Physicochemical and Computational Approaches for the Prediction of the Manufacturability of Active Pharmaceutical Ingredients

DEBBIE HOOPER (MSci)

A thesis submitted in partial fulfilment of the requirements of the University of Greenwich for the Degree of Doctor of Philosophy

This research programme was carried out in collaboration with Pfizer Ltd.

July 2018

DECLARATION

I certify that the work contained in this thesis, or any part of it, has not been accepted in substance for any previous degree awarded to me, and is not concurrently being submitted for any degree other than that of Doctor of Philosophy being studied at the University of Greenwich. I also declare that this work is the result of my own investigations, except where otherwise identified by references and that the contents are not the outcome of any form of research misconduct.

Debbie Hooper   *(Candidate)*

PhD Supervisors

Professor John Mitchell   (1st Supervisor)

Professor Martin Snowden   (2nd Supervisor)

Dr Fiona Clarke   (3rd Supervisor)

ACKNOWLEDGEMENTS

ABSTRACT

Tablets have aided the delivery of active pharmaceutical ingredients (APIs) to patients since the 1800s, however tablet failure, such as punch sticking and tablet hardness issues, during manufacturing is still common. The techniques currently available for the prediction of manufacturability of tablets are not adequately representative of bulk solid properties. There is, therefore, a need to develop new and appropriate characterisation techniques for use in pharmaceutical material evaluation. This is particularly important to ensure that at the manufacturing stage the material properties of medicines are fully understood and predictable to enable optimum manufacturing performance.

This thesis presents a novel approach of experimentally predicting punch sticking and deformation properties of APIs. Four diverse particle shapes of ibuprofen, with similar physicochemical properties are reported herein and a correlation between particle shape and sticking propensity established. Ibuprofen particles with a regular particle shape exhibit a greater tendency to stick compared to particles with a needle like particle shape. Surface energy analysis, both experimentally and computationally, reveals that particles with a more regular shape contain a larger proportion of crystal faces that exhibit a higher surface energy driven by the specific energy component. This provides a link between ibuprofen sticking propensity and surface energy.

The sticking propensity and surface energy of two further APIs, palbociclib and crizotinib, are reported. In general, particles with regular shapes exhibit higher surface energies and a greater propensity to stick. The specific surface energy measured experimentally and total surface energy measured computationally have been shown as useful tools to fundamentally understand the surface chemistry. These attributes can be used to explain different sticking behaviour between different shapes of the same API, where particles with a high proportion of crystal faces containing unsaturated high energy intermolecular interactions at the surface are more likely to stick. This fundamental understanding could be used to engineer API particle shapes through crystallisation to ultimately reduce punch sticking and minimise production issues during tableting processes.

CONTENTS

TABLES

FIGURES

xx

ABBREVIATIONS

API	active pharmaceutical ingredient
CCDC	Cambridge crystallographic data centre
CSD	Cambridge structural database
DS	detachment stress
DSC	differential scanning calorimetry
GTP	Gamlen tablet press
HS-GC	headspace-gas chromatography
ICH	international council for harmonisation
IGC	inverse gas chromatography
MPa	mega pascal
MS	mass spectrometry
PXRD	powder X-ray diffraction
RH	relative humidity
SEM	scanning electron microscopy
TGA	thermal gravimetric analysis

CONFERENCE PRESENTATIONS/PUBLICATIONS

D. Hooper, F.C. Clarke, J.C. Mitchell, and M.J. Snowden, *A Modern Approach to the Heckel Equation: The Effect of Compaction Pressure on the Yield Pressure of Ibuprofen and its Sodium Salt*. Journal of Nanomedicine and Nanotechnology. 2016. **7**(3): p. 381-386.

This publication contains data which is presented in chapter five. See APPENDIX 1 for full publication.

D. Hooper, F.C. Clarke, R. Docherty, J.C. Mitchell, and M.J. Snowden, *Effects of crystal habit on the sticking propensity of ibuprofen—A case study*. International Journal of Pharmaceutics, 2017. **531**(1): p. 266-275.

This publication contains data which is presented in chapters three, six and seven. See APPENDIX 2 for full publication.

AAPS, San Diego, Nov 2017

Poster presentation entitled 'Particle Habit and Surface Energetics to Predict API Punch Sticking'

International Compaction Simulation Forum, Ghent, Jun 2017

Oral presentation entitled 'From Molecule to Material to Medicine: A Case Study of The Sticking Propensity of Ibuprofen'

APS, Glasgow, Sep 2016

Oral presentation entitled 'Evaluating the Impact of Particle Shape on a Materials Tabletability and Sticking Propensity'

Awarded poster prize by GSK during this conference.

1. Chapter One: Thesis Overview

1.1 Purpose of Study

Tablets are the most common dosage form used to administer medicines to patients. The manufacture of tablets in a consistent and reliable manner is crucial in ensuring a robust supply. The physicochemical properties of active pharmaceutical ingredients (APIs) are known to affect the bioperformance of the medicine; therefore these are closely monitored and controlled by specifications. One of the main critical quality attributes of APIs is particle size. Particle size is known to impact on drug product performance such as dissolution, bioavailability and it is for these reasons API particle size specifications are included in the regulatory filing for solid oral dosage forms. Particle size however also affects the manufacturability of tablets as it can impact attributes such as flow and compactability. The size of API particles is controlled during the crystallisation stage or by further processing such as milling. These processes can induce small changes in particle shape and the effect of these changes on drug product processing is not well understood.

Historically, the instrument capabilities for measuring particle shape have been limited but more recently technologies have become available to measure these properties. Another contributing factor to the unknown impact of particle shape changes is the lack of small scale tools e.g. material sparing tableting equipment available to measure mechanical properties. Predicting the mechanical properties of APIs, such as deformation and hardness, can be achieved at a particle level using techniques such as nanoindentation. This capability does not encompass the variation observed in bulk pharmaceutical materials therefore, there is a requirement to address this technology gap and develop suitable small scale predictive characterisation tools for API manufacturability.

Defects in tablets, caused by APIs adhering to the punch tooling, is a major challenge faced by the pharmaceutical industry. Punch sticking has been attributed to many processing and environmental factors; however, no one root cause has been identified.

1

The work reported in this thesis seeks to address these issues by developing a small scale tablet press to predict API manufacturability in terms of punch sticking and tablet hardness. The small scale press will also be used to provide a contemporary approach to the Heckel equation in order to predict API deformation at bulk scale. The root cause of punch sticking will be investigated by modifying the particle shape of APIs and characterising their physicochemical properties using a range of experimental and computational techniques.

1.2   Research Aims

The research reported in this thesis aims to answer the following questions.

- Can a novel bench top tablet press be used to characterise the deformation mechanisms and manufacturability of APIs?
- What impact does API particle shape have on the materials manufacturability, particularly tabletability and sticking propensity?
- Do changes in API particle shape result in surface energy differences and if so do these correlate to the observed manufacturing performance?
- Can the crystal chemistry of APIs be used to explore the surface properties, and can this be used to predict the manufacturing performance of APIs?

1.3   Material Selection

In order to achieve the aforementioned research aims, chemically diverse APIs were selected. The research is centered on ibuprofen which is a solid-state molecular crystal, with only one known room temperature stable polymorphic form. The API has well defined deformation properties making it the ideal candidate for the deformation work. The sodium salt of ibuprofen is also studied in this work for further investigations into the methodologies developed. Ibuprofen is also used for the particle shape investigation since

the effect of solvent on its crystal habit has been well-documented in the literature and is known to exhibit punch sticking.

Two other solid-state molecular APIs (palbociclib and crizotinib) are investigated using the methodologies developed for ibuprofen. Crizotinib and palbociclib are basic compounds, whereas ibuprofen is acidic. Exploration of chemically diverse APIs allows chemical causality as a driving force for punch sticking to be investigated. Crizotinib undergoes a milling stage and the tools developed in this thesis explored the effect of shape/surface changes on sticking propensity. Palbociclib is known to exhibit small changes in particle shape during crystallisation which is of interest in relation to its manufacturability.

1.4   Outline of Thesis

The thesis begins with a literature review of pharmaceutical tablets and the pharmaceutical solid-state landscape. This chapter outlines the manufacture of tablets via direct compression and the problems faced such as tablet hardness and sticking propensity. It also gives a brief introduction to the theory of the solid-state which is then used as a basis for the *in silico* work.

The third chapter describes the theory and reasons of choice for the main experimental materials characterisation techniques utilised. An introduction to the computational tools is also provided.

Chapter four investigates the effect of compaction pressure on the yield stress of ibuprofen and its sodium salt using the Heckel equation. This chapter also demonstrates the use of a novel bench top tablet to characterise deformation properties.

Chapter five provides a detailed discussion of the computational tools used in the theoretical research reported and the crystal chemistry of ibuprofen is explored.

In chapter six, the effect of ibuprofen particle shape on its subsequent manufacturability is presented and chapter seven presents experimental and computational surface energy data on different crystal habits of ibuprofen.

Chapter eight combines the experimental and computational approaches for predicting API sticking propensity and applies these methodologies to investigate chemically diverse APIs: palbociclib and crizotinib.

In chapter nine overall conclusions are provided in relation to all the experimental work reported and how these relate to the original aims of the overall research project. In addition, suggestions for future work which could be conducted, together with the reasons for undertaking such research, in order to enhance/build upon the scientific investigations reported in the thesis.

2. Chapter Two: Literature Review

2.1 Introduction

The pharmaceutical industry discovers, develops, produces, and markets drugs for use as medications. Pharmaceutical companies may deal in generic or brand medications and medical devices. The work reported in this thesis refers only to drug molecules. The workflow summarising the stages of drug discovery, development and manufacture is illustrated in Figure 2.1. Once a molecule that has medicinal properties has been discovered, its solid form and particle properties are optimised by a drug development process. It is then common for the API to be formulated with functional excipients and once combined these mixtures are known as drug products. Drug products are then manufactured into medicines to aid administration to patients, which are known as a dosage forms.
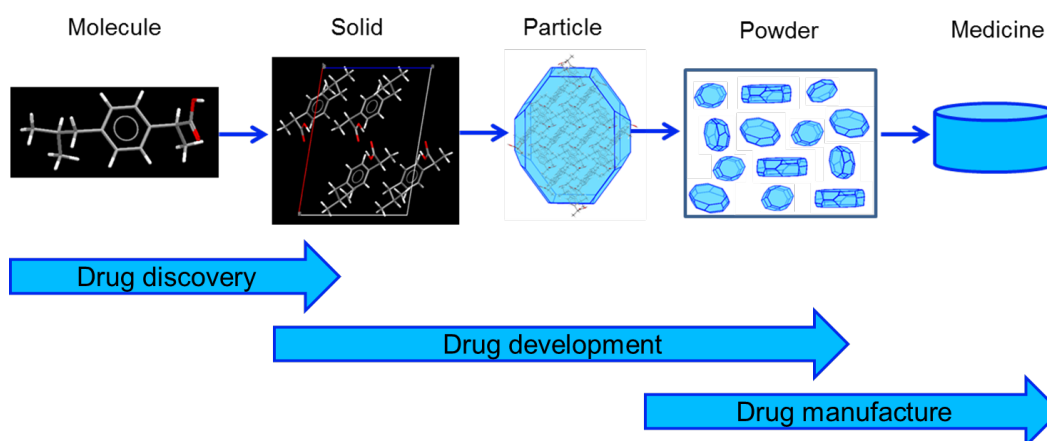
Figure 2.1 – Workflow illustrating the stages of drug discovery, development and manufacture. Adapted from reference [1].

Dosage forms are classified in terms of their physical form: solid, semisolid and liquid and can be further subdivided by their target organ area e.g. a dry powder inhaler is a solid oral dosage form, mixed with a propellant that targets the respiratory tract. Around 70% of all drug products are manufactured as solid oral dosage forms [1]. Solid oral dosage forms include dry powders, tablets and capsules with tablets being the most common type

due to their ease of administration, flexibility in design and because they can be manufactured economically [2].

The work reported in this thesis focuses on understanding some of the properties that affect the manufacture of pharmaceutical tablets.

2.2   Pharmaceutical Tablets

The use of 'pharmaceutical tablets' dates back as far as 1500 BC where it is presumed that pills were invented to enable the administration of measured amounts of medicinal substances to patients.   In 1843, William Brockedon invented the tablet we all know today, still referred to as 'pills' in pharmacy, by placing powder in a tube and hammering it with a mallet [3].

The manufacture of tablets has evolved as well as the types available.   There are four main types which are summarised in Table 2.1.   The type of tablet which is selected will depend on the mechanism of action of the API e.g. APIs which are intended to be dissolved in the gastrointestinal tract and absorbed by the blood will be orally ingested and can include immediate release or delayed action tablets.   APIs that are destroyed by gastric juices can be formulated into oral cavity tablets e.g. buccal or sublingual where they are designed to dissolve in the mouth, usually to treat localised pain.   Patient needs can also be considered when the type of tablet is designed e.g. instantly disintegrating tablets dissolve into a liquid on the tongue that can then be swallowed by patients who find it difficult to swallow whole tablets.

Table 2.1 – Types of pharmaceutical tablets, including examples.

Type of Tablet	Example
Orally Ingested	Compressed tablet, delayed release tablet, multi-layer tablet, instantly disintegrating.
Used in oral cavity	Buccal tablet, sublingual tablet, lozenges.
Used to prepare a solution	Effervescent tablet, hypodermic tablet.
Other route	Implanted tablet, vaginal tablet.

Tablets are manufactured by molding or compression, with the latter being the most common. The work reported in this thesis focuses on understanding the properties that affect the manufacture of orally ingested compressed pharmaceutical tablets; however, the ideas could be expanded to other types of tablets manufactured by compression.

2.2.1 Pharmaceutical Tablet Formulation and Manufacture

Drug products for tablets are made by combining an API with inactive excipients to enhance the properties of the blend that is to be compacted. Excipients are added to aid the medicinal properties of the API e.g. disintegrants which promote the break-up of tablets in the gastrointestinal tract. They are also added to improve the manufacturability of the API e.g., binders, adhesives and lubricants which improve the flow and compaction properties. Other excipients are added to improve the appearance and taste of the tablet e.g. colourings and flavourings.

The final pharmaceutical blend can be processed using conventional methods such as dry/wet granulation; however, direct compression of the APIs and excipients without any prior treatment is the desired tablet manufacturing route due to its simplicity and cost effectiveness [4]. For direct compression, the APIs and excipients are simply mixed before tableting. The blend is then transferred into a commercial tablet press which is used to produce tablets on a mass scale. The compression cycle on a rotary tablet press is shown in Figure 2.2 where it can be seen that the press has a number of positions. The first operation is to overfill the die with the blend shown in Figure 2.2a. The press then rotates and the volume of the powder is reduced to achieve a specific tablet weight. The upper and lower punches then move between large wheels known as pressure rollers to begin the compression event of the powder. Pre-compression (Figure 2.2b) can be used prior to the main compression event to reduce air pockets and, for some blends, can be used to produce harder tablets [5]. The main compression event (Figure 2.2c) follows pre-compression and determines the final thickness/hardness of the tablet. The tablet is then ejected from the die by being pushed up by the

lower punch (Figure 2.2d) and the tablet is moved from the die by a scraper [6].
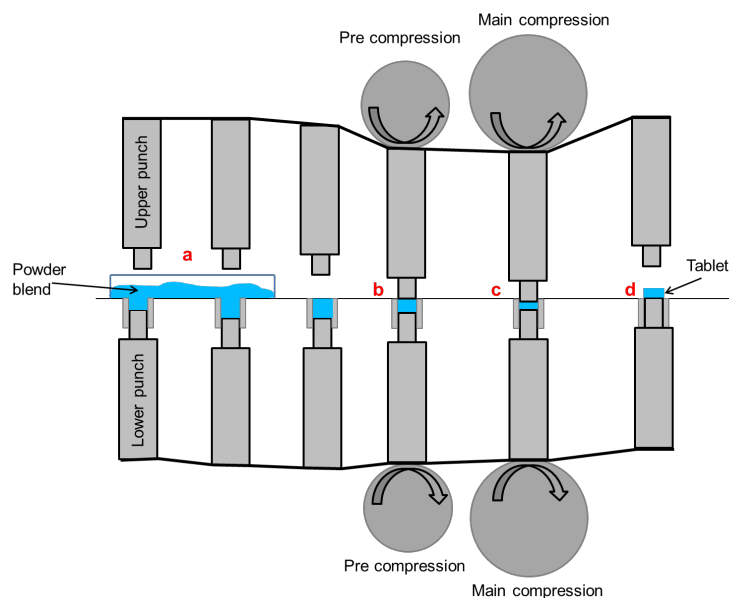
Figure 2.2 – Illustration of the compression process on a rotary tablet press showing four main stages a) die filling b) pre compression c) main compression d) tablet ejection. Adapted from reference 7.

In order for suitable tablets to be obtained the blend must be able to flow uniformly into the die, compress to form acceptable tablets and the final tablet must eject as a solid entity from the press.

2.2.2 Powder Compression and Deformation

There are three stages of powder compression which have been clearly defined in the literature: particle rearrangement and fragmentation, followed by particle deformation and then, finally, elastic recovery of the tablet [7]. As pressure is initially applied to the powder bed the particles rearrange and fragment in order to fill in void space between them. This initial stage brings the particles within close proximity to each other; however, the main mechanism of consolidation is particle deformation [8]. The final stage involves the elastic relaxation of the tablet as the force is withdrawn [8].

Deformation is the action of physically changing the shape of a solid material which can be reversible or irreversible. There are three main types of deformation: elastic, plastic and brittle (Figure 2.3). When a material (point a) is subjected to stress, it relieves the resulting strain by deforming. Materials will firstly exhibit elastic deformation, where the change in shape is reversed once the force has been removed (point b). If the stress applied is beyond the elastic limit of the material, the strain will then be relieved by fracturing (brittle deformation) or plastic deformation, represented by points c and d, respectively. Brittle fracture involves a size reduction and, subsequently, the original material shape is permanently changed. As a result of plastic deformation, an irreversible change in size and shape occurs with no fracturing present.
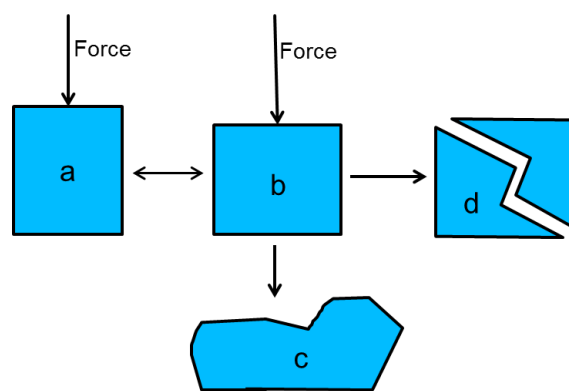
Figure 2.3 – Illustration of the three main types of deformation a) particle b) elastically deformed particle c) plastically deformed particle d) particle undergone brittle fracture. Adapted from reference [9].

The type of deformation that a material will undergo is an intrinsic property that is directly related to its crystal structure [7, 10] but can also be influenced by external factors such as the rate and magnitude of force applied and temperature [11, 12].

The majority of fundamental understanding on deformation arises from industries other than the pharmaceutical industry e.g. geology and transport industries where the deformation of rocks that form mountains and the resistance to car parts on impact are studied [13, 14]. It is only recently with

the growing understanding of how deformation properties affect manufacturing processes such as compaction and milling [15-17] that pharmaceutical formulation scientists have become focused in this area. The Heckel equation is used to calculate compaction properties and is frequently used in the pharmaceutical industry to measure bulk powder deformation [18]. Deformation is measured by calculating the yield pressure (σ) of a material, where low values indicate plastic deformation and high values indicate brittle deformation. The Heckel equation has been heavily criticised in the literature for its variability due to experimental conditions affecting yield pressure results. Despite the criticism the equation is still used today therefore this research aims to explore these variations and standardise them further [19].

2.2.2.1 Tablet Formation

The formation of a tablet can be attributed to two primary factors: dominating bonding mechanisms and the surface area over which these bonds are active [20]. During compaction, increased bonding surface area is achieved through plastic deformation, where the flow of particles increases the bonding surface as highlighted in Figure 2.4. The fragmentation of particles, via brittle deformation, also increases bonding surface area through the exposure of new surfaces [21]. This means that plastic deformation is necessary but not sufficient to create strong tablets; therefore, a direct compression formulation requires the correct balance of both plastic and brittle components.
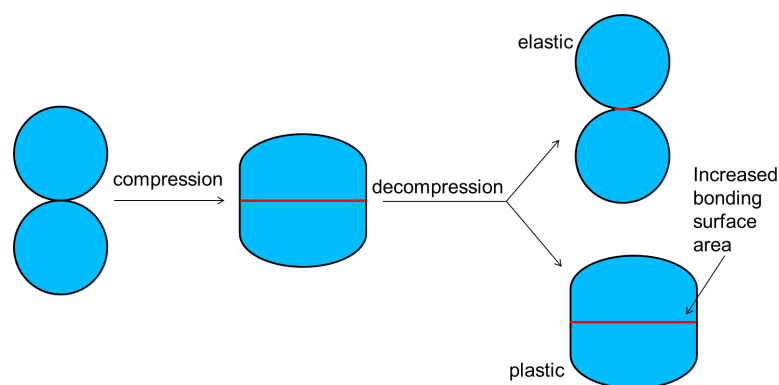
Figure 2.4 – Illustration of particle compression where plastic deformation increases the particle to particle bonding surface area. Adapted from reference [22].

There are three main types of bonding mechanisms present in tablets: 'solid bridges', intermolecular forces and mechanical interlocking. The strongest interactions are 'solid bridges', where atomic contact is present, and is thought to be due to the material melting or recrystallising [20]. Intermolecular forces take into consideration the hydrogen bonding, Van der Waals and electrostatic forces between surfaces that are separated by some distance. These forces are the dominating bonding mechanisms in pharmaceutical tablets [23] and it has been shown that hydrogen bonds are important for the strength of tablets made from microcrystalline cellulose [24]. The third type of bonding mechanism is the mechanical interlocking of irregularly shaped particles [20], where two different shaped particles are able to twist and interlock easier than particles of the same shape.

2.2.3 Active Pharmaceutical Ingredient Target Attribute Profile

Materials Science is an interdisciplinary subject, spanning the physics and chemistry of matter, engineering applications and industrial manufacturing processes. The importance of this discipline to pharmaceuticals has recently been described by the materials science tetrahedron, which depicts the relationships between internal structure, particle properties, material processing and performance of a drug product (Figure 2.5). Pharmaceutical materials science has emerged as a foundation of Quality by Design (QbD)

with solid form, crystallisation and particle engineering being core elements linking the drug product to the final steps of the API manufacturing process [25].
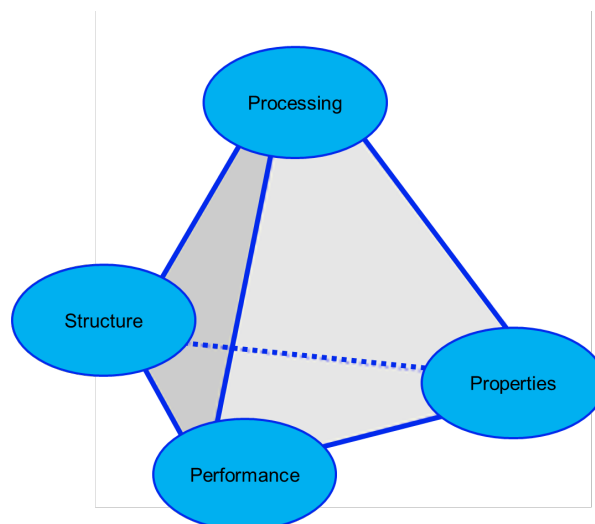
Figure 2.5 – The materials science tetrahedron showing the relationship between structure, properties, process and performance. Adapted from reference [22].

The physicochemical and mechanical properties of APIs that affect the bioavailability, stability and manufacturability of the drug product are defined in an API target attribute profile (API-TAP). These attributes are critical for tablets manufactured by direct compression as the properties are not masked by processing e.g. by a granulation step. Generally, the properties of excipients are well documented in the literature [4, 21] therefore this body of work focuses on understanding the effect of API properties on the manufacturability of tablets. Some important critical quality attributes affecting tablet manufacture are documented below.

2.2.3.1 <u>Crystal Form</u>

An API can exist in more than one crystal form, known as polymorphism (discussed in Section 2.2.3). The crystal form of an API is known to influence

the medicinal properties as well as the manufacturability, with one of the earliest examples of this in the literature being paracetamol. In 1998, Nichols and Frampton reported different deformation behaviour of the two stable forms of paracetamol: form I and form II [10]. The plastic nature of orthorhombic form II was attributed to the existence of slip planes in the structure which do not exist in monoclinic form I. The plastic deformation of form II allowed stronger tablets to be formed over the commercial form I [26]. This demonstrated that making changes to the nature of the polymorphic form is an attractive route to alter the mechanical properties of some APIs.

As the crystal form can alter both the medicinal and mechanical properties of an API these factors need to be balanced during the solid form selection for a new drug candidate. For commercial products where the solid form has already been selected, changing the polymorph to improve manufacturability is undesirable. This study aims to keep the crystal form of APIs the same as the commercial material and samples will be characterised using orthogonal characterisation techniques to confirm no form changes have occurred.

2.2.3.2 Particle Size

Particle size is one of the most important physical properties of an API and has been shown to affect both the drug product performance and the materials manufacturability. The size of particles can influence product safety by affecting dissolution rate, bioavailability, content uniformity and stability and also the manufacturability of products by affecting flow, blending, wetting drying and mechanical properties [27 - 29].

The factors discussed make it of increased importance to control and measure the particle size of materials; acceptable criteria are set by the Food and Drug Administration (FDA) and similar organisations depending on the country for new APIs [30]. The particle size of APIs can be controlled during the crystallisation process; however, processing operations such as milling are often used to decrease/control the size further [17]. The milling of APIs has been shown to affect the crystallinity of materials and also there is no

control of particle shape. This study aims to control the particle size of materials during crystallisation with one milling case study presented.

The effect of particle size on drug product performance has been well documented in the literature (see references [28, 31]) therefore the effect of particle shape will be investigated further.

2.2.3.3 Particle Shape

The particle shape of APIs has been shown to influence the medicinal and manufacturing properties of drug products. This attribute however receives much less attention in the literature in comparison to particle size. It has been shown that dissolution rate and bioavailability are affected by particle shape as well as particle size where generally crystal orientations that grow faster will in turn dissolve faster [32]. It is also well known that spherical particles exhibit better flow in comparison to needle shaped particles [33]. The effects of particle size on manufacturability are better understood and therefore the control of size, during the processing of APIs, often takes priority.

Particle shape (crystal habit) can be described qualitatively, and is often subject to interpretation. It is only recently that viable instrumentation has been developed to quickly provide quantitative shape descriptors. The six basic crystal shapes that an API can exhibit [34] are shown in Figure 2.6. These shape descriptors allow APIs to be classified into groups. However, Yu *et al.* suggested that in order to fully capture particle shape quantitative measurements should be made and several shape descriptors (e.g., aspect ratio, sphericity, elongation) should be reported [35].
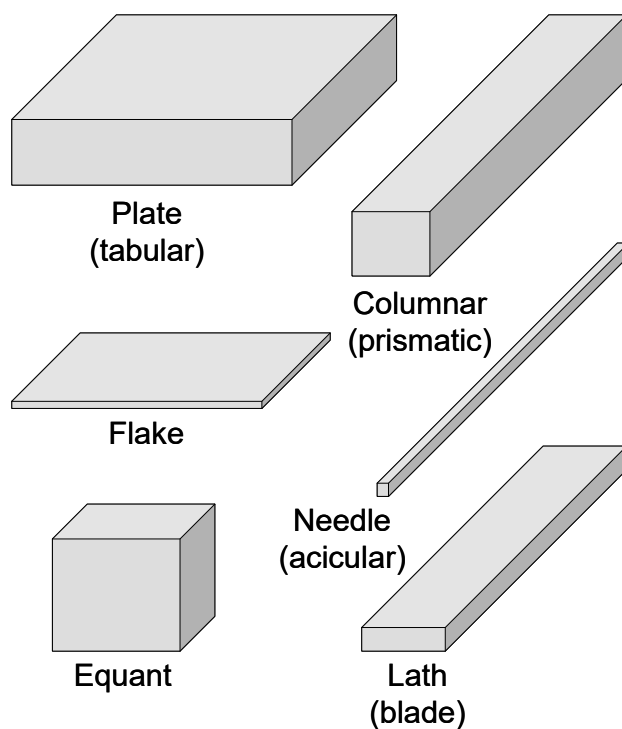
Figure 2.6 – Six basic crystal shapes of APIs. Reproduced with permission from [34].

Particle shape can be altered by a number of routes including how the API is crystallised or by further processing routes. During the crystallisation process the choice of solvent, solvent impurities, cooling rate, seeding and drying conditions can affect the final API particle shape. APIs which are further processed after crystallisation, e.g. by milling or spray drying have their particle shape dictated by the operating conditions used for these additional operations [36].

This study aims to alter the particle shape of APIs via crystallisation and milling in order to better understand the effect on the manufacturability of tablets.

2.2.4 Critical Attributes and Failures of Tablets

As with all drug products, tablets must be of a certain quality and deliver the required safety and efficacy of the product [37]. These specifications have been summarised by Alderborn [7] and include chemical, physical and mechanical properties. Tablets should be of a consistent weight, size and

shape as well as contain the correct dose of API. The API should be stable throughout the shelf-life of the tablet and be released in a controlled and reproducible manner. The final tablet should also be packed in a safe and appropriate manner and have sufficient mechanical strength to avoid fracturing during its handling, packaging and transportation.

Although tablets have existed for many years, the process of making a 'good' tablet is still said to be more of an art rather than a science due to the complex mechanisms involved [38].

2.2.4.1 Hardness

The hardness of a tablet relates to the breaking force or resistance to crushing strength and is often used as a control specification to ensure quality. It can also be used as an indication if other specifications such as disintegration and friability can also be met [39]. The hardness of a tablet will be dependent on the type of tablet; however, in general a balance between 'too soft' and 'too hard' must be achieved. Tablets must have sufficient mechanical strength to avoid breakdown during the lifetime of the product but also be weak enough to breakdown in the body in order to achieve dissolution.

The mechanisms which affect tablet hardness are well documented in the literature and include processing and environmental factors as well as the physicochemical and mechanical properties of the constituent materials.

Parameters used for the operation of a tablet press such as the speeds of the turret and feeder can affect tablet hardness due to the speed causing differences in die filling and particle attrition leading to differences in tablet hardness [38]. Factors such as the speed of compaction, dwell time and pre-compression parameters can influence tablet hardness which is related to the deformation mechanisms of the powders in the blend [5, 40]. Plastic pharmaceutical materials need to be loaded and unloaded from the punches at an adequate speed for permanent deformation to occur. If a material exhibits time dependent deformation properties, such as viscoelastic

behaviour, then then dwell time can affect tablet hardness. For formulations that contain highly elastic materials, pre-compression can be used to increase the tablet hardness and avoid issues such as lamination and capping. The physical geometry of punches has also been shown to affect hardness; for example, a recent study by Anbalagan *et al.*, revealed that radius edge tooling produces stronger tablets compared to bevel edge tooling [41].

The physicochemical and mechanical properties of an API have been shown to affect hardness. The intrinsic deformation properties of an API have been shown to influence the tablet hardness where plastic materials form stronger tablets than brittle materials. The effect of particle size on direct compression has also been well documented in the literature. The tensile strength of compacts has been shown to increase with decreasing particle size by many researchers [28, 31, 42]. This phenomenon can be attributed to the increased surface area of smaller particles, compared to larger particles, resulting in an increased area available for inter-particulate bonding. For a direct compression formulation it is important to achieve a balance between large and small particles to enable the material to flow but also have adequate bonding area.

The effect of particle shape on tablet hardness has also been explored in the literature. Sun *et al.* found that plate shaped particles of L-lysine formed stronger tablets that prism shaped particles [42]. Rather than a physical difference in shape being associated with the variation in hardness the reason was attributed to the shape causing a greater exposure of a slip plane in the plate shaped particles. In 2010, Seton *et al.* compared the hardness of tablets formulated with different crystal shapes of ibuprofen (needle and lath shaped particles) and lactose. This study found no correlation between the API shape and tablet hardness, which could be due to the formulation [43]. The studies reported herein use pure APIs for compaction experiments only.

2.2.4.2 Lamination and Capping

Lamination and capping are two common modes of tablet failure highlighted in Figure 2.7a and Figure 2.7b, respectively. Lamination is the splitting of the

tablet into two distinct layers whereas capping is the removal of the top or bottom of the tablet from the main body.
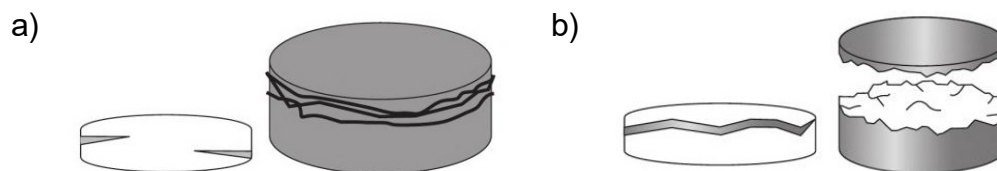
Figure 2.7 – Common modes of tablet failure a) tablet lamination b) tablet capping [44].

Lamination of tablets occur when a material is over compressed due to the shape of the particles/granules becoming flat and not being able to lock together. This would imply that the particle shape of an API may influence lamination, with flatter particles being more prone to this behaviour. Capping is thought to be due to the elastic recovery of the compact being greater than the bonding deformation occurring during compression [45], which is dependent on the materials used in the formulation.

Due to the current amount of research ongoing in this area [46] the mechanisms of lamination and capping will not be investigated in this project, but will be monitored during the compaction of materials.

2.2.4.3 Punch Sticking

One of the major issues affecting the production of pharmaceutical tablets is the formulation adhering to the tooling surfaces, known as sticking or picking. Punch sticking is a general term that refers to the adhesion of powder to a tablet punch whereas picking is more specific in that it refers to the sticking of powders within the embossing or debossing of the tabletting tooling [47]. The differences in these phenomena are highlighted in Figure 2.8. The work reported in this thesis is concerned with punch sticking; however, the concepts discussed could also be extended to tablet picking.
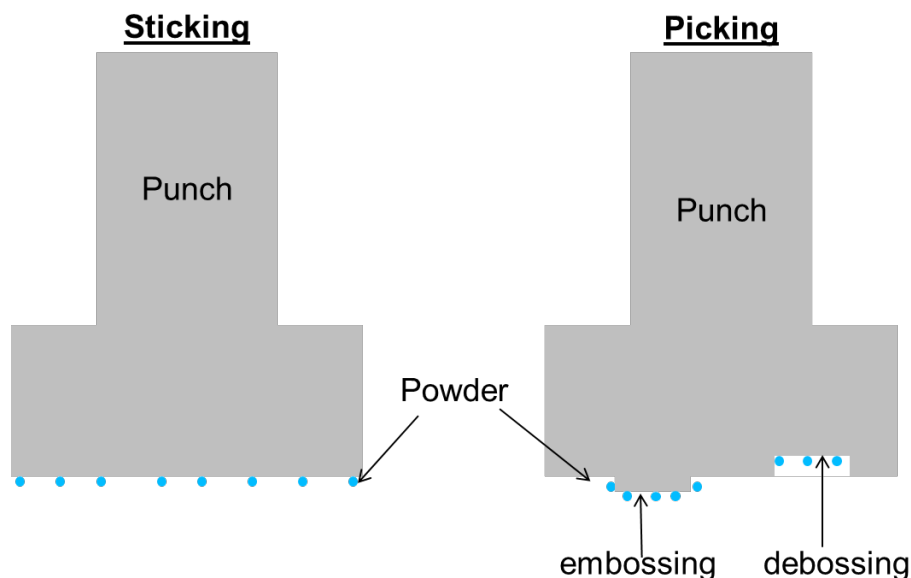
Figure 2.8 – Illustration highlighting the differences between punch sticking and picking.

Punch sticking can reduce the efficiency of drug product manufacture due to presses having to be stopped and cleaned. This can also lead to tablet defects which can result in more serious effects, such as loss of potency of the API and visual defects which can cause possible quality concerns for patients.

Many attempts in the literature have been made to determine the elusive root cause of this phenomenon, however no single root cause has been identified. It is known that sticking is due to API adherence even when it is present in a formulation at low concentrations [48]; however, it is not only caused by the API but many formulation, processing and environmental factors have been shown to contribute.

From a formulation perspective lubricants such as magnesium stearate are added to a formulation to reduce punch sticking by forming a film around the particles therefore reducing the particle-punch friction and in turn reducing the powder sticking to the tabletting equipment. Although generally accepted as a solution to reduce punch sticking, lubricants have been shown to have a negative effect on tablet hardness due to the reduced solid-solid interactions which decrease the available bonding surface area between particles [28]. In

some cases lubricants have also been attributed to the cause of sticking when present in high concentrations (magnesium stearate >1%) [49]. In this study lubrication will not be used during the direct compression of materials.

The processing and environmental factors that have been linked to punch sticking include punch type and quality, how the press is operated and temperature/humidity. Roberts *et al.,* showed that the punch sticking of an ibuprofen formulation decreased as punch curvature increased suggesting that worst case sticking will occur with flat faced tooling which is used in this project [50]. Studies have also shown that the humidity and temperature of the environment influence punch sticking [51, 52], as well as the temperature of the punch and die [53]. The environment was not controlled in the experiments reported herein; however, temperature and humidity parameters were recorded and, due to the small scale equipment used, it was assumed that no significant temperature increase would occur in the die.

To try and overcome the problem of punch sticking some options are available to pharmaceutical scientists, such as different punch coatings, punch modification and the use of different lubricants [54 - 57]. Tablet equipment manufacturers advertise punches coated with chromium nitride to be superior in terms of sticking management and studies have found sodium stearyl fumarate to minimise the sticking tendencies of an ibuprofen formulation in comparison to the traditionally used magnesium stearate [55]. Although these solutions exist there is still a need to understand the role of the API from a particulate level to punch sticking.

Many attempts in the literature have been made to try to correlate sticking to particle properties such as size and shape. It has been shown that particles with a smaller size have a greater propensity to stick [58 - 60]; however, it has also recently been suggested [62] that sticking is an inherent materials property influenced by plastic deformation (meaning it is not unlikely that some large API particles will also stick).

As previously stated, the role of API particle shape with regards to punch sticking has received less attention than particle size in the literature. A study by Seton *et al.,* which measured the hardness of ibuprofen tablets formulated

with different shaped particles and lactose found no correlation between punch adhesion and API shape [43]. This study, as mentioned before, did not examine the API alone and the formulation could be concealing the problem. Rasenack *et al.,* also studied the sticking propensity of different ibuprofen particle shapes and found that when tableting pure API needle shaped particles had a higher tendency to stick compared to lath shaped particles [61].

More recently a study was undertaken to investigate the causes of sticking at a molecular level. Different shaped particles of mefenamic acid were produced and were shown to exhibit difference tendencies to stick (needle shaped particles stuck more than lath shaped particles). The difference was attributed to chemical causality of the different ratios of surfaces exposed in each of the particle shapes [62].

This study aims to investigate further if chemical causality caused by a change in API particle shape is the root cause for tablet sticking.

2.2.5 Compaction Simulation

There is an increased need to understand the processing behaviour of a powder before full scale manufacture in order to try and predict manufacturability and therefore reduce the risk of any tablet failures. Compaction simulators provide a small scale technique for powder compaction but with the same control as a manufacturing tablet press such as a Fette or Korsch press [63].

In general, compaction simulators can perform to the same limits as production presses; however, there can be confusion when interpreting data due to the various ways used to report the results obtained. It has been suggested, by the compaction simulation research community, that data should be normalised to account for differences in tooling e.g. size and shape and to provide a more 'analytical' approach to compaction simulation [64, 65].

A brief review of the way compaction simulators are used to predict manufacturability (tabletability and sticking propensity) is documented below.

2.2.5.1 Tabletability

Compaction simulators can be used to produce small batches of tablets in order to measure their tablet hardness to provide a prediction at small scale. In order for compaction simulator data to be comparable to production press data when the tablet dimensions, shape and size, are different the data can be normalised to tensile strength, σ, (Equation 1):

$$\sigma = \frac{2F}{\pi dh} \tag{1}$$

where F is breaking strength, d is tablet diameter and h is tablet thickness. Equation 1 is only suitable for flat-faced cylindrical tablets but can be used to normalise the hardness of different size tablets [66]. Recently more complicated equations have been developed for concave, elongated tablets allowing different tablet shapes to be compared [67].

In order to achieve a tablet of sufficient strength it has been suggested in the literature that a tensile strength value of greater than 2 MPa must be achieved, with a minimum value of 1.7 MPa being acceptable [68].

The tabletability of a material is a measure of tensile strength at different compaction pressures and is used as a small scale tool to predict material behaviour at different pressures. It is accepted that the tensile strength of compacts will increase as compaction pressure increases. However, a delicate balance between compaction pressure and tensile strength is required to avoid problems such as lamination and chipping (as highlighted in Figure 2.9).
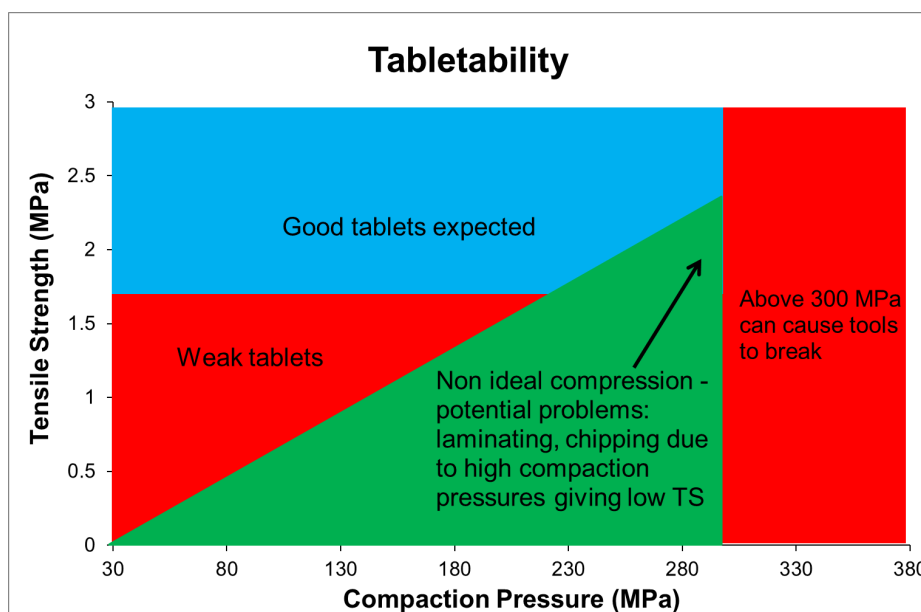
Figure 2.9 – Tabletability plot highlighting the relationship between tensile strength and compaction pressure. Adapted from reference [68].

2.2.5.2 Punch Sticking

There is no set standard for measuring or predicting punch sticking in the pharmaceutical industry and different research groups have proposed a number of different tests.

On a particulate level, atomic force microscopy can be used to measure the tip adhesion to single faces of crystals [62]; however, this is crystal face specific and does not provide a bulk representative of an API sample due to crystals being anisotropic. A bulk test developed by Wang *et al.,* quantified API adherence to a stainless steel surface. This test involved placing a stainless steel ball as well as mefenamic acid into a die before applying force. The ball was then removed from the die and placed in methanol so that any powder adhered to the ball would be dissolved. The amount of powder was then measured using high performance liquid chromatography [69]. Although this is a quantitative measure of adhesion, it involves several pieces of equipment, expertise in many areas and the ball used does not represent the equipment used during tablet manufacture.

The most promising test proposed in the literature to quantify punch sticking is the use of a removal upper punch tip with the compaction simulator. In this

23

test the compaction simulator is run as normal however the tip is removed and weighed at intervals in order to assess how much powder has adhered [70]. This test requires a considerable mass of material (250 g was used in the mass punch test) and error can be introduced from weighing milligrams of powder adhered to a heavy punch tip.

There is still a need to develop a new and appropriate small scale technique to predict the sticking propensity of pharmaceutical powders.

2.3 Pharmaceutical Solid-State Landscape

As most medicines are administered to patients in solid dosage forms it is important to understand the solid-state landscape of APIs. An overview of the pharmaceutical solid-state is shown in Figure 2.10 and can be split into three defined areas: crystalline, liquid crystal and amorphous. The molecules in a crystalline material exhibit three dimensional long range order, liquid crystals exhibit one or two dimensional long range order whereas amorphous materials exhibit only short range order. Although amorphous materials tend to have better bioavailability within the body, the majority of small molecule APIs (>90%) are delivered in the crystalline form [71] due to the unstable nature of amorphous materials. Crystalline APIs will be the main focus of this study.

Crystalline APIs can be split into single and multi-component systems. API molecular crystals contain only one type of API neutral molecule in the unit cell compared to cocrystals, salts and solvates/hydrates which contain more than one component. The components within a salt are bonded together via ionic bonding whereas the others contain intermolecular forces only. API single component molecular crystals will be the focus of this investigation.

24
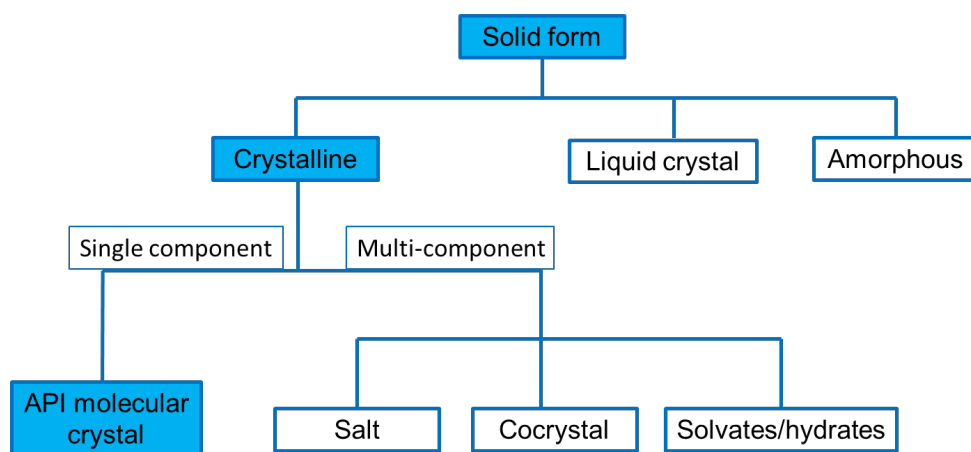
Figure 2.10 – Overview of pharmaceutical solid-state landscape. Adapted from reference [1].

2.3.1   Crystallography

Crystals are solid materials where the constituents (atoms, ions or molecules) are regularly arranged with respect to each other, in three-dimensions. The scientific discipline that governs the formation of a crystal is called crystallography. The pattern of repetition in a crystal can be described by defining the repeating units and the symmetry between them. Due to the regular arrangement of the constituents, these can be replaced by lattice points which are imaginary sets of points in space and when repeated make up the crystal lattice shown in Figure 2.11. The crystal lattice can be described in terms of the unit cell which is the smallest repeating pattern (also highlighted in Figure 2.11). The unit cell is described by the three lengths (a, b and c) and three angles (α, β and γ), known as lattice parameters. The unit cell also compromises of symmetry elements which describe the rotation, translation and inversion (space groups) and together both can be used to define the full crystal lattice. This work focuses on *in silico* modelling of APIs where it is common practice to use the unit cell to minimise the computational cost.
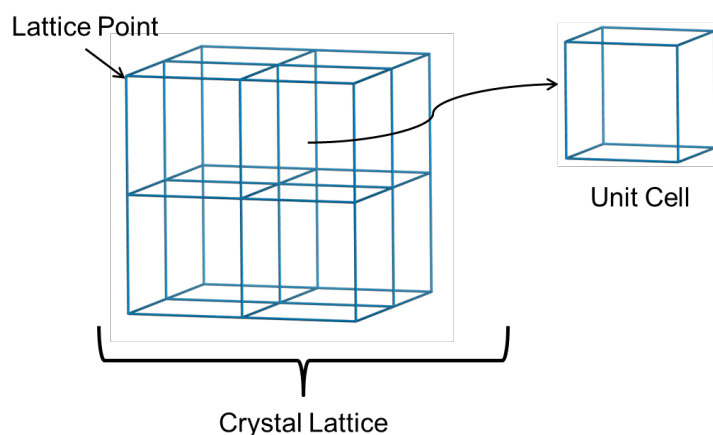
Figure 2.11 – Crystal lattice highlighting lattice points and the unit cell.

Unit cells can be categorised in terms of their geometry and symmetry. There are seven distinct shapes known as the crystal systems: triclinic, monoclinic, orthorhombic, tetragonal, rhombohedral, hexagonal and cubic. Unit cells can be constructed in different ways from a set of lattice points known as the unit cell type. The main unit cell type is the primitive unit cell, where the lattice points are only at the cell corners and there are six others which are variations of this e.g., face-centered where the lattice points are at the cell corners and also at the center of all the faces. The crystal system and unit cell type combined give rise to Bravais lattices of which there are 14 unique types. Pharmaceutical molecules tend to adopt primitive unit cell types of triclinic, monoclinic or orthorhombic systems [72].

2.3.1.1 Crystallographic Planes

Crystallographic planes relate the internal bulk arrangement of molecules to the well-defined faces that are exhibited by crystalline materials. The molecules are arranged in equal distance to each other creating imaginary sheets. Planes can be drawn through unit cells and are defined using Miller indices. Miller indices (hkl) are the inverse of the fractional co-ordinates where the plane intercepts the axis. If a plane does not intercept the axis then it is denoted as zero and negative intercepts can be defined using a

negative Miller index or the positive integer with a bar above. Examples of planes and derived Miller indices are shown in Figure 2.12.

a)   b)   c)

a = 1   a = 1   a = -1
b = ∞   b = ∞   b = 1
c = ∞   c = 1   c = ∞
Miller index (1 0 0)   Miller index (1 0 1)   Miller index (-1 1 0)
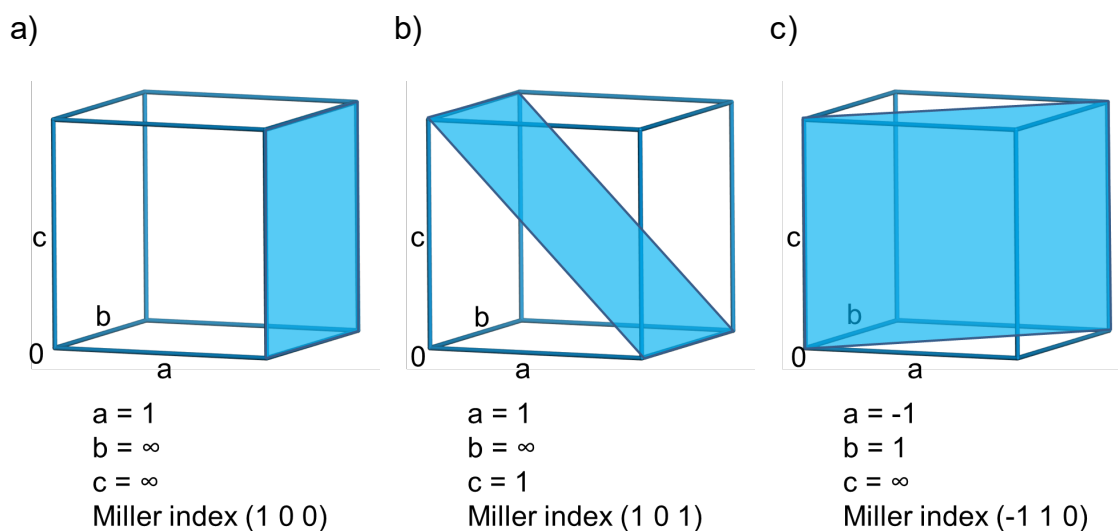
Figure 2.12 – Crystallographic planes and their derived Miller indices a) (1 0 0), b) (1 0 1), and c) (-1 10).

In a full crystal lattice the crystallographic planes run adjacent to each other forming rows. These planes are held together by intermolecular bonds and are separated by interplanar d-spacing (d_{hkl}).

2.3.2   Intermolecular Interactions

In molecular solids the discrete molecules are held together by intermolecular forces only. Intramolecular forces are the bonding forces that hold the atoms together in a molecule whereas intermolecular forces are the interactions that exist between molecules, with an example using water highlighted in Figure 2.13. All states of matter exhibit intermolecular forces and are responsible for the macroscopic properties of material e.g. water existing as a solid, liquid or gas depending on the temperature. Intermolecular interactions are based on atomic and molecular phenomena which relate back to electrostatics. The types of forces are namely Van der Waals and hydrogen bonding and are described in more detail below.

27
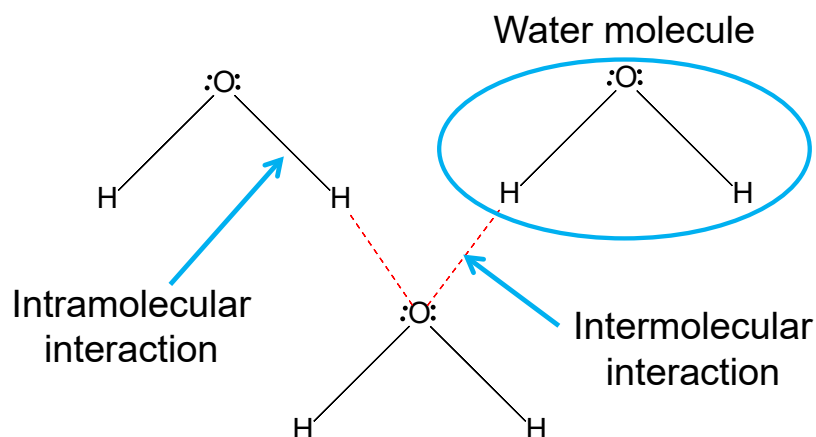
Figure 2.13 – Water molecules highlighting the difference between intramolecular and intermolecular interactions.

2.3.2.1 Van Der Waals Forces

Van der Waals forces are attractive forces that can be split into three types dependent on the dipole formation. If two molecules have a permanent dipole which are aligned this, is a Keesom force. If a molecule which has a permanent dipole induces a dipole in a polarisable molecule this is known as a Debye force. The third type is a dispersive force, which is known as a London force and these occur when instantaneous temporary dipoles are formed by non-even electron distribution in an atom. These dipoles can then induce dipoles in neighbouring atoms. The differences in dipole formation result in these type of interactions having differences in strength where London<Debye<Keesom [73].

2.3.2.2 Hydrogen Bonding

Hydrogen bonds are a special type of permanent dipole interaction that are caused by the force between a highly electronegative atom (nitrogen, oxygen or fluorine) and an electron-poor hydrogen atom. Unlike Van der Waals forces, hydrogen bonds are directional in nature and much shorter in distance. They are the strongest interaction found in molecular solids and are widely studied.

In 1991, Desiraju proposed that hydrogen bonds are responsible for directing the arrangement of molecules in the crystal structure [74] which was backed up by data reported by Aakeröy and Seddon in 1993 [75]. More recently in 2015, Rosbottom *et al.,* showed that for *p*-aminobenzoic acid the strength of the hydrogen bonds was similar to the strength of Van der Waals interactions [76]. From this it is clear that the intermolecular interaction type and strength that a molecular material exhibits is dependent on atomic and molecular phenomena and each case must be studied individually.

2.3.3 Polymorphism

The three dimensional order of a molecule can be changed by rearrangement of the molecules within the unit cell, known as polymorphism. There are different types of polymorphs that can exist e.g. an API molecular crystal can have several forms (packing polymorphism) and also form hydrates or solvates to change its form (pseudopolymorphs).

These form changes are known to influence the chemical and physical properties of the material and often alter the medicinal properties [71, 77] of the drug. Ritonavir is an API used in the treatment of HIV/AIDS and is known to exhibit two common polymorphic forms. However during its release onto the market in 1996 only one form (form I) had been investigated and later in 1998 a second form (form II) was discovered in the product which was much less soluble. This discovery compromised the oral bioavailability of the API and led to a different dosage form being utilised.

As discussed in Section 2.1.4, polymorphism of a molecular API influences the deformation behaviour which in turn affects tablet hardness. Due to this many recent efforts have focused on crystal engineering to change the deformation properties of the API and therefore increase the tablet hardness [78 - 83]. Sun and Hou showed that combining caffeine with methyl gallate significantly improved the hardness of tablets (compared to caffeine alone) due to the presence of flat hydrogen bonded slip planes present in the cocrystal [79]. In support of this theory Chattoraj *et al.,* later showed, using theophylline, that introduction of a cocrystal does not always improve the

mechanical properties and that it is in fact the arrangement of molecules in the three dimensional repeating unit of crystals that drives this manufacturing behaviour [80].

There is, to the author's knowledge, no published work on polymorphism affecting sticking propensity. However, in 2017, Shubhajit *et al.,* proposed that plastic materials have a greater tendency to stick than brittle materials [84]. This means there is the opportunity to engineer different crystal forms of APIs to change the sticking propensity. For marketed products it is unlikely that the polymorphic form of an API would be changed to alter the manufacturability, as this would involve major regulatory impact as well as the potential to alter the drugs mechanism of action. For this reason this study focuses on understanding the surface chemistry of different particle shapes only, which will be discussed in more detail.

2.3.4 Crystal Morphology and Surfaces

The external shape of a crystal will be dictated by the internal structure and can be predicted numerically. Gibbs developed the equilibrium criteria for the solid crystal and solvent interphases and the first approach for determining the shapes of crystals at equilibrium was proposed by Wulff in 1901 [85, 86]. The Gibbs-Thomson formula, shown in Equation 2, relates the surface energies and area of crystal facets to the total surface energy (ΔG) at a specific volume (V):

$$\Delta G = -\frac{V\Delta\mu}{V_M} + \sum \gamma_i A_i \qquad (2)$$

where $\Delta\mu$ is concentration, V_m is volume at equilibrium and γ_i and A_i are the surface energy and surface area of facet I, respectively. The equilibrium crystal shape occurs when the surface energy and area of faces is at a minimum and increasing the surface energy of a crystal face will decrease its morphological importance.

Although this early work was the first of its kind, the limitations of the model were recognised by Gibbs who stated that kinetics was an influencing factor of crystal growth [87]. The model was then improved by the Frank-Chernov

conditions which use crystallographic data and growth rates of crystal faces to predict steady state growth shapes independent of the equilibrium shape [88, 89].

Bravais then proposed a model, Equation 3, showing the inversely proportional relationship between the growth rate of a crystal face (G_{hkl}) and the interplanar d-spacing (d_{hkl}):

$$G_{hkl} \propto \frac{1}{d_{hkl}} \tag{3}$$

The relationship was validated by Friedel and modified by Donnay and Harker (relating to symmetry extinction) and is now known as the Bravais, Friedel, Donnay and Harker (BFDH) model [90-92]. This model is still commonly used to predict crystal shapes due to its simplicity of only requiring crystallographic data.

Although the BFDH model is still commonly used to predict morphologically important crystal faces it does not consider the chemistry of the intermolecular interactions present in molecular crystals (isotropic van der Waals and directional hydrogen bonds) therefore leading to unsuccessful predictions for some molecular crystals [93]. Hartman and Perdock addressed this problem by developing an attachment energy model which takes into account intermolecular interactions [94]. They defined the term attachment energy (E_{att}) which is 'the bond energy released when one building unit is attached to the surface of a crystal' [87]. The lattice energy (E_{latt}), which is the total energy of intermolecular interactions in a crystal lattice, can be calculated and used to determine attachment energy per surface, E_{att}^{hkl} shown by Equation 4:

$$E_{latt} = E_{slice}^{hkl} + E_{att}^{hkl} \tag{4}$$

where E_{slice}^{hkl} is the energy of intermolecular interaction contained within a layer of thickness d_{hkl}.

An assumption of linearity is made between the growth rates of crystal faces (Equation 5), where a surface with a high attachment energy will have a fast growing crystal face therefore will not be morphologically important.

$$G_{hkl} \propto E_{att}^{hkl} \tag{5}$$

Both the BDFH and attachment energy model neglect the external factors that affect solution grown crystals such as solvents, impurities and supersaturation; therefore care must be taken when comparing predicted crystal shapes to 'real' crystals. In this study the intermolecular interaction strength is calculated using atomistic force-fields and both the BDFH and attachment energy morphologies are also calculated.

Differences in the internal packing of molecules (polymorphism) often cause differences in particle shape to arise [95]. Although this is the case the presence of different particle shapes can also arise when the polymorphic form is consistent and is described by the term crystal habit. Differences in crystal habit can exist due to the crystal faces exhibiting different growth rates in solvents with different chemical properties. The crystal habit can also be affected in a less controlled manner during the milling process where new faces are exposed via particle breakage.

At each face of a crystal there are different parts of the API molecule exposed in turn leading to differences in surface energy. Surface energy will be discussed in more detail in the upcoming chapters of this thesis.

This study aims to keep crystal form consistent and seeks to determine the variation in particle surface energy via the change in API shape and the effect of milling. Both computational and experimental methods will be used to determine surface energy and these will be assessed to determine if there is a link to API manufacturability.

3. Chapter Three: Experimental and Computational Materials Characterisation Tools

3.1 Microscopy

Microscopy of pharmaceutical materials is one of the most powerful solid-state materials characterisation techniques. Nichols powerful one line conclusion in the monograph "Polymorphism: In the Pharmaceutical Industry" stated 'look at your samples!' highlighting the significance of this technique when characterising materials [34].

Using only small amounts of material (often milligrams) microscopy magnifies a sample so it can be resolved in fine detail and can provide qualitative physicochemical information regarding particle size, particle shape, crystallography, surface properties, crystallinity and thermal behaviour [34].

The field of microscopy is large and the choice of technique is dependent on the information required. There are three main branches of microscopy: optical, electron and scanning probe. Standard transmission light microscopy allows the observation of particles within a sample and allows qualitative determination of particle size and shape. The sample size required is small and sample preparation is minimal however, the results can be biased due to particle orientation, agglomeration and limited sample size [96]. Scanning electron microscopy (SEM) offers a number of advantages over light microscopy (discussed in more detail below) and was therefore utilised to qualitatively assess the particle size and shape of materials in this research.

3.1.1 Scanning Electron Microscopy

SEM allows the qualitative determination of particle size and shape of powders and offers a number of advantages over conventional light microscopy techniques. SEM can achieve much higher magnifications, has a large depth of field allowing visualisation of surfaces and has increased lateral spatial resolution (around 3 nm compared to 200 nm for a light microscope) [96].

SEM is able to achieve higher resolutions than standard light microscopy as the imaging radiation is decreased. Electrons are produced from an electron gun, the most common being tungsten, which is heated to high temperatures (>2500°C) producing high energy electrons of low wavelengths [97]. Electromagnetic condensers allow the electron beam to be focused on the sample. The beam is then scanned across the sample using scanning coils and loosely bound secondary electrons are emitted from the sample. These electrons are then amplified and converted to an image using a secondary electron detector with an example of an instrument set up shown in Figure 3.1 [98].
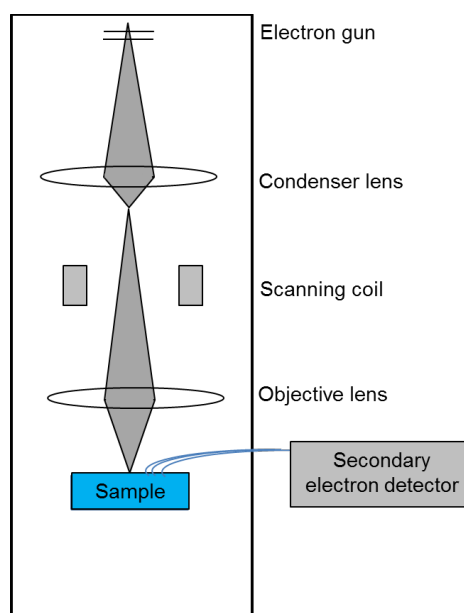
Figure 3.1 – Scanning electron microscopy set-up. Adapted from reference [98].

3.2 Particle Size and Shape Characterisation Techniques

Particle size can be determined qualitatively using microscopy however there are also many techniques available for quantitative determination. The importance of controlling the particle size of APIs is highlighted by guidelines set in ICH Q6a [99] and many processes are moving towards in-line measurements such as focused-beam reflectance measurement (FBRM) to gain tighter control of pharmaceutical processes e.g. API crystallisation [100].

The pharmaceutical industry standard for off-line particle size measurements is laser diffraction due to its reproducibility, fast analysis time and small volumes of material required [30]. Despite this the technique relies on basic assumptions, clearly defined in the review by Jillavenkatesa *et al.* [101], which can introduce error into the measurement. One of the main assumptions is that the particles are spherical in shape meaning that valuable shape data is lost during measurement.

To overcome the drawbacks of laser diffraction other particle sizing techniques will be used in the work reported in this thesis.

3.2.1 Sieving

Powder separation utilising sieving is the oldest and most widely used technique for particle size determination [102]. This technique requires a powder to be passed through a set of sieves with defined decreasing mesh sizes. The particle size can then be reported for each size fraction after being accurately weighed. As well as particle size determination, sieving can also be used as a screen to remove large primary particles or agglomerates present in pharmaceutical powders.

Sieving offers a number of advantages such as the fact that little operator expertise is required and the equipment is simple and inexpensive [103]. The technique also allows a large sample size to be analysed and the different size fractions can be retained for further analysis.

Although analysing a large sample volume can be advantageous this can be a limitation if the quantity of material available is low and, often, loss of material can occur. There are also many other disadvantages to sieving such as the cohesion and adhesion of small particles (<75 µm in diameter) making it unsuitable for the measurement of powders with a small particle size [30]. Calibration of the size aperture is also difficult as well as control of the energy input into manual systems which can cause variation in results due to particle breakage [104]. Automatic shakers and air jet sieves (which offer more control) are available; however, the disadvantages discussed make it more

attractive to use other, more sophisticated, techniques for particle size determination.

Due to the reasons documented sieving will not be used as a particle sizing technique. It will, however, where appropriate, be used as a screening method.

3.2.2 Image Analysis

The use of microscopy for qualitative materials analysis is one of the most powerful materials characterisation tools. But, for quantitative particle size measurements the technique is not recommended due to it being time consuming for an operator to count particles which in turn is subject to operator bias [30]. In addition only a small sample volume can be analysed. Therefore, more sophisticated techniques utilising image based techniques for quantitative particle size analysis have been developed.

Image analysis uses a camera to image particles therefore eliminating the assumptions made during the use of laser diffraction techniques and allowing both size and shape data to be reported. There are two types of imaging techniques used for measurements, static and dynamic, with the instrument set up for both shown in Figure 3.2.

Static Image Analysis **Dynamic Image Analysis**
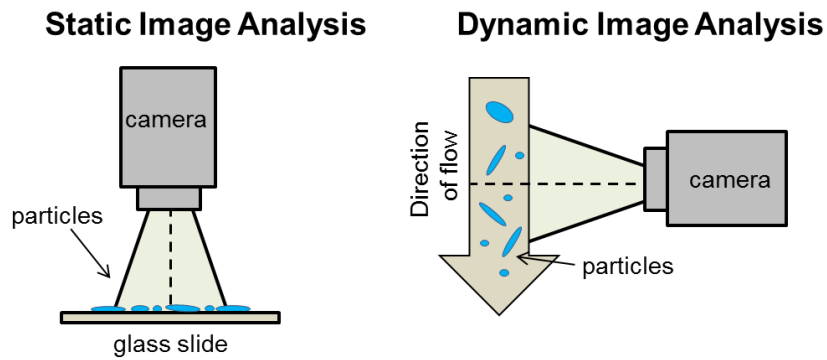
Figure 3.2 – Instrument set up for a static and dynamic image analysis system. Adapted from reference [105].

The difference between techniques is the introduction of particles to the camera. In static image analysis the particles are introduced in a stationary position compared to dynamic image analysis where they flow past the camera. Static image analysis provides detailed size and shape information. This method is not as commonly used as dynamic image analysis due to its disadvantages such as depth of field and long analysis time. Due to the static nature of the measurement, particles with different thicknesses may be captured by the microscope, but they may be out of the depth of field which can introduce error [106]. This problem can be overcome by introducing image stacking measurements; however, this increases analysis time to an already time consuming technique. Static measurements can range from two to six hours depending on the required parameters in comparison to minutes for dynamic systems [106]. Due to the foregoing limitations, static image analysis will not be conducted in this study and instead dynamic image analysis will be utilised.

3.2.2.1 Dynamic Image Analysis

Dynamic image analysis involves the use of a high speed camera to capture images of moving particles as they flow past a light source. This causes a contrast between the particles and the background enabling the size of shape of particles to be analysed simultaneously using a computer. In order to

minimise blurring, due to particle motion, the technique utilises a pulsed light source that can have an exposure time of around 1 ns [107].

The main limitation of dynamic analysis is the lower resolution it offers compared to static image analysis but it has advantages of increased sample size together with decreased analysis time due to the stream of moving particles. Akin to static image analysis, the method provides simultaneous size and shape information.

In the studies reported herein a Sympatec QICPIC system will be used to provide size and shape information of samples. The system contains different evaluation modes in which the particle size of samples can be calculated depending on the information required. The main evaluation modes: Feret-diameter and equivalent projection area of a circle (EQPC) are highlighted in Figure 3.3. EQPC reports the particle size as the diameter of a circle that has the same area as the project area of the particle and the results have been shown to be similar to the results obtained by using laser diffraction techniques [108]. The Feret-diameter of a particle can be described in terms of the maximum and minimum diameter and these measurements are deemed more appropriate when analysing non-spherical shapes [109]. Pharmaceutical powders normally contain a range of particle sizes therefore the data is best represented by particle size distribution curves. In this study the particles will be examined using SEM before choosing an appropriate evaluation mode for the analysis of the results.
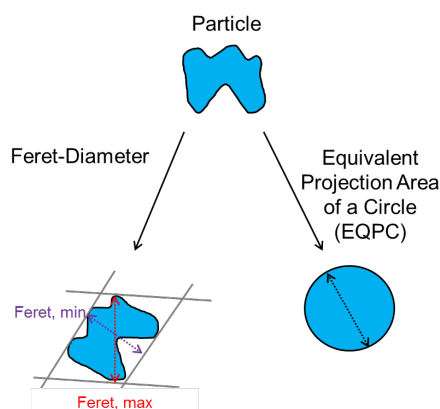
Figure 3.3 – QICPIC dynamic image analysis evaluation modes highlighting feret-diameter and equivalent projection area of a circle.

The Sympatec QICPIC software also allows for the calculation of different shape parameters. Aspect ratio and sphericity are two common parameters which are used to describe the closeness to a perfect sphere and elongation of a particle, respectively. Aspect ratio is calculated using equation 6, and describes how regular the particle is:

$$Aspect\ Ratio = \frac{Feret,min}{Feret,max} \qquad (6)$$

Aspect ratio can be used to describe both regular (aspect ratio close to 1) and elongated shapes (aspect ratio close to 0) [109].

Sphericity is calculated using the equation 7, and relates the perimeter of the predicted equivalent circle (P_{EQPC}) to the real measured perimeter (P_{real}):

$$Sphericity = \frac{P_{EQPC}}{P_{real}} \qquad (7)$$

The research reported in this thesis deals with a range of particle shapes therefore these descriptors will be used where appropriate.

3.3 Solid Form and Analytical Techniques

3.3.1 Differential Scanning Calorimetry

Differential scanning calorimetry (DSC) is a well-established characterisation technique used to measure the physical and chemical properties of pharmaceutical materials. Its popularity over other thermal techniques, such as common capillary melt, is due to its accuracy in measuring the parameters associated with thermal transitions [110]. In crystalline materials, polymorphism and crystallinity can be inferred by examining the enthalpies and endotherm profiles where different polymorphs will exhibit different enthalpies and purely crystalline materials are expected to have a sharp melting endotherm [111].

In DSC, the flow of energy into (endotherms) and/or out of (exotherms) materials is measured as a function of temperature, at a programmed scan rate, allowing transitions in materials to be identified. There are two main types of DSC used in the pharmaceutical industry: double furnace (power-

compensation DSC) and single furnace (heat flux DSC). Both designs use a small pan to encapsulate the material prior to heating or cooling. The double furnace design contains two identical furnaces, where one furnace is used to heat the sample in the pan and the other used to heat a reference pan. The furnaces are heated as specified by the user and the energy used for each furnace is compared and the difference plotted as a function of temperature or time. The single furnace design contains one furnace, such that both the reference and sample pans are placed inside (Figure 3.4). Each pan contains a temperature sensor and when the furnace is heated as specified by the user; a difference in the temperature between these pans arises when a transition in the sample occurs. The difference in temperature is converted to a heat flow equivalent which is plotted as a function of temperature or time [112].
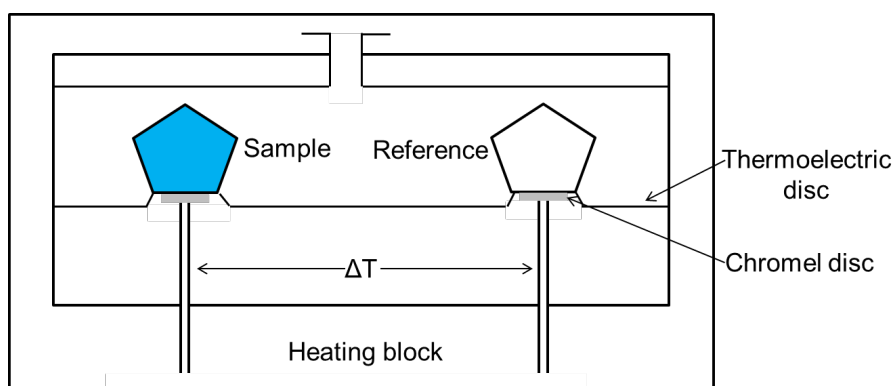
Figure 3.4 – Single furnace (heat flux) differential scanning calorimetry set-up. Adapted from reference [111].

In this study a heat flux "Discovery DSC" will be used to detect changes in crystal form and crystallinity.

3.3.2 Evolved Gas Analysis

Evolved gas analysis (EGA) combines two techniques that allow the weight loss of a sample to be monitored as well as identify what material is being evolved. Firstly a thermogravimetric analyser (TGA), depicted in Figure 3.5,

measures the weight change of a sample as a function of temperature and then a second instrument (usually a Fourier-transform infrared spectrometer or mass spectrometer) identifies the volatile products emitted from the sample.
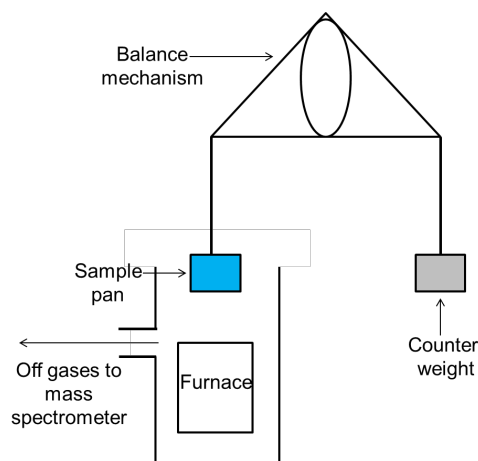
Figure 3.5 – Thermogravimetric analyser set-up. Adapted from reference [113].

The weight changes measured by the balance can often be attributed to solvate or hydrate loss and can be used to help explain energy changes detected in DSC data [112]. In this study a TGA coupled to a mass spectrometer will be used to identify and quantify any weight loss of water or solvents from recrystallisation studies.

Due to the gravimetric nature of the technique the limit of detection of EGA is dependent on sample mass. In order to quantify low levels, parts per million (PPM), of residual solvents a more sensitive analytical technique will be utilised.

3.3.3 Headspace-Gas Chromatography

Headspace-gas chromatography (HS-GC) is an analytical technique used to separate and quantify analytes of interest.   Compared to other chromatographic techniques, such as high performance liquid

chromatography and nuclear magnetic resonance, HS-GC enables highly sensitive measurements of volatile analytes.

The sampling in HS-GC is achieved by dissolving the material in a suitable solvent and shaking and heating until a liquid vapour equilibrium is established.   The head space is then sampled which allows for the quantification of volatile products. The gaseous sample is transferred onto a column where retention (interaction time) and selectivity (resolution) of the analytes is determined by its interaction with the stationary and mobile phase. The separated components are then passed through a flame ionisation, detector where the concentration of analytes is directly proportional to the response.

3.4   X-Ray Diffraction

X-ray diffraction is an important solid-state characterisation tool as it provides information on the three-dimensional structural arrangement of molecules. There are two main types of X-ray diffraction: single crystal X-ray diffraction (SCXRD) and powder X-ray diffraction (PXRD). SCXRD is the 'gold standard' of solid-state analysis and allows the full crystal structure to be determined including unit cell dimensions, relative position of atoms and molecular symmetry [72].   In order to perform SCXRD, high resolution equipment is required as well as a high level of expertise to collect/analyse the data.   In addition crystals of suitable dimensions/diffraction quality are required; obtaining such crystals can-sometimes-be very time consuming. Due to these reasons, SCXRD will not be performed in this study however single crystal structures will be accessed from the Cambridge Structural Database (discussed in Section 3.6.1).

Every crystalline material exhibits a unique PXRD pattern. The technique can be used to identify changes in polymorphic form as well as crystallinity; the latter can be inferred by the sharpness of the peaks in the difractogram [34]. For a powder diffraction pattern to be obtained X-rays, of known frequency, are produced by a diffractometer via the rapid deceleration of high energy electrons and the emission of radiation when an electron decays.   The

incident X-rays are then accelerated towards the powder sample where the electrons of the atoms arranged in a periodic array scatter coherently. Diffraction only occurs if Bragg's law, shown in Figure 3.6, is satisfied.

Incident X-rays of
known wavelength λ

Diffracted X-rays

θ_{hkl}

interplanar
d-spacing
d_{hkl}

Bragg's Law
$n\lambda = 2d_{hkl}sin\theta_{hkl}$
n is an integer (n ≠ 0)
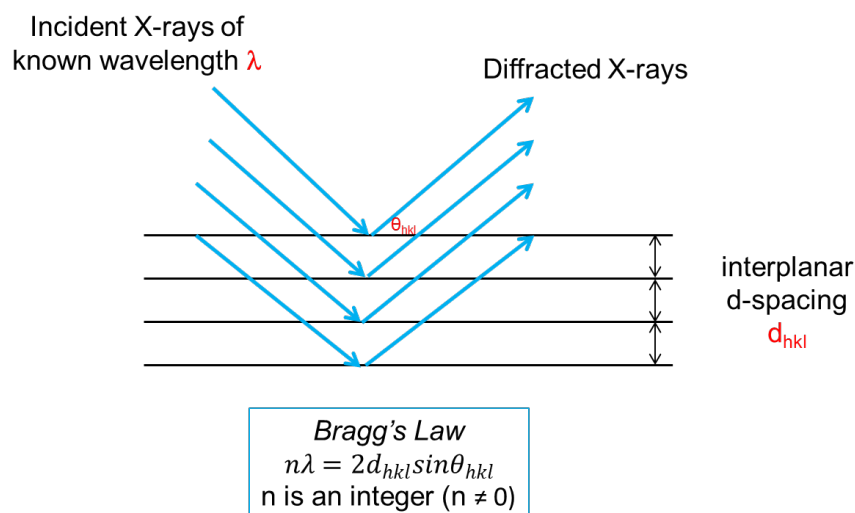
Figure 3.6 – Incident X-ray of known wavelength (λ) is pushed towards lattice planes of a crystal (d_{hkl}) at incident angle θ_{hkl}. Diffraction only occurs if Bragg's law is satisfied: $n\lambda = 2d_{hkl}sin\theta_{hkl}$ where n is an integer (n ≠ 0). Adapted from reference [72].

The interaction between the X-rays and crystallographic planes is converted to a unique fingerprint pattern that can be used to distinguish between materials with different arrangement of molecules. In pharmaceutical powders it is common to identify intensity differences in peaks which are due to preferred orientation effects. When the powder sample is prepared on a plate this can occur when different shaped particles orientate themselves in a preferred position e.g. plates stacking up. Sample preparation including grinding and spray drying as well as capillary tubes can be used to overcome this effect.

In this study PXRD will be utilised, where appropriate, to ensure that all crystal forms are the same and samples will be prepared using flat plates.

3.5 <u>Surface Analysis</u>

Characterising the surface properties of powders is becoming increasingly important in the pharmaceutical industry due to the ever growing understating of their importance. In the manufacture of tablets, each operation will involve a particle interaction with another substrate which can be influenced by both the surface area and surface energetics of particles. Literature studies have described how characterisation of the physical and chemical properties of powders has revealed them to be similar; however, changes in surface properties have led to different manufacturing behaviour [23, 114, 115]. This section reviews the techniques used to characterise surface properties of powders in the pharmaceutical industry.

3.5.1 Surface Area

Differences in surface area can cause the particles to interact differently, ultimately affecting their behaviour. Generally as particle size decreases, surface area increases. Surface area can be measured using gas adsorption, mercury porosimetry or gas permeametry techniques with the former being the most common. Gas adsorption involves using an inert probe molecule, commonly nitrogen or krypton, of known size to calculate the amount of available surface. Nitrogen isotherms are measured and the Brunauer, Emmett and Teller (BET) equation is commonly used to determine surface area:

$$\frac{P}{V(P_0-P)} = \frac{1}{V_m C} + \frac{(c-1)P}{V_m C P_0} \tag{8}$$

Where P is the partial pressure of the adsorbate, P_0 is the saturation pressure of adsorbate at experimental temperature, V is the volume of gas adsorbed at pressure P, V_m is the volume of gas adsorbed as a monolayer and C is a constant relating the heat of adsorption and condensation of the adsorbate.

Different concentrations of adsorbate can be used and then $P/V(P_0-P)$ plotted against P/P_0. V_m is calculated from the reciprocal of the sum of the slope (the low end of the isotherm) and intercept and the total surface area (S_t) is given by Equation 9:

44

$$S_t = \frac{V_m N_0 A_{cs}}{M_W} \tag{9}$$

Where N_0 is Avogrado's number, A_{cs} is the cross-sectional area of the adsorbent molecule and M_W is the molecular weight of the adsorbent. The specific surface area is calculated by dividing the total surface area by the mass of the powder measured.

The pore volume of particles can also be calculated using the nitrogen isotherm. It is assumed that at relative pressures higher than where the nitrogen monolayer has formed, capillary condensation of the nitrogen will occur. At high pressures the particle pores will contain condensed liquid nitrogen. The total pore volume is calculated by assuming the density of liquid nitrogen is the same in the bulk as it is in the pores [116].

In this study the surface area, pore area and volume will be calculated using the gas adsorption method for ibuprofen particles exhibiting different particle shapes.

3.5.1.1 True Density

The skeletal density which is also referred to as the true density represents the density of the solid portion of the material and is an important parameter in the use of compaction equations. True density is measured by pycnometry which involves a displacement gas e.g. helium being purged into a specific volume containing a known mass of material. The gas penetrates between the voids in the samples (measuring the molecular volume) and therefore the true density can be calculated using Equation 10:

$$True\ density = \frac{mass}{molecular\ volume} \tag{10}$$

In this study the true density will be calculated for use with the Heckel equation.

3.5.2 Surface Energy

The surface energy of powders can be measured at a single particle or bulk scale level. Atomic force microscopy can be used to measure the surface energy of individual crystal faces as well as contact angle measurements; however, the results from this technique do not represent the bulk powder [117]. Techniques used to measure the bulk surface energy of powders include inverse gas chromatography (IGC), centrifugal detachment and contact angle with the former being the most common. Contact angle measurements require a flat surface of powder in order for a liquid to interact; therefore, the particle properties of the bulk powder may be changed due to the compaction event [118]. Centrifugal detachment involves deriving surface energy by measuring the detachment of particles from a stub which may not provide the scientific accuracy required from these measurements [119]. IGC gains its popularity due to the characterisation of the bulk powder, minimal surface modifications being made and analytical accuracy which has shown to discriminate between different batches of the same material [120].

3.5.2.1 Inverse Gas Chromatography

IGC utilises the basis of classical gas chromatography (GC) however the stationary and mobile phase are different. In GC the analytes of interest are passed through in the mobile phase and their interaction with the stationary phase is used for characterisation. In IGC the stationary phase is the pharmaceutical powder and different mobile phases are passed through the column and the surface energy determined by analysing their interaction with the stationary phase. A typical set-up is shown in Figure 3.7 where an inert carrier gas is used to inject probes (typically liquids which are vaporised) across the powder sample contained within a glass column. The probes used differ in terms of their chemistry e.g. acidity, basicity and molecular area. Common detectors can be used in conjunction with an IGC e.g. thermal conductivity detector or flame ionisation detector (FID) with the latter being used in this study due to its high sensitivity to most hydrocarbons.
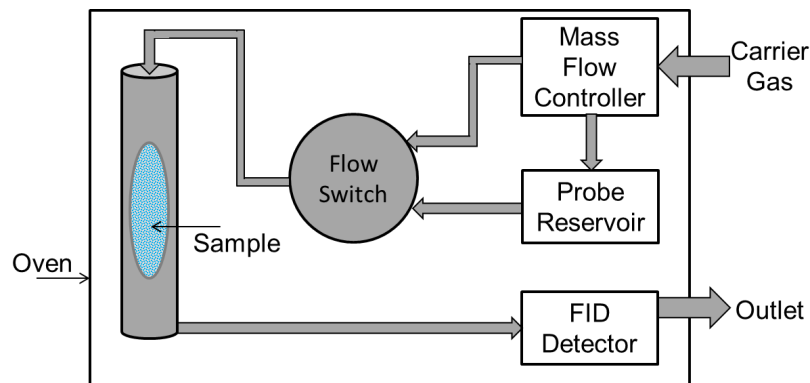
Figure 3.7 – Inverse gas chromatography set-up. Adapted from reference [121].

Surface energy data can be collected using two different chromatographic conditions relating to the concentration of probe used. The most common experiments are conducted at infinite dilution where only small concentrations of probes are used.   It is assumed that the interactions between the adsorbate and the surface occur only at high energy sites making this the most common method used to report surface energy. Higher concentrations of probes can be used (finite concentration) as a complimentary analysis to infinite dilution and provide a measure of surface energy heterogeneity [121].

This study will use IGC to measure the surface energy heterogeneity of APIs with different particle shapes.   Further information on the IGC methodologies used will be described in chapter seven.

3.6   Compaction Simulation

Tablet presses used in the manufacture of pharmaceutical tablets are generally large pieces of equipment that provide streamlined and automated control of the production line and can generate up to one million tablets per hour [122].   Compaction simulators are material sparing tools that mimic production presses enabling scientists to characterise, scale-up and troubleshoot the tablet production process [123].

Tablet production presses come in two forms: single station or rotary press. Many processes use the rotary design which contain several punch stations to maximize the tablet output. Conventional compaction simulators are single station presses which can be fitted with same type, size and shape of tooling as a production press. Some can also replicate the movement of the punches, as in a production press, while capturing significant amounts of accurate data such as force displacement, compaction speed, die-wall pressure and ejection force. This data can be used to aid formulation development as well as provide insights into the manufacturing performance of commercial products [124].

Compaction simulators use less material than production presses; however, depending on the type of investigation required they still require a large volume of material (typically between 50 – 100 g). They are also expensive and require extensive user training and user expertise which has led to the development of miniaturised 'compaction simulators'.

3.6.1 Gamlen Tablet Press

The Gamlen tablet press (GTP), shown in Figure 3.8, was the first computer controlled bench top tablet press which can precisely control and monitor the production of tablets at a small scale [125]. The press contains a single station punch which uses a uni-axial saw tooth displacement profile (Gamlen Tableting, UK).
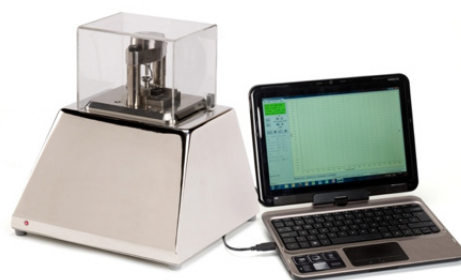
Figure 3.8 – Gamlen tablet press.

The press contains a novel die design, illustrated in Figure 3.9. The main difference between this and a conventional punch and die is the stationery base die which is moved horizontally after compression to allow for ejection of the tablet.
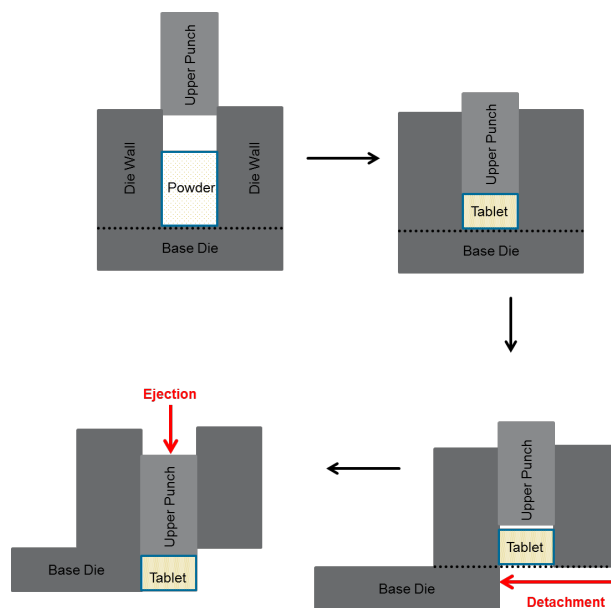
Figure 3.9 – Illustration of the Gamlen tablet press die design and operation.

It is the detachment force, which is converted to detachment stress (DS), shown by Equation 11, which is used as a novel small scale tool to predict punch sticking in this study.

$$DS = \frac{DF * G}{\pi r^2} \qquad (11)$$

Where DF is detachment force, r is the radius of the tablet and G is the gravitational constant.

As with any new technique in the scientific community, its suitability for use has been tested and published in the literature. Pitt *et al.* compared the tabletability of two different formulations, direct compression and wet granulation, showing a substantial comparability in the tensile strength and ejection stress of tablets produced from the GTP and a rotary process press [126].

The GTP will be used in this study to measure the deformation, tabletability and sticking propensity of materials possessing different physicochemical properties.

3.7   Computational Tools

In 1994, Gavizotti entitled a publication: 'Are Crystal Structures Predictable', and in the first line of the article answered 'no' [127].   This publication summarised the potential use for computational tools in the organic solid-state chemistry field however acknowledged these tools were still developing. More than twenty years later this field is still developing but substantial progress has been made in employing predictive computational tools to aid almost every stage of the pharmaceutical discovery / design and manufacturing process [1, 128, 129].

Pharmaceutical industries are aiming to deliver medicines to patients more effectively and in doing so are involved with emerging computational tools to aid this journey [1].   Computational tools cover a broad spectrum from modelling the API molecule using quantum or molecular mechanics to solid particles using discrete and finite element methods.   This diversity enables various stages of the drug discovery and development process to be modelled such as crystallisation, polymorph screening and unit operations e.g. compaction.

This study focuses on the physicochemical properties of APIs therefore modelling will be used to explore the crystal chemistry and morphology / surface properties using the techniques described below.

3.7.1   Cambridge Structural Database

The crystal structure of an API can be solved using X-ray diffraction as detailed in Section 3.3.4. However, in this study the relevant structures will be retrieved from the CSD. The CSD was established in 1965 by the Cambridge Crystallographic Data Centre (CCDC) and is a non-profit organisation and registered charity which mainly gains support from software subscriptions.

The database contains entries for over 900 000 organic and organometallic small molecule structures which are evaluated before entry [130].

When retrieving crystal structures it is important to determine the most suitable for the study to be undertaken, as chemical structures can contain more than one entry. The different entries arise from using different experimental conditions i.e., temperature, studies by different scientists and improved refinement of structures [131].

The CCDC have developed a number of software packages which enable users to search and analyse the data, a number of which are discussed below.

3.7.1.1 Conquest

Each individual crystal structure forms an entry in the CSD which can be searched on using many criteria: formula, structure, reference code (unique six letter identification code referred to in this thesis as REFCODE) etc., using ConQuest [132]. ConQuest retrieves the standard text file format containing the crystallographic information of interest, known as a CIF (crystallographic information file) for use in other software packages.

3.7.1.2 Mercury and Materials Studio

Mercury and Materials Studio are the two main software packages used to import CIF files and provide advanced functionality for viewing crystal structures [132]. Mercury provides the ability to measure distances and angles within crystal structures as well as calculating the BFDH morphology. Materials studio contains more sophisticated tools where as well as the BFDH morphology the attachment energy morphology can be viewed.

3.7.1.3 Habit 98

The Habit98 programme, developed by Roberts *et al.* [133, 134], enables the prediction of the lattice energy of a crystal along with the strength and directivity of the intermolecular interactions present. The lattice energy can also be broken down in terms of slice and attachment energy per crystal face allowing surface energies to be predicted.

In the work reported herein, a combination of the software packages described will be utilised to explore the crystal chemistry of the APIs being evaluated.

4. Chapter Four: The Crystal Chemistry of Ibuprofen

4.1 Introduction

Ibuprofen is a non-steroidal anti-inflammatory API that is used for treating medical conditions such as pain and inflammation [135]. The API is usually formulated into a tablet or capsule for administration to patients. During the manufacture of ibuprofen tablets the drug product has been shown to undergo punch sticking [55]. It is for this reason together with it being a molecular crystal that it is of interest for this study.

A recent publication by Nguyen *et al.,* documented the computational analysis of ibuprofen in relation to its molecular and syntonic structure; however, this publication focused on the growth behaviour of the crystal as a function of the crystallisation conditions [136]. To the best of the authors' knowledge, no study has explored the relationship between the crystal chemistry of ibuprofen and its manufacturability. Computational tools are therefore utilised to explore the crystal chemistry of ibuprofen and, in subsequent chapters, are used to provide an insight into the relationship between the crystal chemistry and resultant physicochemical and mechanical properties. In order to achieve this, the Cambridge Structural Database base will be explored for ibuprofen structures. The structure will then be optimised using an appropriate force field (an introduction to force fields is given below). The strength of the intermolecular interactions will then be calculated and used to help understand the surface properties of the dominant crystal faces of iburpofen.

4.1.1 Force Field Fitting

Force fields are used in molecular modelling to optimise a structure by calculating the potential energy of a system. Force fields are used to compute the total lattice energy of a system (E_{latt}) by considering the energies of the bonded (intramolecular) and non-bonded (intermolecular) interactions, shown by Equation 12.

$$E_{latt} = E_{bonded} + E_{non-bonded} \qquad (12)$$

The bonded interactions are modelled by harmonic energy functions accounting for bond stretching, bond angle bending and torsional distortions. The different types of intermolecular interactions present in molecular crystals of an API are modelled in different ways. Van der Waals interactions are usually computed using a 12-6 Lennard-Jones potential (V_{LJ}), Equation 13, which balances the repulsive and attractive forces between two atoms:

$$V_{LJ} = 4\varepsilon \left[\frac{\sigma}{r}\right]^{12} - \left[\frac{\sigma}{r}\right]^{6} \tag{13}$$

Where ε is the depth of the well, r is the distance between the particles and σ is the collision diameter. Modifications of the conventional 12-6 Lennard-Jones potential have been made to represent these types of interactions in molecular crystals such as a 9-6 potential which reduces the repulsive part of the interaction [137]. The electrostatic charges are modelled by assigning partial charges to the atoms and then using Coulombs law to calculate their energetic contribution. Some force fields also contain an explicit hydrogen bonding term but this is not always the case and is force field dependent [138].

The importance of selecting a suitable force field has been stresses by Datta and Grant where they stated that different force fields may only change the total lattice energy by less than 5%; however, the difference can lead to inaccurate predictions [139]. The suitability of a force field can be determined by comparing the calculated lattice energy to experimental sublimation enthalpies as the relationship, Equation 14, shows:

$$E_{latt} = \Delta H_{sub} - 2RT \tag{14}$$

Where R is the gas constant and T is temperature (in Kelvin).

In this study, calculated lattice energy values will be compared to experimental data for validation of the force field used.

4.2 Materials and Methods

4.2.1 Materials

The molecular structure of ibuprofen consists of a phenyl ring with a propanoic acid group and isobutyl in the *para* position (Figure 4.1). The structure also contains a chiral centre denoted by the star sign in Figure 4.1.
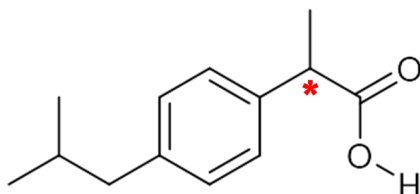
Figure 4.1 – The molecular structure of ibuprofen. Functionality consists of one hydrogen bond donor (carboxylic acid hydrogen) and one hydrogen bond acceptor (carboxylic acid oxygen).

The two enantiomers are shown in Figure 4.2 where (S)(+) ibuprofen is the bioactive isomer and (R)(-) ibuprofen is inactive [140]. The commercially available racemic mixture of ibuprofen will be the focus of this study.

(S)(+) ibuprofen   (R)(-) ibuprofen
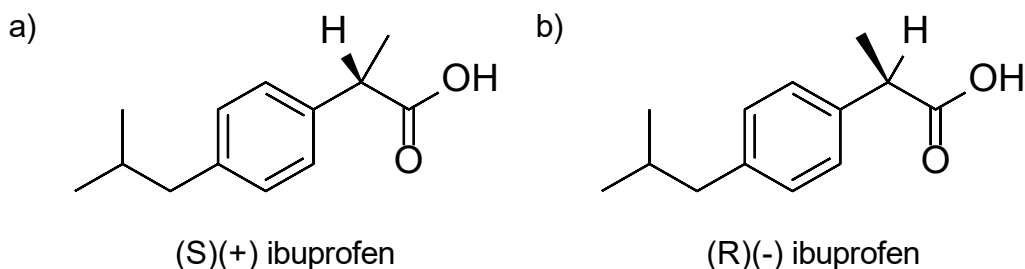
Figure 4.2 – Ibuprofen enantiomers where a) is a schematic representation of (S)(+) ibuprofen and b) a schematic representation of (R)(-) ibuprofen.

Racemic (RS)-ibuprofen has two known polymorphic forms (form I and form II). Form I was reported in the literature in 1974 [141] whereas form II was only reported, more recently, in 2010 [142] due to its metastable nature. Both forms crystallise in a monoclinic structure in the $P2_1/c$ space group. Form II

has a larger cell volume by 5% and different orientation of the carboxylic acid group compared to form I, thereby altering the orientation of the hydrogen bonded dimers. Unit cell diagrams of form I and form II are shown in Figure 4.3a and Figure 4.3b respectively. There structural differences have been used to explain the metastable nature of form II [142] and this study will focus on describing the crystal chemistry of racemic (RS) form I ibuprofen.
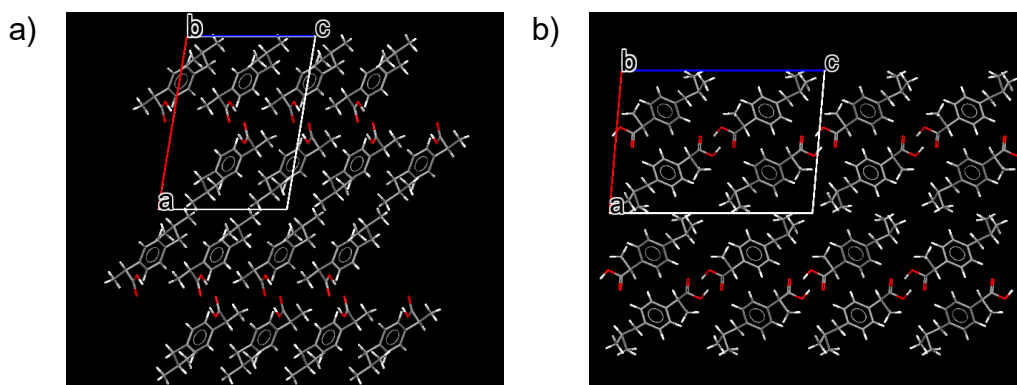
Figure 4.3 – Unit cell of a) RS-ibuprofen form I [REFCODE: IBPRAC] b) RS-ibuprofen form II [REFCODE: IBPRAC04].

4.2.2 Methods

4.2.2.1 Analysis of the Cambridge Structural Database

The Cambridge Structural Database (CSD) was interrogated for ibuprofen structures using ConQuest (CCDC 1.18, 2016). The criteria for this search were: R-factor of less than 0.075 and the absence of metal ions. The selection of ibuprofen structure was based on R-factor (agreement between predicted and observed structure) compared to other structures. The crystal structure selected for ibuprofen was IBPRAC.

The carboxylic acid hydrogen bonding distance for this hit was measured and compared to all other hits with this functionality included in the CSD. The query for this search is shown in Figure 4.4 and the same criteria as above were used.
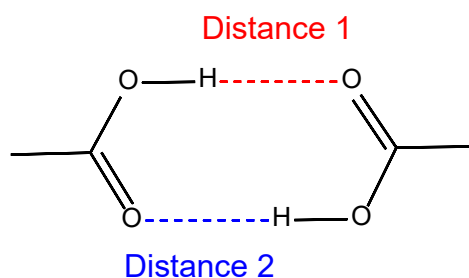
Figure 4.4 – Query for the search of the CSD for carboxylic acid hydrogen bonded dimers measuring the hydrogen bond distance.

4.2.2.2 Structure File Preparation

The crystal structure for IBPRAC was exported from Mercury (CCDC 3.9, 2016) as a .cif file. The .cif file was imported into Materials Studio (v7.0, 2013) and the crystal structure was built to apply the symmetry. The structure was then exported as a .car file (Cartesian coordinates) and converted to fractional coordinates, .cssr, for use in Habit98 [133, 134].

4.2.2.3 Force Field Fitting

The .cif for IBPRAC, was imported into Materials Studio and the fractional charges were assigned using COMPASS II [143], as this was the most suitable force field present in the software used.

The lattice energy of ibuprofen was calculated using two common force fields: UNI and Tripos 5.2, in order to determine the suitability of each. The UNI force field includes an explicit six exponential term to describe hydrogen bonding [127, 144], whereas Tripos 5.2 does not include an explicit term to describe hydrogen bonding but includes a scaling factor in the Lennard-Jones potential.

The computed lattice energy for each force field was compared to experimental sublimation enthalpies. To further validate the force field, the strength of the most dominant intermolecular interaction was compared to validation work published by Dunitz and Gavezzotti [145]. All further calculations were performed using the Tripos 5.2 force field.

57

4.2.2.4 <u>Lattice Energy and Intermolecular Interactions</u>

HABIT98 [133, 134] was used to calculate the strength of the non-bonded intermolecular interactions (intrinsic synthons) and lattice energy. The software was run in DEBUG-1 Latt mode to achieve the pairwise interaction strengths. The atomic energy contribution to the lattice energy was computed by running HABIT98 in DEBUG-2 Latt mode.

4.2.2.5 <u>Morphology Prediction</u>

The Bravais, Friedel, Donnay and Harker (BFDH) [90 - 92] method was used to predict the most likely growth surfaces of crystals based on the rule which states the crystal faces with the largest interplanar spacing (d_{hkl}) are likely to be the most morphologically important at the surface of the particle [76, 146].

4.2.2.6 <u>Attachment Energy Calculations</u>

HABIT98 was run in FULL mode to break down the slice and attachment energy per morphologically important crystal face.

4.3   Results and Discussion

4.3.1   Analysis of Cambridge Structural Database

The search for the molecular structure of ibuprofen in the CSD returned twenty-five hits of which seven were *(RS)*-ibuprofen, form I. The unit cell dimensions for these together with the R-factors are displayed in Table 4.1. It can be seen that there are subtle differences between the unit cell dimensions which can be caused by different refinements of structures and also the temperature at which the data was collected. For example, IBPRAC has a β value of 99.362° and was collected at 283 K whereas IBPRAC01 has a β value of 99.700° and was collected at 100 K. IBPRAC contains the lowest R-factor therefore this structure was chosen for further analysis.

Table 4.1 – Unit cell dimensions and R-factor for seven solved structures of ibuprofen in the CSD.

REFCODE	R-factor	a (Å)	b (Å)	c (Å)	β (°)
IBPRAC	3.9	14.667	7.886	10.730	99.362
IBPRAC01	5.3	14.397	7.818	10.506	99.700
IBPRAC06	5.4	14.674	7.895	10.735	99.541
IBPRAC16	4.2	14.485	7.832	10.491	99.743
IBPRAC17	4.5	14.514	7.843	10.530	99.609
IBPRAC18	4.6	14.561	7.857	10.587	99.563
IBPRAC19	4.8	14.605	7.872	10.651	99.525

The molecular structure of ibuprofen was divided into four molecular components as shown in Figure 4.5.
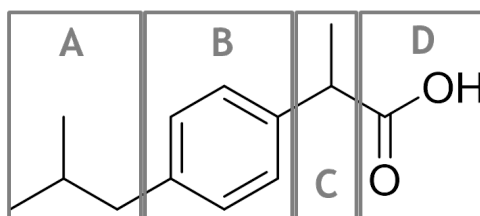
Figure 4.5 – Ibuprofen structure divided into molecular components A) isobutyl B) phenyl C) methyl attached to a carbon backbone and D) carboxylic acid.

The unit cell, for the crystal structure of IBPRAC, is comprised of four molecules arranged in centro-symmetric hydrogen bonded dimers with dimensions a = 14.667 Å, b = 7.886 Å, c = 10.730 Å and β = 99.362° (Figure 4.6).
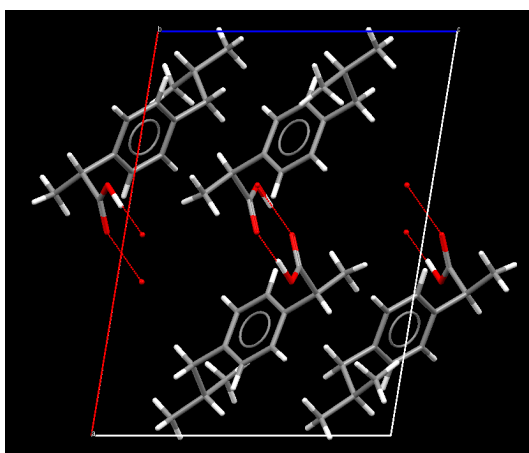
Figure 4.6 – Ibuprofen unit cell displaying hydrogen bonded carboxylic acid dimers.

4.3.1.1 Carboxylic Acid Hydrogen Bond Distance

The hydrogen bonding distance of IBPRAC's centro-symmetric dimer was measured and found to be 1.624 Å. The CSD was interrogated for other structures containing this functionality and 1601 hits were returned. Of these hits 78% were centro-symmetric, highlighted by the dominance of the linear relationship between distance 1 and distance 2, shown in Figure 4.7.
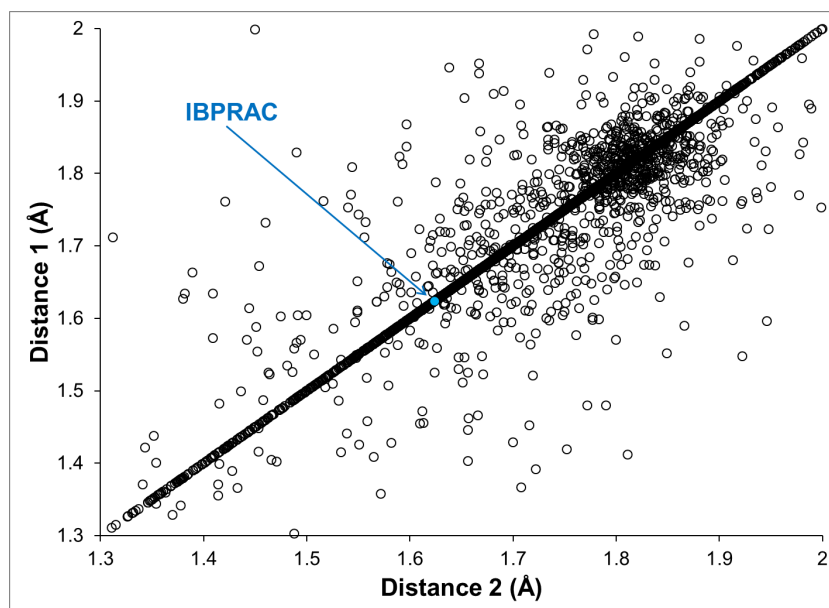
Figure 4.7 – Hydrogen bond distance (distance 1 and 2) plotted against each other for the 1601 carboxylic acid dimers found in the CSD.

The frequency of hits was plotted against the O-H bond distance and, in comparison, ibuprofen falls below the average of 1.743 Å (Figure 4.8).
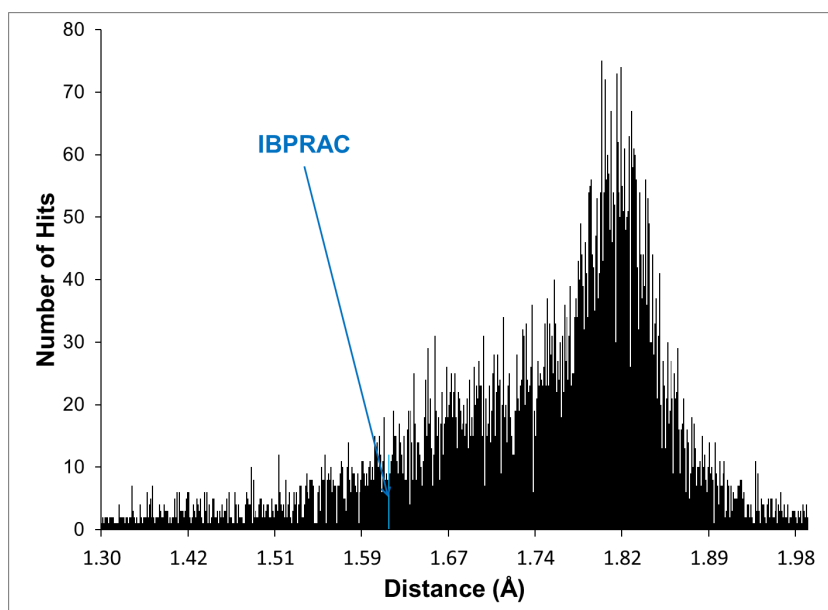
Figure 4.8 – Number of hits plotted against hydrogen bond distances for structures within the CSD containing carboxylic acid dimers.

The differences in extremes can be explained in terms of the electronegativity of substituent atoms. Diphenic acid, which is at the high end of the spectrum, contains a centro-symmetric carboxylic acid hydrogen bonded dimer of 1.951 Å. The hydrogen bonded structure is shown in Figure 4.9a where it can be seen that the benzene ring where the acid is attached also contains an amine group which is involved in the hydrogen bonded network. The amine group pulls electronegativity away from the acid group to form its own hydrogen bond thereby increasing the length of the carboxylic acid bond hydrogen bond. On the other end of the spectrum is anthranilic acid with a centro-symmetric carboxylic acid hydrogen bonded dimer of 1.346 Å (Figure 4.9b). This molecule contains no other atoms which are available to hydrogen bond and the lone pair of electrons on the two ether groups attached to the phenyl will increase the electronegativity of the carboxylic acid via delocalisation, thereby decreasing its bond length.

a)   b)
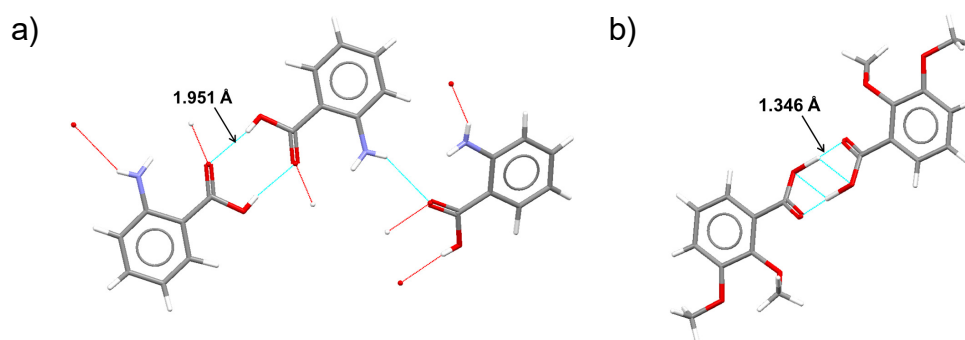
Figure 4.9 – Molecules containing different carboxylic acid hydrogen bonds of different lengths a) diphenic acid [REFCODE: AMBACO03], b) anthranilic acid [REFCODE: OJENIA].

Ibuprofen contains no other hydrogen bonding donors/acceptors and is a relatively planar molecular which will contribute to a short hydrogen bonding distance.

4.3.2   Force Field Fitting

The calculation of lattice energy using two different force fields gives rise to very similar results where E_{latt} displays values of -120.8 kJ/mol and -125.2 kJ/mol for UNI and Tripos 5.2, respectively. The small difference of 4.4 kJ/mol between the force fields leads to both calculated lattice energy values having comparable values to literature enthalpies of sublimation: 125.9 kJ/mol [147] and 115.9 kJ/mol [148].

For this reason a further comparison step was made whereby the strength of the most dominant interaction (hydrogen bonded carboxylic acid) was compared to literature values. The UNI force field calculated the strength of this interaction to be -22.9 kJ/mol compared to the one and half times higher value of -33.7 kJ/mol using Tripos 5.2. Dunitz and Gavezzotti's analysis of these types of interactions revealed the strength to be around -35 kJ/mol [145]. All further calculations were performed using the Tripos 5.2 force field as it shows excellent agreement to the literature values.

4.3.3   Lattice Energy and Intermolecular Interactions

The intermolecular interactions (intrinsic synthons) were examined for their contribution to the lattice energy; the contributions for the first twelve are shown in Figure 4.10. This plot highlights the fact that by only considering twelve interactions, 90% of the lattice energy is accounted for. It is clear that as the interaction number increases the contribution to the lattice energy decreases, meaning the interaction is of less importance in the stabilisation of the crystal lattice.
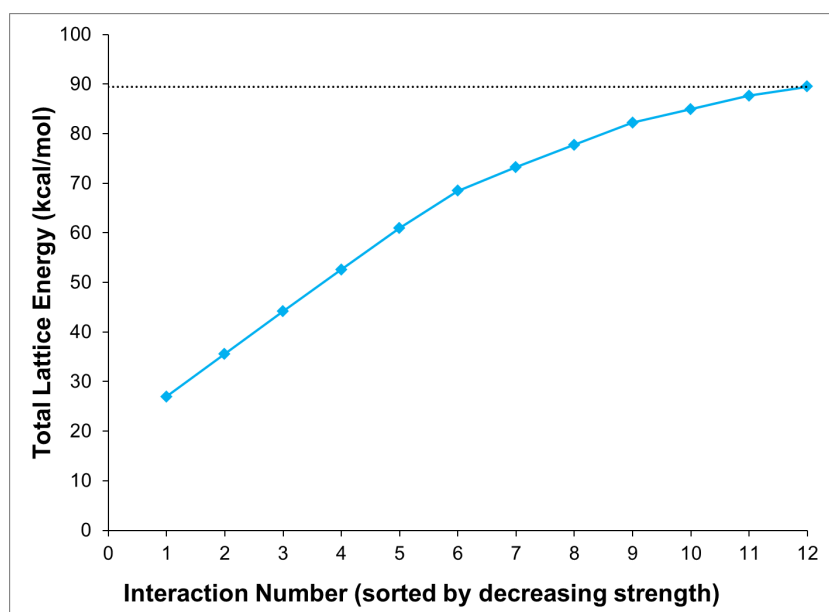
Figure 4.10 – Energetic contribution to the total lattice energy of ibuprofen from the first twelve intermolecular interactions (interaction number is sorted by decreasing strength).

The different intrinsic synthon types were investigated further and the six key interaction types (>4 kJ/mol) are shown in Figure 4.11.   A total of nine interactions, compromising of six types make up 82% of the lattice energy, with the largest contribution arising from the hydrogen bonded carboxylic acid dimer with a value of -33.7 kJ/mol.   The high strength of this interaction is highlighted by comparing its contributions to the lattice energy with the next strongest π-π stacking interaction which contributes 9% compared to 27%, a three-fold difference.   The five other interaction types are Van der Waals

interactions and despite being crucial for the formation of the crystal are all relatively weak in comparison to the carboxylic acid dimer.
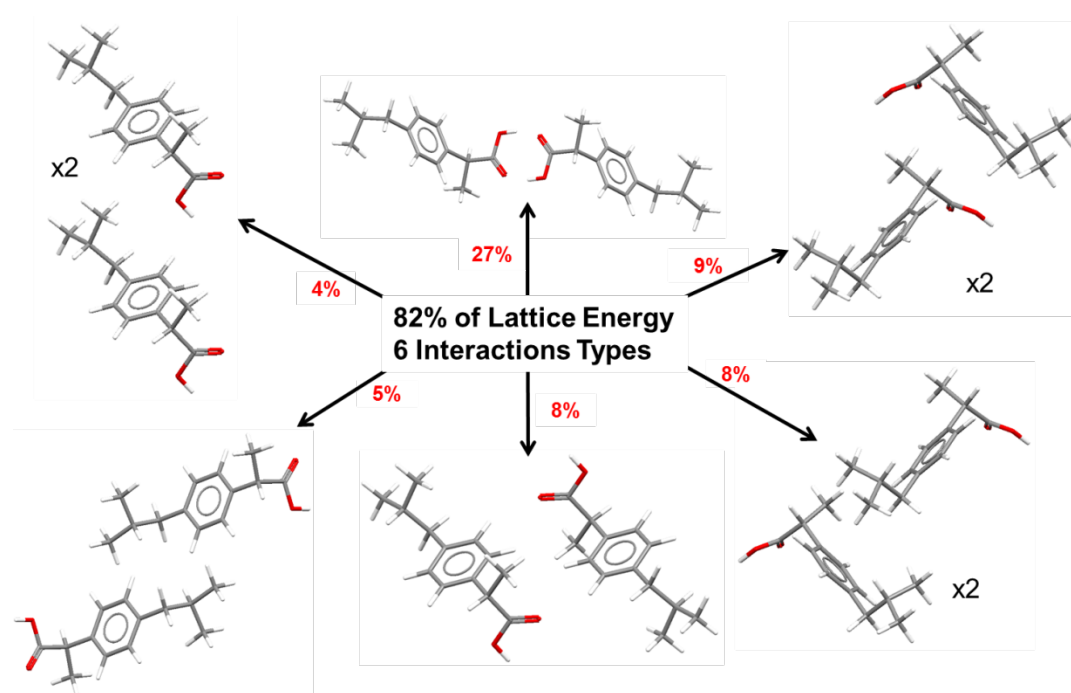
Figure 4.11 – Ibuprofen key intermolecular interaction types and their contribution to the total lattice energy.

The lattice energy was collapsed onto the individual atoms and summed across each molecular component, shown in Figure 4.12. If the percentage of atoms in each component is considered together with the percentage contribution to the lattice energy then it is clear that the lattice energy is not evenly distributed across the molecule. Despite containing the lowest number of atoms (12.1%), molecular component D makes the greatest contribution to the lattice energy (37.5%), which is attributed to the strong hydrogen bonded intermolecular interaction. All other molecular components, therefore, have a lower energy contribution compared to the number of atoms they contain. The molecular components can be ranked in terms of their increasing contribution to the lattice energy: D>A>B>C.
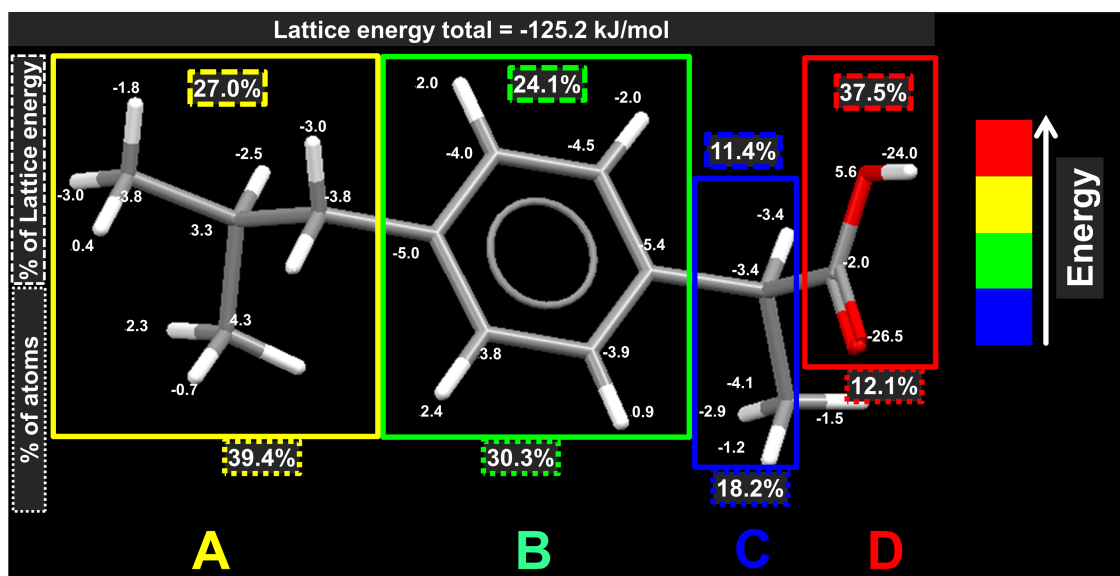
Figure 4.12 – Ibuprofen lattice energy collapsed onto atoms, summed over molecular components and ranked in terms of energy.

4.3.4 Morphological Simulations

The Bravais, Friedel, Donnay and Harker (BFDH) morphology of ibuprofen is shown in Figure 4.13a and reveals six predicted morphologically important crystal faces. The attachment energy morphology is shown in Figure 4.13b and reveals a flatter habit with the disappearance of faces (1 0 -2), (0 1 1) and the appearance of (1 1 1). Although this morphology is similar to what is observed experimentally, literature reveals that the three dominant faces during crystallisation are (1 0 0), (0 0 2) and (0 1 1) [147, 149, 150]. The first two faces are present in both the BDFH and attachment energy models however face (0 1 1) is only present in the BDFH prediction. The attachment energy model was altered to include the three faces present during crystallisation and this is shown in Figure 4.13c.
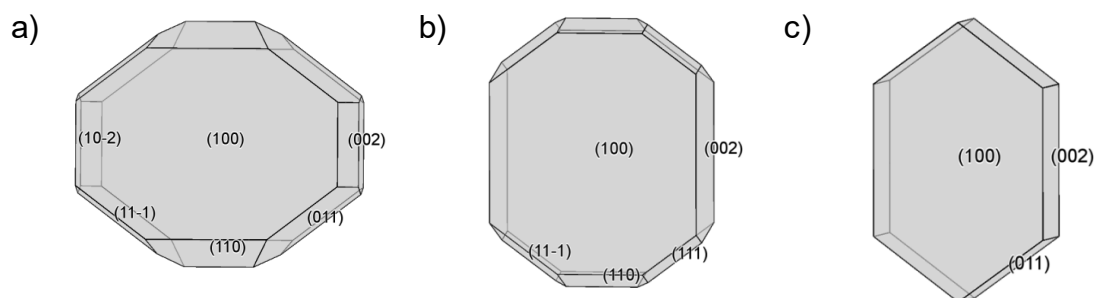
Figure 4.13 – Predicted morphology of ibuprofen a) BDFH highlighting six morphologically important crystal faces b) attachment energy morphology highlighting five morphologically important crystal faces and c) attachment energy morphology edited to only include the three faces observed during crystallisation.

The d spacing (d_{hkl}), calculated slice (E_{slice}) and attachment energies (E_{att}) for the morphologically important crystal faces of ibuprofen are shown in Table 4.2.

Table 4.2 – The d spacing, slice and attachment energy per morphologically important crystal face of ibuprofen.

Face (hkl)	d_{hkl} Å	E_{slice} (kJ/mol)	E_{att} (kJ/mol)
(1 0 0)	14.5	-110.5	-14.6
(1 1 0)	6.9	-54.8	-70.3
(0 1 1)	6.3	-44.4	-80.8
(1 1 -1)	6.0	-52.3	-72.9
(1 1 1)	5.6	-52.9	-72.3
(2 1 0)	5.3	-46.9	-78.2
(0 0 2)	5.3	-63.6	-61.5

4.3.5   Quantitative Surface Analysis

Analysis of the three main faces reveals different crystal chemistry present at the surface of each, as shown in Figure 4.14. The dominant (1 0 0) surface contains the aliphatic chains; group A at the surface with the molecules linked by the carboxylic acid dimers in the centre of the bulk. This high energy interaction accounts for the directional growth of ibuprofen crystals in the (1 0 0) direction and is confirmed by the lath shaped particles usually

produced during crystallisation from non-polar solvents, such as hexane [147]. The (0 1 1) and (0 0 2) faces have the carboxylic acid group exposed at the surface allowing for potential hydrogen bonding to occur with Lewis acids. This is confirmed by the habit change when polar crystallisation solvents, such as ethanol, are used and result in a plate like habit due to the slower growth of the (0 1 1) and (0 0 2) crystal face [147, 149].

Dominant surfaces of ibuprofen

(1 0 0) **(0 1 1)** **(0 0 2)**
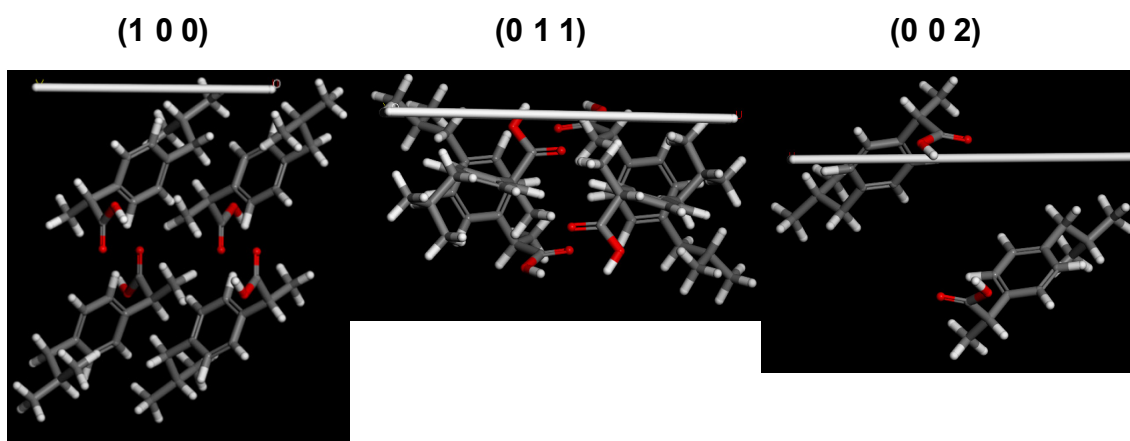
Figure 4.14 – Crystal chemistry of the morphologically important faces of ibuprofen, (1 0 0), (0 1 1) and (0 0 2).

It can be hypothesised from this analysis that the (1 0 0) face will exhibit a lower surface energy than the other two faces, (0 1 1) and (0 0 2) due to the high energy carboxylic acid dimer being contained within the bulk of the structure.

4.4   Conclusions

The research reported in this chapter demonstrates the application of molecular modelling techniques to explore the crystal chemistry of ibuprofen. The solid-state of ibuprofen was explored and this study focused only on racemic (RS)-ibuprofen form I. The CSD was interrogated and structure (REFCODE: IBPRAC) was chosen for analysis.

The crystal structure of ibuprofen was shown to contain a hydrogen bonded centrosymmetric dimer which contains a short length when compared to all other structures with this functionality within the CSD. Comparison of two different force fields was presented such that the Tripos 5.2 force field was shown to be in excellent agreement with the enthalpy of sublimation and carboxylic acid dimer strength values in the literature. Further analysis of the strengths of the intermolecular interactions revealed the carboxylic acid dimer energy to dominate the lattice energy. This interaction was shown to be three times stronger than the next strongest interaction (carboxylic acid contributes 27% whereas the second dominant interaction contributes 9%). The structure was divided into molecular components and the lattice energy collapsed onto individual atoms then summed across these components. A novel approach using a colour coded diagram to represent the contribution of each molecular component to the total lattice energy is presented. This revealed that the lattice energy is not evenly distributed across the molecule and, as expected, the carboxylic acid interaction dominates.

The morphology of ibuprofen was predicted using two classical approaches and then further modified to represent what it expected during crystallisation using literature analysis. The attachment energy values, per dominant surface, are presented which will enable future calculations of surface energy. It is predicted, via qualitative analysis, that the surface energy of different faces of ibuprofen will vary due to the different crystal chemistry present at each surface. By using the colour coded diagram, in relation to the surface chemistry, it is predicted that the crystal faces that contain the unsaturated carboxylic acid, (0 0 1) and (0 0 2), will exhibit a higher energy than the (1 0 0) crystal face where the dimer is within the bulk.

5. Chapter Five: Development of The Heckel Equation

5.1 Introduction

As tablets are the most common dosage platform, understanding the deformation behaviour of the individual molecular components is critical. Despite the importance of the foregoing statement, especially in the design and manufacture of direct compression formulations, there are no set analytical testing standards or materials classification guidelines. Instead many workers have attempted to develop techniques for the measurement and classification of a material's deformation but there is still confusion and contradiction present in this field.

Recently many efforts have focused on the study of the deformation of materials at the single crystal level [151 - 154]. Techniques such as nanoindentation provide information using minimal quantities of material; however, the relationship between single crystal and bulk mechanical behaviour is not well understood. This had led to the continued use of compaction equations to classify materials in terms of their deformation.

Despite being heavily criticised in the literature the most widely used and accepted compaction equation is the Heckel equation, proposed by Heckel in 1961 [18]. Its presence in the literature for 55 years is due to the ease with which it can distinguish between plastic and brittle materials. Achieving the correct balance of plastic and brittle materials in a formulation is critical to ensure adequate tablet strength is achieved; therefore, classifying materials using the Heckel equation is attractive to pharmaceutical formulation scientists.

The model proposed by Heckel is represented by the expression:

$$\ln(1/1 - D) = K \cdot P + A \qquad (15)$$

where D is the relative density of the compact, P is the applied pressure, A is a constant suggested to represent particle rearrangement and the reciprocal of K is used to calculate apparent mean yield pressure (P_y). The density / pressure relationship is based on first order kinetics and has been defined as the stress at which plastic deformation of a particle is initiated,

where low P_y values represent plastically deforming materials and high P_y values represent brittle materials [7]. In the pharmaceutical industry, the deformation of excipients has been most widely characterised [21] and it is accepted that microcrystalline cellulose (MCC) and dibasic calcium phosphate (DCP) form the extremes of the deformation spectrum, with MCC (Avicel PH-101) exhibiting a yield pressure of 50 MPa and DCP exhibiting a yield pressure value of 957 MPa [155].

The yield stress values of well characterised materials become important when attempting to classify new materials. Often a comparison with materials whose deformation behaviour is well understood will be made due to the absence of defined standard class limits on yield pressure in terms of a plastic or brittle material. Roberts and Rowe attempted to set limits on these values together with other mechanical descriptors including Young's modulus, hardness and strain rate sensitivity which allowed materials to be categorised [155]. Materials with P_y <80 were classified as soft/plastic materials whereas P_y >80 indicated hard/brittle substances. Although these limits are available they are difficult to adhere to due to the variation in P_y values presented for the same material between different research groups. The variation presented is due to many experimental and physical factors (experiment type, compaction speed, compaction pressure and particle size) affecting derived values and no standardisation being set on these.

The Heckel equation can be fitted to data collected from 'in-die' or 'out-of-die' compaction experiments. These different experiment types have been shown to affect yield pressure measurements due to the contribution of elastic energy [156, 157]. Ilić *et al.*, measured the yield pressure of MCC (Avicel PH 101) in-die and out-of-die and the respective yield pressure values were 61.7 MPa and 98.3 MPa. This difference of 36.6 MPa between experiment types is one of many factors contributing to discrepancies in yield pressure data published from different research groups.

As well as experiment type, it is also well documented that experimental conditions can affect yield pressure. It has been shown by numerous workers that compaction speed and final compaction pressure can affect yield

pressure [158 - 160]. Roberts and Rowe [160] proposed a term, strain rate sensitivity, which describes the relationship between yield pressure values collected at two different compaction speeds. Since then it has been shown that plastic materials are more sensitive to strain rate compared to brittle materials [12]. This means that when reporting the yield pressure of plastic materials, the compaction speed will alter the yield pressure value.

The variation detected in yield pressure is not only due to experimental conditions but can be attributed to the physical effect of particle size. The yield pressure of a material is an intrinsic property and therefore should not be affected by physical properties such as particle size; however, there is contradicting information in the literature. Fell and Newton [161] reported that the yield pressure of lactose was influenced by particle size. However, in 1982 a study by McKenna and McCafferty [162] revealed that during their calculation of yield pressure for lactose, particle size was irrelevant. Another study by Patel *et al.*, [163] found that the yield pressure of paracetamol was dependent on particle size, where increasing particle size resulted in higher yield pressure values. Recent studies have suggested that as the yield pressure is derived from the density pressure relationship this value is actually an indication of powder densification rate that may be effected by particle size [19]. Nevertheless, yield pressure calculated from the Heckel equation is still derived to provide information on bulk deformation behaviour and particle size is one of the many variables affecting the outcome.

One area which may account for variability in the yield pressure value, but has been neglected in the literature, is the way in which the K value from the Heckel equation is derived. This is due to the fact that although it is accepted that yield pressure is derived from the gradient of a linear slope, Heckel plots are not completely linear and contain deviations at low and high pressures. These deviations are due to particle rearrangements at low pressures [7], and elastic deformation as pressure increases [156]. It is the responsibility of the analyst to select the most appropriate region in which to calculate yield pressure. This method is susceptible to user subjectiveness and has the potential to cause error in derived values which could lead to mistakes in material classification. Despite this, there are no standards or

recommendations in the literature to define what area of the Heckel profile should be used in order to calculate yield pressure

The type of variation in yield pressure that can be obtained for a material, due to the factors discussed, can be significant e.g., ibuprofen which has a reported values of 21 – 1139 MPa. The compressibility of ibuprofen has been studied by many workers [164 - 167] and a listing of the reported yield pressure values are shown in Table 5.1. The small variations present in studies, 4 MPa [165] and 3 MPa [167], are due to particle shape and particle size differences, respectively. The study by Patel *et al.* reveals large differences accounted for by the effect of compaction pressure. This would suggest, according to the limits set by Roberts and Rowe [155], that ibuprofen changes from a plastic to a brittle material. In an attempt to further understand yield pressure variations within the literature this study will focus on the effect of compaction pressure on ibuprofen yield pressure and a method to determine the linear region of the Heckel plot using a novel bench top tablet press.

Table 5.1 – Reported yield pressure values of ibuprofen from literature.

Py (MPa)	Reference	Comment
54 – 58	Di Martino *et al.*, 2002 [165]	Particle shape dependent
21 – 24	Liu *et al.*, 2013 [167]	Particle size dependant
98 – 1139	Patel *et al.*, 2010 [166]	Compaction pressure dependant

5.2   Materials and Methods

5.2.1   Materials

Ibuprofen (40 μm grade) was supplied by Pfizer Ltd. Ibuprofen sodium dihydrate was purchased from Sigma Aldrich, Dorset, UK.

5.2.2 Methods

5.2.2.1 Scanning Electron Microscopy

Scanning electron microscopy (SEM) was used to qualitatively assess particle size and shape. Electron micrographs were captured using a Zeiss SUPRA 40VP (Carl Zeiss Microscopy GmbH, Cambridge, UK). The samples were mounted onto an aluminium pin stub containing sticky carbon tabs and sputter coated with platinum. A voltage of 3.0 kV and working distance of 10 mm were used.

5.2.2.2 Dynamic Image Analysis

Particle size and shape values of the samples were measured using a dynamic image analysis system QICPIC (Sympatec Ltd., Clausthal-Zellerfeld, Germany). A vibratory feeder system (VIBRI, Sympatec) was combined with a dry air disperser (RODOS, Sympatec) and was operated at 0.5 bar pressure. The system operates using a pulsed light source with sub-nanosecond illumination, and the particles were imaged by a high speed camera with a frame rate of 400 frames per second. Single measurements were made using the M6 lens (measuring range of 5 – 1705 µm) and a minimum of 700,000 particles were imaged for each run. Images were analysed using WINDOX (Sympatec) software and size / shape distributions reported using the maximum Feret diameter.

5.2.2.3 True Density

The true density of 2.5 ± 0.2 g samples were measured in duplicate using a Pentapyc 5200e helium pycnometer (Quantachrome UK Ltd., Hook, UK).

5.2.2.4 Compression Studies

A Gamlen GTP-1 single punch bench top tablet press (Gamlen Tableting, United Kingdom) was used to complete the compression experiments. The

deformation of the punch was corrected by running a measurement with no material in the die and then using these values to correct the in-die thickness.

Tablets of 100 ± 5 mg were produced using a 6 mm flat-faced punch and die. Compression experiments were undertaken at a speed of 0.033 mm/s, following the same methodology described by Roberts and Rowe [158].

In order to investigate the effect of compression pressure on yield pressure ibuprofen and ibuprofen sodium were compacted at five different compaction pressures (52, 87, 121, 156 and 173 MPa). Six individual measurements were made at each compaction pressure for both materials, to enable the variation in the yield pressure for each material to be determined.

5.3 Results and Discussion

5.3.1 Scanning Electron Microscopy

SEM was conducted to visually assess and qualitatively determine particle size and shape information. The electron micrographs of ibuprofen and ibuprofen sodium, shown in Figure 5.1a and Figure 5.1b, respectively reveal a difference in size and shape between the two materials. The majority of ibuprofen particles are smaller than 100 μm whereas the ibuprofen sodium batch contains both small (around 100 μm) and larger particles (around 200 μm). Differences in particle shape are also revealed, with ibuprofen consisting of smooth lath shaped particles compared to ibuprofen sodium which has both rough prismatic and lath shaped particles.
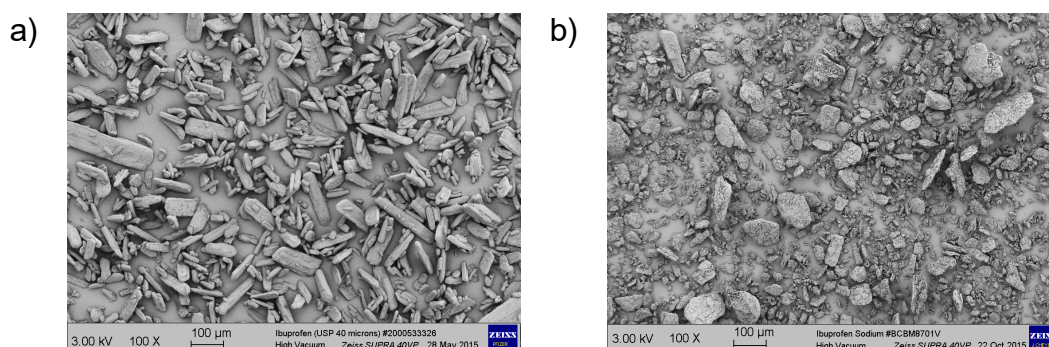
Figure 5.1 – Scanning electron micrographs a) ibuprofen and b) ibuprofen sodium. All images captured using x100 magnification and scale bar is 100 μm.

5.3.2 Dynamic Image Analysis

Ibuprofen and ibuprofen sodium were characterised using QICPIC to enable a quantitative measure of particle size. The volume distributions (most sensitive to larger particles) are shown in Figure 5.2a and the number distributions (most sensitive to the smaller particles) are shown in Figure 5.2b. The numerical values for both volume and number distributions are shown in Table 5.2.

The volume distributions reveal that ibuprofen contains a primary mode centring around 100 µm, which is in agreement with the visual observation. This distribution for ibuprofen sodium is wider and centres around 200 µm. The larger size of this material can be seen when comparing the average mean by volume, D[4,3], for both batches: ibuprofen is 114.7 µm compared to ibuprofen sodium which is 186.3 µm.
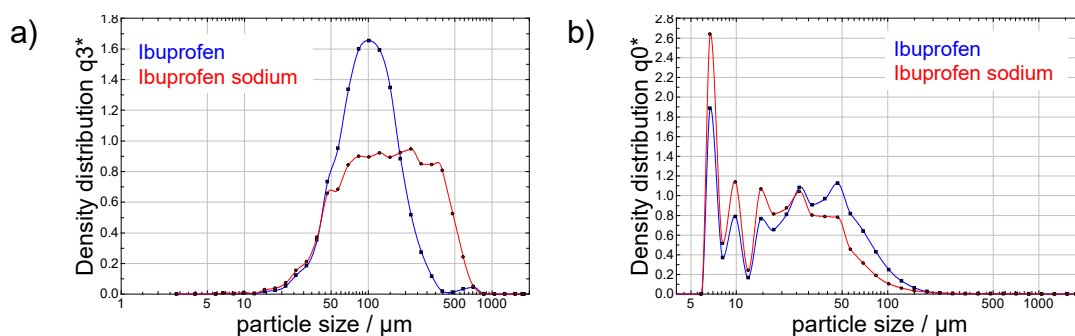
Figure 5.2 – QICPIC a) volume and b) number weighted distributions for ibuprofen and ibuprofen sodium.

The number distributions reveal that ibuprofen sodium contains a higher proportion of fine particles (around 5 µm) compared to ibuprofen. Ibuprofen contains a higher proportion of larger particles (between 50 – 100 µm) compared to ibuprofen sodium resulting in a larger mean by number: 33.5 µm compared to 25.2 µm for ibuprofen and ibuprofen sodium, respectively.

Table 5.2 – QICPIC number and volume particle size values for ibuprofen and ibuprofen sodium.

Sample	Number				Volume			
	D[n,0.1] µm	D[n,0.5] µm	D[n,0.9] µm	Mean by Number µm	D[v,0.1] µm	D[v,0.5] µm	D[v,0.9] µm	D[4,3] µm
Ibu	6.9	26.0	70.0	33.5	47.8	99.0	193.8	114.7
Ibu sodium	6.7	17.5	51.5	25.2	46.5	141.0	401.6	186.3

5.3.3 True Density

Helium pycnometry was used to measure the true density of the materials. The true density values of ibuprofen and ibuprofen sodium were 1.12 g/cm^3 and 1.17 g/cm^3, respectively. The standard error of measurement for each material was calculated and determined to be 0.0013 g/cm^3 (0.11%) for ibuprofen and 0.007 g/cm^3 (0.61%) for ibuprofen sodium.

It has previously been reported that Heckel plots are sensitive to variations in measured density. A 1% error in density can lead to a 10% error in yield pressure [19], therefore it is important to report density values used and include the standard error in the measurement for transparency. Since the error values are low it is predicted that this will have minimal effect on derived values; however, the impact or error in density will be investigated during yield pressure calculations.

5.3.4 Yield Pressure Determination

5.3.4.1 In-Die Heckel Calculation

In-die Heckel plots were obtained by calculating the relative density (D) in-die using the true density and compact thickness (derived from corrected punch displacement measurements). The value for ln(1/1-D) was determined for each measurement at each compaction pressure and these were plotted against each other to enable yield pressure to be determined.

5.3.4.2 <u>Linear Regression Fitting</u>

To enable accurate determination and eliminate subjective selection of the linear region of the Heckel plot, linear regression analysis was performed. A visual assessment of the Heckel plot was made and the regression co-efficient calculated for this part only. The linear region was then extended in both directions by decreasing the compaction pressure of x_1 and increasing the compaction pressure of x_2 in approximately 10 MPa sequential steps (Figure 5.3). After each step the regression coefficient was recalculated.
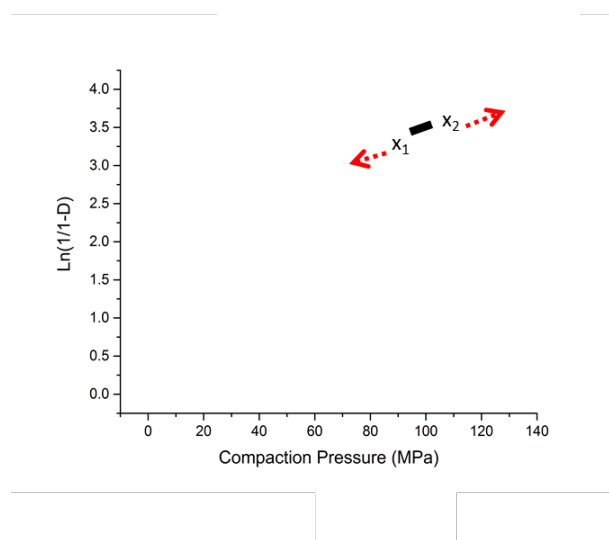
Figure 5.3 – Linear region of Heckel equation selected by visual inspection illustrating the direction of decreasing x_1 and increasing x_2.

Once the region which contained the highest regression coefficient (specific to the x coordinate) was established the step size was decreased until an accuracy of 1 MPa was reached. The regression coefficients with regards to the x coordinates are shown in Table 5.3 for ibuprofen compacted to 156 MPa (repeat 1). For this particular example the compaction pressure range used to derive the yield pressure was 76.2 – 111.1 MPa with a corresponding r^2 value of 0.9993.

Table 5.3 – Example of extending the linear region of the Heckel plot for ibuprofen compacted to 156 MPa with corresponding regression coefficient values. Highlighted value is linear range used to calculate yield pressure.

Action	Compaction pressure range (MPa)			r^2
	x_1	x_2	$x_2 - x_1$	
visual selection	80.1	90.2	10.1	0.99395
x_2 increase	80.1	100.2	20.1	0.99817
x_2 increase	80.1	110.1	30.0	0.99916
x_2 increase	80.1	120.2	40.1	0.99898
x_2 increase	80.1	130.3	50.2	0.99749
x_2 decrease	80.1	115.2	35.1	0.99907
x_2 decrease	80.1	112.2	32.1	0.99907
x_2 decrease	80.1	105.1	25.0	0.99877
x_2 increase	80.1	109.2	29.1	0.99911
x_2 increase	80.1	111.1	31.0	0.99921
x_1 decrease	70.2	111.1	40.9	0.99886
x_1 increase	75.1	111.1	36.0	0.99914
x_1 increase	77.2	111.1	33.9	0.99929
x_1 increase	78.0	111.1	33.1	0.99927
x_1 decrease	76.2	111.1	34.9	0.99930

The effect of the regression coefficient on the gradient of the slope and hence the yield pressure is highlighted using an example of ibuprofen compacted to 121 MPa (repeat 1) in Figure 5.4. This reveals the importance of selecting the most representative linear region, as selecting only a small portion of the plot, where r^2 is 0.984, gives rise to a yield pressure value of 85 MPa compared to a larger portion of the plot (r^2 is 0.999) which gives rise to a yield pressure value of 76 MPa, a difference of around 10%. According to Rowe and Roberts [155], this would classify ibuprofen in two different deformation categories, changing from hard / brittle to soft / plastic.
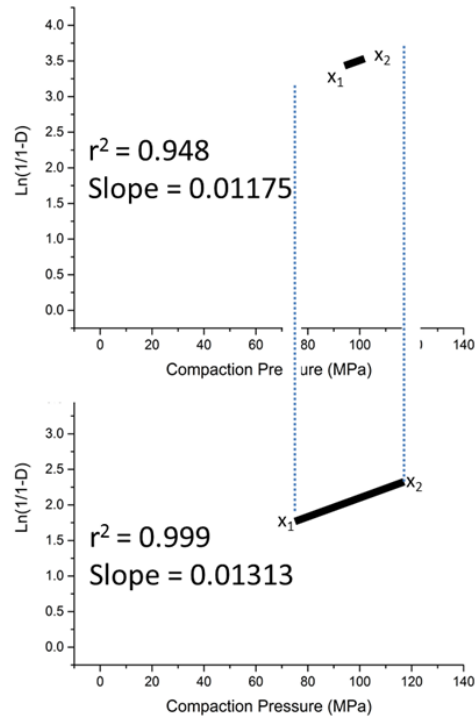
Figure 5.4 – An example of the extension of the linear range of the Heckel model in order to achieve the highest regression coefficient.

5.3.4.3 Effect of Compaction Pressure on Yield Pressure

Heckel transformations for ibuprofen at the different compaction pressures analysed are shown in Figure 5.5. The plots produced at each compaction pressure overlay suggesting that, in principal, the same linear region for each pressure could be selected and therefore deriving the same yield pressure results. However, the plot also reveals that the full linear range of the Heckel plot may only become apparent when higher final pressures are used.
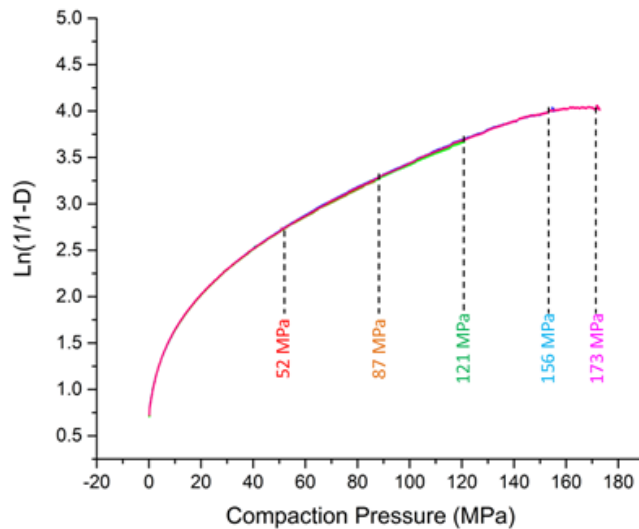
Figure 5.5 – Heckel transformations of ibuprofen at varying compaction pressures.

Linear regression was performed on six Heckel plots at each compaction pressure for ibuprofen and ibuprofen sodium. During analysis it became apparent that differences in yield pressures arise due to the range of the linear region available for selection at different compaction pressures. Figure 5.6 shows an example where ibuprofen compacted to 52 MPa returns a yield pressure value of 48 MPa compared to 76 MPa for ibuprofen compacted to 121 MPa. The visually subtle difference in gradient due to the compaction pressure used causes a significantly large difference in yield pressure, 28 MPa. Compacting ibuprofen to higher compaction pressures extends the rate of powder densification which in turn lowers the gradient of the slope and explains the increase in yield pressure values.
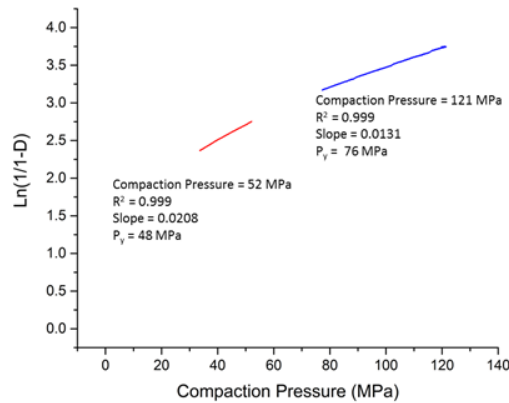
Figure 5.6 – Derived yield pressure from Heckel plot at 52 MPa and 121 MPa.

5.3.4.4 Investigation the Effect of Error in True Density

As discussed previously, it is known that errors in measured true density can affect derived yield pressure values. To investigate this further a worst case scenario of ibuprofen sodium compacted to 52 MPa was chosen for investigation, due to ibuprofen sodium containing 0.5% higher error in density compared to ibuprofen. This measurement gave a yield pressure of 50 MPa and when the error in density was included returned values of 46 MPa and 53 MPa, which is a difference of around 14%. This large error associated with density is unavoidable due to the logarithmic transformation of the Heckel equation; therefore alternative methods to reduce error are of upmost importance.

5.3.4.5 Comparison of Ibuprofen and Ibuprofen Sodium

The effect of compaction pressure on yield pressure for ibuprofen and ibuprofen sodium is displayed in Figure 5.7. The derived value for ibuprofen ranges from 52 – 78 MPa and ranges from 48 – 75 MPa for ibuprofen sodium. At the very high compaction pressures (>156 MPa) it is observed that the yield pressure values for both materials reaches a plateau where the standard deviations overlap. This would suggest that at these compaction pressures the highest possible rate of powder densification has been reached. However,

examination of Figure 5.4 reveals that in order to utilise the greatest range of linearity, final compaction pressures of 121 MPa should be used to report yield pressure values.
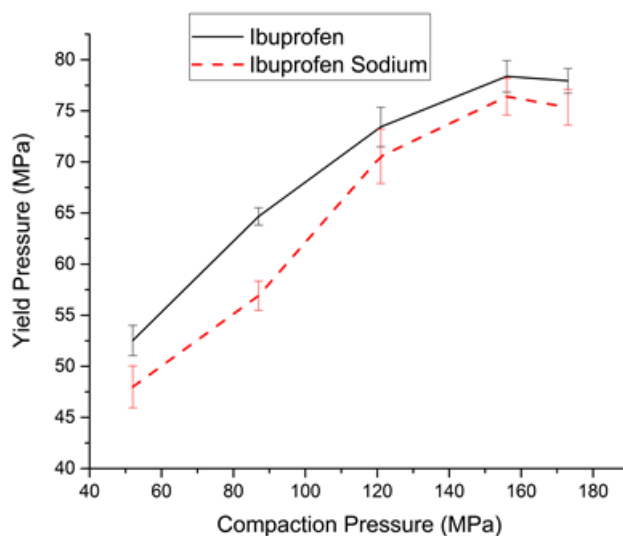
Figure 5.7 – Effect of compaction pressure on yield pressure for ibuprofen and ibuprofen sodium.

The comparison of ibuprofen yield stress to its sodium salt dihydrate reveals that at all compaction pressures ibuprofen sodium exhibits lower yield stress values. It would be expected, from the results of previous studies, that ibuprofen sodium would exhibit a smaller particle size distribution which would account for the differences [163]. However, examination of the particle size data (Figure 5.2) reveals that the salt contains a larger particle size. Therefore regardless of particle size, ibuprofen sodium dihydrate possesses an increased powder densification rate suggesting higher plasticity compared to the free acid. A possible reason for this is the water contained within the crystal structure of the sodium salt could be acting as a plasticiser allowing easier slip to take place. This could explain the lower yield stress and therefore plasticity of ibuprofen sodium dihydrate compared to ibuprofen free base.

5.4 Conclusions

A new approach utilising linear regression has been developed to analyse Heckel plots. Examination of regression coefficients of the linear region of the plot has allowed the selection of the most representative area in which yield stress can be derived. The variation due to the linear region selection has been reviewed and revealed that variations of 10% are possible, dependent on which part of the plot is selected.

This linear regression method has been effectively applied to ibuprofen and ibuprofen sodium dihydrate and the results highlight the fact that increasing compaction pressure results in the calculation of higher yield pressure values. This phenomena reaches its peak at very high compaction pressures (>156 MPa); however the greatest range of linearity is observed when pressures of 121 MPa were used in this study. Therefore it is proposed that in order to enable a useful comparison of yield pressure, high compaction pressures (around 121 MPa) should be used for analysis.

It is also proposed from this research that, when reporting yield pressure values from the Heckel equation, all experimental conditions and linear regression methods should be clear and transparent in order to reliably classify materials.

The study also revealed ibuprofen sodium to exhibit increased plasticity compared to ibuprofen. This could be due to water molecules contained within the crystal structure acting as a plasticiser. From this study, it is suggested that the presence of these molecular entities creates a greater presence of slip planes within the crystal lattice allowing the sodium salt of ibuprofen to exhibit greater plastic deformation than ibuprofen alone.

6. Chapter Six: The Impact of Particle Shape on the Manufacturability of Ibuprofen

6.1 Introduction

The particle shape of APIs gains much less attention in the pharmaceutical industry than other physicochemical properties such as particle size or solid form. Slight changes in API particle shape may arise during the crystallisation or processing of the API / drug product. The effect that this may have on the manufacturability of the drug product in terms of direct compression is unknown. The work reported in this chapter aims to crystallise ibuprofen into diverse particle shapes and measure the impact on the tabletability and sticking propensity of the API.

A brief overview of crystallisation theory and the crystallisation of ibuprofen will be given below.

6.1.1 Crystallisation Theory

Crystallisation is widely used within the pharmaceutical industry to manufacture, purify or modify the physicochemical properties of APIs [95]. The particle size, shape, crystal structure and degree of crystal imperfection can be altered by the crystallisation process; therefore, the fundamental properties need to be understood to achieve the desired product [168].

Crystallisation of a solid can take place via solidification of melts or by liquid crystallisation (which is the crystallisation of a solid from a solvent suspension); the latter will be used in this study. The crystallisation of a powder from a suspension involves the nucleation and growth of crystals from a supersaturated solution [169]. Supersaturated solutions can be achieved by increasing the temperature or pressure of a solution; temperature will be the parameter used in this study. A typical solubility curve is shown in Figure 6.1 where, generally, the solubility of a solid in a solution increases as temperature increases. A solution can be heated prior to cooling to produce a supersaturated or metastable solution. The metastable zone width is the

temperature range in which a solution will remain in its supersaturated state before precipitating into crystals.
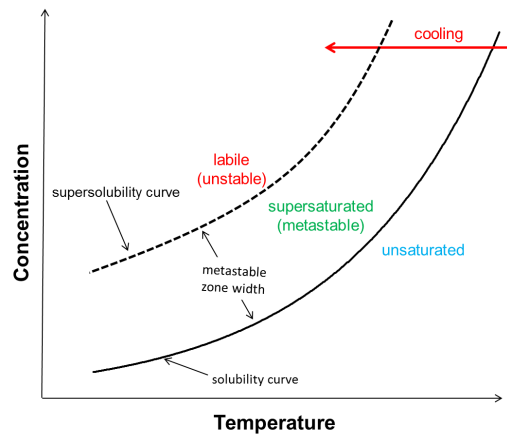
Figure 6.1 – Typical solubility curve highlighting the metastable zone width of a solution. Adapted from reference [170].

The first stage in the crystallisation of solid material is known as the nucleation process. There are three types of nucleation that can occur: primary homogeneous, primary heterogeneous and secondary nucleation. Primary homogenous nucleation forms crystal embryos in which new surfaces can grow; however, most primary nucleation events that occur are heterogeneous and are induced by the presence of other surfaces with lower surface energy. Secondary nucleation results from the presence of other solute particles in the solution and is said to be the most significant nucleation mechanism. In order to promote secondary nucleation a seed material can be added to the supersaturated solution in the metastable zone and can influence the particle size and form of the resultant crystals [169]. In this study a seeding material will be added to supersaturated solutions in order to promote controlled secondary nucleation.

Once stable nuclei have been formed crystals can start to grow from the supersaturated solution. The growth of crystals can be described using many theories such as surface energy, adsorption layers, kinematic and diffusion-reaction theories [171] and are governed by both "internal" and "external" factors. Internal factors (such as the strength of the intermolecular

interactions) as well as external factors (such as temperature, supersaturation, and solvent type) will affect the growth of the crystals. The particle shape of crystals is generally controlled by kinetic factors, where the slowest growing crystal faces give rise to the largest crystal surfaces. The particle size of crystals formed can be influenced by the seed material as well as the cooling rate of the supersaturated solution [172].

In industry, once the product has been formed via crystallisation it is normally washed and filtered to obtain a clean, pure product [173]. In this study products will not be washed and will be filtered using small scale equipment.

6.1.1.1 Crystallisation of Ibuprofen

The crystallisation and solubility of ibuprofen has been well documented in the literature with a solubility curve for common solvents shown in Figure 6.2. This highlights the soluble nature of ibuprofen in a range of solvents with varying polarities. It is most soluble in 95% ethanol followed by toluene then acetonitrile. This solubility data will be used to derive the conditions for the recrystallisation experiments in this study.
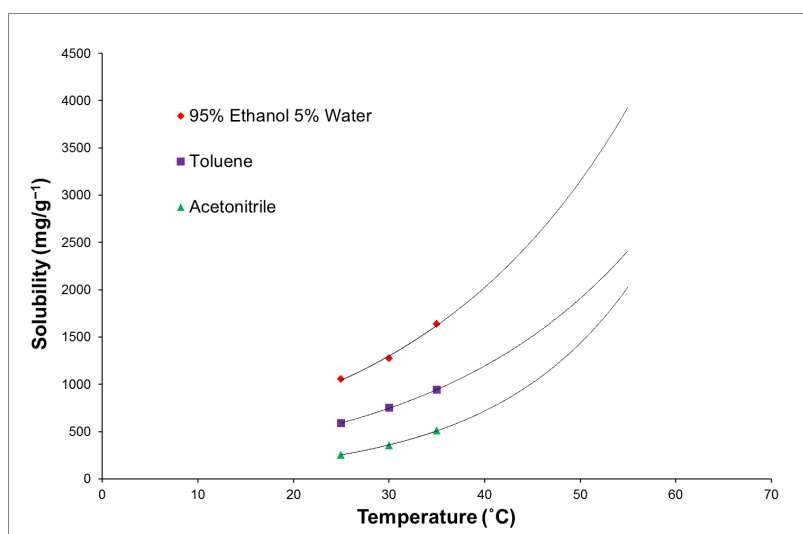
Figure 6.2 – Solubility of ibuprofen in 95% ethanol, toluene and acetonitrile. Adapted from reference [174].

The impact of solvents on the crystal habit of ibuprofen is well understood with Bunyan *et al.,* first reporting the effects in 1991 [147]. These are schematically shown in Figure 6.3. This work revealed that elongated lath shaped particles are produced from non-polar solvents (such as hexane and toluene) and the crystal habit becomes more regular as solvent polarity increases. Particles produced from polar solvents (such as ethanol and methanol) contain a greater exposure of the side crystal faces resulting in a prismatic shape.
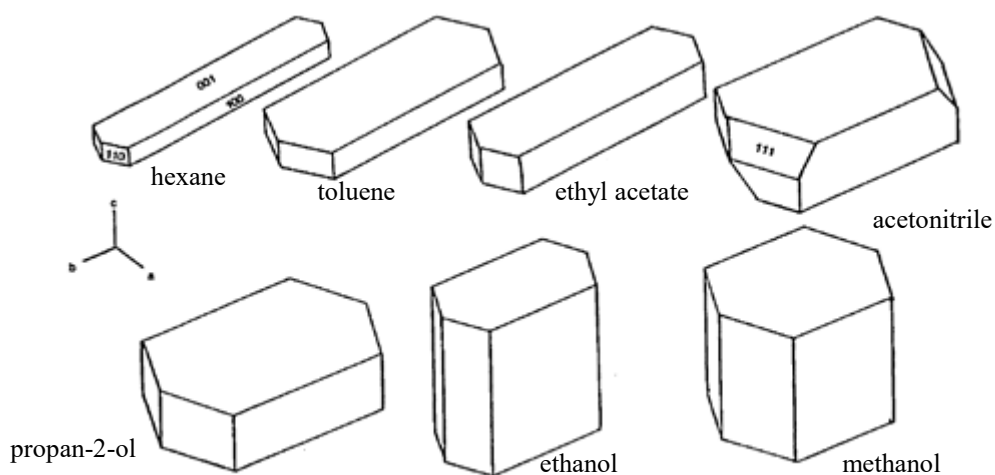
Figure 6.3 – The effect of solvents on the crystal habit of ibuprofen. Adapted from reference [147].

More recently the chemistry of ibuprofen has been studied at a molecular level and the effect of solvent on crystal habit has been explained [136, 149]. Ibuprofen particles contain four dominant crystal faces: (1 0 0), (0 0 2), (1 1 0) and (0 1 1). The differences in crystal habit can be explained by focusing on the main two crystal faces: (1 0 0) and (0 0 2). The main (1 0 0) crystal face present in lath shaped particles contains layers of polar and non-polar functionalities. Due to the hydrogen bonded dimers it is unlikely that the polar functionality would be presented at the surface, thereby allowing alkyl groups from non-polar solvents to form interactions with the non-polar groups.

As the solvent polarity is increased, so does the interaction between these solvents and the side (0 0 2) crystal face. The (0 0 2) crystal face exposes

the carboxylic acid allowing hydrogen bonding interactions between the molecule and solvent therefore slowing down the growth rate of this face which in turn results in a more regular shaped particle.

The solvent effect on ibuprofen crystal habit can be explained using the crystal chemistry of the crystal faces and in turn suggests that ibuprofen particles with varying habits will have different surface energies due to the variations in surface chemistry exposed.

This chapter focuses on the recrystallisation and characterisation of ibuprofen batches with different crystal habits.

6.2 <u>Materials and Methods</u>

6.2.1 Recrystallisation of Ibuprofen using the Optimax Reactor

(RS)-ibuprofen, (40 µm grade, ≥99.8%) was supplied by Pfizer Ltd and was recrystallised from hexane (95%), toluene (>99.5%), acetonitrile (99.8%) and ethanol (>99.5%) purchased from Fisher Scientific (Loughborough, UK). The experimental conditions used in these experiments are shown in Table 6.1. Supersaturated solutions were prepared at the following concentrations: hexane 1.1 g/mL, toluene 1.5 g/mL, acetonitrile 1.3 g/mL and ethanol 1.5 g/mL. These solutions were heated to the temperatures shown in Table 6.1 in a jacketed Optimax reactor (Mettler Toledo, Leicester, UK). The stirred solutions were cooled linearly to 0°C at a rate of 1°C/min and seeded with 1% of the starting material prior to nucleation. The product was obtained by filtering through general-purpose laboratory filter paper (Whatman, UK) and dried in an oven at 50°C for 24 hours.

Table 6.1 – Experimental conditions for the recrystallisation of ibuprofen using ethanol, acetonitrile, toluene and hexane.

Solvent	Initial mass of ibuprofen (g)	Heating temperature (°C)	Seeding temperature (°C)	Recovered mass of ibuprofen (g)	Yield (%)
Ethanol	215.4	43	30	142.0	66
Acetonitrile	206.5	55	45	161.3	78
Toluene	211.6	55	48	171.4	81
Hexane	208.6	61	50	127.0	61

6.2.2 Physical Characterisation of Ibuprofen

6.2.2.1 Scanning Electron Microscopy

Scanning electron microscopy (SEM) images were captured using a Zeiss SUPRA 40VP (Carl Zeiss Microscopy GmbH, Cambridge, UK). The samples were mounted onto an aluminium pin stub containing sticky carbon tabs and sputter coated with platinum. A voltage of 3.0 kV and working distance of 10 mm were used.

6.2.2.2 Sieve Analysis

Sieve analysis was performed as a screen on recrystallised samples using a mesh size of 1.25 mm. The stainless steel sieve (Endecotts Ltd., London, UK) was manually tapped 60 times.

Further to this all batches were then passed through a 150 μm stainless steel sieve (Endecotts Ltd., London, UK) using the same method described above.

6.2.2.3 Dynamic Image Analysis

Particle size and shape values of the samples were measured with a dynamic image QICPIC (Sympatec Ltd., Clausthal-Zellerfeld, Germany) analysis system. A vibratory feeder system (VIBRI, Sympatec) was combined with a

dry air disperser (RODOS, Sympatec) and was operated at 0.5 bar pressure. The system operates using a pulsed light source with sub-nanosecond illumination, and the particles were imaged by a high speed camera with a frame rate of 400 frames per second. Single measurements were made using the M6 lens (measuring range of 5 – 1705 µm) and a minimum of 200,000 particles were imaged for each run. Images were analysed using WINDOX (Sympatec) software, and size and shape distributions reported using the maximum Feret diameter.

6.2.3 Solid Form and Analytical Characterisation of Ibuprofen

6.2.3.1 Powder X-ray Diffraction

Powder X-ray diffraction (PXRD) was performed by preparing the samples using a flat plate and diffraction patterns collected on a D4 Endeavor (Bruker Corporation, Billerica, Massachusetts, USA). The scan was carried out between 2° and 55° 2θ using CuKα radiation with a secondary graphite monochromator.

6.2.3.2 Differential Scanning Calorimetry

Differential scanning calorimetry (DSC) studies were performed using a Discovery DSC (TA Instruments, Herts, UK). The samples were analysed in a T-zero standard pan at a heating rate of 10°C/min over a temperature range of 30°C to 100°C and using an atmosphere of dry nitrogen.

6.2.3.3 Evolved Gas Analysis

Evolved gas analysis (EGA) was performed using a thermogravimetric analyser (PerkinElmer Inc., Llantrisant, UK) coupled to a mass spectrometer (Hiden Analytical Ltd., Warrington, UK). The samples were heated over the range from 30°C to 100°C at a heating rate of 10°C/min and the mass ion related to the recrystallisation solvent for each batch was monitored: ethanol

mass ion 45, acetonitrile mass ion 41, toluene mass ion 91 and hexane mass ion 86. The mass ion for water was also monitored for each batch.

6.2.3.4 Headspace-Gas chromatography

Headspace-gas chromatography (HS-GC) was performed using a 6892N Network GC system coupled to a 7694 HS sampler (Agilent Technologies, CA, US). Around 20 mg of each sample was dissolved in N,N-dimethylacetamide (≥99%) purchased from Sigma Aldrich (Dorset, UK). A liquid-vapour equilibrium was established by heating the solution in a sealed vial and an aliquot of the headspace vapour was analysed by capillary GC. Quantification of each volatile impurity was achieved by comparison of the chromatographic peak areas of external reference standards with the peak areas of the test sample solutions.

6.2.4 Blending of Ibuprofen Mixtures

Ibuprofen batches containing different particle shapes were prepared by preparing small laboratory scale mixtures on a 5 g scale. The mixtures were blended using a TURBULA® shaker-mixer (Glen Mills Inc, New Jersey, USA) at a rate of 49 rotations per minute for 5 minutes.

6.2.5 Manufacturability of Ibuprofen

6.2.5.1 Tabletability

The ibuprofen samples were compacted using a Gamlen tablet press (GTP-1, Gamlen Tableting Limited, Nottingham, UK). The samples were compacted using a 6 mm die containing 101 ± 4 mg of material at a speed of 60 mm/min. Tablets were made in triplicate at three compaction pressures: 40 MPa, 120 MPa and 180 MPa.

After ejection, the compacts were left overnight to allow for elastic recovery and then the compact thickness measured using calipers (Mitutoyo Ltd.,

Hampshire, UK). The tablet hardness was tested using the GTP at a speed of 1 mm/min.

6.2.5.2 Sticking Propensity

The sticking propensity of the powder to the base die was captured during the tabletability measurements using a novel approach, shown in Figure 6.4. After tablet compression (prior to ejection), the detachment stress of the base die was measured manually using a 50 kg hand held force gauge (Mecmesin, Slinfold, UK) placed at the side of the base die. Detachment measurements were made in triplicate.
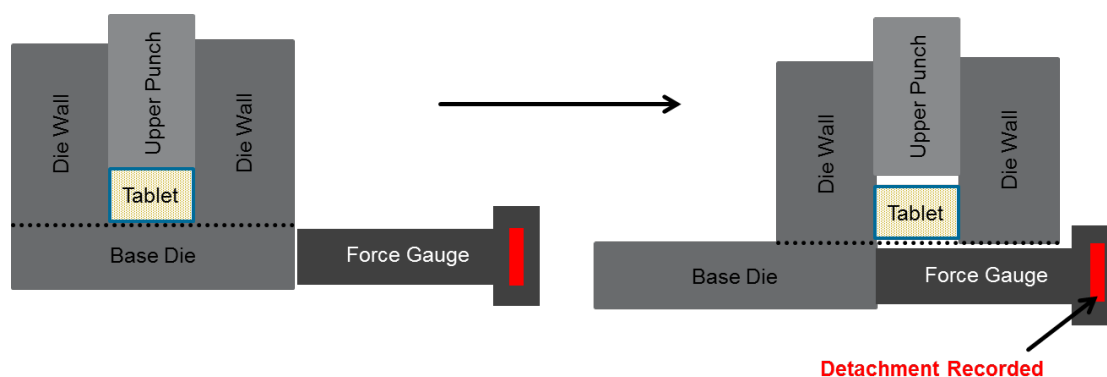
Figure 6.4 – Detachment test developed to measure sticking propensity on the Gamlen tablet press.

6.3   Results and Discussion

6.3.1   Recrystallisation of Ibuprofen

The yield for each crystallisation reaction was variable with hexane only returning 61% of starting material whereas toluene returned the most with 81% yield (Table 6.1). The low yields are not typical for pharmaceutical processes however the supersaturated solutions that were prepared were viscous which resulted in product coating the reactor vessel. Care was also taken when the product was removed from the vessel to try and minimise

particle breakage. The foregoing factors contribute to the low yield. There is no correlation between the polarity of the recrystallisation solvent and yield.

The sample names used to represent each product are shown in Table 6.2. Each sample is also represented by a colour and these names and colours will be used to represent each sample in the materials characterisation sections.

Table 6.2 – Sample names and colours used to represent each ibuprofen recrystallisation product.

Recrystallisation Solvent	Sample Name	Colour used to Represent Samples
Hexane	IbuHex	Blue
Toluene	IbuTol	Purple
Acetonitrile	IbuAce	Green
Ethanol	IbuEth	Red

6.3.2 Particle Size and Shape Characterisation

Scanning electron microscopy (SEM) was utilised to visualise the particle morphology of each crystallised batch. The electron micrographs are shown in Figure 6.5 and confirm the crystallisation was successful in producing particles with different particle shapes.

As expected, from data in the literature [136, 147], increasing the solvent polarity (hexane<toluene<acetonitrile<ethanol) increases the particle shape regularity. The non-polar solvents, hexane and toluene, produce needle and lath shaped particles, respectively whereas acetonitrile produces plate shaped particles. The most polar solvent used, ethanol, results in both plate and prismatic shaped ibuprofen particles.
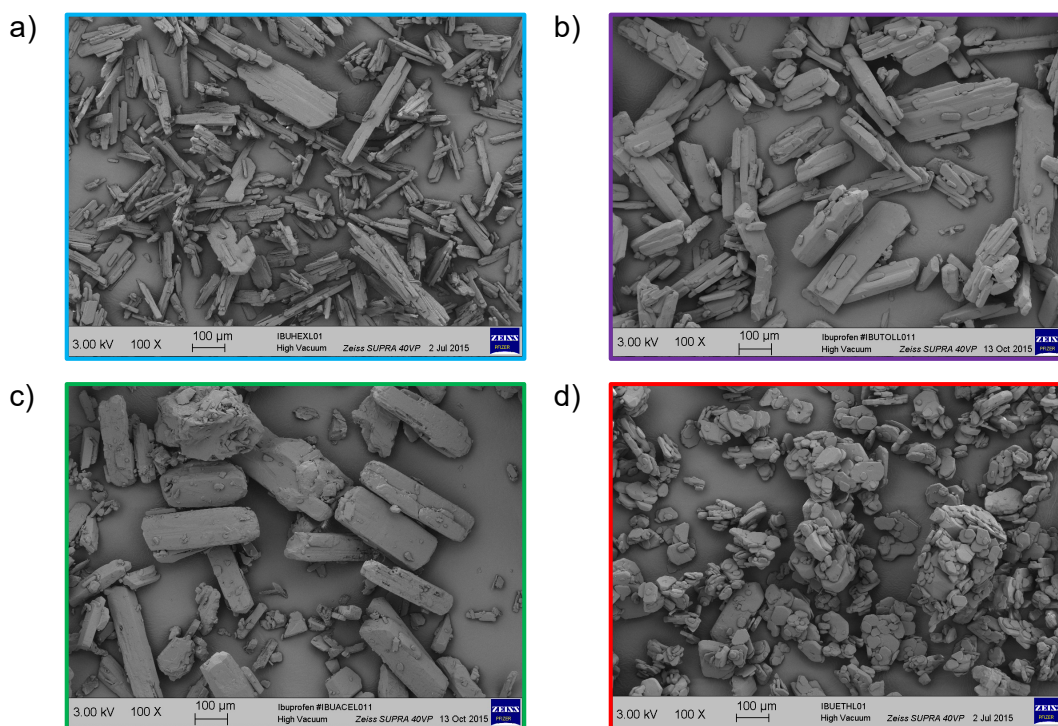
Figure 6.5 – Scanning electron micrographs of recrystallised ibuprofen showing changes in particle shape a) IbuHex (needle/lath shaped) b) IbuTol (lath shaped) c) IbuAce (plate shaped) d) IbuEth (plate/prismatic shaped). All images captured using x100 magnification and the scale bar represents 100 µm.

6.3.2.1 Sieving

In order to remove any large agglomerates formed during the crystallisation, all batches were passed through a 1.25 mm sieve. In order to try and achieve a consistent size distribution between shapes the batches were passed through a 150 µm mesh and details of all batches produced are listed in Table 6.3.

Table 6.3 – Sample names and details of mesh sizes produced from sieving crystallised ibuprofen.

Crystallised sample name (bulk)	0 – 1.25 mm sample name	0 – 150 µm sample name
IbuHex	IbuHex (0 – 1.25 mm)	IbuHex (0 – 150 µm)
IbuTol	IbuTol (0 – 1.25 mm)	IbuTol (0 – 150 µm)
IbuAce	IbuAce (0 – 1.25 mm)	IbuAce (0 – 150 µm)
IbuEth	IbuEth (0 – 1.25 mm)	IbuEth (0 – 150 µm)

6.3.2.2 Dynamic Image Analysis

QICPIC particle size analysis was performed on all samples and the number distributions (most sensitive to smaller particles in the sample) for the 0 – 1.25 mm samples are shown in Figure 6.6a. The number values are provided in Table 6.4. The data reveals that batches IbuHex and IbuTol, which contain needle/lath shaped particles, contain a similar distribution of particles. Batches IbuAce and IbuEth which contain plate/prismatic shaped particles also contain a similar distribution of particles.

Table 6.4 – QICPIC number particle size values for ibuprofen (0 – 1.25 mm mesh size).

Sample	D[n,0.1] (µm)	D[n,0.5] (µm)	D[n,0.9] (µm)	Mean by number (µm)
IbuHex (0 – 1.25 mm)	6.9	27.8	83.5	38.6
IbuTol (0 – 1.25 mm)	6.9	27.7	92.4	42.2
IbuAce (0 – 1.25 mm)	6.8	22.4	73.9	35.7
IbuEth (0 – 1.25 mm)	6.9	28.0	82.9	39.1

The volume distributions (most sensitive to larger particles in the sample) are shown in Figure 6.6b and the volume particle size values are shown in Table 6.5. The data reveals that, by volume, all samples exhibit non-normal distributions and there is a large variation between samples. In general, the distributions contain a primary mode which is related to the primary particle size and then secondary modes which are shown to be both large primary particles and agglomerates by examination of the SEM micrographs and QICPIC particle gallery.

Table 6.5 – QICPIC volume particle size values for ibuprofen (0 – 1.25 mm mesh size).

Sample	D[v,0.1] µm	D[v,0.5] µm	D[v,0.9] µm	D[4,3] µm
IbuHex (0 – 1.25 mm)	62.4	138.1	329.1	173.1
IbuTol (0 – 1.25 mm)	95.1	295.0	1011.7	435.1
IbuAce (0 – 1.25 mm)	116.7	360.2	724.8	397.6
IbuEth (0 – 1.25 mm)	74.5	267.8	530.6	295.0
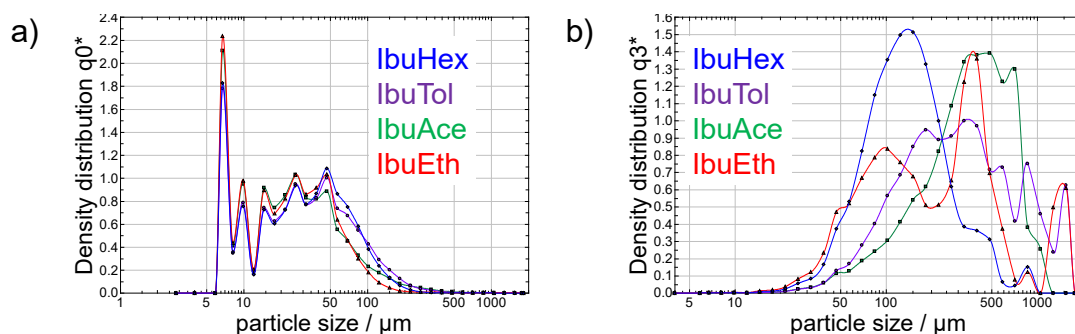
Figure 6.6 – QICPIC a) number and b) volume weighted distributions for ibuprofen (0 - 1.25 mm mesh size).

Example QICPIC particle images are shown in Figure 6.7 where the agglomerated particles and large primary particles for batch IbuAce are highlighted.   The average volume data, D[4,3], ranks the batches as follows; IbuHex>IbuEth>IbuAce>IbuTol revealing that there is no correlation between crystallisation solvent polarity and size.
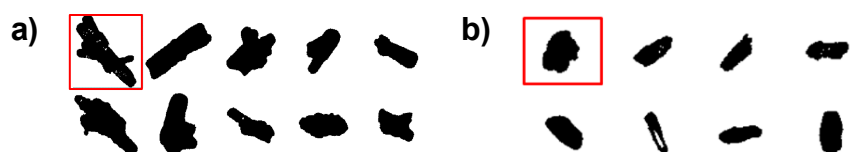
Figure 6.7 – QICPIC particle images for IbuAce (0 – 1.25 mm) a) large agglomerated particles, where the particle highlighted has a maximum feret diameter of 850.9 µm, and b) large primary particles, where the particle highlighted has a maximum Feret diameter of 440 µm.

The number distributions (most sensitive to smaller particles in the sample) for the 0 – 150 μm samples are shown in Figure 6.9a. The number values are provided in Table 6.6. It should be noted that although the batches were passed through a 150 μm sieve they all contain a proportion of particles greater than the sieve mesh size. This can be attributed to two causes: elongated particles passing through the mesh along their shortest axis and also the data is reported using Feret max, the particles longest diameter, giving rise to values larger than 150 μm. The distributions reveal that IbuAce contains a higher proportion of fine (around 5 μm) particles and the lowest proportion of coarse material (50 – 400 μm).

Table 6.6 – QICPIC number particle size values for ibuprofen (0 – 150 μm mesh size).

Sample	D[n,0.1] μm	D[n,0.5] μm	D[n,0.9] μm	Mean by number (μm)
IbuHex (0 – 150 μm)	6.9	27.2	80.9	37.3
IbuTol (0 – 150 μm)	7.0	32.2	101.1	45.1
IbuAce (0 – 150 μm)	6.9	24.0	85.5	38.0
IbuEth (0 – 150 μm)	7.0	33.6	104.3	46.0

The volume distributions, shown in Figure 6.9b (volume number values: Table 6.7), reveal that for IbuAce the primary mode is centered at ~250 μm which is higher than all other batches (centered at ~125 μm), inferring that this batch has the widest size distribution. All other batches contain a similar proportion of particles by number and have primary modes centering around 125 μm by volume.

The images of the particles analysed were examined and revealed that the sieving was successful in removing the agglomerated and large primary particles in all batches and the size distributions represent primary particle sizes (an example for IbuAce is shown in Figure 6.8a). The small second peak (~1000 μm) in the volume distribution of IbuAce was shown to be a single fibrous particle and therefore can be excluded from analysis (Figure 6.8b).
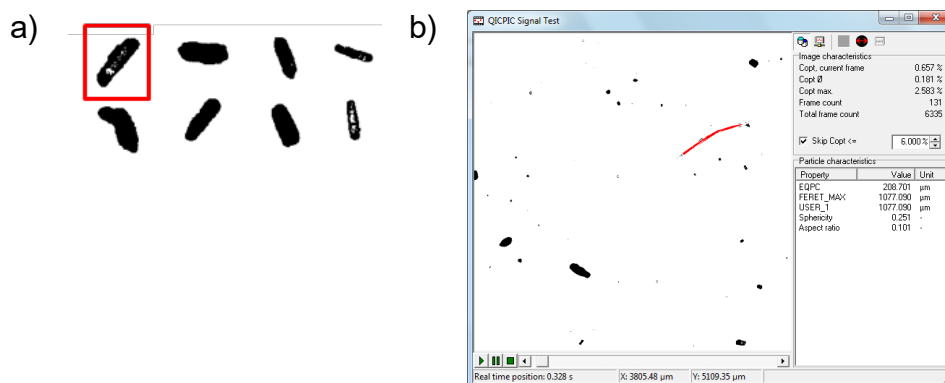
Figure 6.8 – QICPIC particle images for IbuAce (0-150 µm) a) primary particles where the particle highlighted has a maximum feret diameter of 445.3 µm and b) fibrous particle highlighted in red giving rise to the second peak in IbuAce volume distribution.

Table 6.7 – QICPIC volume particle size values for ibuprofen (0-50 µm mesh size).

Sample	D[v,0.1] µm	D[v,0.5] µm	D[v,0.9] µm	D[4,3] µm
IbuHex (0 – 150 µm)	57.7	122.9	237.3	138.5
IbuTol (0 – 150 µm)	71.6	145.3	257.2	156.7
IbuAce (0 – 150 µm)	84.7	206.5	361.3	225.4
IbuEth (0 – 150 µm)	70.7	134.2	227.8	143.0
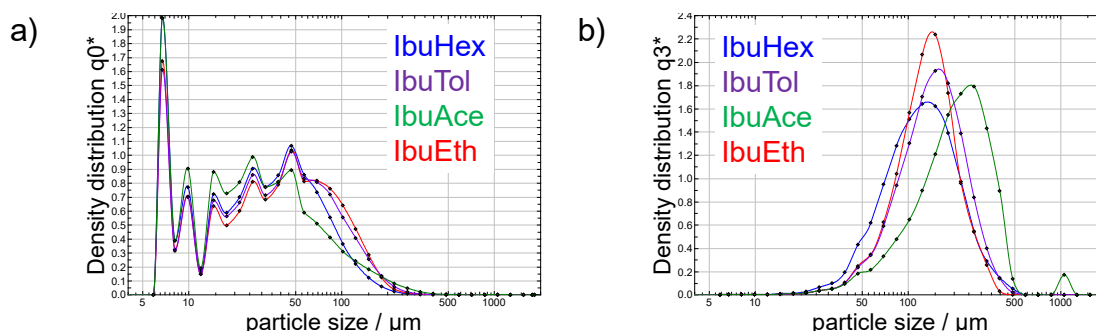
Figure 6.9 – QICPIC a) number and b) volume weighted distributions for ibuprofen (0 – 150 µm mesh size).

The aspect ratio (width / length) versus particle size for 0 – 1.25 mm batches and 0 – 150 µm batches is shown in Figure 6.10a and Figure 6.10b, respectively. The aspect ratio for both size fractions confirms the visual observations made from the SEMs that shape changes trend with

crystallisation solvent polarity. The aspect ratio of all batches decreases as size increases. The most polar solvent, ethanol, results in particles with the highest aspect ratio, 0.55 – 0.73 for 0 – 1.25 mm batch and 0.40 – 0.73 for 0 – 150 μm batch compared to the least polar solvent, hexane, which contains particles with the lowest aspect ratios, 0.40 – 0.70 for both 0 – 1.25 mm and 0 – 150 μm batches.

These extreme batches exhibit the greatest difference in aspect ratio, 0.25, around 300 μm for 1.25 mm batches. For the smaller size range material, 0 – 150 μm, the greatest difference, 0.23, is observed around 190 μm.
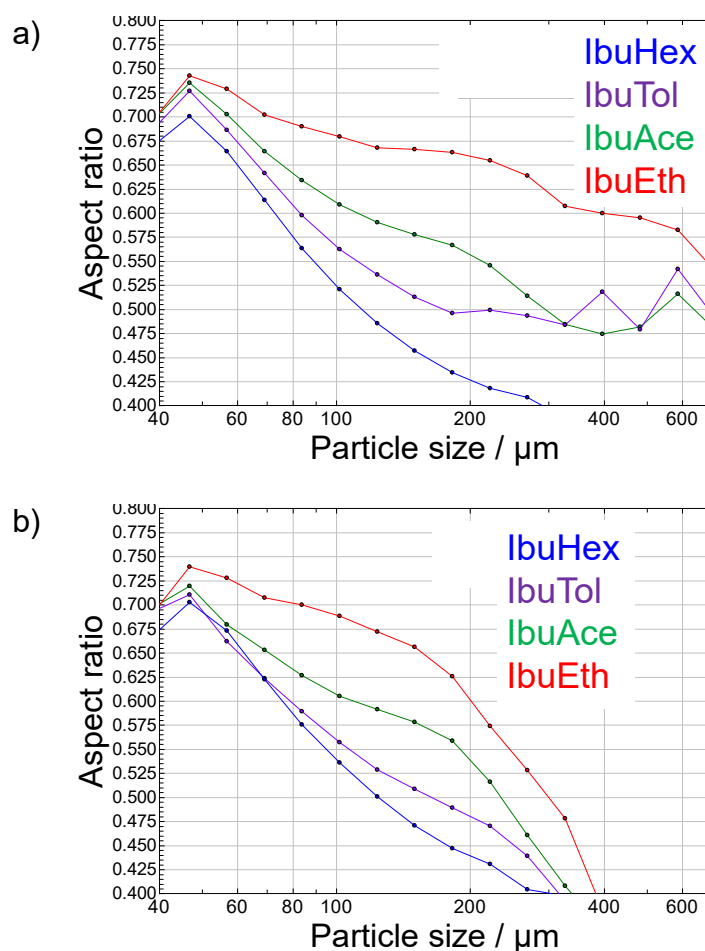
Figure 6.10 – QICPIC aspect ratio (width/length) a) ibuprofen (0 – 1.25 mm) and b) ibuprofen (0 – 150 μm).

6.3.3 Solid Form and Analytical Characterisation

This section describes the material characterisation techniques utilised to determine that no form changed had occurred during recrystallisation and also that the batches were dry from both water and recrystallisation solvent.

6.3.3.1 Powder X-ray Diffraction

It was expected that no form change, from *(RS)*-ibuprofen form I, would occur during the recrystallisation of ibuprofen as the only other form reported, form II [175], was prepared by annealing. PXRD was performed to confirm this result. The diffraction patterns for the recrystallised samples are shown in Figure 6.11 and reveal that all peaks present in the diffractograms are aligned. Perhaps, not unexpectedly, there is some impact on the PXRD intensities due to the morphology of the samples. Some preferred orientation is seen in Figure 6.11, especially from needles crystallised from hexane (a). This data confirms that no form change has occurred during the recrystallisation and that the form present is *(RS)*-ibuprofen form I due to the mild crystallisation conditions used.
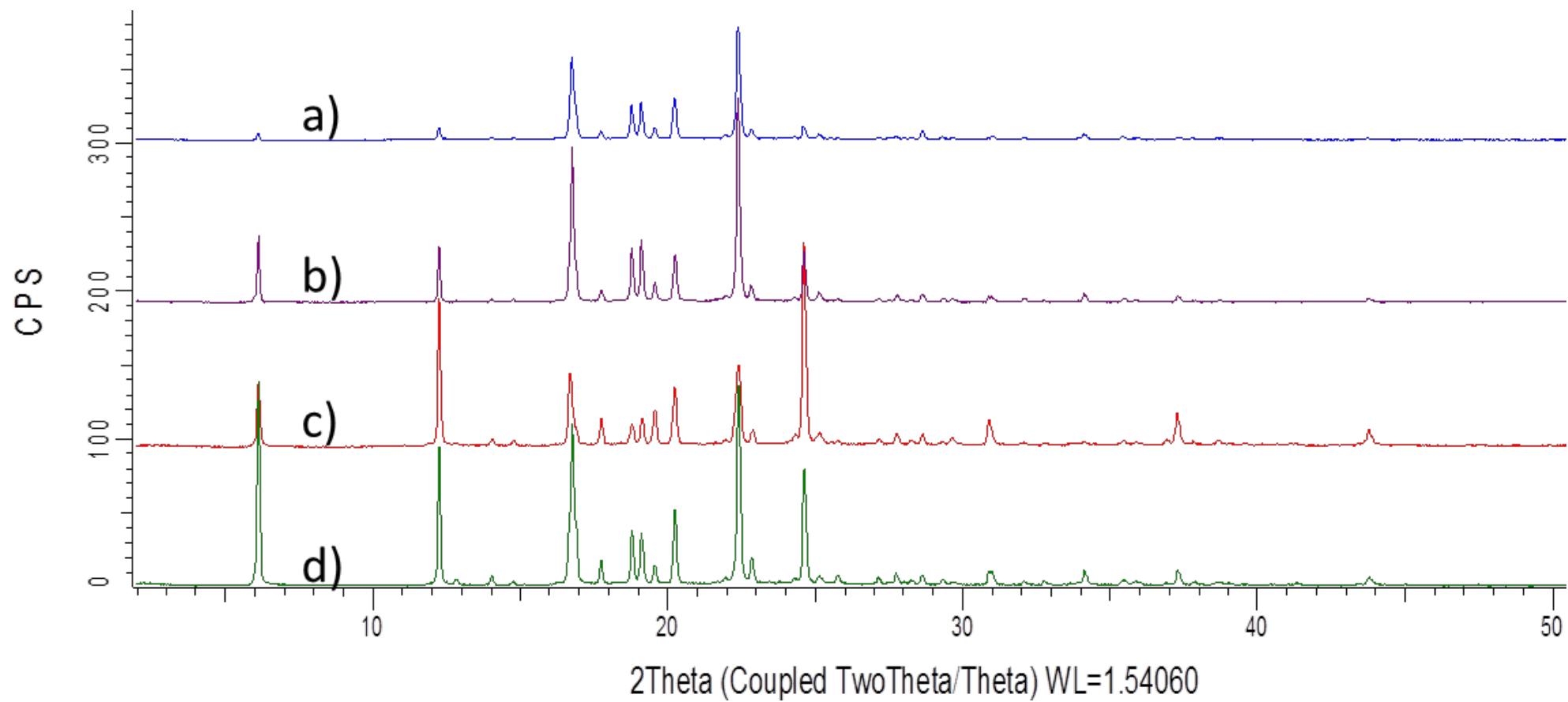
Figure 6.11 – Powder X-ray diffraction patterns for recrystallised ibuprofen batches a) IbuHex, b) IbuTol, c) IbuEth, and d) IbuAce.

6.3.3.2 Differential Scanning Calorimetry

The DSC thermograms for all samples are shown in Figure 6.12 and reveal no major differences between the melt of the samples. The onset of the melt was extrapolated using Trios software (TA Instruments, Herts, UK) and was shown to be similar for all samples, with the melt range being 73.6 – 74.5°C. The peak melting temperatures were found to be within the range 75.8 – 76.1°C. The enthalpy of fusion values for recrystallised ibuprofen batches were shown to be; 123.2 J/g for IbuHex, 126.8 J/g for IbuTol, 127.4 J/g for IbuAce and 118.6 J/g for IbuEth. It can be seen that there is some variation between the samples with IbuEth exhibiting the lowest enthalpy and IbuAce exhibiting the highest, however they are all form I as the reported enthalpy of fusion for form II is 33.9 J/g and this form is unstable at room temperature [175].
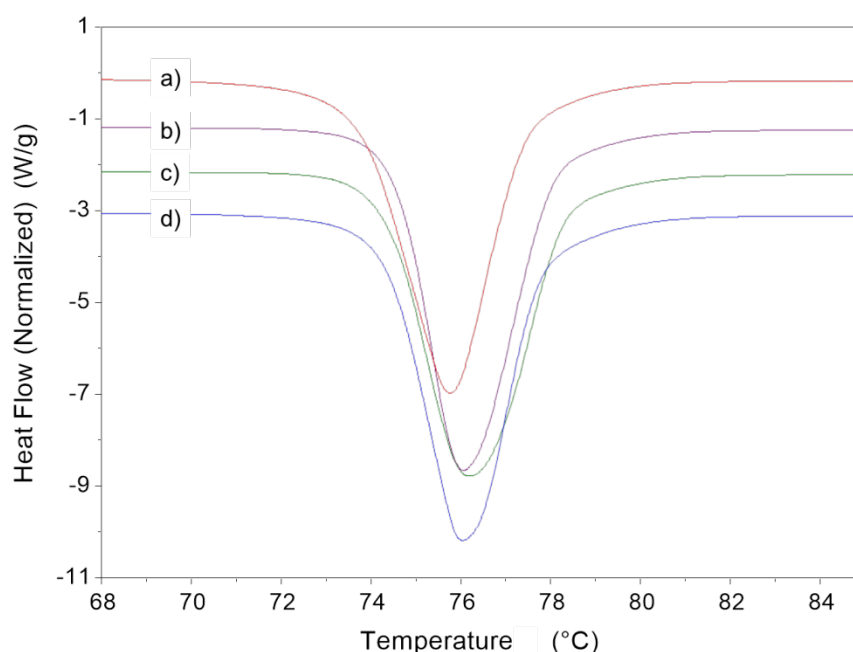
Figure 6.12 – DSC thermograms of recrystallised ibuprofen a) IbuEth, b) IbuTol, c) IbuAce and d) IbuHex.

6.3.3.3 Evolved Gas Analysis

Evolved gas analysis was conducted to monitor the weight loss of ibuprofen samples due to water or crystallisation solvents. The combined TGA and MS

traces for all samples are shown in Figure 6.13. The TGA trace shows no significant weight loss for each sample up to and after the melt (30 – 100°C). There is also no significant response from the MS for the mass ions monitored, therefore suggesting that the samples are free from water/solvent.

a)

b)

c)

d)
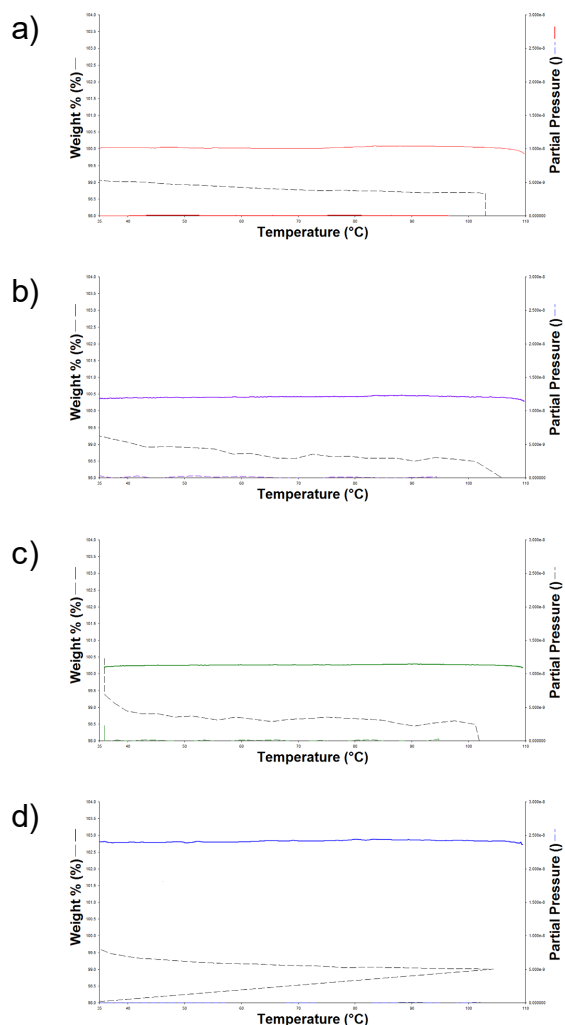
Figure 6.13 – EGA traces for recrystallised ibuprofen batches a) IbuEth, b) IbuTol, c) IbuAce and d) IbuHex.

6.3.3.4 <u>Headspace-gas Chromatography</u>

The respective volatile organic solvent for each recrystallised batch was quantified using HS-GC and the resultant residual solvent levels are shown in Table 3.2. The residual solvent levels are low (≤180 PPM) and are below the

maximum acceptable daily exposure guidelines, as set by ICH Q3C (R6) 2016 [99].

Table 6.8 – Residual solvent revels for recrystallised ibuprofen batches.

Batch	Solvent tested for	Residual solvent levels (PPM)	Maximum daily exposure: ICH Q3C(R6) Guidelines (PPM)
IbuHex	Hexane	20	290
IbuTol	Toluene	20	890
IbuAce	Acetonitrile	Not detected	410
IbuEth	Ethanol	180	5000

The characterisation of these batches of ibuprofen using PXRD, DSC, EGA and HS-GC revealed that they were of the same form, highly crystalline and dry from both recrystallisation solvent and water.

6.3.4 Investigating the Effect of Particle Shape on Ibuprofen Manufacturability

To investigate the impact of particle shape with minimal impact from particle size on ibuprofen manufacturability, batches (0 – 150 µm) were analysed in this study.

6.3.4.1 Tabletability

The tabletability of recrystallised ibuprofen batches (0 – 150 µm) is shown in Figure 6.14. At the lowest compaction pressure, around 40 MPa, the tensile strength of tablets increases as the aspect ratio decreases. Tablets produced from batch IbuEth (plate/prismatic shaped particles) exhibited the lowest tensile strength, 0.4 MPa, compared to batch IbuHex (needle/lath shaped particles) which produced tablets with the highest tensile strength, 1.0 MPa.

This trend still holds true for batches IbuHex, IbuTol and IbuEth at the middle compaction pressure, around 120 MPa; however, batch IbuAce is the exception. Batch IbuAce, which contains only plate shaped particles, exhibited tablet lamination at the middle and highest compaction pressure; therefore, the tensile strength of these tablets is compromised. This is evident at the middle and highest compaction pressure where this batch produced tablets with the lowest tensile strength compared to all other batches and a large error is present at the highest compaction pressure due to the lamination. The other batches did not laminate (including batch IbuEth which contains a mixture of plate/prismatic shaped particles), therefore a cause of lamination in batch IbuAce may be due to the purely plate shaped particles lying flat during compaction preventing interlocking. The particle size data from this batch revealed it to have the widest size distribution as well as the largest size by volume which could be causing weak tablets, as smaller particles generally increase tensile strength.

At the highest compaction pressure, around 180 MPa, it is clear that batch IbuHex still produces tablets with higher tensile strengths compared to the other materials. For all the batches, except IbuEth, there is little increase in the tensile strength between the middle and highest compaction pressure which suggests that a high tablet density may have been reached. The physical differences in shape will affect the initial packing of particles where it is assumed elongated particles will lie flat and when compressed the maximum tensile strength will be reached with less pressure compared to more regular shaped particles which will have greater spacing between them, meaning more pressure is required to reach the maximum tensile strength.
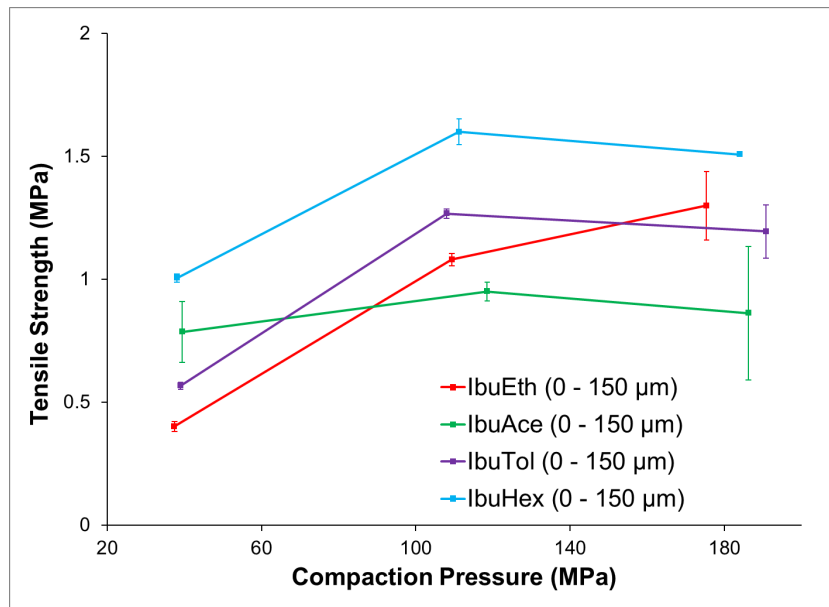
Figure 6.14 – Tabletability of recrystallised ibuprofen. Error bars represent standard deviation of three measurements.

This data reveals that there is an optimum particle shape for direct compression of ibuprofen tablets dependent on compaction pressure. At all compaction pressures needle/lath shapes particles have a greater tabletability performance over other batches; however, purely plate shaped particles show lamination.

6.3.4.2 Sticking Propensity

The sticking propensity of the batches was measured by recording the detachment stress from the base die post compaction. It is proposed that higher stresses relate to more powder adhering to the die, in turn inferring a greater sticking propensity. The detachment stress measurements at three compaction pressures are shown in Figure 6.15.
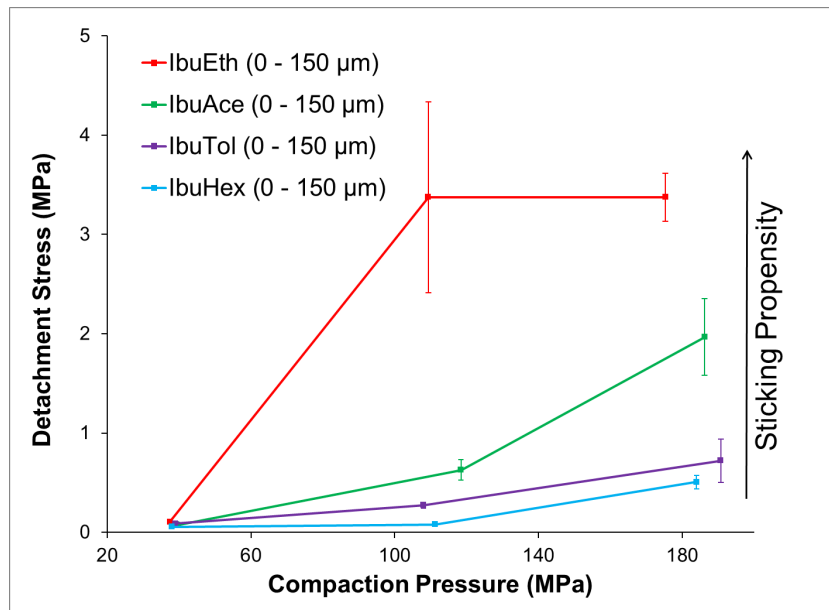
Figure 6.15 – Sticking propensity of recrystallised ibuprofen to the base die. Error bars represent standard deviation of three measurements.

At the lowest compaction pressure all samples exhibit no sticking and low detachment stress readings (≤0.1 MPa). As the pressure increases the detachment stress values diverge and the largest difference is observed at the highest compaction pressure (around 180 MPa). Representative images of the base die are shown in Figure 6.16 and the visual observation of material adhered correlate with the detachment stress values. Thus the batches can be clearly ranked in terms of their shape, where sticking increases as aspect ratio increases: IbuHex<IbuTol<IbuAce<IbuEth. When sticking is detected the standard deviations of the measurements generally increase, and large variation is observed at 108 MPa for IbuEth. This variation could be attributed to the random nature of the sticking event or could be a limitation of the hand held force gauge used in this measurement. Despite this, the sticking trend is still clear and it can be concluded that the sticking propensity of ibuprofen increases as a result of a higher aspect ratio.

IbuHex   IbuTol   IbuAce   IbuEth

Sticking Propensity
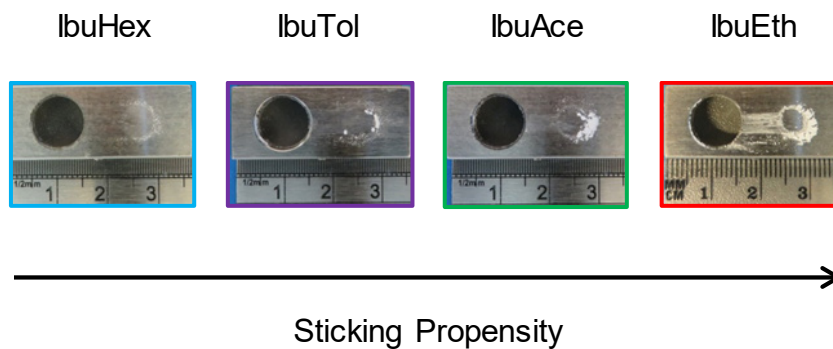
Figure 6.16 – Images of the base die after compaction of recrystallised ibuprofen.

This study reveals that ibuprofen needle/lath shaped particles crystallised from hexane show the best manufacturing performance in terms of tabletability and sticking propensity.

6.3.5 Investigating the Effect of Particle Size on Ibuprofen Manufacturability

To understand the impact that particle size has on the manufacturability of the different particle shape the two different sieve fraction of the extreme crystal habits (IbuHex: needle/lath shaped particles and IbuEth: plate/prismatic shaped particles) will be compared in this study.

6.3.5.1 Tabletability

The tabletability of recrystallised ibuprofen sieve fractions 0 – 150 μm and 0 – 1.25 mm for batches IbuEth and IbuHex are shown in Figure 6.17. Despite the difference in size it is clear that at all compaction pressures the needle/lath shaped particles (IbuHex) produce tablets with a higher tensile strength than prismatic/plate shaped particles (IbuEth). At the highest compaction pressure (around 180 MPa) the greatest difference between particle shape exists. The larger sieve fraction (0 – 1.25 mm) for IbuEth produces slightly weaker tablets compared to the smaller sieve fraction (0 –

108

150 µm). From the size analysis it was shown that the larger sieve fraction contained a proportion of large primary particles and agglomerates which were removed in the smaller sieve fraction. It is possible that reducing the agglomeration in the smaller sieve fraction has allowed the smaller regular shaped particles to be in closer contact therefore resulting in stronger tablets. The opposite trend is observed for the needle/lath shaped particles, where the larger sieve fraction forms stronger tablets than the smaller sieve faction. In the case of the needle shaped particles it is likely that these will pack horizontally the same whether they are small / large in size and in fact the agglomeration is providing a variety of shapes and sizes increasing particle interlocking therefore increasing tablet tensile strength. The needle shaped particles are also more likely to break than the regular shaped particles; therefore, the proportion of fines could increase giving rise to stronger tablets in both cases.

From this study it is clear that the size of the different particle shapes has minimal impact on the tablet tensile strength and it is in fact particle shape that is driving the differences observed in tabletability.
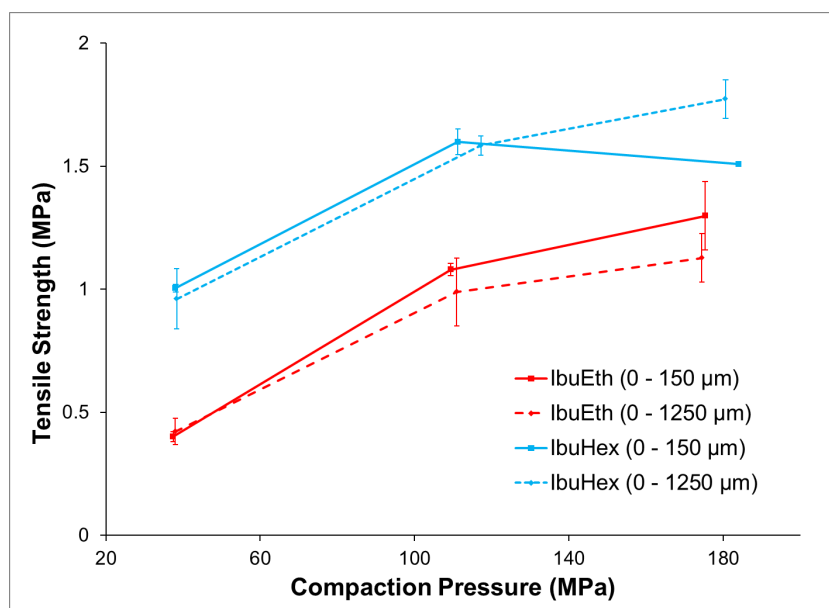
Figure 6.17 – Tabletability of recrystallised ibuprofen batches (IbuHex and IbuEth) with different size fractions (0 – 150 µm and 0 – 1.25 mm). Error bars represent standard deviation of three measurements.

6.3.5.2 <u>Sticking Propensity</u>

The detachment stress measurements at three compaction pressures for sieve fractions 0 – 150 µm and 0 – 1.25 mm for batches IbuEth and IbuHex are shown in Figure 6.18. The larger size fractions (0 – 1.25 mm) follow the same trend as the small size fractions (0 – 150 µm), indicating that the differences observed are due to the differences in particle shape not particle size.

At the highest compaction pressures (around 180 MPa) the smaller sieve fraction for IbuHex shows slightly higher sticking (0.5 MPa) than the larger sieve fraction (0.1 MPa). This slight increase in sticking could be due to particle size where the smaller sieve fraction contains a higher proportion of fine particles compared to the larger sieve fraction.
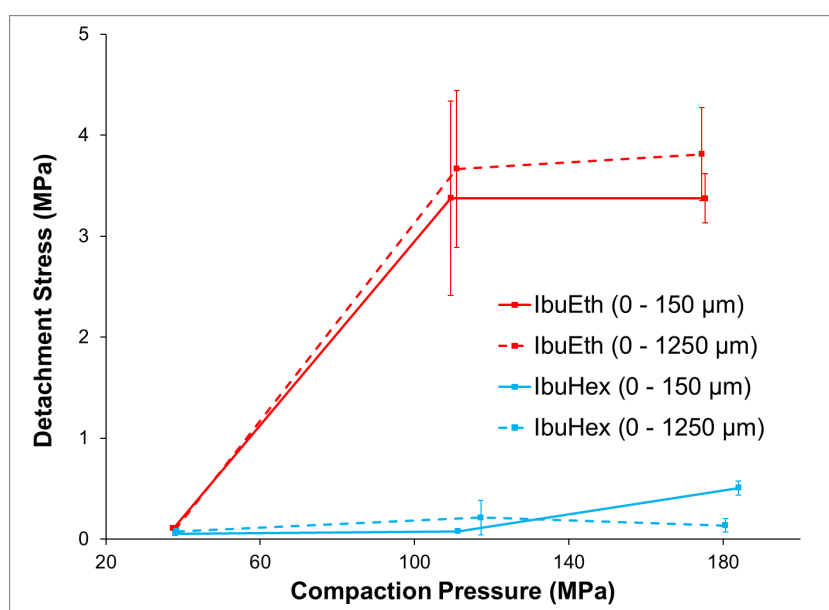
Figure 6.18 – Sticking propensity of recrystallised ibuprofen with different size fractions. Error bars represent standard deviation of three measurements.

From this study it is clear that the size of the different shapes has minimal impact on the sticking propensity and it is in fact particle shape that is driving the behaviour.

6.3.6 Investigating the Effect of Particle Shape Mixtures on Ibuprofen Manufacturability

Ibuprofen shape mixtures were prepared by mixing different concentrations of shapes. The extreme particle shape batches with similar particle size, IbuHex 0 – 150 µm and IbuEth 0 – 150 µm, were used and labelled as needles and cubes, respectively for the ease of display. Due to the low sample size blend homogeneity was assumed.

6.3.6.1 Tabletability

The tabletability of four ibuprofen mixtures containing different concentrations of particle shapes (75% needles:25% cubes, 50% needles:50% cubes, 25% needles:75% cubes and 10% needles:90% cubes) were compared against the 'as crystallised' batches (100% needles and 100% cubes) are shown in Figure 6.19. At all compaction pressures the tensile strength of tablets decreases as the percentage of cubes in the mixture increases. The outlier to this trend is the mixture which contains 10% needles and 90% cubes where this batch performs the worst out of all.
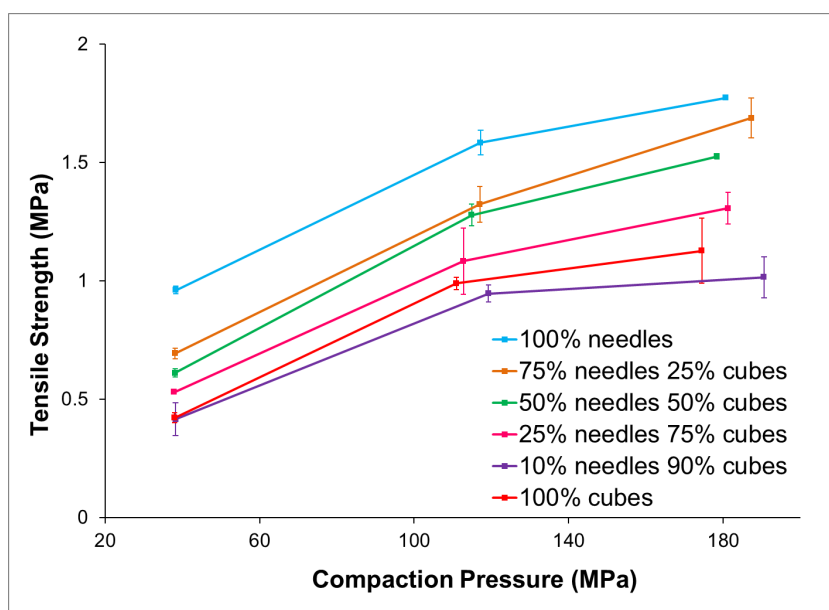
Figure 6.19 – Tabletability of ibuprofen API shape mixtures. Error bars represent standard deviation of three measurements.

Despite this outlier a correlation can be made between the tensile strength of tablets at 180 MPa and the percentage of cubes in the mixtures, shown in Figure 6.20. As the percentage of cubes in the blend increases, the tensile strength of the tablets decreases linearly with an R^2 value of 0.9253.
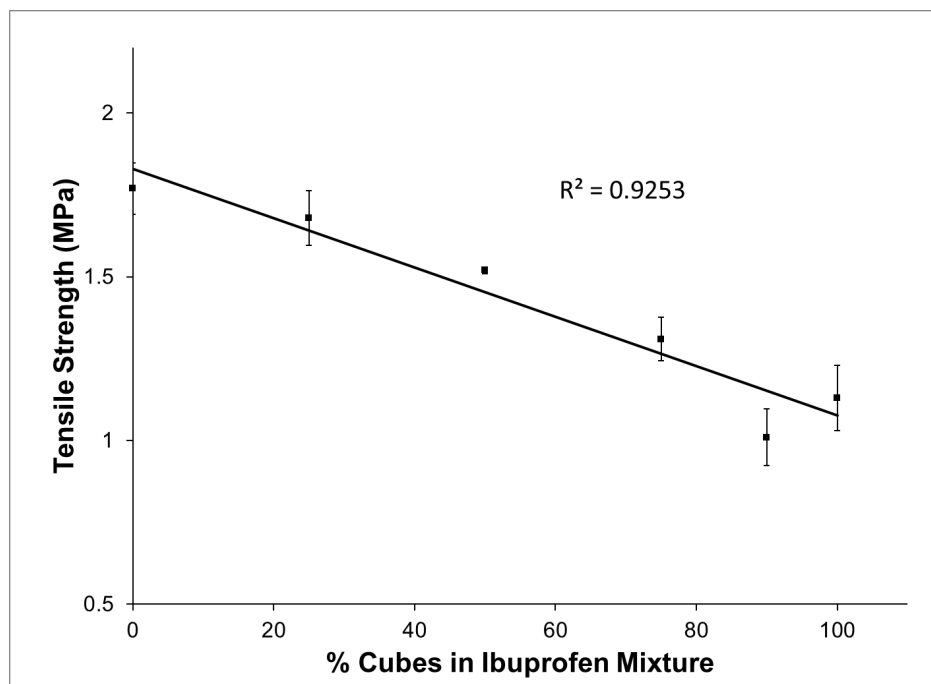
Figure 6.20 – Linear relationship between the tensile strength of tablets made at 180 MPa with different percentages of cube shaped particles in the mixture.

This research has shown that more needle shaped particles form stronger tablets than more regular shaped particles. It is known that particle shapes influences the flow of powders where spherical particles have enhanced flow properties over needle shaped particles. It is therefore unlikely that the high tensile strength values alone would drive a change in API particle shape and instead formulators may try to add excipients to mask sticking and improve the formulation. This study has revealed that a mixture of particle shapes could be used to gain optimum tensile strength of ibuprofen tablets (1.7 MPa for 80% needles 20% cubes). Although the flow of the mixtures was not measured in this study it is thought that a mixture containing a percentage of cube shaped particles would flow better than a batch which contained 100% needle shaped particles.

112

6.3.6.2 <u>Sticking Propensity</u>

The detachment stress measurements of four ibuprofen mixtures containing different concentrations of particle shapes (75% needles:25% cubes, 50% needles:50% cubes, 25% needles:75% cubes and 10% needles:90% cubes) compared against the 'as crystallised' batches (100% needles and 100% cubes) are shown in Figure 6.21.

At the lowest compaction pressure all samples exhibit no sticking and low detachment stress readings (≤0.1 MPa). At the middle compaction pressure all mixtures exhibit low detachment stress readings and cannot be ranked apart from 10% needles:90% cubes where the detachment stress value is 1.5 MPa. At the highest compaction pressure more divergence between the mixtures is observed where all mixtures exhibit some degree of sticking, except 75% needles:25% cubes which behaves more similarly to the 100% needle batch.
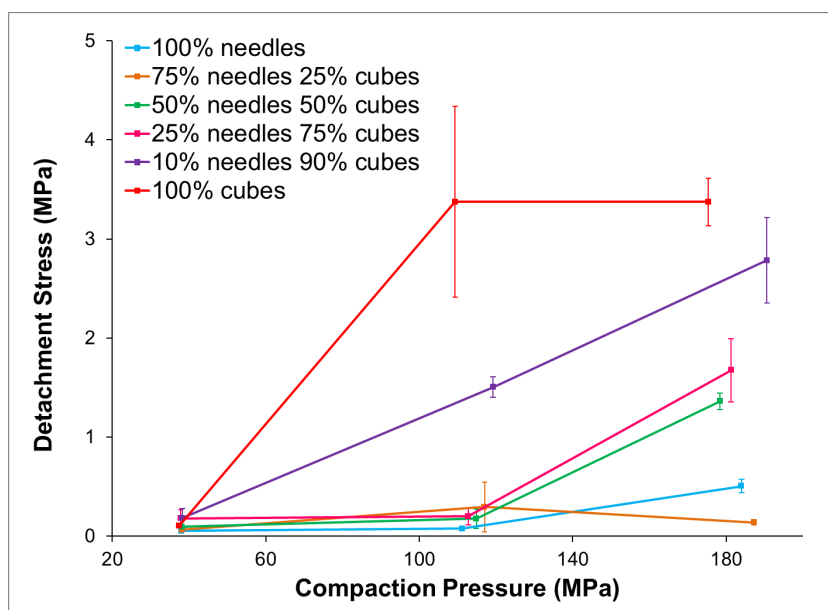
Figure 6.21 – Sticking propensity of ibuprofen API shape mixtures to the base die. Error bars represent standard deviation of three measurements.

An exponential trend can be seen between the sticking propensity of mixtures at 180 MPa and the percentage of cubes in the mixture. This trend is different to the linear trend observed for the tensile strength and its exponential nature may be due to the fact that once sticking has occurred more material is likely to stick because of different surface properties of the punch. As mentioned previously, needles are not optimum for flow reasons, therefore a mixture of shapes may be more convenient. The 80% needle:20% cube mixture exhibits high tensile strengths (1.7 MPa) and low sticking propensity (<0.1 MPa) meaning that this mixture may be ideal for direct compression of ibuprofen tablets.
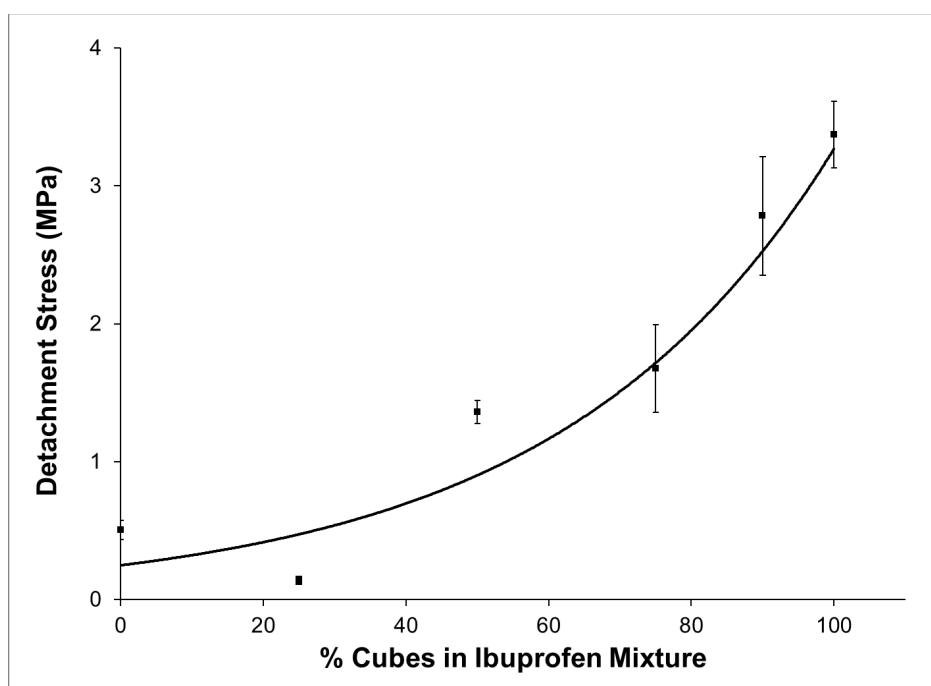
Figure 6.22 – Relationship between the detachment stresses of tablets made at 180 MPa with different percentage of cube shaped particles in the mixture.

The differences in the tensile strength of tablets could be attributed to the physical differences in particle shape, however a trend between sticking and tensile strength of tablets can also be made between the mixtures. As sticking increases tensile strength decreases, which may be due the surface defects in the tablets caused by the powder sticking.

114

6.4 Conclusions

A suite of materials characterisation tools have been utilised to understand the effect of API particle shape on its subsequent manufacturability. Ibuprofen was recrystallised using four solvents of varying polarity and produced diverse particle habits: needle/lath shaped, lath shaped, plate shaped and plate/prismatic shaped. The batches were shown to be of the same form, highly crystalline and free from both recrystallisation solvent and water.

The batches were sieved to give comparable size distributions and the effect of shape on tabletability and sticking propensity measured using a GTP-1. The tensile strength of tablets could not be directly correlated with aspect ratio however differences in tensile strength between the different particle shapes were revealed.   The needle/lath shaped particles formed the strongest tablets at all compaction pressures, which could be due to the initial packing arrangement of particles.   The sticking propensity correlated with aspect ratio where a higher aspect ratio (plate/prismatic shaped particles) resulted in tablets that were more likely to stick than particles with a lower aspect ratio (needle/lath shaped particles).   From this is can be concluded that in terms of manufacturability, needle/lath shaped particles are the optimum shapes producing tablets with high tensile strengths and low propensity to stick.

As needles can compromise other parts of the manufacturing process, such as flow, the tabletability and sticking propensity of API mixtures containing varying proportions of different shaped particles were measured. It was found that increasing the concentration of plate/prismatic shaped particles in a mixture decreased the tensile strength of compacts linearly (measured at 180 MPa, starting with 100% needle/lath shaped mixture).   The sticking propensity of these mixtures increased exponentially as the percentage of cubes was increased therefore suggesting that there may be a middle ground where a mixture could be used to minimise sticking and maximise tensile strength but also produce suitable flow properties.

The tabletability and sticking propensity of two size fractions (0 – 150 μm and 0 – 1.25 mm) of the extreme particle shapes (needle lath shaped and plate prismatic shaped) were compared. The effects on tabletability and sticking propensity relating to differences in particle size were shown to be minimal; again confirming that the observed difference in manufacturability is driven by particle shape.

7. Chapter Seven: Towards a Grammar of Surface Chemistry

7.1 Introduction

The surface energy of powders has been shown to affect API properties such as dissolution, flowability and cohesion and adhesion [176 - 178]. Despite this, it is difficult to rank powders in terms of their surface energy due to pharmaceutical powders all having relatively similar values. In terms of manufacturability, previous work has shown that a higher powder surface energy leads to greater interparticulate cohesion, hence a higher tensile strength of tablets [179].

It is known that surface energy is affected more by a change in particle shape rather than particle size, due to the different chemical functionalities present at each surface [180]. The research reported in chapter six revealed that a change in particle shape drove the subsequent manufacturing behaviour of APIs in terms of tabletability and sticking propensity. The sticking propensity directly correlated with aspect ratio therefore the work reported in this chapter seeks to investigate links between surface properties and manufacturing behaviour. A brief theoretical review of surface energy techniques is provided.

7.1.1 Surface Energy Theory

In chapter two a description of a crystal lattice was given, where crystalline materials are formed of repeating molecules in three-dimensional space. When a solid surface is created the molecular interactions at the surface have been disrupted and, therefore, display a higher energy compared to the molecules within the bulk. The surface free energy quantifies this distribution and is defined as the energy required to produce a unit area of surface. The total surface energy (γ_t) of a surface can be split into two different types, as described by Fowkes [181],:

$$\gamma_t = \gamma_d + \gamma_{ab} \qquad\qquad (16)$$

Where γ_d represents dispersive interactions and γ_{ab} is a specific interaction(s). Dispersive interactions are due to non-polar interaction, such as London

interactions at the surface, whereas specific contributions result from polar interactions such as hydrogen bonding. There are several techniques which can be used to characterise the surface energy of pharmaceutical powders, detailed in chapter three. For the foregoing purpose, this research focuses on inverse gas chromatography (IGC).

7.1.1.1 <u>Inverse Gas Chromatography</u>

IGC is used to quantify the surface energy of a powder sample by using it as the stationary phase and measuring the retention volumes of well-characterised probes of varying molecular size. The dispersive and specific interactions that occur between the adsorbate (probe) and adsorbent (powder sample) are calculated by the use of thermodynamic equations, e.g., Equation 17, where the Gibbs free energy change is defined by the net retention volume (*Vn*):

$$\Delta G_{ad} = \Delta G_{de} = RT ln V_N + C \tag{17}$$

Where ΔG_{ad} and ΔG_{de} are molar Gibbs free energy changes of adsorption and desorption, respectively, R is the gas constant, T is the temperature (in Kelvin) and C is a constant related to reference states.

Similar to Equation 16, described by Fowkes [181], the free energy of adsorption can be split into dispersive (ΔG_d) and specific (ΔG_{ad}) components given by the following expression:

$$\Delta G_{ad} = \Delta G_d + \Delta G_{ab} \tag{18}$$

The dispersive component of the total surface energy can be calculated using two common approaches: the Schultz method and the Dorris-Gray method [182, 183] . Studies have been carried out in which the dispersive surface energy values from the two methodologies have been compared [121, 184]. In general, the two methodologies were found to give similar results and in this study the Dorris-Gray approach will be used.

7.1.1.2 Dispersive Surface Free Energy

In 1980, Dorris-Gray determined the thermodynamics of adsorption of a series of liquid n-alkane probes (displaying only dispersive interactions) at infinite dilution. Flame ionisation detection was utilised, as a method of detection, due to its high sensitivity at low surface coverages making it the ideal candidate for measuring thermodynamic parameters under these conditions. In theory, the presence and absence of probe interactions are considered and therefore Henry's law is obeyed. This was confirmed in Dorris-Gray's work by the Gaussian peaks of the IGC chromatogram and a constant retention time for different injection volumes.

When dispersive surface energy is determined via the Dorris-Gray approach only the energy of adsorption of methylene groups (ΔG^{CH2}) is taken into account. This can be calculated from the gradient of a line by plotting the adsorption energy of the probes ($-\Delta G^{AD}$) versus the carbon number of the probe (n):

$$\Delta G^{CH2} = -RTln(\frac{V_{N,n+1}}{V_{N,n}}) \tag{19}$$

Where $V_{N,n}$ is the retention volume of the n-alkane probe with carbon number *n*, R is the gas constant and T is temperature in K.

According to Fowkes the work of adhesion for one methylene group (W_{aCH2}) follows the relationship between the phases shown in the following expression:

$$W_{aCH} = 2\sqrt{\gamma_d \gamma_d^{CH2}} \tag{20}$$

Where γ_d is the dispersive surface energy of the stationary phase and γ_d^{CH2} is the dispersive surface energy of a solid material only containing methylene groups.

As there are no specific interactions the energy of adsorption of a series of alkanes ($-\Delta G_{CH2}$) can be described as follows:

$$-\Delta G_{CH2=} N_A \, a \, W_{aCH} \tag{21}$$

119

Where N_A is Avogadro's number, a is the cross-sectional area of an adsorbed methylene group (6 Å^2).

The relationship between dispersive surface energy and temperature is commonly quoted for polyethylene as:

$$\gamma_d^{CH2} = 35.6 - 0.058t \qquad (22)$$

Where t is the temperature in $^\circ$C.

The dispersive surface free energy of the solid stationary phase can therefore be obtained by using the expression [183] :

$$\gamma_d = \frac{1}{4\gamma_{CH2}} \left(\frac{RTln(\frac{V_{N,n+1}}{V_{N,n}})}{Na_{CH2}}\right)^2 \qquad (23)$$

7.1.1.3 Specific Surface Free Energy

The difficulties in characterising the specific surface energy of a solid using IGC have been discussed in the literature with the main challenge being that polar materials interact via both the specific and dispersive interactions, present at a surface [185]. In order to overcome this, the specific surface energy (γ_{ab}) is determined by measuring the retention parameters of well characterised polar adsorbates, such as ethanol and acetone, and then subtracting the dispersive component.

It is possible to measure the specific surface energy by characterising the surface using only two polar probes: one monopolar acid (electron acceptor: γ^+) and one monopolar base (electron donor γ^-):

$$\gamma_{ab} = 2\sqrt{\gamma^+ \gamma^-} \qquad (24)$$

The specific surface energy can be further divided into the components from acidic and basic contributions; however, this will not be studied in this research.

7.2 Materials and Methods

7.2.1 Ibuprofen Samples

The ibuprofen samples used were recrystallised by the methods detailed in chapter six. A summary of the sample properties are shown in Table 7.1.

Table 7.1 – Samples analysed in this chapter with a summary of their manufacturability ranking, from chapter six.

Sample	Shape	Manufacturability Ranking	
		Tabletability Best=1 Worst=4	Sticking Low=1 High=4
IbuHex (0 – 150 µm)	Needle/lath	1	1
IbuTol (0 – 150 µm)	Lath	2	2
IbuAce (0 – 150 µm)	Plate	4	3
IbuEth (0 – 150 µm)	Plate/prismatic	3	4

7.2.2 Surface Area

The specific surface area, pore size distributions and pore volume of the samples was measured using a TriStar II 3020 surface area and porosity analyser (Micromeritics U.K. Ltd., Hexton, UK). Between 450 – 850 mg of sample was filled into a 3/8" flat bottom cell with filler rods and conditioned under a helium purge at 40°C for 16 hours. Nitrogen isotherms were measured at -196°C. The BET model [186], based on the linear region of the nitrogen adsorption isotherm (from $P/P_0 = 0.05 – 0.3$) for pore volume and area, was used for data calculation. Each batch was measured in duplicate. For the extreme particle shapes, IbuHex and IbuEth, krypton was also used as an adsorption probe (following the methodology described above) for comparison.

7.2.3 Surface Energy

7.2.3.1 <u>Inverse Gas Chromatography</u>

Surface energy heterogeneity was measured using inverse gas chromatography − surface energy analyser 2.0 (IGC-SEA; Surface Measurement Systems (SMS) Ltd., Alperton, UK). The samples were packed into 4 mm pre-salinised glass columns and mechanically tapped for 10 minutes using a SMS sample packing device. All samples were packed to yield a total surface area of approximately $0.13 \, m^2$. The columns were pre-conditioned at 30°C and 0% RH using helium (carrier gas) at a flow rate of $7 \, cm^3/min$ for 120 minutes and these conditions were maintained throughout the experiment duration. A range of dispersive (non-polar) probes (decane, nonane, octane, heptane and hexane) and specific (polar) probes (ethyl acetate, chloroform, ethanol, acetone and acetonitrile) were injected into the columns at a range of surface coverages (n/n_m) ranging from 1 to 20%; the dead volume of the chromatographic column was determined using methane. Data analysis was performed using Cirrus Plus SEA Data Analysis software (v1.2, SMS Ltd., Alperton, UK). The Dorris-Gray approach [183] was used to determine the dispersive energy contribution, whereas the specific energy contribution was determined by measuring the free energy desorption of a pair of mono-functional acidic and basic probes (chloroform and ethyl acetate), based on the polarisation approach [187] and Della Volpe scale [188]. The polar probes were chosen on the basis of the most suitable retention times. The repeatability and reproducibility of the IGC-SEA system is quoted by the manufacturer as RSD = 1% [189] which is lower than traditional IGC techniques due to the system using the same pipeline and injection manifold for every injection [190]. To assess the instrument repeatability, batches of IbuEth were run in triplicate, but all other batches were run once due to limitations in availability of the IGC-SEA system.

7.2.3.2 Computational Methods

The methodologies used in chapter four were expanded in this section to investigate the surface properties further. The parts of the molecule present at the surface of each crystal face were coloured in relation to their atomic contribution to lattice energy.

The surface energy per crystal face (γ_{hkl}) was calculated using the attachment energy calculation:

$$\gamma_{hkl} = \frac{ZE_{att}d_{hkl}}{2V_{cell}N_A} \tag{25}$$

Where Z is the number of molecules in the unit cell, V_{cell} is the unit cell volume, E_{att} is the attachment energy, d_{hkl} is the d spacing and N_A is Avogadro's number.

7.3   Results and Discussion

7.3.1   Surface Area of Different Particle Shapes

The BET surface area values are presented in Table 7.2 and show that despite the change in particle shape the surface area of particles remains similar, with values between 0.082 - 0.109 m^2/g. The cumulative pore area and volume are also shown in Table 7.2, where no correlations with particle shape or manufacturability are observed.

Table 7.2 – BET surface area, cumulative pore volume and cumulative pore area for recrystallised ibuprofen samples. Reported values are mean of two measurements.

Batch	BET surface area (m^2/g)	Cumulative pore volume (mm^3/g)	Cumulative pore area (m^2/g)
IbuHex	0.109	0.183	0.114
IbuTol	0.082	0.111	0.070
IbuAce	0.101	0.095	0.054
IbuEth	0.082	0.153	0.074

It is proposed that when surface area values are below 1.0 m^2/g krypton should be used as an adsorbent gas due to its smaller area [30]. The two extreme particle shapes, IbuHex and IbuEth, which also represent the highest and lowest surface area results were obtained in the presence of krypton. The analysis using krypton increased the surface area of IbuHex and IbuEth by 0.013 m^2/g and 0.036 m^2/g, respectively. These increases are relatively small and show less discrimination between batches; hence, the data does not provide any additional information. It was therefore determined that running other batches using krypton was not necessary.

Typical isotherms for all batches are shown in the data in Figure 7.1 and classify all batches as Type II, non-porous or macroporous according to the IUPAC guidelines [191]. These results suggest that surface area and pore size are not contributing factors to the observed differences in the manufacturability of the different particle shapes.
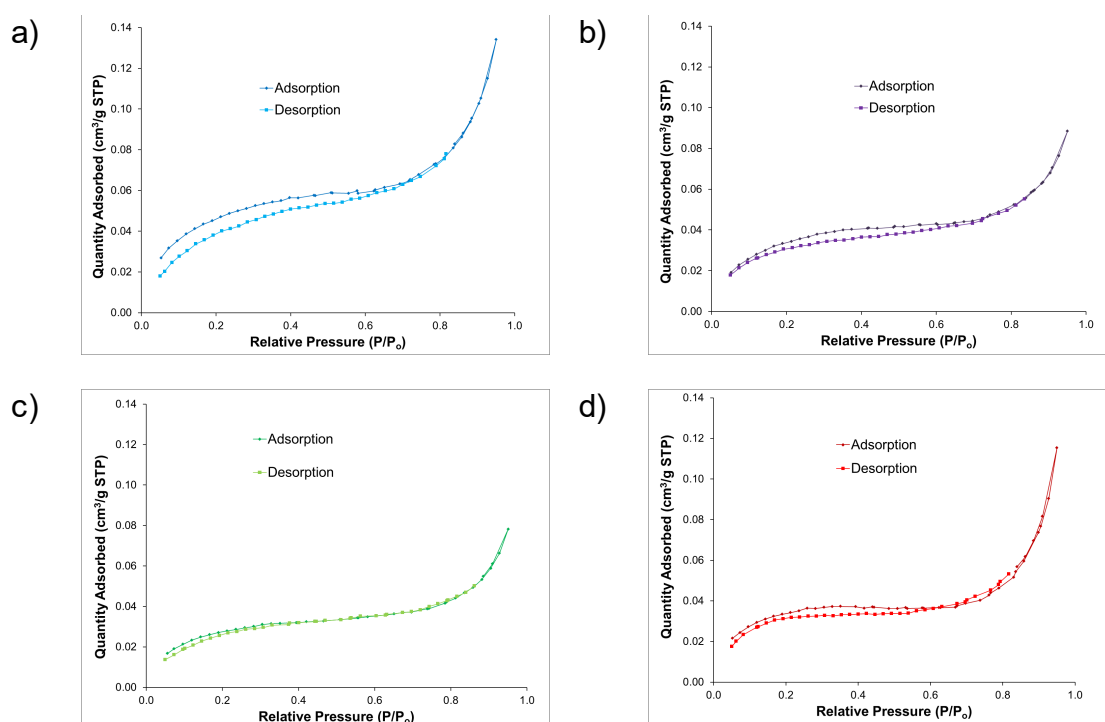
Figure 7.1 – Typical adsorption/desorption isotherms for recrystallised ibuprofen batches a) IbuHex, b) IbuTol, c) IbuAce and d) IbuEth.

7.3.2   Computational Surface Energy of Ibuprofen

Work published in 1994 by Brock and Dunitz recognises the analogies between the grammar of a language and the regularities between crystal packing and proposes ideas of how to best articulate such concepts [192]. The similarities do not end there and can be extended to describe the complex interactions present at the surface of APIs.

The surface chemistry of the different faces of ibuprofen were examined, qualitatively, in chapter four where it was revealed that different parts of the molecule were exposed at each surface.   It is expected that the different crystal faces will exhibit different surface energies and in order to investigate this further a novel visualisation approach is used.   The molecular components are coloured in relation to their lattice energy contribution and a side/top view of each crystal surface is shown in Figure 7.2.
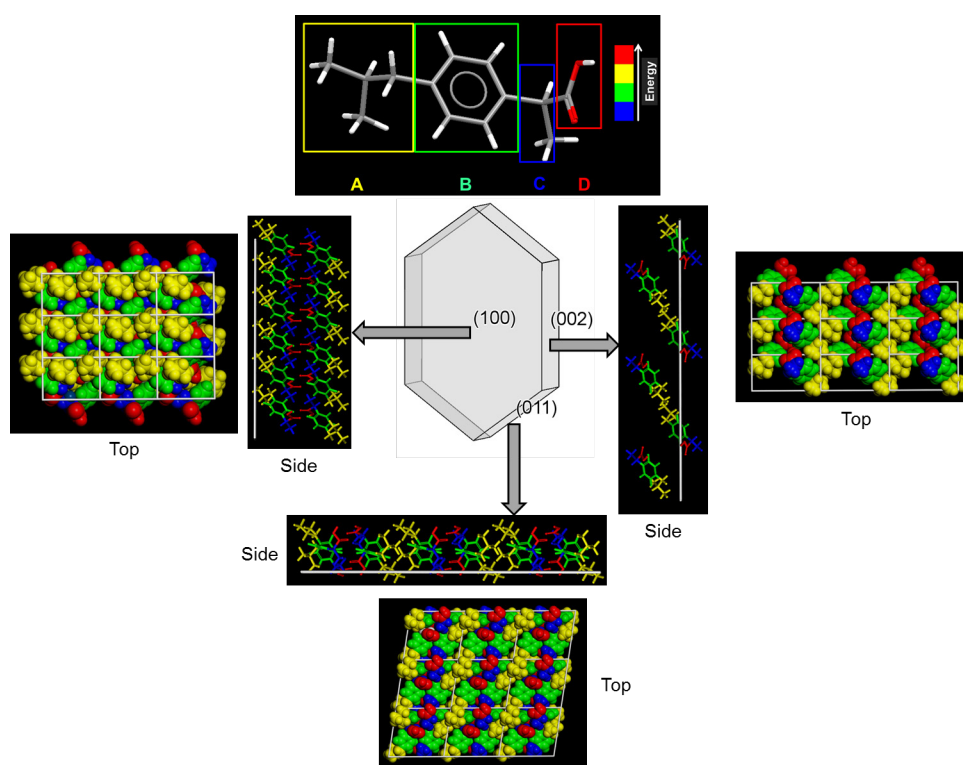
Figure 7.2 – Top and side view of the surface chemistry of ibuprofen where each molecular component is coloured relating to its atomic contribution to lattice energy.

The side view of the (1 0 0) crystal face reveals that there is one type of surface interaction (Figure 7.3). The surface is smooth with the aliphatic chains of the second highest energy group (yellow) close to the crystal surface. The other parts of the molecule are contained within the bulk of the surface and the highest energy group can be seen in the middle of the bulk meaning this interaction is saturated in the formation of this face. The top view shows the yellow group slightly protruding from the surface (Figure 7.2). Channels can be seen between the yellow groups leaving the green group slightly exposed however this is sunken into the surface. The calculated surface energy of this face is 30.7 mJ/m^2.
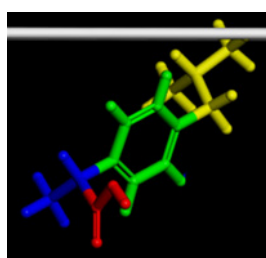
Figure 7.3 – The single interaction type present at (1 0 0) surface of ibuprofen.

The side view of the (0 0 2) face reveals that there are two types of surface interaction (Figure 7.4). The molecules in interaction 1 run at 45° angles to the surface leaving the blue, red and half of the green group fully exposed above the surface. The surface is rough, with over 50% of the atoms in this interaction type sticking out of the top. All the atoms in interaction 2 are below the surface with the yellow group pointing towards the top and the red group pointing towards the bulk. The top view shows the blue group protruding from the surface with the red group underneath, but still visible. Large gaps between the groups are visible where the green and yellow groups are exposed and spaces available where the red group (highest energy) is not fully saturated. The calculated surface energy of this face is shown to be one and a half times higher than the (0 0 1) crystal face with a value of 47.1 mJ/m^2.

Interaction 1   Interaction 2
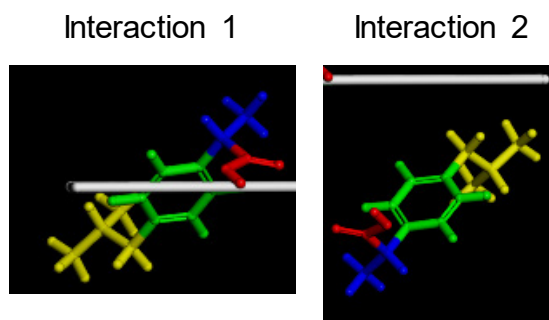
Figure 7.4 – The two types of interaction present at the (0 0 2) surface of ibuprofen.

The side view of the (0 1 1) face reveals that there are four types of surface interactions (Figure 7.5). The majority of the atoms lie on or beneath the surface for all interactions. The red group can be seen sticking out of the surface in interaction 1 and 4 and the yellow group sticking out in interaction 2 and 3. The red group is running parallel to the surface in interaction 1 and perpendicular in interaction 4. The top view reveals a relatively flat surface with all of the groups exposed. The yellow and green groups are seen lying between clusters of the red and blue group. The red group is fully exposed relating to interaction 1 and 4, meaning in relation to the intermolecular interaction these interactions are not bonded/unsaturated. The calculated surface energy of this face was shown to be almost two and a half times higher in energy than the (1 0 0) face with a value of 73.8 mJ/m^2.

Interaction 1   Interaction 2   Interaction 3   Interaction 4
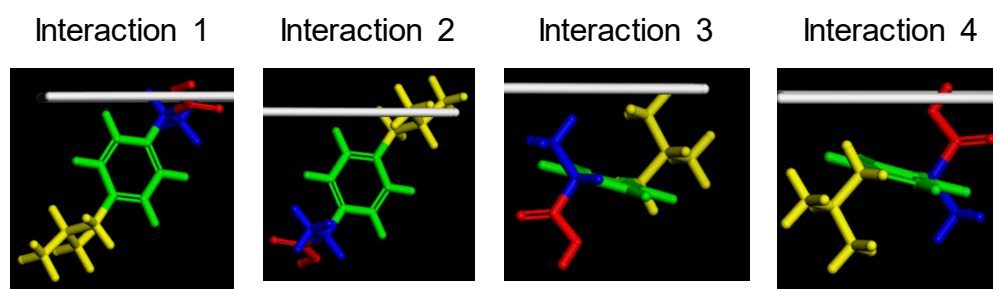
Figure 7.5 – The four types of interaction present at the (0 1 1) surface of ibuprofen.

The areas of each face contained within the modified attachment energy morphology were exported using Mercury and used to calculate a predicted particle surface energy, shown in Table 7.3.

Table 7.3 – The main faces of ibuprofen showing their multiplicity, computational surface energy and percentage area contribution to the modified attachment energy morphology and predicted particle surface energy.

Face	Multiplicity	% Area	Computed Surface Energy (mJ/m^2)	Contribution to Particle Surface Energy (mJ/m^2)
(1 0 0)	2	35.6	30.7	21.9
(0 0 2)	2	6.0	47.1	5.6
(0 1 1)	4	4.2	73.8	12.4
Predicted Particle Surface Energy (mJ/m^2)				**39.9**

It was shown during the crystallisation of ibuprofen (chapter six) that the particle shape can be modified by altering the recrystallisation solvent polarity. Needle/lath shaped particles were produced from non-polar solvent hexane whereas plate/prismatic shaped particles were produced from polar solvent ethanol. The change in particle shape resulted in the side, (0 0 2) and (0 0 1), faces being more exposed. In order to investigate the effect this has on particle surface energy two extreme particle morphologies were modelled and shown in Figure 7.6 together with scanning electron micrographs in which they were derived from. It should be noted that there was no one particle shape present in the micrographs; therefore, the image was visually assessed and a particle representing the average crystal habit produced.
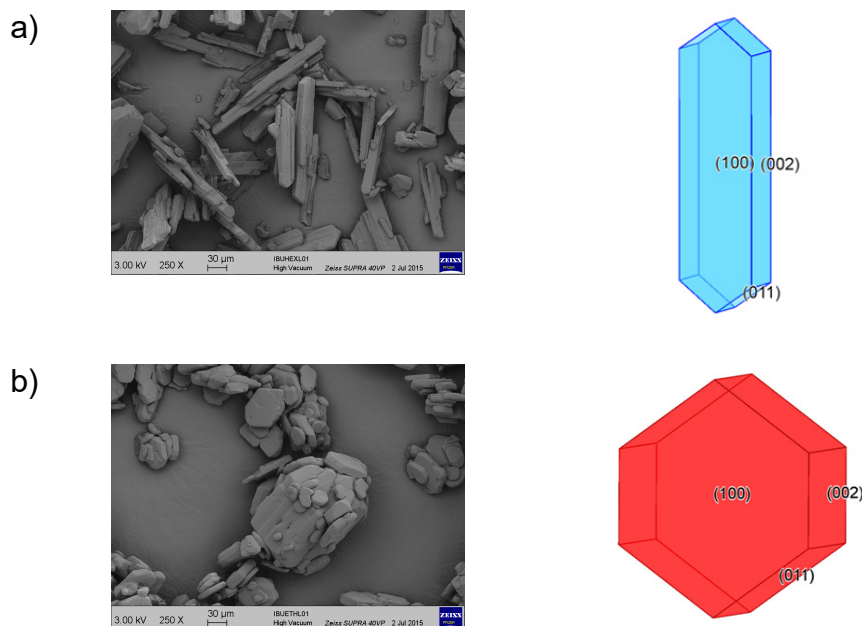
Figure 7.6 – Scanning electron micrographs and modelled extreme particle shapes of ibuprofen a) needle/lath shaped b) plate/prismatic shaped.

The areas of each face contained within the modified particle shapes were exported using Mercury and used to calculate a predicted particle surface energy for each crystal habit. Needle/lath shaped particles exhibited a surface energy of 38.8 mJ/m^2 whereas plate/prismatic shaped particles exhibited a higher particle surface energy of 48.4 mJ/m^2. This 9 mJ/m^2 difference can be explained by the plate/prismatic shaped particles containing a higher percentage area of the particle side faces which exhibit a higher surface energy.

7.3.3 Surface Energy of Different Particle Shapes – Experimental

IGC was used to experimentally determine the surface energy of different particle shapes of ibuprofen. Studies have suggested surface energy values close to 'infinite dilution' should occur due to the high energy sites being analysed and hence these values being representative of the entire material surface properties [190]. In order to achieve this, energy values are typically reported at surface coverages of <5%.

Total surface energy heterogeneity was calculated for all batches and split into dispersive/specific contributions. The total surface energy is shown in Figure 7.7 and reveals that batches IbuAce, IbuTol and IbuHex would rank differently depending on what surface coverage value below 5% was reported. Despite this it is clear that batch IbuEth exhibits the highest total surface energy of all the analysed surface coverages (at 1% surface coverage IbuEth has a total surface energy of 67.3 mJ/m^2 whereas all other batches exhibit lower values between 61.1 – 62.0 mJ/m^2).
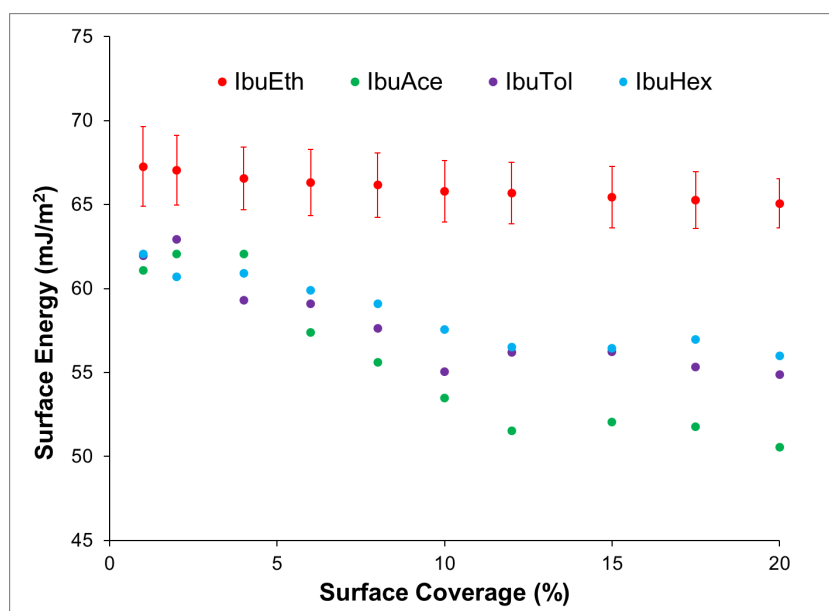
Figure 7.7 – Total surface energy heterogeneity plot for recrystallised ibuprofen. Error bars represent the standard deviation of three measurements made on sample with highest variation in surface energy (IbuEth).

The same trends are found for the specific surface energy (γab) values, Figure 7.8, where IbuEth exhibits a higher specific component at all surface coverages compared to the other batches (at 1% surface coverage batch IbuEth has a specific surface energy of 26.4 mJ/m^2 whereas all other batches exhibit lower values between 20.7 – 20.8 mJ/m^2). These results concur with the computational work described, where regular shaped particles (IbuEth) exhibit a higher surface energy due to the presence of a higher proportion of the side (0 0 2) and (0 1 1) faces. These faces contain a higher surface

energy due to the presence of the carboxylic acid groups at the surface and in turn increase the specific surface energy.
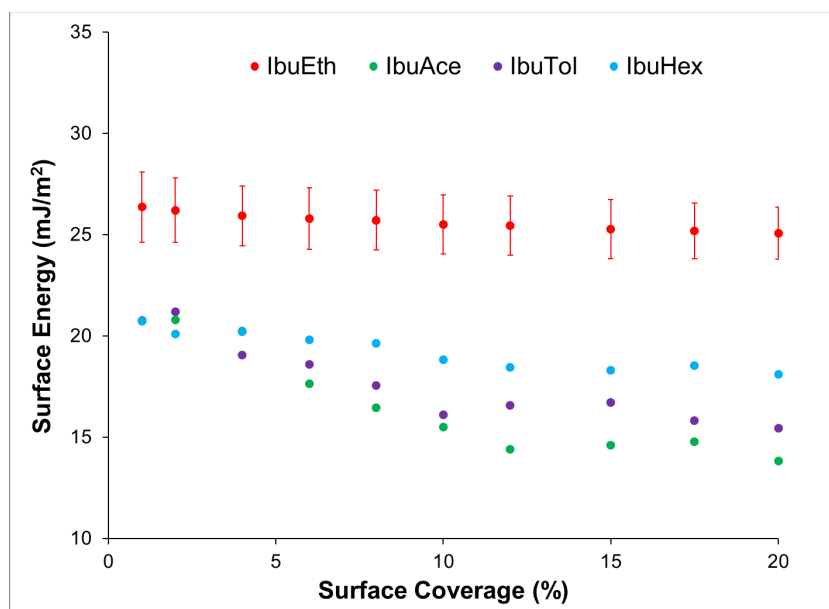
Figure 7.8 – Specific surface energy heterogeneity plot for recrystallised ibuprofen. Error bars represent the standard deviation of three measurements made on sample with highest variation in surface energy (IbuEth).

At surface coverages below 5% the dispersive surface energy for all batches is similar, with values between $40.3 – 41.8 \, mJ/m^2$. It was not possible to rank the dispersive surface energy, because the changes in the total surface energy are due to the variations in specific surface energy only. This implies that the proportion of the main (1 0 0) face stays constant during particle growth and only the proportion of the (0 0 2) and (0 1 1) faces are altered when the polarity of the crystallisation solvent is increased.
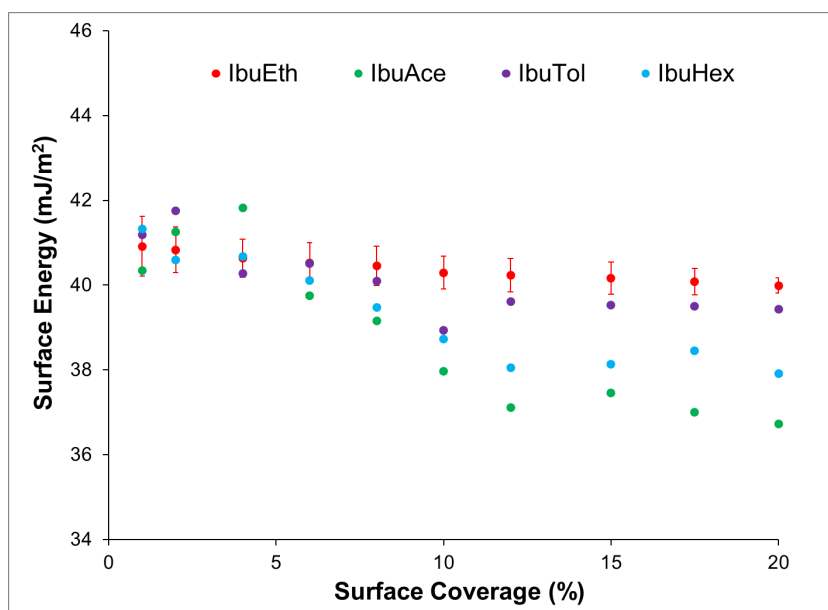
Figure 7.9 – Dispersive surface energy heterogeneity plot for recrystallised ibuprofen. Error bars represent the standard deviation of three measurements made on sample with highest variation in surface energy (IbuEth).

It would be expected that the total surface energy (influenced by the specific surface energy) would decrease as the aspect ratio of particles decreases. These trends are not found for IbuAce, IbuHex and IbuTol, and these batches would be ranked the same if error is accounted for. This could be due to instrument sensitivity; however, an increase in specific surface energy as aspect ratio increases can be inferred from the computational work.

7.3.4 Comparison between Computational and Experimental Surface Energy

The experimental and computational methods used to determine surface energy in this study are derived from different approaches. The computational method uses a bottom-up approach, where the surface energy is calculated from the unsaturated interactions at the surface (extrinsic synthons). The experimental, IGC, method is based on a top-down approach where the surface energy is calculated from the interactions of a probe molecule at the highest energy surface sites. In order to compare the two techniques caution must be taken when reporting IGC data due to the

132

different surface coverages analysed. In order to provide a reasonable comparison between these different approaches it is proposed that reporting IGC at infinite dilutions is not suitable due to computational modelling considering the complete surface. For comparison, IGC data at 20% surface coverage will be reported.

A comparison between the surface energies of the extreme particle shapes is shown in Table 7.4 where it can be seen that both techniques show around a 9 mJ/m^2 difference between needle/lath and plate/prismatic shaped particles. These values are not aligned due to the divergent approaches described above; however, they do show agreement in the discrimination between different particle shapes.

Table 7.4 – Comparison of the computational and experimental surface energies of ibuprofen particle shapes.

	Total Surface Energy (IGC at 20% surface coverage) (mJ/m^2)	Calcuated Surface Energy (mJ/m^2)
Needles/laths	56.0	38.8
Plate/prismatic	65.1	48.4
Difference (mJ/m^2)	**9.1**	**9.6**

Using a combination of experimental and computational techniques it is concluded that changing the particle shape of ibuprofen drives differences in surface energy, such that a particle with a more regular shape exhibits a higher surface energy than a needle shaped particle. The increase in surface energy is driven purely by an increase in specific surface energy caused by a greater exposure of the (0 0 2) and (0 1 1) faces containing the carboxylic acid functionality at the surface.

7.3.5 Surface Energy Relationship and Manufacturability

There is a strong correlation between the surface energy and sticking propensity of ibuprofen batches, whereby batch IbuEth exhibited the highest

surface energy and the greatest sticking propensity. The surface energy of the other three batches could not be distinguished using IGC. Computational results suggest that the specific component of the surface energy decreases as aspect ratio decreases, which correlates with the observed sticking behaviour.

There is no clear trend between the surface energy of ibuprofen particles and their tableting performance. Despite Gindy [179] suggesting that particles with a higher surface energy will form stronger tablets, this is not observed in this study, where the batch with the highest surface energy (IbuEth) ranks third in terms of tabletability. This batch also exhibited the highest sticking propensity, which may have caused weaker tablets as the powder adhered to the punch rather than itself to form a strong tablet. Batch IbuAce ranked worst in terms of tabletability, but stuck less than IbuEth, suggesting that the physical shape of the powder is also contributing to the resultant tensile strength of the tablets.

The computational work suggests that the surface energy differences are caused by the side faces being exposed in different ratios in turn altering the specific component part caused by exposure of the carboxylic acid functionality. This carboxylic acid functionality will contain a negatively charged dipole and it is probable that the metal on the punch tips could be slightly positively charged causing an attraction which leads to increased sticking propensity. This hypothesis would explain why a high surface energy, driven by the specific component, favours powder adhesion to punches over cohesion to form strong tablets.

7.4   Conclusions

The surface properties of recrystallised ibuprofen samples with four diverse particle shapes were characterised using both experimental and computational techniques in order to investigate differences in manufacturing behaviour (tabletability and sticking propensity). The surface area and porosity of the materials were found to be similar and did not correlate with observed manufacturing behaviour. Plate/prismatic ibuprofen particles were

found to have the highest surface energy, caused by an increase in specific surface energy, compared to all other batches by IGC. The surface energy of the other batches could not be ranked using this technique.

The surface chemistry of each ibuprofen crystal face was visualised computationally and a novel approach used to qualitatively assess surface energy presented. This approach allows for a quick and easy assessment of the surface chemistry to be made providing a grammar to those who are not familiar with computational approaches. The surface energy of each face was found to increase as the exposure of the most dominant intermolecular interaction (carboxylic acid hydrogen bonded dimer) increased at the surface. Two extreme particle shapes of ibuprofen were modelled where it was found that plate/prismatic shaped particles exhibited a higher surface energy of 9 mJ/m^2 compared to needle/lath shaped particles, which was in agreement with the experimental work. Despite IGC being unable to discriminate between all batches, the computational model suggested that as the aspect ratio of particles increases (particles become more regular in shape) then the surface energy will increase due to a greater exposure of the side (0 0 2) and (0 1 1) crystal faces containing the high energy carboxylic interaction.

A strong link between the surface energy of particles and sticking propensity was found, where particles with a high surface energy, caused by specific surface energy, exhibited a greater sticking propensity. It is hypothesised that the polar nature of the carboxylic acid dimer exposed in the ibuprofen faces could be attracted to metal punches, if they were to become positively charged during manufacture.

A previous study in the literature revealed that a higher surface energy leads to greater cohesion resulting in a higher tensile strength of tablets [179]. The findings, from this study, suggest that the specific contribution to the total surface energy may alter the adhesive properties and a higher specific component leads to greater adhesion and therefore sticking propensity. A link between tensile strength and surface energy could not be found and the differences in tensile strength observed are thought to be driven by the

physical change in crystal habit rather than chemically driven by surface energy.

8. Chapter Eight: From Molecule to Material to Medicine

8.1 Introduction

Punch sticking is a major issue for the pharmaceutical industry and the work reported in this thesis has presented links between API particle shape/surface energy and sticking propensity. For ibuprofen, a change in particle shape from needle/lath to plate/prismatic shape increased the concentration of side crystal faces which contained a polar intermolecular interaction at the surface. The change in particle shape resulted in an increase in specific surface energy which was shown to drive the sticking propensity of the powder to metal punches during tableting.

Crystal engineering of pharmaceuticals has become increasingly common in academia where, often, the polymorphic form is changed to gain the desired mechanical properties e.g. increased plasticity [79]. If the hypothesis between particle shape / specific surface energy and sticking holds true then it may be possible to crystal engineer an API with certain physicochemical properties in order to reduce sticking propensity.

So far the change in particle shape of an API has been explored by crystallisation; but, other routes such as milling can also cause changes in particle shape. Milling has been shown to increase the total surface energy of pharmaceutical powders and the work reported in this chapter will probe this further [193].

The results of experiments reported in this chapter aim to further investigate the link between the crystal structure of APIs, physicochemical properties and sticking propensity using predictive computational and experimental tools. Chemically diverse APIs will be studied to determine if chemical causality is a root cause for punch sticking.

8.2   Materials and Methods

8.2.1   Palbociclib Crystallisation

The commercial manufacturing process for palbociclib has been documented in a publication by Chekal *et al.,* where a crystallisation step using *n*-butanol / anisole mixture was developed in order to obtain the desired API particle properties [194].   This publication also documents some qualitative particle shape changes which are dependent on the solvent used for crystallisation. It was noted that recrystallisation, from both anisole and m-xylene, resulted in lath shaped particles that were different from the conventional needle shapes that are usually produced.   In this study palbociclib was crystallised using anisole and *m*-xylene in the attempt to generate different particle shapes. Unfortunately, these crystallisation reactions were unsuccessful and the resultant particles were needle-like in shape.

Two batches of palbociclib, which contain slightly different particle shapes (needle and lath shaped particle) were received from Pfizer for use in this research.   The different shapes, which were produced from confidential modifications to the crystallisation process, will be characterised in the work reported herein.

8.2.2   Crizotinib Milling

Crizotinib was supplied by Pfizer for use in this study.   The API undergoes hammer milling and two samples of the same lot were received for analysis; one before and the other after milling.   The material was used as received.

8.2.3   Particle Morphology Characterisation

Scanning electron microscopy (SEM) images were captured using a Zeiss SUPRA 40VP (Carl Zeiss Microscopy GmbH, Cambridge, UK).   The samples were mounted onto an aluminium pin stub containing sticky carbon tabs and sputter coated with platinum.   A voltage of 3.0 kV and working distance of 10 mm were used.

Particle size and shape values of the samples were measured with a QICPIC dynamic image analysis system (Sympatec Ltd., Clausthal-Zellerfeld, Germany). A vibratory feeder system (VIBRI, Sympatec) was combined with a dry air disperser (RODOS, Sympatec) and was operated at 0.5 bar pressure. The system operates using a pulsed light source with sub-nanosecond illumination, and the particles were imaged by a high speed camera with a frame rate of 400 frames per second. Single measurements were made using the M6 lens (measuring range of 5 – 1705 µm) and a minimum of 200,000 particles were imaged for each run. Images were analysed using WINDOX (Sympatec) software and size and shape distributions reported using the maximum Feret diameter and EQPC for palbociclib and crizotinib, respectively.

8.2.4 Sticking Propensity Measurements

The APIs were compacted using a Gamlen tablet press (GTP-1, Gamlen Tableting Limited, Nottingham, UK). Between 90 – 100 mg of powder was compacted in a 6 mm die at a speed of 60 mm/min. After tablet compression (prior to ejection), the detachment stress of the base die was measured manually using a 50 kg hand held force gauge (Mecmesin, Slinfold, UK) placed at the side of the base die. Detachment measurements were undertaken in triplicate.

8.2.5 Surface Energy

Surface energy heterogeneity was measured using inverse gas chromatography − surface energy analyser 2.0 (IGC-SEA, Surface Measurement Systems (SMS) Ltd., Alperton, UK). The samples were packed into 4 mm pre-salinised glass columns and mechanically tapped for 10 minutes using an SMS sample packing device. All samples were packed to yield a total surface area of approximately 0.13 m^2. The columns were pre-conditioned at 30°C and 0% RH using helium (carrier gas) at a flow rate of 7 standard cubic centimetres per minute for 120 minutes and these conditions

were maintained throughout the duration of the experiments. A range of dispersive (non-polar) probes (decane, nonane, octane, heptane and hexane) and specific (polar) probes (ethyl acetate, chloroform, ethanol, acetone and acetonitrile) were injected at a range of surface coverages (n/n_m) ranging from 1 to 20%; the column dead volume was determined using methane. Data analysis was performed using the Cirrus Plus SEA Data Analysis software (v1.2, SMS Ltd., Alperton, UK). The Dorris/Gray approach [183] was used to determine the dispersive energy contribution, whereas the specific energy contribution was determined by measuring the free energy desorption of a pair of mono-functional acidic and basic probes (chloroform and ethyl acetate), based on the polarisation approach [187] and Della Volpe scale [188]. The polar probes were chosen based on the most suitable retention times. The repeatability of the measurements was assessed in chapter seven and all batches were run once due to limitations in availability of the IGC-SEA system.

8.2.6 Computational Tools

The crystal structures of palbociclib and crizotinib were solved within Pfizer, and are not available in the public domain.

The lattice energy of the two materials was calculated using the Dreiding II force field. This force field compromises of a 6 - 12 potential and a 10 - 12 hydrogen bond potential with parameters from Mayo *et al.* and Williams [195, 196]. This force field was deemed to be the most appropriate one available in Materials Studio for dealing with organic molecules.

8.3   Results and Discussion

8.3.1   Investigating the Effect of Particle Shape Change on Palbociclib Sticking Propensity

8.3.1.1   Crystal Chemistry of Palbociclib

A schematic of the chemical structure and unit cell of palbociclib are shown in Figure 8.1a and Figure 8.1b, respectively.   Palbociclib is a weak base and there are four molecules in the unit cell, where hydrogen bonding between the amine group and nitrogen on the six membered ring can be seen.
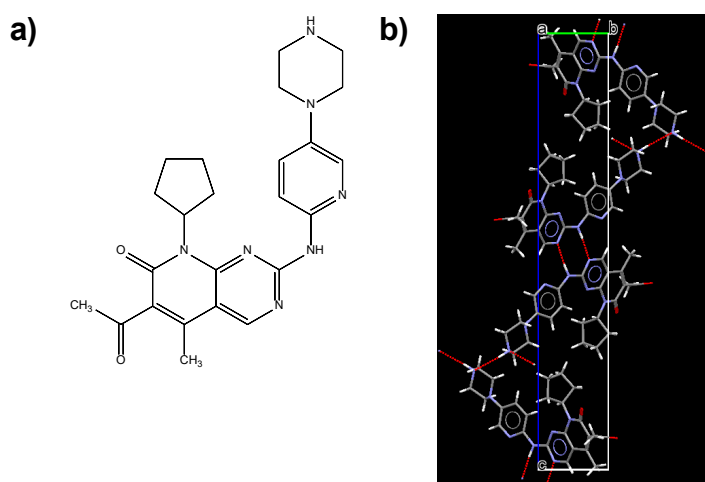
Figure 8.1 – Palbociclib a) chemical structure b) unit cell (crystallographic information not in the public domain).

The crystal lattice energy was calculated to be -146.7 kJ/mol.   Unfortuntely, no sublimation enthaplies were available for comparison; therefore, the work was continued using the force field selected (Dreiding II).

The intermolecular interactions (intrinsic synthons) were examined for their contribution to the crystal lattice energy where nine interactions compromising of six interaction types, were shown to make up 93% of the total lattice energy (Figure 8.2).   Despite the structure containing hydrogen bonds, the lattice energy is dominated by a π-π stacking interaction, contributing 27%, followed by a hydrogen bonding interaction contribution of 10%.   The cyclic, relatively flat structure of palbociclib allows close packing of the molecules and is

thought to be the reason for this dominant interaction. All other interactions are Van der Waals and contribute less than 7% to the total lattice energy.
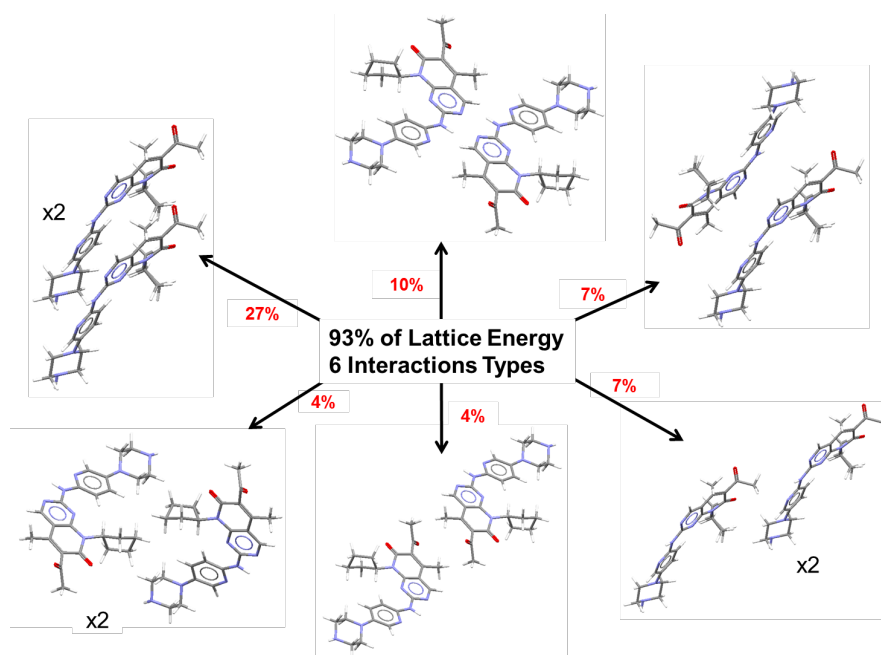
Figure 8.2 – Key types of intermolecular interaction for Palbociclib and their contribution to the total crystal lattice energy.

The creation of strong intermolecular interactions can, sometimes, arise at a cost by causing repulsive interactions and during examination of the molecular interactions a repulsion between the amine groups, shown in Figure 8.3, was noted. This repulsion has a positive value of 14 kJ/mol which negatively impacts the lattice energy (making it more positive). The packing of palbociclib accommodates for this repulsion by maximising the π-π stacking interactions; the intermolecular interaction strengths may be augmented by this repulsive interaction.
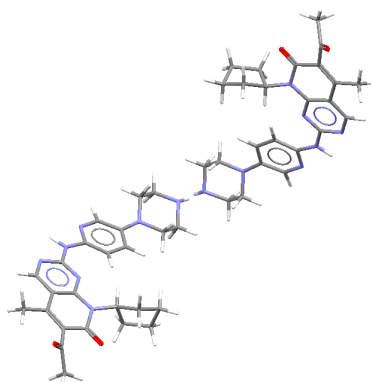
Figure 8.3 – Repulsion present in palbociclib packing which negatively impacts the lattice energy by 9%.

Palbociclib was then divided into molecular components and the lattice energy collapsed onto the individual atoms and summed across each fragment (Figure 8.4). The molecular components were ranked in terms of energy contribution to the total lattice energy. It can be seen that the cyclic rings containing the amine group contributes to over half the lattice energy (54.36%) despite containing only 29% of the atoms present within the molecule. This can be explained by the π-π stacking interaction and the hydrogen bonding interaction being contained within this component. From the data gained from the ibuprofen work, the surface energy will be higher when this molecular component is present at the surface of a crystal.
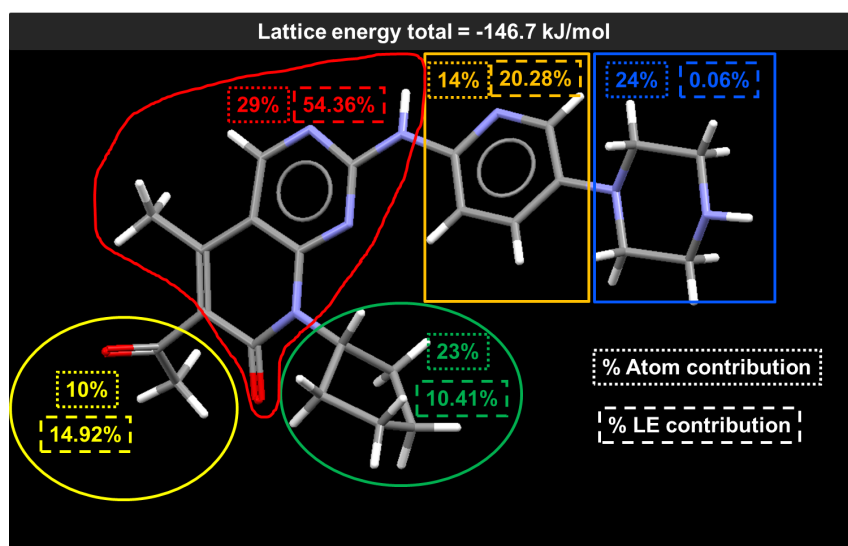
Figure 8.4 – Palbociclib lattice energy collapsed into atoms, summed over molecular components and ranked in terms of energy.

The attachment energy morphology of palbociclib was calculated and a needle like shape with three dominant faces predicted: (0 0 2), (-1 0 1) and (-1 1 1). The surface chemistry of these faces was viewed and the surface energy calculated using the attachment energy equation (Figure 8.5).

The side view of the dominant (0 0 2) face reveals that there is one type of surface interaction (Figure 8.5a). The surface is relatively smooth with the aliphatic chains of the highest energy group (red) sticking out the top. The majority of the molecules are contained within the bulk of the surface and the highest energy group can be seen running perpendicular to the surface. The top view (Figure 8.5b) reveals that although the highest energy group (red) is present at the surface of this face, the π-π staking interaction which contributes 26.9% to the total lattice energy is saturated due to the molecules running perpendicular to the surface. This means that, despite this high energy group being present at the surface, this interaction will not be affected in the formation of this face resulting in a low surface energy of 10.2 mJ/m^2. The top view also reveals that there are small gaps between the red groups, where the orange and yellow groups can be seen, but they are sunk into the bulk of the crystal face.

Surface energy shown in grey box (mJ/m^2)
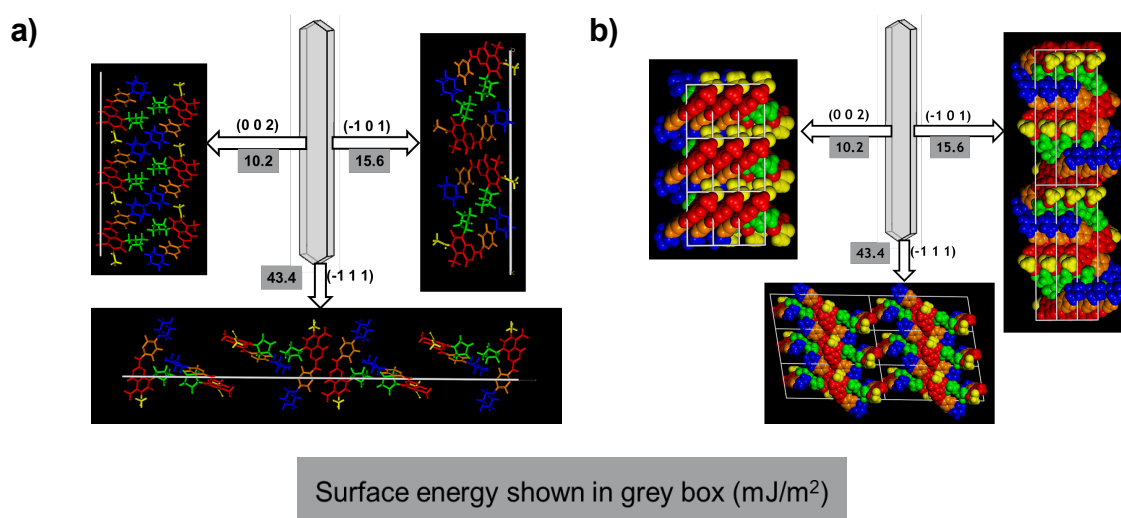
Figure 8.5 – Surface chemistry of palbociclib, where each molecular component is coloured in relation to its atomic contribution to the lattice energy; a) side view and b) top view.

144

The side view of the (-1 0 1) face reveals two types of surface interactions, shown in Figure 8.6. Interaction 1 shows the third highest energy group (yellow) sticking out of the surface and interaction 2 shows the lowest energy group (blue) sitting on the surface. The yellow group contains carbonyl functionality which will increase the specific surface energy of this face due to its polarity. Just below the surface the highest energy group (red) can be seen in interaction 1 and the second highest energy group (orange) for interaction 2. The top view of this face (Figure 8.5b) shows that the lowest energy group (blue) and third highest energy group (yellow) protruding from the surface; there are, however, large gaps between the molecular components meaning other parts of the molecule are exposed. The highest energy group (red) is orientated at an angle of 45° in relation to the surface, meaning these interactions are not fully saturated at this face leading to a surface energy of around one and a half times higher than the (0 0 2) face with a value of 15.6 mJ/m^2.

Interaction 1   Interaction 2
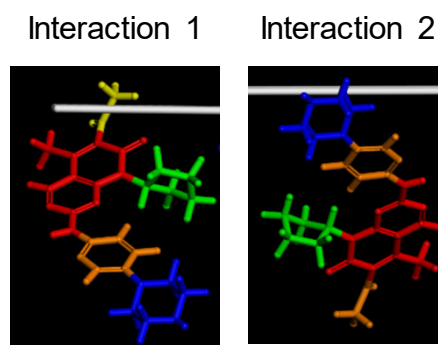
Figure 8.6 – The two types of interaction present at the (-1 0 1) surface of palbociclib.

The side view of the (-1 1 1) face reveals four types of interactions, shown in Figure 8.7. The surface is "bumpy" with many parts of the molecule sticking out. Interaction 1 shows the lowest energy group (blue) sticking out of the surface and half of the second highest energy group orange sticking out. All the atoms for interaction 2 are contained within the bulk where the majority of the molecule lies parallel to the surface. The highest energy group (red) and the green group are sticking out of the surface in interaction 3 and again the

molecules run parallel to the surface. Interaction 4 shows the third highest energy group (yellow) sticking out of the crystal surface as well as half of the red. In general for this interaction, the molecular geometry runs perpendicular to the crystal surface. The top view reveals a bumpy surface with almost all of the groups exposed in some way (Figure 8.5b). The highest energy group, red, is shown to be unsaturated (not involved in the intermolecular bonding) at the top of the surface (relating to interaction 3) therefore this will contribute to a high surface energy. The surface energy of this face is predicted to be 43.4 mJ/m^2, approximately four times higher than the (0 0 2) face.
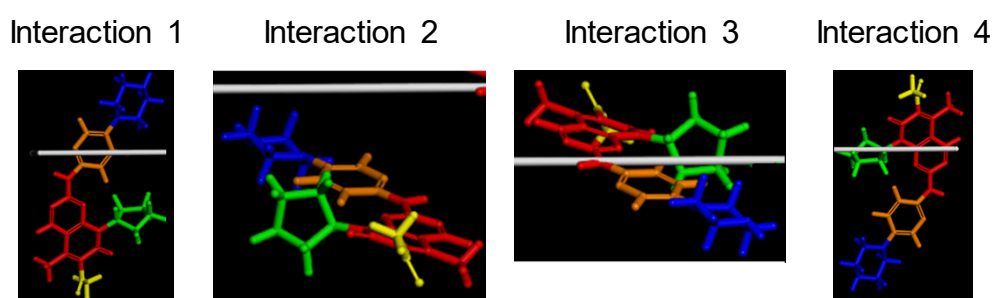
Figure 8.7 – The four types of interaction present at the (-1 1 1) surface of palbociclib.

8.3.1.2 Particle Morphology of Palbociclib

Scanning electron microscopy (SEM) was utilised to visualise the particle morphology of the batches supplied by Pfizer. The electron micrographs are shown in Figure 8.8 and reveal physical differences between the two batches. The particles shown in Figure 8.8a are shown to be needle like, with a particle size centring around 100 µm. The particles shown in Figure 8.8b are shown to be of a similar size to the first batch. However, they contain a needle/lath shaped crystal habit and also contain less fine particles (around 5 µm). The batches shown in Figure 8.8a and Figure 8.8b will be referred to as needles and lath, respectively.
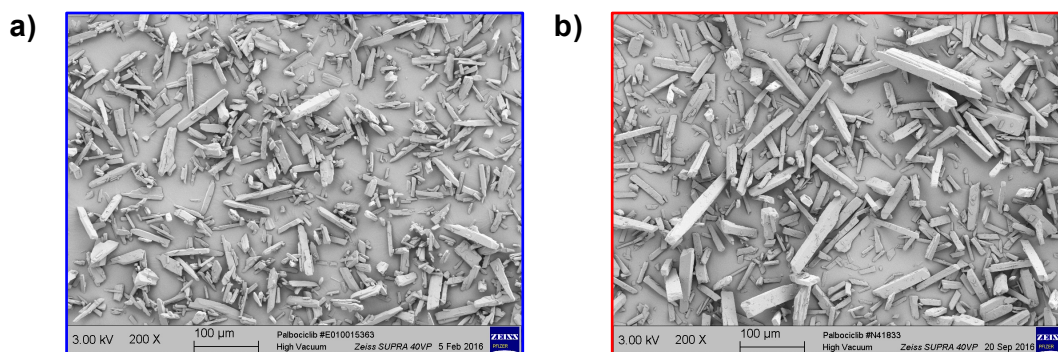
Figure 8.8 – Scanning electron micrographs of palbociclib showing changes in particle shape a) Palbo1 (needle/lath shaped) b) Palbo2 (lath shaped). All images captured using x200 magnification and the scale bar represents 100 μm.

The attachment energy morphology of palbociclib was altered to be more representative of the two shapes imaged by SEM. The predicted shape was placed on top of selected particles (fifteen shapes in each image) and altered accordingly. The image shown in Figure 8.9 shows a selection of six particles selected to gain a representation on the shape present in the batches.
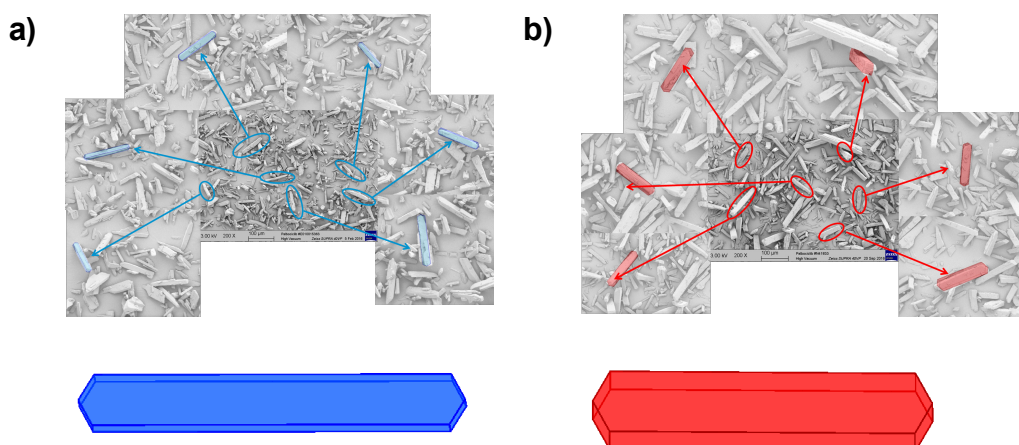
Figure 8.9 – Method used to alter the attachment energy morphology of palbociclib and resultant shapes for a) needles and b) laths.

QICPIC particle size analysis was performed on the two batches and the number distributions (most sensitive to smaller particles in the sample) are shown in Figure 8.10a. As expected from the electron micrographs, the needle batch contains the highest proportion of fine particles (around 5 μm),

compared to the lath batch. The volume distributions (most sensitive to larger particles in the sample) are shown in Figure 8.10b where it can be seen that the needle batch is slightly smaller in size than the lath batch. The average particle size, by volume, for the two batches is 87.7 µm and 73.7 µm for laths and needles, respectively. It should be noted that the difference in fine particles could lead to a greater sticking propensity of the needle particles.
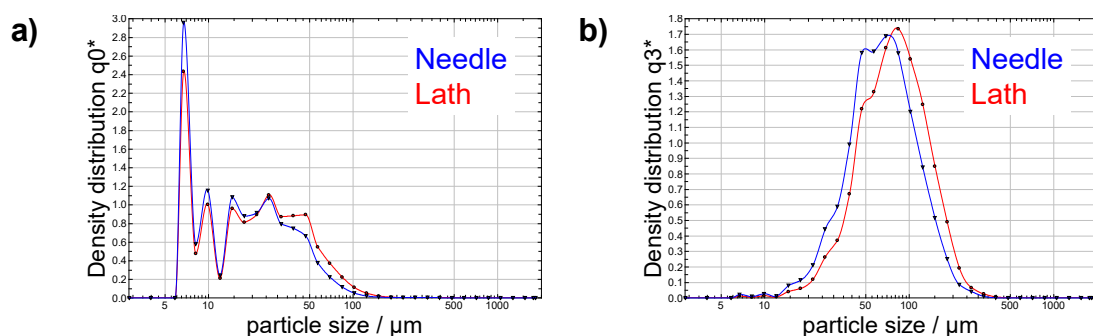
Figure 8.10 - QICPIC a) number and b) volume weighted distributions for palbociclib.

The QICPIC aspect ratio versus particle size for the two batches was calculated and the resultant plot is shown in Figure 8.11. Despite the lath shaped particles containing a visually higher aspect ratio than the needles; the aspect ratio for needles is shown to be slightly higher than the laths. This method was deemed unsuitable for these particles and could be due to differences in the proportion of fine particles. For this reason the sphericity was calculated, shown in Figure 8.11b, and the lath shaped particles are shown to have a higher value, meaning they are more spherical in nature and in agreement with the SEM observations.
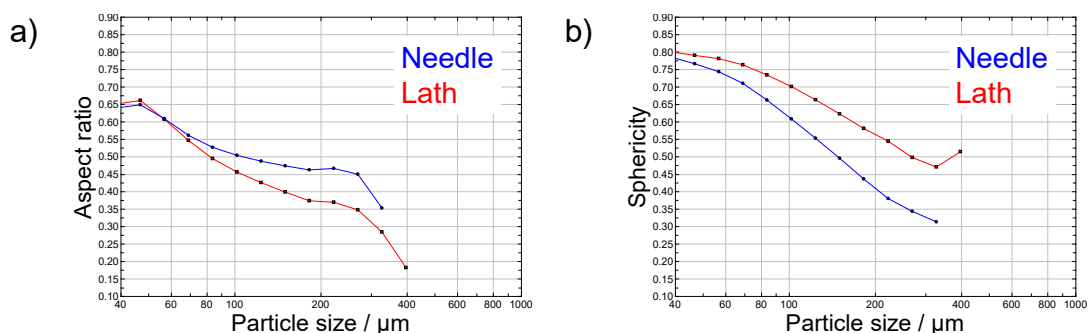
Figure 8.11 – QICPIC shape values for palbociclib a) aspect ratio and b) sphericity.

8.3.1.3 Surface Energy of Palbociclib

Surface energy heterogeneity was calculated for the two batches using IGC and split into dispersive and specific components. The total surface energy plot (Figure 8.12) reveals that, below 5% surface coverage, the needle shaped particles have a slightly higher total surface energy than the laths. It would be expected from the modelling work that as the lath shapes contain a higher proportion of the high energy side faces, (-1 0 1) and (-1 1 1), then these would have a higher total surface energy than the needles.
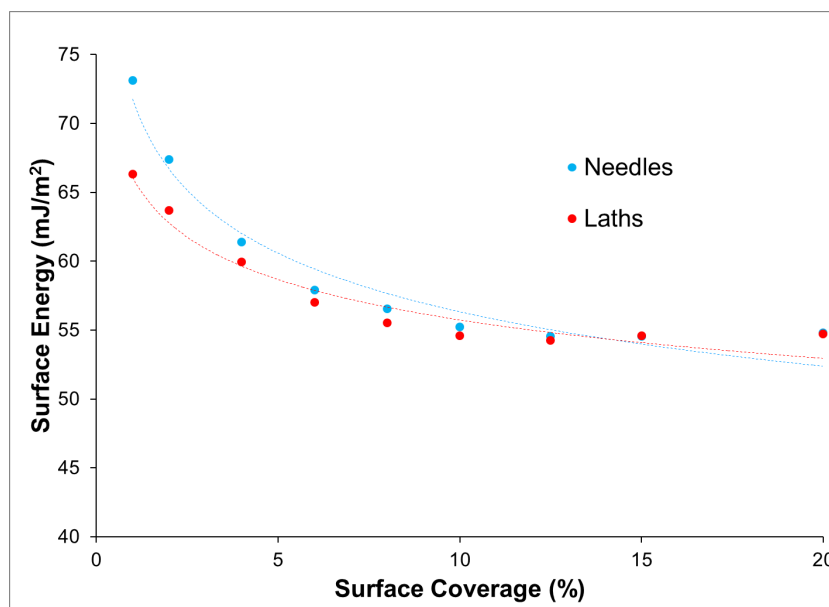
Figure 8.12 – Total surface energy heterogeneity plot for palbociclib.

The total surface energy obtained from IGC results does not agree with this prediction. However, if the specific surface energy is taken as a percentage contribution to the total surface energy, highlighted by the pie charts in Figure 8.13, then it can be seen that the lath shaped particles have a higher total contribution from specific surface energy. The total surface energy of the laths is made up of 29.7% from specific surface energy compared to the needle shaped particles only being made up of 27.6% from specific surface energy .
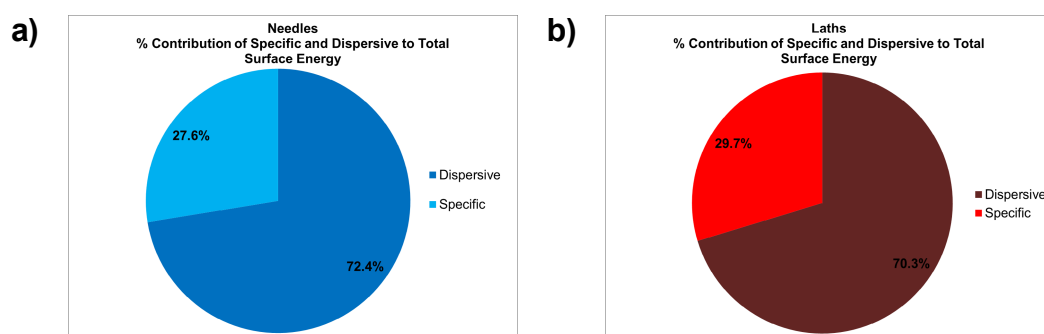
Figure 8.13 – Pie chart representing the percent contribution from dispersive and specific surface energy to the total surface energy of palbociclib a) needles and b) laths.

The total surface energy of the modified particles shown in Figure 8.9 were calculated and, as expected, the surface energy of the laths was shown to be higher than the needles with values of 15.7 mJ/m^2 and 12.8 mJ/m^2, respectively.   These values are lower than the total surface energy values calculated using IGC which may be due to the differences in approaches used, as discussed in chapter seven.

8.3.1.4 Sticking Propensity of Palbociclib

The sticking propensity of the batches was measured by recording the detachment stress from the base die post-compaction.   The detachment stress measurements at three compaction pressures are shown in Figure 8.14, where it can be seen that at the middle and highest compaction

pressure the laths have a greater propensity to stick to the base die than the needles.

Despite the needles containing a higher proportion of fine particles the change in particle shape is shown to be a more dominant factor in driving the sticking propensity than particle size. This observation is similar to the ibuprofen case study where again a more regular shape exhibited a higher sticking propensity. In terms of surface energy, the computational work predicts that the laths would stick more than the needles due to the highest energy intermolecular interaction being unsaturated at the faces with a greater exposure for the laths. The total surface energy calculated using IGC does not trend with this data; however, if viewed with regard to specific contribution to the total surface energy this prediction would hold true.
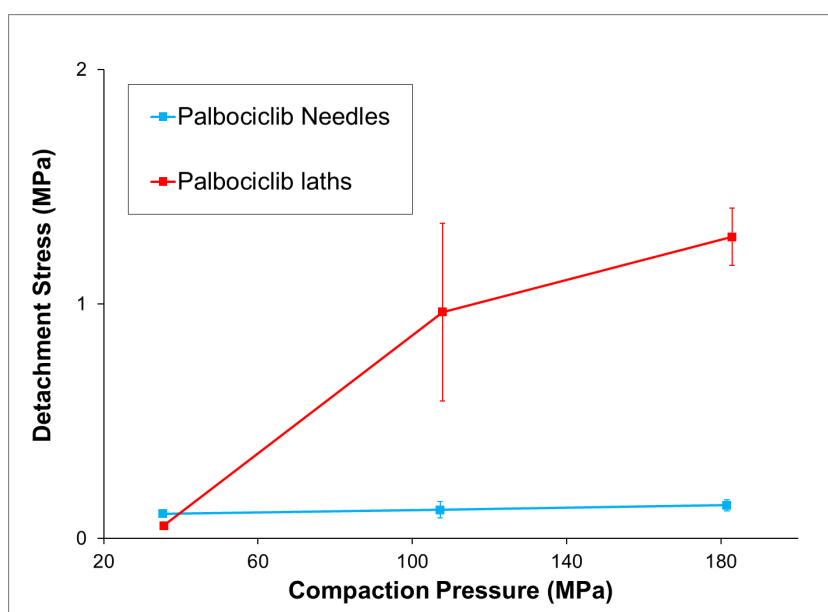
Figure 8.14 – Sticking propensity of palbociclib to the base die. Error bars represent standard deviation of three measurements.

It was noticed, during the tableting of palbociclib, that not only did the lath batch stick to the base die but both batches adhered to the upper punch. Representative images captured at 180 MPa (Figure 8.15) show yellow powder stuck to the upper punch. Unfortunately, the GTP-1 sticking test does

not quantify this phenomenon. To measure this, the mass punch test described in chapter three could be utilised.
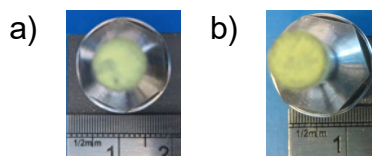
Figure 8.15 – Representative images showing upper punch sticking of palbociclib after compaction at 180 MPa a) needles and b) laths.

This case study has revealed that there is link between particle shape / specific surface energy and API sticking propensity. The more regular shape of palbcoclib was shown to have a higher propensity to stick; however, the total surface energy from IGC could not be used to predict this sticking behaviour. The specific surface energy, if taken as a contribution to the total surface energy, showed a trend with sticking behaviour such that a higher specific surface energy led to greater sticking propensity. The computational surface energy showed a correlation where particles with higher predicted surface energy values were shown to have a greater propensity to stick.

8.3.2 Investigating the Effect of Particle Shape Change Induced by Milling on Crizotinib Sticking Propensity

8.3.2.1 Crystal Chemistry of Crizotinib

A schematic of the chemical structure and unit cell of crizotinib are shown in Figure 8.16a and Figure 8.16b, respectively. Crizotinib is a base and there are four molecules in the unit cell where there is a hydrogen bonded network between the ether, primary and secondary amine.
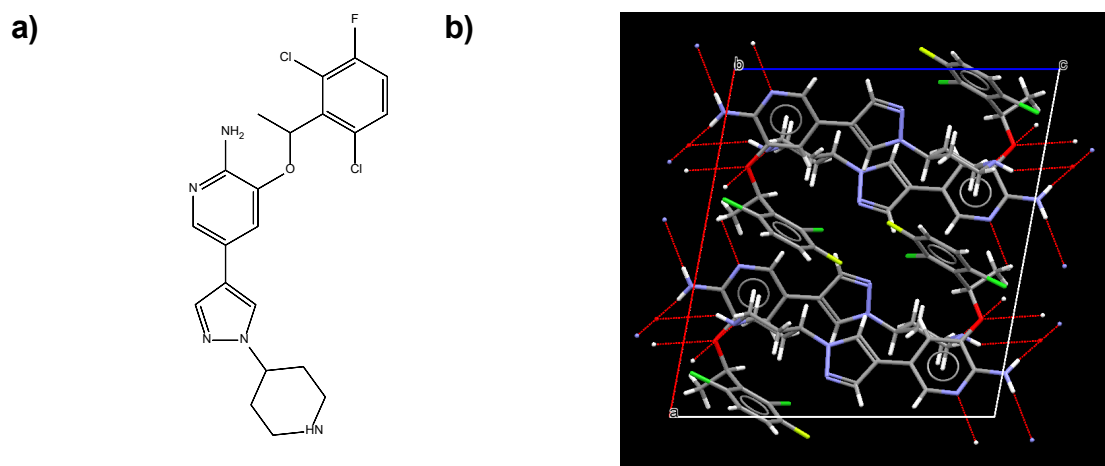
Figure 8.16 – Crizotinib a) chemical structure and b) unit cell.

The lattice energy was calculated to be -167.3 kJ/mol. Unfortuntely no sublimation enthaplies were available for comparison; therefore, the work was continued using the force field selected (Dreiding II).

The intermolecular interactions (intrinsic synthons) were examined for their contribution to the lattice energy, where nine interactions compromising of six interaction types are shown to make up 85% of the total lattice energy (Figure 8.17). Unlike the previous molecular crystals investigated, crizotinib does not contain one dominant interaction but, instead, there are two dominant interactions contributing to the total lattice energy. The highest energy intermolecular interaction is shown to be a π-π stacking interaction, contributing 20%, followed by the second strongest, another π-π stacking interaction which contributes 15%. All other interactions are shown to be dispersive and the hydrogen bonding does not contribute to the top nine interactions suggesting that this interaction is relatively weak compared to the others.
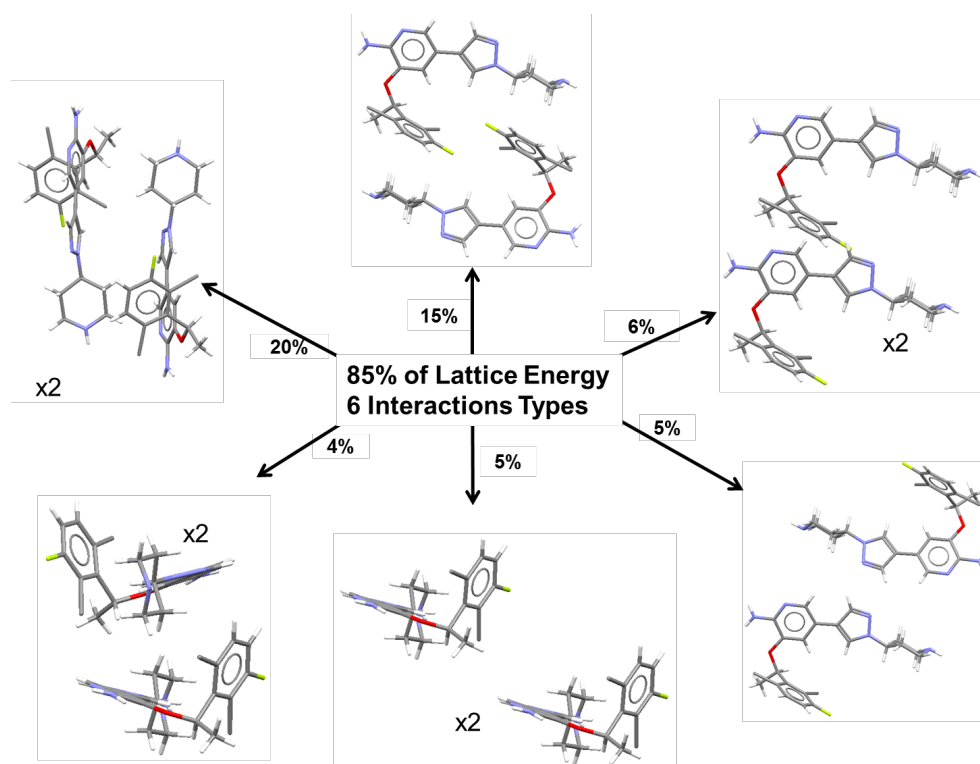
Figure 8.17 – Key types of intermolecular interactions in crizotinib and their contribution to the total lattice energy.

Crizotinib was then divided into molecular components and the lattice energy collapsed onto the individual atoms and summed across each fragment (Figure 8.18). The molecular components were ranked in terms of energy contributions to the total lattice energy, where it can be seen that the lattice energy is fairly evenly distributed across the molecule. The highest energy interaction, shown in red, contributes to 28.5% of the total lattice energy and contains 30.8% of the atoms. The lowest energy interaction, shown in blue, contributes 11.1% to the total lattice energy but contains 13.5% of the atoms. This is in agreement with the intermolecular interaction survey where there was no one dominant interaction and all of the atomic parts play a substantial role in stabilisation of the lattice. From the foregoing information it is predicted that the surface energy of the faces should be reasonably similar.
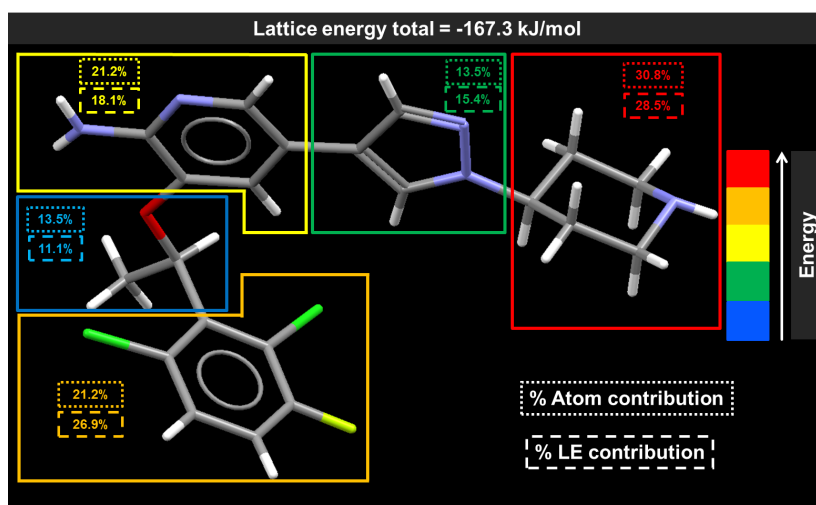
Figure 8.18 – Crizotinib lattice energy collapsed onto atoms, summed over molecular components and ranked in terms of energy.

The attachment energy morphology of crizotinib was calculated and a plate/rhombic like particle shape with four dominant faces was predicted: (0 0 1), (2 0 0), (-1 1 0) and (-1 -1 0). The surface chemistry of these faces was viewed and the surface energy calculated using the attachment energy equation (Figure 8.19). The surface energy of the main (0 0 1) face is shown to be the lowest with a value of 29.9 mJ/m^2. All other faces are shown to be similar in terms of energy with their predicted surface energies lying between 40.1 mJ/m^2 – 41.0 mJ/m^2. It is clear from the images that despite the (0 0 1) face containing the highest energy group at the surface it is lowest in terms of surface energy. As the lattice energy is distributed evenly across the molecule this method of viewing surface energy may be deemed inappropriate for this API. Another approach could be used where the percentage molecular contribution to the lattice energy is divided by the total number of atoms present in the molecular component, which may be more representative for this structure.

a)

b)

Surface energy shown in grey box (mJ/m^2)
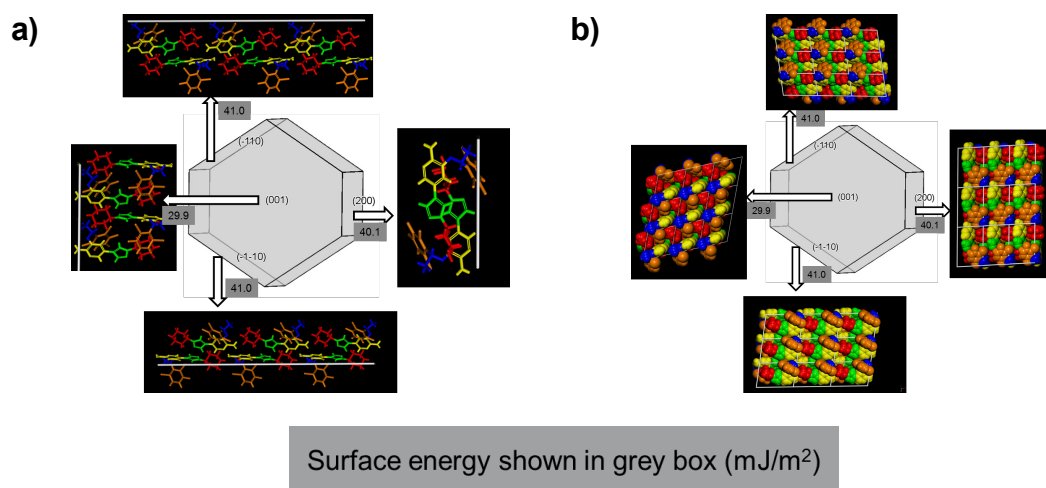
Figure 8.19 – Surface chemistry of crizotinib, where each molecular component is coloured relating its atomic contribution to its lattice energy, a) side view and b) top view.

8.3.2.2 Particle Morphology of Crizotinib

Scanning electron microscopy (SEM) was utilised to visualise the particle morphology of the unmilled and milled batches of crizotinib (Figure 8.20a and Figure 8.20b, respectively). As expected, due to the milling, physical property differences between the two batches are observed. The unmilled batch contains plate/rhombic shaped particles whereas the milled batch contains angular irregular shaped particles. Both batches contain a similar proportion of fine particles however the large particles have decreased in size in the milled batch. The particle surfaces of the unmilled batch are also smoother than the milled batch.

a)

b)
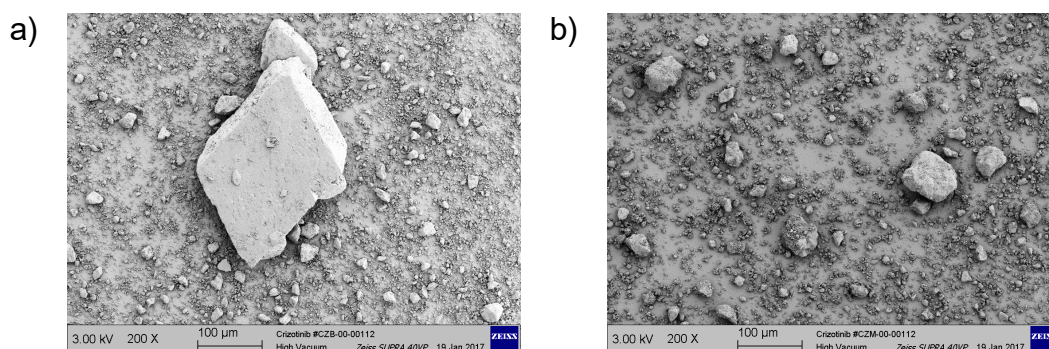
Figure 8.20 – Scanning electron micrographs of crizotinib before and after milling, a) unmilled (plate/rhombic/irregular shaped) and b) milled (angular shaped). All images captured using x200 magnification and the scale bar represents 100 µm.

156

Particle size analysis, using QICPIC, was performed on the two batches and the number distributions (most sensitive to smaller particles in the sample) are shown in Figure 8.21a. Both the unmilled and milled batch are shown to contain a similar proportion of particles by number, despite the material undergoing milling. The volume distributions (most sensitive to larger particles in the sample) are shown in Figure 8.21b, where it can be seen that the unmilled batch contains a bimodal and wider size distribution than the milled batch. The average, by volume, for the unmilled batch is 187.6 μm compared to 69.9 μm for the milled batch, confirming that the milling step has caused a reduction in particle size.
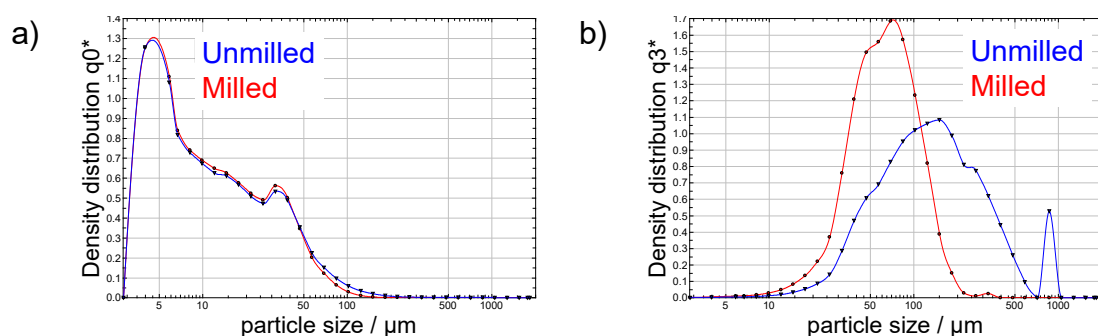
Figure 8.21 – QICPIC a) number and b) volume weighted distributions for crizotinib.

The QICPIC aspect ratio versus particle size for the two batches was calculated and the data in the resultant plot (Figure 8.22) shows that the milled batch has a higher aspect ratio than the unmilled batch. This data agrees with the data from the SEM electron micrographs, where the milling step has produced more regular particles.

157
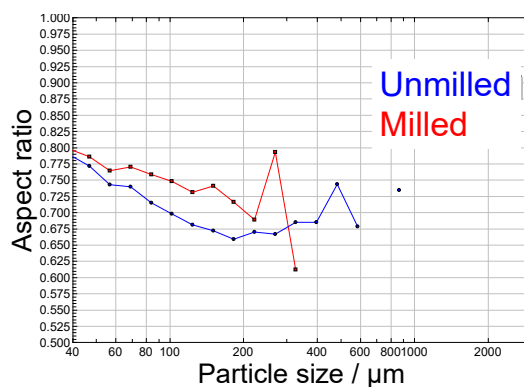
Figure 8.22 – QICPIC aspect ratio of crizotinib.

8.3.2.3 Surface Energy of Crizotinib

Surface energy heterogeneity was calculated for the two batches using IGC and split into dispersive and specific components. The total surface energy plot is shown in Figure 8.23 where, at all surface coverages analysed, the milled batch exhibits a higher surface energy than the unmilled batch. This is expected, as milling has been shown to increase the surface energy of pharmaceutical powders [193].
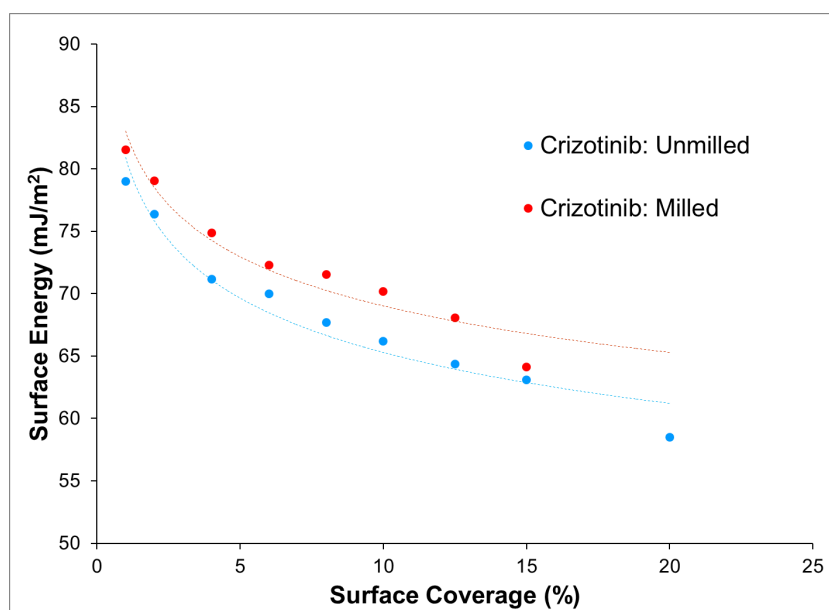
Figure 8.23 – Total surface energy heterogeneity plot for unmilled and milled batches of crizotinib.

To understand the contribution from specific surface energy to the total surface energy, pie charts (Figure 8.24) were constructed. Despite the milled material containing a slightly higher total surface energy, the contribution from specific surface energy is shown to be similar for each batch: 23.1% for unmilled and 23.2% for milled. From the IGC data it is predicted that the milled and unmilled batches would exhibit similar sticking propensity, due to similar specific surface energy contributions.
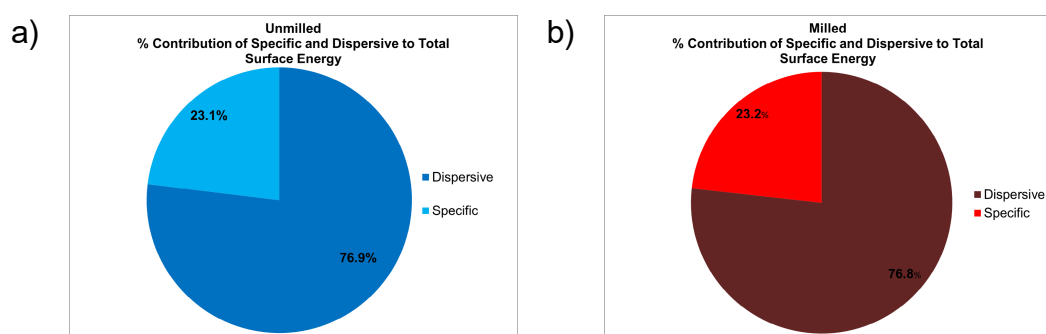
Figure 8.24 – Pie chart representing the percent contribution from dispersive and specific surface energy to total surface energy of a) unmilled and b) milled crizotinib.

The surface energy of the attachment energy morphology was calculated and revealed to be 35.0 mJ/m^2. This value is much is much lower than the experimental value for the unmilled batch (58.5 mJ/m^2 at 20% surface coverage). Again, this difference could be due to the different approaches used in the computational and experimental determination of surface energy.

In this project the surface energy of the milled batch could not be determined using the computational methodologies described, due to the milling causing an unknown impact to the crystal surfaces. The particle surfaces present in milled crystals are thought to be those with the lowest attachment energy [197] and disorder in the crystallinity could also be induced after milling [198]. In order to model the surface energy, further interrogation of the intermolecular interactions would be needed and this is outside the scope of this project; therefore, the predicted milled surface energy will not be considered.

8.3.2.4 <u>Sticking Propensity of Crizotinib</u>

The sticking propensity of the milled and unmilled batches were measured by recording the detachment stress from the base die post compaction. The data for the detachment stress measurements, at two compaction pressures, are shown in Figure 8.25. At the highest compaction pressure (180 MPa) no data could be recorded using the hand held force gauge due to the material sticking the instrument die parts together. The force required to overcome this sticking was too high for the user operating the instrument to successfully move the parts. Readings were captured at the lowest (40 MPa) and middle (120 MPa) compaction pressures, where it is shown that the unmilled batch exhibits a higher sticking propensity then the milled batch. This is an unexpected trend as the specific surface energy values would predict these batches to behave similarly. If the total surface energy, from IGC results, is considered the milled batch is shown to have a higher surface energy; so, again, there is no correlation. If size and shape are considered, the milled batch contains the smallest particle size and highest aspect ratio; therefore, it would be expected that this batch would stick more. From this data it can be concluded that there are no correlations with the physicochemical data and the sticking propensity, as found for ibuprofen and palbociclib, suggesting other factors may be influencing this behaviour.
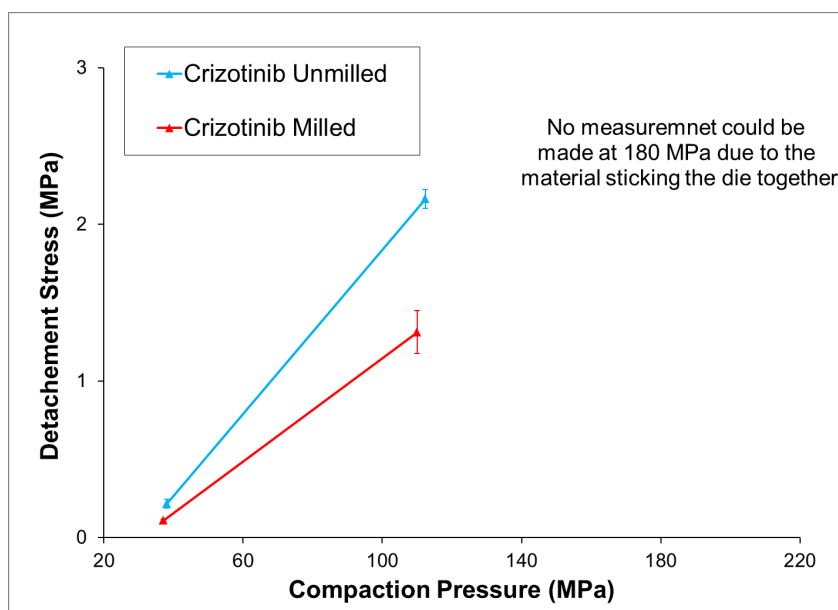
Figure 8.25 – Sticking propensity of crizotinib to the base die. Error bars represent standard deviation of three measurements.

8.3.3   Ranking of the Sticking Propensity of Ibuprofen, Palbociclib and Crizotinib in Relation to their Physicochemical Properties

In order to compare the APIs studied in terms of their sticking propensity and physicochemical properties the following data was selected: aspect ratio (between 50 µm – 350 µm), sticking propensity at 180 MPa and the total surface energy at 4% surface coverage.   The computational data was not available for all shapes analysed; therefore, it is only included where data is available.   As no sticking propensity data was available for crizotinib at the highest compaction pressure, it was assumed that this material exhibited a higher value than the other APIs studied; therefore a value of 10 kg is used.

The comparison, shown in Table 8.1, reveals that as the sticking propensity decreases the batches typically rank lower in terms of total surface energy and aspect ratio.   Crizotinib (referred to as Criz), exhibits the highest punch sticking and rank the highest in terms of total surface energy and aspect ratio. The ranking of the sticking propensity of palbociclib was dependent on particle shape, where low aspect ratio (needles) resulted in a lower sticking propensity compared to laths which were places fifth in terms of sticking propensity.   Again, the sticking propensity of ibuprofen was highly dependent

on particle shape, where batches with low aspect ratios exhibited lower sticking propensity.

The contribution of the specific surface energy to the total surface energy and the predicated computational surface energy do not exhibit a trend with the sticking propensity data for different APIs. Although these properties do not show a strong correlation between different API molecular crystals, previous work has shown they are a useful tool when considering crystal shape differences that may arise between the same API.

Table 8.1 – API sticking propensity (at 180 MPa), total surface energy (at 4% surface coverage), contribution from specific surface energy, aspect ratio (50 μm – 350 μm) and computational surface energy. 1 = high and 8 = low.

API	Shape	Sticking Propensity	Total Surface Energy	Specific Surface Energy	Aspect Ratio	Comp Surface Energy
Criz	Rhomb	1	2	9	2	3
Criz	Angular	2	1	8	1	
Ibu	Prism	3	3	1	3	1
Ibu	Plate	4	4	4	4	
Palbo	Lath	5	7	6	8	4
Ibu	Lath	6	8	5	5	
Ibu	Needle	7	6	3	6	2
Palb	Needle	8	5	7	7	5

When considering a comparison of the sticking propensity data, between different APIs, other factors which may affect this data must be considered. The environmental humidity at time of compaction may be an influencing factor as the experiments were run on different days. The ibuprofen data was collected when the humidity was between 27 – 30% RH and the crizotinib data was collected when the humidity was 36% RH. The palbociclib analysis was performed on a day when the humidity was much higher (52% RH); therefore, if this material is hygroscopic then this may influence the behaviour.

In general, it has been shown that the smaller particle size of an API leads to a greater propensity to stick. If a holistic view of particle size is considered

then the sticking propensity of the APIs compared do not rank in terms of size. The stickiest material, unmilled crizotinib, has a volume weighted average of 187.6 µm compared to the least sticky material, palbociclib needles, which has a volume weighted average of 73.7 µm. This data reveals that particle size is not the only root cause for sticking and other factors such as particle shape and surface energy are important factors to be considered.

8.4 Conclusions

This chapter utilises the computational and experimental methodologies developed in previous chapters to explore different API molecular crystals. The crystal chemistry of palbociclib and crizotinib were explored as well as the size/shape and surface energy. Characterisation of palbociclib revealed that changes in particle shape resulted in different degrees of sticking, where particles with a more regular shape resulted in a higher sticking propensity. Exploration of the crystal chemistry revealed that this may be due to the exposure of unsaturated high energy intermolecular interactions present in greater proportion in these crystals. The total surface energy, measured by IGC, did not trend with this observation, where the lath shaped particles which exhibited the highest sticking propensity had a lower surface energy compared to the needles. The specific surface energy was considered as a percentage contribution of the total surface energy and the lath shaped particles showed a greater contribution from the specific surface energy component, in agreement with the work reported for ibuprofen that the specific surface energy part may be influencing the sticking propensity.

Characterisation of unmilled and milled crizotinib revealed differences in physical properties between the two batches. The unmilled batch contained rhomb shaped particles of a larger size compared to the milled batch which contained smaller, irregular shaped particles. As expected, the surface energy, measured by IGC, was shown to be higher for the milled batch compared to the unmilled batch. Computational surface energy was not predicted for the milled material due to the crystal faces present being unknown. The sticking propensity of the two batches was measured, where

163

the unmilled batch was shown to be stickier than the milled batch. Both batches were revealed to have a similar contribution from specific surface energy; therefore, it is hypothesised that factors other than particle size/shape/surface energy are influencing the sticking propensity of crizotinib.

A comparison between the sticking propensity, aspect ratio, total surface energy, specific surface energy and computational surface energy for all API shapes considered in this thesis was made. It was revealed that particle shape and total surface energy show a strong correlation between the sticking propensity where a high aspect ratio (regular shape) and high surface energy lead to a greater propensity to stick. The specific surface energy measured experimentally and total surface energy measured computationally have been shown as useful tool to fundamentally understand the surface chemistry. These attributes can be used to explain different sticking behaviour between different shapes of the same API, where particles with a high proportion of faces that contain unsaturated, high energy intermolecular interactions at the surface are more likely to stick. If high energy intermolecular interactions are known to be present at the surface of the face it may be possible to engineer different particle shapes through crystallisation processes to reduce the presence these interactions and therefore minimise sticking propensity.

9. Chapter Nine: General Conclusions and Future Work

9.1 Conclusions

The research reported in this thesis has successfully demonstrated the use of a novel bench top tablet press to predict the deformation mechanisms, tabletability and sticking propensity of APIs. The plasticity of ibuprofen and its sodium salt were confirmed and a clear methodology reported to determine the yield pressure of pharmaceutical powders using the Heckel equation. It was found that for ibuprofen, the greatest range of linearity is observed when pressures of 121 MPa were used for analysis. Therefore, it is proposed that in order to enable a useful comparison of yield pressure, high compaction pressures (around 121 MPa) should be used for future analysis as well as transparency around experimental conditions used.

In general, a correlation between an APIs particle shape and sticking propensity was found, where particles with a high aspect ratio (regular shape) exhibit a higher sticking propensity than low aspect ratio particles (needle shape). For ibuprofen, it was found that needle shaped particles formed stronger tablets compared to regular shaped particles making needle shaped particles optimum for direct compression with regards to tensile strength and sticking propensity. It has been noted that needle shaped particles can be problematic for other unit operations during the manufacturing process such as filtration and flow. The research presented in this thesis revealed that sticking propensity increased exponentially and tensile strength decreased linearly, with respect to the percentage of cubes in an API mixture. This suggests that it may be possible to find an optimum mixture of API particle shape in order to balance the many aspects of direct compression manufacturing e.g. tablet hardness, sticking propensity and flow.

The effect of particle shape on sticking propensity was probed further where, through the use of computational and experimental techniques, a link between a specific surface energy and sticking propensity was made. It is hypothesised that during tablet manufacture, punches may become positively charged which could attract particles containing a higher proportion of negatively charged surfaces leading to a greater sticking propensity. For

ibuprofen, no link between the surface energetics of the powder and tensile strength of tablets could be made. It is therefore hypothesised that differences in tensile strength arise due to the physical effects of changing particle shape.

The crystal chemistry of each API investigated was explored and provided useful insights to the surface chemistry. A novel, user-friendly approach of viewing surfaces at a molecular level was presented. Molecular components were colour coded in relation to their contribution to lattice energy which allowed a qualitative assessment of surface energy of individual faces. Surface energy values were also calculated for each modelled particle shape. This work correlated with the experimental surface energy work where particles with a greater presence of crystal faces containing high energy intermolecular interactions at the surface were shown to stick more. This work was useful when dealing with API shape changes that were driven by the crystallisation process. In the case of crizotinib where the shape was changed via milling the surface energy was not predicted due to the crystal faces present not being known.

9.2   Future Work

In order to understand the Heckel equation in relation to pharmaceutical powders further, it is proposed that other APIs as well as excipients are investigated using the linear regression methodology described in this thesis. These experiments would give a greater understanding of the optimum yield pressure for compaction and allow for alignment in these measurements across different research groups. A greater understanding of both APIs and excipients deformation properties would ultimately aid formulators in making tablets more efficiently for patients.

A limitation of the sticking test developed was the hand held instrumentation used to measure the detachment force. The vendor of the instrument now provides a fully automated instrument therefore it is suggested that sticking measurements should be made to understand if the variation present in results is due to an inherent property of the test or the handheld

instrumentation. It is proposed that sticking data from the instrument should be compared to production data in order to assess its accuracy of prediction. The sticking propensity measured in this thesis was to the bottom punch only, however different types of sticking are present within the pharmaceutical industry e.g. upper punch, die wall sticking. A suggestion for future work would be to investigate different types of punch sticking and try to understand the root cause for these.

This work reports that needle shaped particles are less likely to stick to punches compared to regular shaped particles, however needle shaped particles can be problematic for other unit operations. It is also noted that a mixture of shapes (needles and cubes) could be used to minimise sticking propensity and aid flow. Further characterisation work in this area could include flow testing of the API mixtures in order to provide details on an optimum API shape mixture for use in formulations. Work should also include full scale formulation and manufacture e.g. on a production press, of API shapes in formulation to confirm the commercial benefit of shape changes.

Future work could include using imaging techniques, such as X-ray microtomography, to image particles during compaction to understand how they rearrange. In this study, differences in tensile strengths were found between laths and a lath/needle mixture and visualising the compaction process could provide useful insights into the particle rearrangement.

The investigation into surface chemistry was limited to materials that had undergone changes in shape via crystallisation only. To explore the effect of milling behaviour on surface chemistry, intermolecular interactions could be probed further to determine what the weakest interactions are and therefore what faces are more likely to undergo attrition and be present in milled material.

Finally, expanding these ideas to other crystalline solid-state APIs e.g. co-crystals or hydrates would be advantageous. Experimentally the methodologies could be used as presented however further work would be needed to develop the computational work as modelling two component systems is not always reliable.

REFERENCES

1. Abramov, Y.A., *Computational Pharmaceutical Solid-State Chemistry*, in *Computational Pharmaceutical Solid State Chemistry*. 2016, John Wiley & Sons, Inc. 1-13.

2. Shergill, M., M. Patel, S. Khan, A. Bashir, and C. McConville, *Development and characterisation of sustained release solid dispersion oral tablets containing the poorly water soluble drug disulfiram.* International Journal of Pharmaceutics, **497**(1–2), 3-11, 2016

3. Mestel, R., *The Colourful History of Pills Can Fill Many a Tablet*, in *Los Angeles Times*. 2002, Los Angeles Times: L.A., USA.

4. Gohel, M.C. and P.D. Jogani, *A review of co-processed directly compressible excipients.* Journal of Pharmacy & Pharmaceutical Sciences **8**(1), 76-93, 2005

5. Mohan, S., *Compression Physics of Pharmaceutical Powders: A Review.* International Journal of Pharmaceutical Sciences and Research, **3**, 1580-1592, 2012

6. Gerhardt, A.H., *Fundamentals of Tablet Compression.* Journal of GXP Complaince, **14**, 70-79, 2010

7. Alderborn, G., *Tablets and compaction* in *Aulton's pharmaceutics : the design and manufacture of medicines*, M.E. Aulton, Editor. 2007, Churchill Livingstone.

8. Tye, C.K., C. Sun, and G.E. Amidon, *Evaluation of the effects of tableting speed on the relationships between compaction pressure, tablet tensile strength, and tablet solid fraction.* Journal of Pharmaceutical Sciences, **94**(3), 465-472, 2005

9. Carstensen, J.T., *Pharmaceutical Principles of Solid Dosage Forms*. 1993: CRC Press.

10. Nichols, G. and C.S. Frampton, *Physicochemical characterization of the orthorhombic polymorph of paracetamol crystallized from solution.* Journal of Pharmaceutical Sciences, **87**(6), 684-693, 1998

11. Nermoen, A., R.I. Korsnes, O. Aursjø, M.V. Madland, T.A.C. Kjørslevik, and G. Østensen, *How Stress and Temperature Conditions Affect Rock-Fluid Chemistry and Mechanical Deformation.* Frontiers in Physics, **4**(2), 2016

12. Katz, J.M. and I.S. Buckner, *Characterization of strain rate sensitivity in pharmaceutical materials using indentation creep analysis.* International Journal of Pharmaceutics, **442**(1–2), 13-19, 2013

13. Evin, E., M. Tomáš, J. Kmec, S. Németh, B. Katalinic, and E. Wessely, *The Deformation Properties of High Strength Steel Sheets for Auto-body Components.* Procedia Engineering, **69**, 758-767, 2014

14. John M. Cottle, Michael P. Searle, Matthew S. A. Horstwood, and David J. Waters, *Timing of Midcrustal Metamorphism, Melting, and Deformation in the Mount Everest Region of Southern Tibet Revealed by U(-Th)-Pb Geochronology.* The Journal of Geology, **117**(6), 643-664, 2009

15. Perkins, M., S.J. Ebbens, S. Hayes, C.J. Roberts, C.E. Madden, S.Y. Luk, and N. Patel, *Elastic modulus measurements from individual*

lactose particles using atomic force microscopy. International Journal of Pharmaceutics, **332**(1–2), 168-175, 2007

16. Buckner, I.S., D.E. Wurster, and A. Aburub, *Interpreting deformation behavior in pharmaceutical materials using multiple consolidation models and compaction energetics.* Pharmaceutical Development and Technology, **15**(5), 492-499, 2010

17. Taylor, L.J., D.G. Papadopoulos, P.J. Dunn, A.C. Bentham, N.J. Dawson, J.C. Mitchell, and M.J. Snowden, *Predictive Milling of Pharmaceutical Materials Using Nanoindentation of Single Crystals.* Organic Process Research & Development, **8**(4), 674-679, 2004

18. Heckel, R.W., *Density-Pressure Relationship in Powder Compaction.* Trans. Met. Soc. AIME, **221**, 671–675, 1961

19. Sonnergaard, J.M., *A critical evaluation of the Heckel equation.* Int. J. Pharm., **193**, 63-71, 1999

20. Nystrom, C. and P.-G. Karehill, *The Importance of Intermolecular Bonding Forces and the Concept of Bonding Surface Area*, in *Pharmaceutical Powder Compaction Technology*, G. Alderborn and C. Nystrom, Editors. 1995, Marcel Dekker, Inc.

21. Jivraj, M., L.G. Martini, and C.M. Thomson, *An overview of the different excipients useful for the direct compression of tablets.* Pharmaceutical Science & Technology Today, **3**(2), 58-63, 2000

22. Sun, C.C., *Materials science tetrahedron—A useful tool for pharmaceutical research and development.* Journal of Pharmaceutical Sciences, **98**(5), 1671-1687, 2009

23. Modi, S.R., K.S. Khomane, and A.K. Bansal, *Impact of differential surface molecular environment on the interparticulate bonding strength of celecoxib crystal habits.* International Journal of Pharmaceutics, **460**(1–2), 189-195, 2014

24. Reier, G.E. and R.F. Shangraw, *Microcrystalline cellulose in tableting.* Journal of Pharmaceutical Sciences, **55**(5), 510-514, 1966

25. Shekunov, B.Y., P. Chattopadhyay, H.H.Y. Tong, and A.H.L. Chow, *Particle Size Analysis in Pharmaceutics: Principles, Methods and Applications.* Pharmaceutical Research, **24**(2), 203-227, 2007

26. Joiris, E., P.D. Martino, C. Berneron, A.-M. Guyot-Hermann, and J.-C. Guyot, *Compression Behavior of Orthorhombic Paracetamol.* Pharmaceutical Research, **15**(7), 1122-1130,

27. Iacocca, R.G., C.L. Burcham, and L.R. Hilden, *Particle engineering: A strategy for establishing drug substance physical property specifications during small molecule development.* Journal of Pharmaceutical Sciences, **99**(1), 51-75,

28. Almaya, A. and A. Aburub, *Effect of Particle Size on Compaction of Materials with Different Deformation Mechanisms with and without Lubricants.* AAPS PharmSciTech, **9**(2), 414-418, 2008

29. Mosharraf, M. and C. Nyström, *The effect of particle size and shape on the surface specific dissolution rate of microsized practically insoluble drugs.* International Journal of Pharmaceutics, **122**(1), 35-47, 1995

30. Zeng, X.-M., *Particulate Analysis - Particle Size*, in *Solid State Characterization of Pharmaceuticals*, R.A. Storey and I. Ymen, Editors. 2011, Blackwell Publishing Ltd. 387-425.

31. Kelemen, A., A. Szalay, T. Sovány, and K. Pintye-Hódi, *Role of the particle size of sorbitol during the compression of common tablets and prediction of mini-tablet compression parameters.* Chemical Engineering Research and Design, **104**, 814-818, 2015

32. Stoica, C., P. Verwer, H. Meekes, P.J.C.M. van Hoof, F.M. Kaspersen, and E. Vlieg, *Understanding the Effect of a Solvent on the Crystal Habit.* Crystal Growth & Design, **4**(4), 765-768, 2004

33. Ma, J.K.H. and B. Hadzija, *Pharmaceutical Powders*, in *Basic Physical Pharmacy*. 2013, Jones and Bartlett Learning. 220-247.

34. Nichols, G., *Light Microscopy*, in *Polymorphism: in the Pharmaceutical Industry*, R. Hilfiker, Editor. 2006, WILEY-VCH Verlag GmbH & Co. KGaA: Weinheim 167-209.

35. Yu, W., K. MUTEKI, L. ZHANG, and G. KIM, *Prediction of Bulk Powder Flow Performance Using Comprehensive Particle Size and Particle Shape Distributions.* J. Pharm. Sci, **100**(1), 284-293, 2011

36. Yu, W., L. Liao, R. Bharadwaj, and B.C. Hancock, *What is the "typical" particle shape of active pharmaceutical ingredients?* Powder Technology, **313**, 1-8, 2017

37. Maguire, J. and D. Peng, *How to Identify Critical Quality Attributes and Critical Process Parameters*, in *FDA/PQRI 2nd Conference*. 2015: North Bethesda, Maryland.

38. Kirsch, D., *Fixing Tableting Problems.* Pharmaceutical Technology, **39**(5), 2015

39. Pharmatron, D.S. http://www.pharmatron.com/newsroom/news/article/key-factors-influencing-measured-tablet-hardness/. 2011 [cited 2017, September].

40. Akande, O.F., J.L. Ford, P.H. Rowe, and M.H. Rubinstein, *Pharmaceutics: The Effects of Lag-time and Dwell-time on the Compaction Properties of 1:1 Paracetamol/microcrystalline Cellulose Tablets Prepared by Pre-compression and Main Compression.* Journal of Pharmacy and Pharmacology, **50**(1), 19-28, 1998

41. Anbalagan, P., P.W.S. Heng, and C.V. Liew, *Tablet compression tooling – Impact of punch face edge modification.* International Journal of Pharmaceutics, **524**(1–2), 373-381, 2017

42. Sun, C. and D.J.W. Grant, *Effects of initial particle size on the tableting properties of L-lysine monohydrochloride dihydrate powder.* Int J Pharm, **215**, 221-228, 2001

43. Seton, L., M. Roberts, and F. Ur-Rehman, *Compaction of recrystallised ibuprofen.* Chemical Engineering Journal, **164**(2–3), 449-452, 2010

44. Natoli, D., M. Levin, L. Tsygan, and L. Liu, *Development, Optimization and Scale-up of Process Parameters: Tablet Compression*, in *Developing Solid Oral Dosage Forms: Pharmaceutical Theory & Practice*, Y. Qiu, Y. Chen, and G.G.Z. Zhang, Editors. 2009, Elsevier.

45. Wu, C.Y., B.C. Hancock, A. Mills, A.C. Bentham, S.M. Best, and J.A. Elliott, *Numerical and experimental investigation of capping mechanisms during pharmaceutical tablet compaction.* Powder Technology, **181**(2), 121-129, 2008

46. Mazel, V., H. Diarra, V. Busignies, and P. Tchoreloff. *Capping: A Mechanical Perpestive*. in *Compaction Simulation Forum*. 2017. Ghent.

47. Tousey, M.D., *Tablet Press Operation.* Tablets and Capsules, **October**, 2003

48. McDermott, T.S., J. Farrenkopf, A. Hlinak, J.P. Neilly, and D. Sauer, *A material sparing method for quantitatively measuring tablet sticking.* Powder Technology, **212**(1), 240-252, 2011

49. Roberts, M., J.L. Ford, P.H. Rowe, A.M. Dyas, G.S. MacLeod, J.T. Fell, and G.W. Smith, *Effect of lubricant type and concentration on the punch tip adherence of model ibuprofen formulations.* Journal of Pharmacy and Pharmacology, **56**(3), 299-305, 2004

50. Roberts, M., J.L. Ford, G.S. MacLeod, J.T. Fell, G.W. Smith, P.H. Rowe, and A.M. Dyas, *Effect of punch tip geometry and embossment on the punch tip adherence of a model ibuprofen formulation.* Journal of Pharmacy and Pharmacology, **56**(7), 947-950, 2004

51. Danjo, K., S. Kojima, C.Y. Chen, H. Sunada, and A. Otsuka, *Effect of Water Content on Sticking during Compression.* CHEMICAL & PHARMACEUTICAL BULLETIN, **45**(4), 706-709, 1997

52. Corn, M., *The Adhesion of Solid Particles to Solid Surfaces. I. A Review.* Journal of the Air Pollution Control Association, **11**, 523-528, 1961

53. Danjo, K., K. Kamiya, and A. Otsuka, *Effect of Temperature on the Sticking of Low Melting Point Materials.* CHEMICAL & PHARMACEUTICAL BULLETIN, **41**(8), 1423-1427, 1993

54. Uchimoto, T., Y. Iwao, T. Yamamoto, K. Sawaguchi, T. Moriuchi, S. Noguchi, and S. Itai, *Newly developed surface modification punches treated with alloying techniques reduce sticking during the manufacture of ibuprofen tablets.* International Journal of Pharmaceutics, **441**(1), 128-134, 2013

55. Al-Karawi, C., I. Lukášová, A. Sakmann, and C.S. Leopold, *Novel aspects on the direct compaction of ibuprofen with special focus on sticking.* Powder Technology, **317**, 370-380, 2017

56. Reed, K., C. Davies, and K. Kelly, *Tablet sticking: Using a 'compression toolbox' to assess multiple tooling coatings options.* Powder Technology, **285**, 103-109, 2015

57. *iHolland http://tablettingscience.com/steel-and-coating-technology_pharmacote.asp*. 2015 [cited 2017, August].

58. Shimada, Y., Y. Yonezawa, and H. Sunada, *Measurement and Evaluation of the Adhesive Force between Particles by the Direct Separation Method.* Journal of Pharmaceutical Sciences, **92**(3), 560-568, 2003

59. Lam, K.K. and J.M. Newton, *Investigation of applied compression on the adhesion of powders to a substrate surface.* Powder Technology, **65**(1), 167-175, 1991

60. Lam, K.K. and J.M. Newton, *Influence of particle size on the adhesion behaviour of powders, after application of an initial press-on force.* Powder Technology, **73**(2), 117-125, 1992

61. Rasenack, N. and B.W. Muller, *Crystal habit and tableting behavior.* Int. J. Pharm., **244**, 45-57, 2002

62. Waknis, V., E. Chu, R. Schlam, A. Sidorenko, S. Badawy, S. Yin, and A. Narang, *Molecular Basis of Crystal Morphology-Dependent*

Adhesion Behavior of Mefenamic Acid During Tableting. Pharmaceutical Research, **31**(1), 160-172, 2014

63. Metzler, K. *Tablet Press Simulation.* in *Compaction Simulation Forum.* 2012. Cambridge, MA.

64. Gamlen, M., *The Importance of Normalisation when Comparing Tablet Properties*, G.T. Ltd., Editor. 2015: Online.

65. Alderborn, G. *Analytical Powder Compression.* in *Compaction Simulation Forum.* 2015. Copenhagen.

66. Newton, J.M., I. Haririan, and F. Podczeck, *The influence of punch curvature on the mechanical properties of compacted powders.* Powder Technology, **107**(1–2), 79-83, 2000

67. Pitt, K.G. and M.G. Heasley, *Determination of the tensile strength of elongated tablets.* Powder Technology, **238**, 169-175, 2013

68. Pitt, K. *Simulation of tabletting and the real-world payoff.* in *Compaction Simulation Forum.* 2013. Cambridge.

69. Wang, Z., U.V. Shah, D. Olusanmi, A.S. Narang, M.A. Hussain, J.F. Gamble, M.J. Tobyn, and J.Y.Y. Heng, *Measuring the sticking of mefenamic acid powders on stainless steel surface.* International Journal of Pharmaceutics, **496**(2), 407-413, 2015

70. Hutchins, A., B.C. MacDonald, and M.P. Mullarney, *Assessing Tablet-Sticking Propensity.* Pharmaceutical Technology, **36**(1), 2012

71. Variankaval, N., A.S. Cote, and M.F. Doherty, *From form to function: Crystallisation of active pharmaceutical ingredients.* AIChE Journal, **54**(7), 1682-1688, 2008

72. Gilmore, C.J., *X-Ray Diffraction*, in *Solid State Characterization of Pharmaceuticals*, R.A. Storey and I. Ymen, Editors. 2011, Blackwell Publishing

73. Heng, J.Y.Y. and D.R. Williams, *Vapour Sorption and Surface Analysis*, in *Solid State Characterization of Pharmaceuticals.* 2011, John Wiley & Sons, Ltd. 245-285.

74. Desiraju, G.R., *The C-H...O hydrogen bond in crystals: what is it?* Accounts of Chemical Research, **24**(10), 290-296, 1991

75. Aakeroy, C.B. and K.R. Seddon, *The hydrogen bond and crystal engineering.* Chemical Society Reviews, **22**(6), 397-407, 1993

76. Rosbottom, I., K.J. Roberts, and R. Docherty, *The solid state, surface and morphological properties of p-aminobenzoic acid in terms of the strength and directionality of its intermolecular synthons.* CrystEngComm, **17**(30), 5768-5788, 2015

77. Bastin, R.J., M.J. Bowker, and B.J. Slater, *Salt Selection and Optimisation Procedures for Pharmaceutical New Chemical Entities.* Organic Process Research & Development, **4**(5), 427-435, 2000

78. Feng, Y., D.J.W. Grant, and C.C. Sun, *Influence of crystal structure on the tableting properties of n-alkyl 4-hydroxybenzoate esters (parabens).* Journal of Pharmaceutical Sciences, **96**(12), 3324-3333, 2007

79. Sun, C.C. and H. Hou, *Improving Mechanical Properties of Caffeine and Methyl Gallate Crystals by Cocrystallisation.* Crystal Growth & Design, **8**(5), 1575-1579, 2008

80. Chattoraj, S., L. Shi, and C.C. Sun, *Understanding the relationship between crystal structure, plasticity and compaction behaviour of*

theophylline, methyl gallate, and their 1 : 1 co-crystal. CrystEngComm, **12**(8), 2466-2472, 2010

81.   Bag, P.P., M. Chen, C.C. Sun, and C.M. Reddy, *Direct correlation among crystal structure, mechanical behaviour and tabletability in a trimorphic molecular compound.* CrystEngComm, **14**(11), 3865-3867, 2012

82.   Upadhyay, P., K.S. Khomane, L. Kumar, and A.K. Bansal, *Relationship between crystal structure and mechanical properties of ranitidine hydrochloride polymorphs.* CrystEngComm, **15**(19), 3959-3964, 2013

83.   Perumalla, S.R. and C.C. Sun, *Enabling Tablet Product Development of 5-Fluorocytosine Through Integrated Crystal and Particle Engineering.* Journal of Pharmaceutical Sciences, **103**(4), 1126-1132, 2014

84.   Paul, S., K. Wang, L.J. Taylor, B. Murphy, J. Krzyzaniak, N. Dawson, M.P. Mullarney, P. Meenan, and C.C. Sun, *Dependence of Punch Sticking on Compaction Pressure—Roles of Particle Deformability and Tablet Tensile Strength.* Journal of Pharmaceutical Sciences, **106**(8), 2060-2067, 2017

85.   Gibbs, W.J., *The Scientific Papers of J. Willard Gibbs*, in *Thermodynamics*. 1961. 382-404.

86.   Wulff, G., Z. Kryst. Mineral, **34**, 449, 1901

87.   Lovette, M.A., A.R. Browning, D.W. Griffin, J.P. Sizemore, R.C. Snyder, and M.F. Doherty, *Crystal Shape Engineering.* Ind. Eng. Chem. Res, **47**, 9812-9833, 2008

88.   Frank, F.C., *On the Kinematic Theory of Crystal Growth and Dissolution Processes, II.* Zeitschrift für Physikalische Chemie, **77**, 84-92, 1972

89.   Gaylord, N.G. and B.G. Rånby, *Growth and perfection of crystals.* Journal of Polymer Science, **38**(133), 279-279, 1959

90.   Bravais, A., *Etudes Crystallographiques*. 1866, Paris: Gauthiers Villars.

91.   Donnay, J.D.H. and D. Harker, *A new law of crystal morphology extending the law of bravais.* Am Mineral, **22**, 446-467, 1937

92.   Friedel, G., *Bulletin De La Societe Francaise De Mineralogie Et De Crystallographie.* **30**, 326, 1907

93.   Docherty, R. and K.J. Roberts, *Modelling the morphology of molecular crystals; application to anthracene, biphenyl and β-succinic acid.* Journal of Crystal Growth, **88**(2), 159-168, 1988

94.   Hartman, P. and P. Bennema, *The attachment energy as a habit controlling factor.* Journal of Crystal Growth, **49**(1), 145-156, 1980

95.   El-Zhry El-Yafi, A.K. and H. El-Zein, *Technical crystallisation for application in pharmaceutical material engineering: Review article.* Asian Journal of Pharmaceutical Sciences, **10**(4), 283-291, 2015

96.   Nichols, G., S. Luk, and C. Roberts, *Microscopy*, in *Solid State Characterization of Pharmaceuticals*, R.A. Storey and I. Ymen, Editors. 2011, Blackwell Publishing Ltd. 287-355.

97.   Vernon-Parry, K.D., *Scanning electron microscopy: an introduction.* III-Vs Review, **13**(4), 40-44, 2000

98.   Jeol. *Scanning Electron Microscope A to Z* http://www.jeol.co.jp/en/applications/detail/891.html. 2009 [cited 2016, March].

99.   *http://www.ich.org/*.   [cited 2017, May].

100.   Li, M., D. Wilkinson, and K. Patchigolla, *Obtaining Particle Size Distribution from Chord Length Measurements.* Particle & Particle Systems Characterization, **23**(2), 170-174, 2006

101.   Jillavenkatesa, A., S.J. Dapkunas, and L.-S.H. Lum, *Size Characterization by Laser Light Diffraction Techniques*, in *Particle Size Characterization*. 2001, U.S. Government Printing Office: Washington. 93-125.

102.   Liu, K., *Some factors affecting sieving performance and efficiency.* Powder Technology, **193**(2), 208-213, 2009

103.   Merkus, H.G., *Sieves and Sieving*, in *Particle Size Measurements: Fundamentals, Practice and Quality*. 2009, Springer: Netherlands. 219-239.

104.   Allen, T., *Particle Size Analysis by Sieving* in *Powder Sampling and Particle Size Determination*. 2003, Elsevier 208-250.

105.   Sympatec. *Image Analysis for Particle Size and Shape Analysis* *https://www.sympatec.com/EN/ImageAnalysis/ImageAnalysis.html*. 2016 [cited 2017, February].

106.   Gamble, J.F., M. Tobyn, and R. Hamey, *Application of Image-Based Particle Size and Shape Characterization Systems in the Development of Small Molecule Pharmaceuticals.* Journal of Pharmaceutical Sciences, **104**(5), 1563-1574, 2015

107.   Yu, W. and B.C. Hancock, *Evaluation of dynamic image analysis for characterizing pharmaceutical excipient particles.* International Journal of Pharmaceutics, **361**(1–2), 150-157, 2008

108.   Kohler, U., T. Stubinger, and W. Witt. *Laser Diffraction Results From Dynamic Image Analysis* in *World Congress of Particle Technology*. 2010. Nuremberg, Germany.

109.   Hollek, M. *Dynamic Image Analysis for size and shape characterisation*. in *Particle Measurement*. 2016.

110.   Coleman, N.J. and D.Q.M. Craig, *Modulated temperature differential scanning calorimetry: A novel approach to pharmaceutical thermal analysis*. International Journal of Pharmaceutics, **135**(1), 13-29, 1996

111.   Clas, S.-D., C.R. Dalton, and B.C. Hancock, *Differential scanning calorimetry: applications in drug development.* Pharmaceutical Science & Technology Today, **2**(8), 311-320, 1999

112.   Saunders, M. and P. Gabbott, *Thermal Analysis - Conventional Techniques*, in *Solid State Characterization of Pharmaceuticals*. 2011.

113.   Song, H., K. Shah, E. Doroodchi, T. Wall, and B. Moghtaderi, *Analysis on Chemical Reaction Kinetics of CuO/SiO2 Oxygen Carriers for Chemical Looping Air Separation.* Energy & Fuels, **28**(1), 173-182, 2014

114.   Buckton, G., *Surface Characterization: Understanding Sources of Variability in the Production and Use of Pharmaceuticals*.* Journal of Pharmacy and Pharmacology, **47**(4), 265-275, 1995

115.   Buckton, G. and H. Gill, *The importance of surface energetics of powders for drug delivery and the establishment of inverse gas chromatography.* Advanced Drug Delivery Reviews, **59**(14), 1474-1479, 2007

116. Zielinksi, J.M. and L. Kettle, *Physical Characterization: Surface Area and Porosity.* Interek: White Paper, 2013

117. Heng, J.Y.Y., A. Bismarck, A.F. Lee, K. Wilson, and D.R. Williams, *Anisotropic surface chemistry of aspirin crystals.* Journal of Pharmaceutical Sciences, **96**(8), 2134-2144, 2007

118. Grimsey, I.M., J.C. Feeley, and P. York, *Analysis of the surface energy of pharmaceutical powders by inverse gas chromatography.* Journal of Pharmaceutical Sciences, **91**(2), 571-583, 2002

119. Zafar, U., C. Hare, A. Hassanpour, and M. Ghadiri, *Drop test: A new method to measure the particle adhesion force.* Powder Technology, **264**, 236-241, 2014

120. Newell, H.E., G. Buckton, D.A. Butler, F. Thielmann, and D.R. Williams, *The Use of Inverse Phase Gas Chromatography to Measure the Surface Energy of Crystalline, Amorphous, and Recently Milled Lactose.* Pharmaceutical Research, **18**(5), 662-666, 2001

121. Mohammadi-Jam, S. and K.E. Waters, *Inverse gas chromatography applications: A review.* Advances in Colloid and Interface Science, **212**(Supplement C), 21-44, 2014

122. http://www.americanpharmaceuticalreview.com/25310-Pharmaceutical-Manufacturing/25344-Pharmaceutical-Tablet-Press-Machine-Rotary-Tablet-Press/. [cited 2017, August].

123. Bourland, M.E. and M.P. Mullarney, *Compaction Simulation*, in *Pharmaceutical Dosage Forms*, S.W. Hoag, Editor. 2008, CRC Press. 519-553.

124. Osamura, T., Y. Takeuchi, R. Onodera, M. Kitamura, Y. Takahashi, K. Tahara, and H. Takeuchi, *Prediction of effects of punch shapes on tableting failure by using a multi-functional single-punch tablet press.* Asian Journal of Pharmaceutical Sciences, **12**(5), 412-417, 2017

125. http://gamlentableting.com/. [cited 2017, July].

126. Pitt, K.G., R.J. Webber, K.A. Hill, D. Dey, and M.J. Gamlen, *Compression prediction accuracy from small scale compaction studies to production presses.* Powder Technology, **270, Part B**, 490-493, 2015

127. Gavezzotti, A., *Are Crystal Structures Predictable?* Accounts of Chemical Research, **27**(10), 309-314, 1994

128. Abramov, Y.A., *Current Computational Approaches to Support Pharmaceutical Solid Form Selection.* Organic Process Research & Development, **17**(3), 472-485, 2013

129. Price, S.L., *Predicting crystal structures of organic compounds.* Chemical Society Reviews, **43**(7), 2098-2111, 2014

130. *The Cambridge Structural Database (CSD)* https://www.ccdc.cam.ac.uk/solutions/csd-system/components/csd/ 2016 [cited 2017, September].

131. Allen, F., *The Cambridge Structural Database: a quarter of a million crystal structures and rising.* Acta Crystallographica Section B, **58**(3 Part 1), 380-388, 2002

132. Bruno, I.J., J.C. Cole, P.R. Edgington, M. Kessler, C.F. Macrae, P. McCabe, J. Pearson, and R. Taylor, *New software for searching the Cambridge Structural Database and visualizing crystal structures.* Acta Crystallographica Section B, **58**(3 Part 1), 389-397, 2002

133. Clydesdale, G., R. Docherty, and K.J. Roberts, *HABIT - a program for predicting the morphology of molecular crystals.* Computer Physics Communications, **64**(2), 311-328, 1991

134. Clydesdale, G., K.J. Roberts, and R. Docherty, *HABIT95 — a program for predicting the morphology of molecular crystals as a function of the growth environment.* Journal of Crystal Growth, **166**(1–4), 78-83, 1996

135. *https://www.nhs.uk/conditions/nsaids/*. 2016 [cited 2017, Oct].

136. Nguyen, T.T.H., I. Rosbottom, I. Marziano, R.B. Hammond, and K.J. Roberts, *Crystal Morphology and Interfacial Stability of RS-Ibuprofen in Relation to Its Molecular and Synthonic Structure.* Crystal Growth & Design, **17**(6), 3088-3099, 2017

137. Gonzalez, M.A., *Force fields and molecular dynamics simulations.* SFN, **12**, 169-200, 2011

138. Paton, R.S. and J.M. Goodman, *Hydrogen Bonding and π-Stacking: How Reliable are Force Fields? A Critical Evaluation of Force Field Descriptions of Nonbonded Interactions.* Journal of Chemical Information and Modeling, **49**(4), 944-955, 2009

139. Datta, S. and D.J.W. Grant, *Crystal structures of drugs: advances in determination, prediction and engineering.* Nat Rev Drug Discov, **3**(1), 42-57, 2004

140. Nguyen, L.A., H. He, and C. Pham-Huy, *Chiral Drugs: An Overview.* International Journal of Biomedical Science : IJBS, **2**(2), 85-100, 2006

141. McConnell, J.F., Crystal structure communications, **3**, 73-75, 1974

142. Derollez, P., E. Dudognon, F. Affouard, F. Danede, N.T. Correia, and M. Descamps, *Ab initio structure determination of phase II of racemic ibuprofen by X-ray powder diffraction.* Acta Crystallographica Section B, **66**(1), 76-80, 2010

143. Sun, H., *COMPASS: An ab Initio Force-Field Optimized for Condensed-Phase Applications Overview with Details on Alkane and Benzene Compounds.* The Journal of Physical Chemistry B, **102**(38), 7338-7364, 1998

144. Gavezzotti, A. and G. Filippini, *Geometry of the Intermolecular X-H...Y (X, Y = N, O) Hydrogen Bond and the Calibration of Empirical Hydrogen-Bond Potentials.* The Journal of Physical Chemistry, **98**(18), 4831-4837, 1994

145. Dunitz, J.D. and A. Gavezzotti, *Supramolecular Synthons: Validation and Ranking of Intermolecular Interaction Energies.* Crystal Growth & Design, **12**(12), 5873-5877, 2012

146. Docherty, R., G. Clydesdale, K.J. Roberts, and P. Bennema, *Application of Bravais-Friedel-Donnay-Harker, attachment energy and Ising models to predicting and understanding the morphology of molecular crystals.* Journal of Physics D: Applied Physics, **24**(2), 89, 1991

147. Bunyan, J., N. Shankland, and D. Sheen, *Solvent Effects on The Morphology of Ibuprofen.* AIChE Symp. Ser., 45-57, 1991

148. Perlovich, G.L., S.V. Kurkov, L.K. Hansen, and A. Bauer-Brandl, *Thermodynamics of Sublimation, Crystal Lattice Energies, and Crystal Structures of Racemates and Enantiomers: (+)- and (±)-Ibuprofen.* Journal of Pharmaceutical Sciences, **93**(3), 654-666, 2004

149. Cano, H., N. Gabas, and J.P. Canselier, *Experimental study on the ibuprofen crystal growth morphology in solution.* J. Cryst. Growth, **224**, 335–341, 2001

150. Winn, D. and M.F. Doherty, *Modeling crystal shapes of organic materials grown from solution.* AIChE Journal, **46**(7), 1348-1367, 2000

151. Taylor, L.J., D.G. Papadopoulos, P.J. Dunn, A.C. Bentham, J.C. Mitchell, and M.J. Snowden, *Mechanical characterisation of powders using nanoindentation.* Powder Technology, **143–144**, 179-185, 2004

152. Meier, M., E. John, D. Wieckhusen, W. Wirth, and W. Peukert, *Influence of mechanical properties on impact fracture: Prediction of the milling behaviour of pharmaceutical powders by nanoindentation.* Powder Technology, **188**(3), 301-313, 2009

153. Egart, M., I. Ilić, B. Janković, N. Lah, and S. Srčič, *Compaction properties of crystalline pharmaceutical ingredients according to the Walker model and nanomechanical attributes.* International Journal of Pharmaceutics, **472**(1–2), 347-355, 2014

154. Egart, M., B. Janković, N. Lah, I. Ilić, and S. Srčič, *Nanomechanical Properties of Selected Single Pharmaceutical Crystals as a Predictor of Their Bulk Behaviour.* Pharmaceutical Research, **32**(2), 469-481, 2015

155. Rowe, R.C. and R.J. Roberts, *Mechanical Properties* in *Pharmaceutical Powder Compaction Technology*, G. Alderborn and C. Nystrom, Editors. 1996, Marcel Dekker, Inc.

156. Sun, C. and D.J.W. Grant, *Influence of Elastic Deformation of Particles on Heckel Analysis.* Pharmaceutical Development and Technology, **6**(2), 193-200, 2001

157. Ilić, I., B. Govedarica, R. Šibanc, R. Dreu, and S. Srčič, *Deformation properties of pharmaceutical excipients determined using an in-die and out-die method.* International Journal of Pharmaceutics, **446**(1–2), 6-15, 2013

158. Roberts, R.J. and R.C. Rowe, *The effect of punch velocity on the compaction of a variety of materials.* Journal of Pharmacy and Pharmacology, **37**(6), 377-384, 1985

159. Gabaude, C.M.D., M. Guillot, J.-C. Gautier, P. Saudemon, and D. Chulia, *Effects of true density, compacted mass, compression speed, and punch deformation on the mean yield pressure.* Journal of Pharmaceutical Sciences, **88**(7), 725-730, 1999

160. Denny, P.J., *Compaction equations: a comparison of the Heckel and Kawakita equations.* Powder Technology, **127**(2), 162-172, 2002

161. Fell, J.T. and J.M. Newton, *Effect of particle size and speed of compaction on density changes in tablets of crystalline and spray-dried lactose.* Journal of Pharmaceutical Sciences, **60**(12), 1866-1869, 1971

162. McKenna, A. and D.F. McCafferty, *Effect of particle size on the compaction mechanism and tensile strength of tablets.* Journal of Pharmacy and Pharmacology, **34**(6), 347-351, 1982

163. Patel, S., A. Kaushal, and A. Bansal, *Effect of Particle Size and Compression Force on Compaction Behavior and Derived Mathematical Parameters of Compressibility.* Pharmaceutical Research, **24**(1), 111-124, 2007

164. Marshall, P.V. and P. York, *An investigation of the effect of punch velocity on the compaction properties of ibuprofen* Powder Tech., **74**, 171-177, 1993

165. Di Martino, P., M. Beccerica, E. Joiris, G.F. Palmieri, A. Gayot, and S. Martelli, *Influence of crystal habit on the compression and densification mechanism of ibuprofen.* Journal of Crystal Growth, **243**(2), 345-355, 2002

166. Patel, S., A.M. Kaushal, and A.K. Bansal, *Mechanistic investigation on pressure dependency of Heckel parameter.* International Journal of Pharmaceutics, **389**(1–2), 66-73, 2010

167. Liu, L.X., I. Marziano, A.C. Bentham, J.D. Litster, E.T. White, and T. Howes, *Influence of particle size on the direct compression of ibuprofen and its binary mixtures.* Powder Tech., **240**, 66-73, 2013

168. Fujiwara, M., Z.K. Nagy, J.W. Chew, and R.D. Braatz, *First-principles and direct design approaches for the control of pharmaceutical crystallisation.* Journal of Process Control, **15**(5), 493-504, 2005

169. Dirksen, J.A. and T.A. Ring, *Fundamentals of crystallisation: Kinetic effects on particle size distributions and morphology.* Chemical Engineering Science, **46**(10), 2389-2427, 1991

170. Barrett, P., B. Glennon, and B. O'Sullivan. *Solubility Curve and Metastable Zone Width using Lasentec FBRM & PVM*. in *Lasentec Users Forum*. 2002. Charleston.

171. Mullin, J., *Crystal Growth*, in *Crystallisation* 2001, Butterworth.

172. Rodríguez-hornedo, N. and D. Murphy, *Significance of controlling crystallisation mechanisms and kinetics in pharmaceutical systems.* Journal of Pharmaceutical Sciences, **88**(7), 651-660, 1999

173. Mullin, J., *Industrial Techniques and Equipment*, in *Crystallisation*. 2001, Butterworth.

174. Nguyen, T.T.H., R.B. Hammond, K.J. Roberts, I. Marziano, and G. Nichols, *Precision measurement of the growth rate and mechanism of ibuprofen {001} and {011} as a function of crystallisation environment.* CrystEngComm, **16**, 4568-4586, 2014

175. Dudognon, E., F. Danède, M. Descamps, and N.T. Correia, *Evidence for a New Crystalline Phase of Racemic Ibuprofen.* Pharmaceutical Research, **25**(12), 2853-2858, 2008

176. Lippold, B.C. and A. Ohm, *Correlation between wettability and dissolution rate of pharmaceutical powders.* International Journal of Pharmaceutics, **28**(1), 67-74, 1986

177. Han, X., C. Ghoroi, D. To, Y. Chen, and R. Davé, *Simultaneous micronization and surface modification for improvement of flow and dissolution of drug particles.* International Journal of Pharmaceutics, **415**(1), 185-195, 2011

178. Clint, J.H., *Adhesion and components of solid surface energies.* Current Opinion in Colloid & Interface Science, **6**(1), 28-33, 2001

179. El Gindy, N.A. and M.W. Samaha, *Tensile strength of some pharmaceutical compacts and their relation to surface free energy.* International Journal of Pharmaceutics, **13**(1), 35-46, 1982

180. Ho, R., D.A. Wilson, and J.Y.Y. Heng, *Crystal Habits and the Variation in Surface Energy Heterogeneity.* Crystal Growth & Design, **9**(11), 4907-4911, 2009

181. Fowkes, F.M., *ATTRACTIVE FORCES AT INTERFACES.* Industrial & Engineering Chemistry, **56**(12), 40-52, 1964

182. Schultz, J., L. Lavielle, and C. Martin, *The Role of the Interface in Carbon Fibre-Epoxy Composites.* The Journal of Adhesion, **23**(1), 45-60, 1987

183. Dorris, G.M. and D.G. Gray, *Adsorption of n-alkanes at zero surface coverage on cellulose paper and wood fibers.* Journal of Colloid and Interface Science, **77**(2), 353-362, 1980

184. Schultz, J. and L. Lavielle, *Interfacial Properties of Carbon Fiber—Epoxy Matrix Composites*, in *Inverse Gas Chromatography*. 1989, American Chemical Society. 185-202.

185. Voelkel, A., *Physicochemical Measurements (Inverse Gas Chromatography)*, in *Gas Chromatography*, C. Poole, Editor. 2012, Elsevier. 477-494.

186. Brunauer, S., P.H. Emmett, and E. Teller, *Adsorption of Gases in Multimolecular Layers.* Journal of the American Chemical Society, **60**(2), 309-319, 1938

187. Dong, S., M. Brendlé, and J.B. Donnet, *Study of solid surface polarity by inverse gas chromatography at infinite dilution.* Chromatographia, **28**(9), 469-472, 1989

188. Volpe, C.D. and S. Siboni, *Some Reflections on Acid–Base Solid Surface Free Energy Theories.* Journal of Colloid and Interface Science, **195**(1), 121-136, 1997

189. SMS. *iGC-SEA compared to Contact Angle (CA) and Atomic Force Microscopy (AFM)* - *www.surfacemeasurementsystems.com/solutions/inverse-gas-chromatography-sea/*. 2016 [cited 2017, August].

190. Gamble, J.F., M. Leane, D. Olusanmi, M. Tobyn, E. Šupuk, J. Khoo, and M. Naderi, *Surface energy analysis as a tool to probe the surface energy characteristics of micronized materials—A comparison with inverse gas chromatography.* International Journal of Pharmaceutics, **422**(1–2), 238-244, 2012

191. Sing, K.S.W., D.H. Everett, R.A.W. Haul, L. Moscou, R.A. Pierotti, J. Rouquerol, and T. Siemieniewska, *Reporting physisorption data for gas/solid systems with special reference to the determination of surface area and porosity.* Pure Appl. Chem., **57**(4), 603-619, 1985

192. Brock, C.P. and J.D. Dunitz, *Towards a Grammar of Crystal Packing.* Chemistry of Materials, **6**(8), 1118-1127, 1994

193. Shah, U.V., Z. Wang, D. Olusanmi, A.S. Narang, M.A. Hussain, M.J. Tobyn, and J.Y.Y. Heng, *Effect of milling temperatures on surface area, surface energy and cohesion of pharmaceutical powders.* International Journal of Pharmaceutics, **495**(1), 234-240, 2015

194. Chekal, B.P., J. Ewers, S.M. Guinness, N.D. Ide, K.R. Leeman, R.J. Post, A.M. Rane, K. Sutherland, K. Wang, M. Webster, G.J. Withbroe, J. Draper, D. Lynch, M. McAuliffe, and J. Keane, *Palbociclib Commercial Manufacturing Process Development. Part III. Deprotection Followed by Crystallisation for API Particle Property Control.* Organic Process Research & Development, **20**(7), 1217-1226, 2016

195. Mayo, S.L., B.D. Olafson, and W.A. Goddard, *DREIDING: a generic force field for molecular simulations.* The Journal of Physical Chemistry, **94**(26), 8897-8909, 1990

196. Williams, D.E., *Nonbonded Potential Parameters Derived from Crystalline Hydrocarbons.* The Journal of Chemical Physics, **47**(11), 4680-4684, 1967

197. Roberts, R.J., R.C. Rowe, and P. York, *The relationship between indentation hardness of organic solids and their molecular structure.* Journal of Materials Science, **29**(9), 2289-2296, 1994

198. Lefort, R., A. De Gusseme, J.F. Willart, F. Danède, and M. Descamps, *Solid state NMR and DSC methods for quantifying the amorphous content in solid dosage forms: an application to ball-milling of trehalose.* International Journal of Pharmaceutics, **280**(1), 209-219, 2004

A Modern Approach to the Heckel Equation: The Effect of Compaction Pressure on the Yield Pressure of Ibuprofen and its Sodium Salt

Hooper D[1,2*], Clarke FC[2], Mitchell JC[1*] and Snowden MJ[1]

[1]Faculty of Engineering and Science, University of Greenwich, Medway, ME4 4TB, UK
[2]Pfizer Sandwich, Ramsgate Road, CT13 9ND, UK

Abstract

Despite being heavily criticised in the literature the most widely used and accepted compaction equation is the Heckel equation proposed by Heckel in 1961. Its presence in literature for 55 years is due to the ease in which it can distinguish between plastic and brittle materials. Achieving the correct balance of plastic and brittle materials in a formulation is critical to ensure adequate tablet strength is achieved therefore classifying materials using the Heckel equation is attractive. Despite the importance of this understanding, especially in the design and manufacture of direct compression formulations, there are no set analytical testing standards or materials classification guidelines. Instead many workers have attempted to develop techniques for the measurement and classification of a materials deformation but there is still confusion and contradiction present in this field.

In this study we report the effect of compaction pressure on the yield pressure of ibuprofen and its sodium salt. Ibuprofen and its sodium salt were selected as models for study due to the availability of comparative literature yield pressure values. The reported variation in yield pressure can be significant e.g. ibuprofen which has literature values of 21-1139 MPa. This study proposes an approach to determine yield pressure from the Heckel equation using a linear regression method. The full linear regression methodology utilised is described and is used to report the yield pressure of ibuprofen and its sodium salt dihydrate. This technique reveals the most representative compaction pressure in order to derive yield pressure to be 121 MPa.

The yield pressure of ibuprofen and its sodium salt have been shown to increase with increasing compaction pressure. The reported values lie between 52-78 MPa for ibuprofen and 48-75 MPa for ibuprofen sodium dihydrate. The slightly lower reported yield pressure values for ibuprofen sodium suggest increased plasticity which could be attributed to the water contained within the structure acting as a plasticiser.

Ibuprofen Heckel transformation at varying compaction pressures.
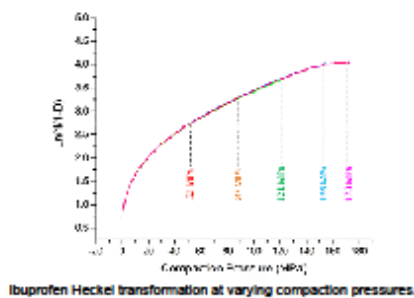
Keywords: Heckel equation; Deformation; Yield pressure; Linear regression; True density

Introduction

As tablets are the most common dosage platform understanding the deformation behaviour of the individual components is critical. Despite the importance of this understanding, especially in the design and manufacture of direct compression formulations, there are no set analytical testing standards or materials classification guidelines. Instead many workers have attempted to develop techniques for the measurement and classification of a materials deformation but there is still confusion and contradiction present in this field.

Recently many efforts have focused on the study of a materials deformation at single crystal level [1-4]. Techniques such as nanoindentation provide information using minimal quantities of material however the relationship between single crystal and bulk mechanical behaviour is not well understood. This had led to the continued use of compaction equations to classify materials in terms of their deformation.

181

Despite being heavily criticised in the literature the most widely used and accepted compaction equation is the Heckel equation proposed by Heckel in 1961. Its presence in literature for 55 years is due to the ease in which it can distinguish between plastic and brittle materials. Achieving the correct balance of plastic and brittle materials in a formulation is critical to ensure adequate tablet strength is achieved therefore classifying materials using the Heckel equation is attractive.

The model proposed by Heckel [5] is represented by the following equation:

$$\ln(1/1-D)=K \cdot P+A \qquad (1)$$

where D is the relative density of the compact, P is the applied pressure, A is a constant suggested to represent particle rearrangement and the reciprocal of K is used to calculate apparent mean yield pressure (P_y). The density pressure relationship is based on first order kinetics and has been defined as the stress at which plastic deformation of a particle is initiated, where low P_y values represent plastically deforming materials and high P_y values represent brittle materials [6]. In the pharmaceutical industry, the deformation of excipients has been most widely characterised [7] and it is accepted that microcrystalline cellulose (MCC) and dibasic calcium phosphate (DCP) form the extremes of the deformation spectrum with MCC (Avicel PH-101) exhibiting a yield pressure of 50 MPa and DCP exhibiting a yield pressure value of 957 MPa [8].

The yield stress values of well characterised materials become important when attempting to classify new materials. Often a comparison to materials whose deformation behaviour is well understood will be made due to the absence of defined standard class limits on yield pressure in terms of a plastic or brittle material. Roberts and Rowe attempted to set limits on these values along with other mechanical descriptors including young's modulus, hardness and strain rate sensitivity which allowed materials to be categorised [8]. Materials with P_y <80 were classified as soft/plastic materials whereas P_y >80 indicated hard/brittle substances. Although these limits are available they are difficult to adhere to due to variation present in P_y values for the same material between research groups. The variation present is due to many experimental and physical factors (experiment type, compaction speed, compaction pressure and particle size) affecting derived values and no standardisation being set on these.

The Heckel equation can be fitted to data collected from 'in-die' or 'out-of-die' compaction experiments. These different experiment types have been shown to affect yield pressure measurements due to the contribution of elastic energy [9,10]. Ilić et al., measured the yield pressure of MCC (Avicel PH 101) in-die and out-of-die and the respective yield pressure values were 61.7 MPa and 98.3 MPa. This difference of 36.6 MPa between experiment types is one of many factors contributing to discrepancies in yield pressure data published from different research groups.

As well as experiment type, it is also well documented that experimental conditions can affect yield pressure. It has been shown by numerous workers that compaction speed and final compaction pressure can affect yield pressure [11-13]. Roberts and Rowe proposed a term, strain rate sensitivity [14], which describes the relationship between yield pressure values collected at two different compaction speeds. Since then it has been shown that plastic materials are more sensitive to strain rate compared to brittle materials [15]. This means that when reporting the yield pressure of plastic materials, the compaction speed will alter the yield pressure value.

The variation seen in yield pressure is not only due to experimental conditions but can be attributed to the physical effect of particle size. A materials yield pressure is an intrinsic property and therefore should not be affected by physical properties such as particle size however there is contradicting information in the literature. Fell and Newton [16] described early on that the yield pressure of lactose was influenced by particle size. However, in 1982 a study by McKenna and McCafferty [17] revealed that during their calculation of yield pressure, particle size was irrelevant for lactose. Another study by Patel et al. [18] found that the yield pressure of paracetamol was dependant on particle size, where increasing particle size resulted in higher yield pressure values. Recent studies have suggested that as the yield pressure is derived from the density pressure relationship this value is actually an indication of powder densification rate that may be effected by particle size [19]. Nevertheless, yield pressure calculated from the Heckel equation is still derived to provide information on bulk deformation behaviour and particle size is one of the many variables affecting the outcome.

One area which may account for variability in the yield pressure value, but has been neglected in the literature, is the way in which K from the Heckel equation is derived. This is due to the fact that although it is accepted that yield pressure is derived from the gradient of a linear slope, Heckel plots are not completely linear and contain deviations at low and high pressures. These deviations are due to particle rearrangements at low pressures [6], and elastic deformation as pressure increases [9]. It is the responsibility of the analyst to select the most appropriate region in which to calculate yield pressure. This method is susceptible to user subjectiveness and has the potential to cause error in derived values which could lead to mistakes in material classification. Despite this, there are no standards or recommendations in the literature to define what area should be used in order to calculate yield pressure.

The type of variation in yield pressure that can be seen for a material, due to the factors discussed, can be significant e.g. ibuprofen which has reported values of 21-1139 MPa. The compressibility of ibuprofen has been studied by many workers [20-23] and a table listing the reported yield pressure values is shown in Table 1. The small variations present in studies, 4 MPa for Di Martino et al. [21] and 3 MPa for Liu et al. [23], are due to particle habit and particle size differences, respectively. The study by Patel et al. [22] reveals large differences accounted for by the effect of compaction pressure. This would suggest, according to the limits set by Rowe and Roberts, [8], that ibuprofen is changing from a plastic to brittle material. In an attempt to further understand these variations within the literature this study will focus on the effect of compaction pressure on ibuprofen yield pressure and the method to determine the linear region.

Materials and Methods

Materials

Ibuprofen (40 μm grade) was supplied by Pfizer Ltd. Ibuprofen sodium dihydrate was purchased from Sigma Aldrich, Dorest, UK.

Methods

Scanning electron microscopy: Scanning Electron Microscopy (SEM) was used to qualitatively assess particle size and shape. Electron micrographs were captured using a Zeiss SUPRA 40VP (Carl Zeiss Microscopy GmbH, Cambridge, UK). The samples were mounted onto an aluminium pin stub containing sticky carbon tabs and sputter

Py (MPa)	Lead Author	Comment
54-58	Di Martino et al. [21]	Particle habit dependant
21-24	Liu et al. [23]	Particle size dependant
98-1139	Patel et al., [22]	Compaction pressure dependant

Table 1: Reported yield pressure values from literature.

182

coated with platinum. A voltage of 3.0 kV and working distance of 10 mm were used.

Laser diffraction: Laser diffraction was utilised to measure the particle size of the ibuprofen samples. Dry dispersion measurements using 200 mg (±5 mg) of sample were made at a pressure of 1 bar using a Sympatec HELOS laser diffraction system with an R5 lens in conjunction with a RodosM disperser and an Aspiros feeder controlled by WINDOX software (Sympatec GmbH, Germany). Samples were measured in triplicate.

True density: The true density of 2.5 g (±0.2 g) samples were measured in duplicate using a Pentapyc 5200e helium pycnometer (Quantachrome UK Ltd., Hook, UK).

Compression studies: A Gamlen GTP-1 single punch bench top tablet press which has a uni-axial saw tooth displacement profile (Gamlen Tableting, United Kingdom) was used to complete the compression experiments. The deformation of the punches was corrected by compacting an un-deformable metal disk.

Tablets of 100 mg (±5 mg) were produced using a 6 mm flat-faced punch and die. Compression events were made at a speed of 0.033 mm second⁻¹, following the same methodology described by Roberts and Rowe [11].

In order to investigate the effect of compression pressure on yield pressure ibuprofen and ibuprofen sodium were compacted to five different compaction pressures (52, 87, 121, 156 and 173 MPa). Six individual measurements were made at each compaction pressure for both materials, to enable the variation in the yield pressure for each material to be determined.

Results and Discussion

Scanning electron microscopy

Scanning electron microscopy was conducted to visually assess and qualitatively determine particle size and shape information. The electron micrographs of ibuprofen and ibuprofen sodium, shown in Figure 1a and 1b respectively, reveal a difference in size and shape between the two materials. The majority of ibuprofen particles are smaller than 100 µm and have a size of around 40 µm whereas the ibuprofen sodium batch contains both small (around 40 µm) and larger particles (around 200 µm). Differences in particle shape are also revealed, with ibuprofen consisting of smooth lath shaped particles compared to ibuprofen sodium which has both rough prismatic and lath shaped particles.

Particle size distribution

Ibuprofen and ibuprofen sodium were characterised using laser diffraction to enable a quantitative measure of particle size. The volume based particle size distribution for both materials are shown in Figure 2. The distributions reveal that ibuprofen contains a primary mode centring around 40 µm, which is in agreement with the visual observation. The distribution for ibuprofen sodium reveals that the main mode centres around 200 µm and has a wider distribution compared to ibuprofen. The cumulative underscore values are presented in Table 2 and shows that 50% of particles are <39.3 ± 0.2 µm for ibuprofen whereas this value is almost doubled at 71.7 ± 2.4 µm for ibuprofen sodium.

True density

Helium pycnometry was used to measure the true density of the materials. The true density values of ibuprofen and ibuprofen sodium
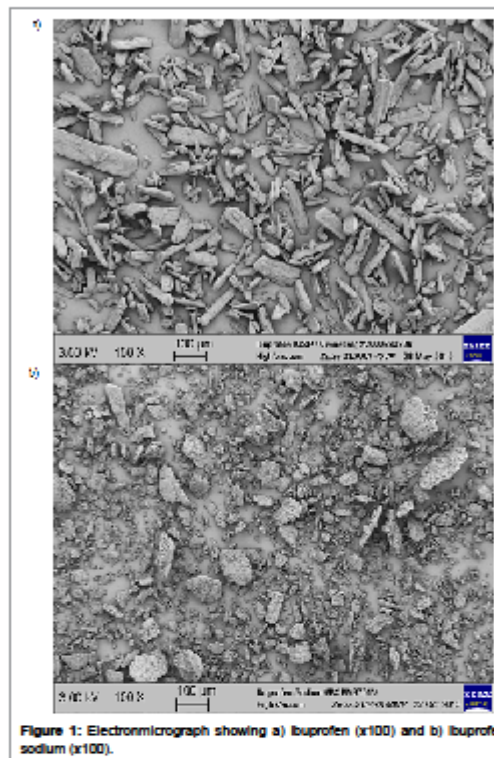
Figure 1: Electronmicrograph showing a) Ibuprofen (x100) and b) Ibuprofen sodium (x100).

Material	d10 (µm)	d50 (µm)	d90 (µm)
Ibuprofen	13.5 (0.2)	39.3 (0.2)	86.4 (0.4)
Ibuprofen sodium	6.2 (0.4)	71.7 (2.4)	253.6 (4.6)

Table 2: Particle size values calculated by laser diffraction for Ibuprofen and Ibuprofen sodium where standard deviations of 3 runs are shown in brackets.

were 1.12 g/cm³ and 1.17 g/cm³, respectively. The standard error of measurement for each material was calculated and determined to be 0.0013 g/cm³ (0.11%) for ibuprofen and 0.007 g/cm³ (0.61%) for ibuprofen sodium.

It has previously been reported that Heckel plots are sensitive to variations in measured density, 1% error in density can lead to 10% error in yield pressure estimate [19], therefore it is important to report density values used and include the standard error in the measurement for transparency. Since the error values are low it is predicted that this will have minimal effect on derived values however the impact or error in density will be investigated during yield pressure calculations.

Yield pressure determination

In Die Heckel calculation: In-die Heckel plots were obtained by calculating the relative density (D) in-die using the true density and compact thickness (derived from corrected punch displacement). The $\ln(1/1-D)$ was determined for each measurement at each compaction pressure and these were plotted against each other to enable yield pressure to be determined.

183

Figure 2: Laser diffraction particle size distribution for ibuprofen and ibuprofen sodium.
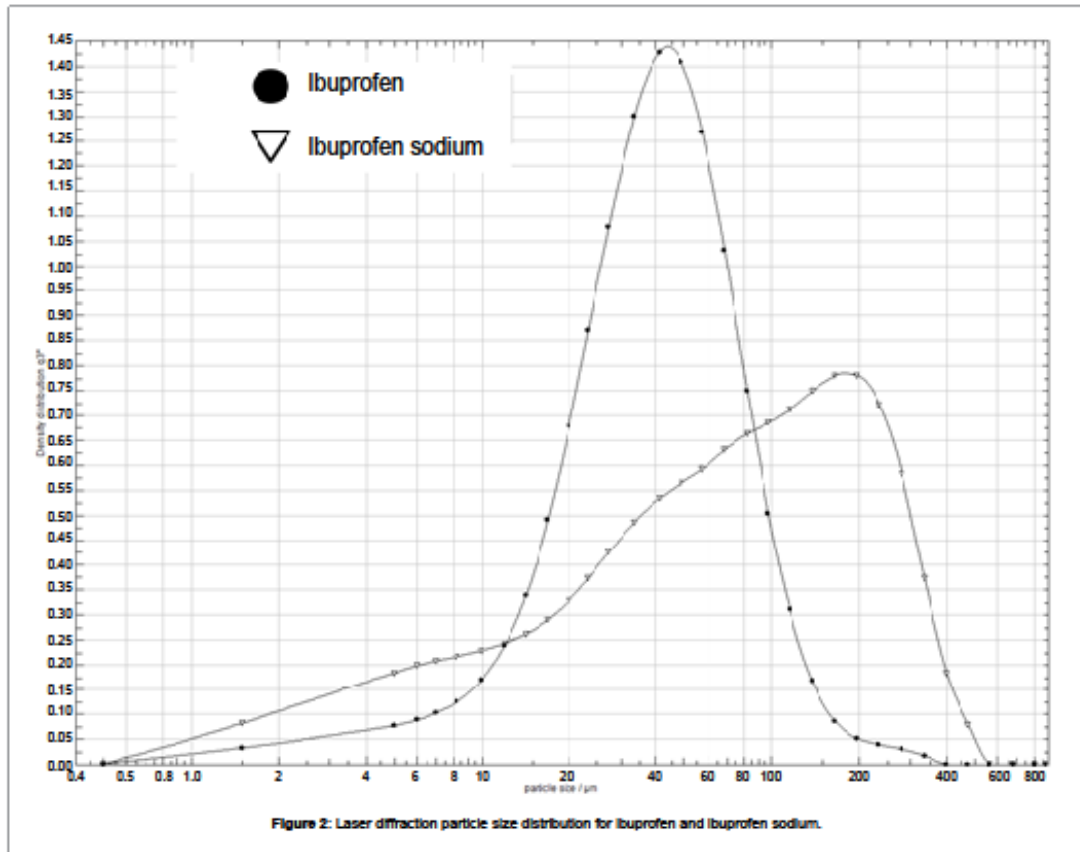
Linear regression fitting: To enable accurate determination and eliminate subjective selection of the linear region of the plot, linear regression analysis was performed. A qualitative assessment to select the most central part of the linear region was made. The regression coefficient for this selected region was calculated. The linear region was then extended in both directions and on each occasion the regression coefficient recalculated. This was achieved by extending the linear range, one x coordinate at a time, in approximately 10 MPa steps. Once the region which contained the highest regression coefficient (specific to x coordinate) was established the step size was decreased until an accuracy of 1 MPa was reached.

The effect of the regression coefficient on the gradient of the slope and hence the yield pressure is highlighted using an example of ibuprofen compacted to 121 MPa (repeat 1) in Figure 3. This reveals the importance of selecting the most representative linear region as selecting only a small portion of the plot, where r^2 is 0.984, gives rise to a yield pressure value of 85 MPa compared to a larger portion of the plot (r^2 is 0.999) which gives rise to a yield pressure value of 76 MPa, a difference of around 10%. According to Rowe and Roberts, [8] this would classify ibuprofen in two different categories, changing from hard/brittle to soft/plastic.
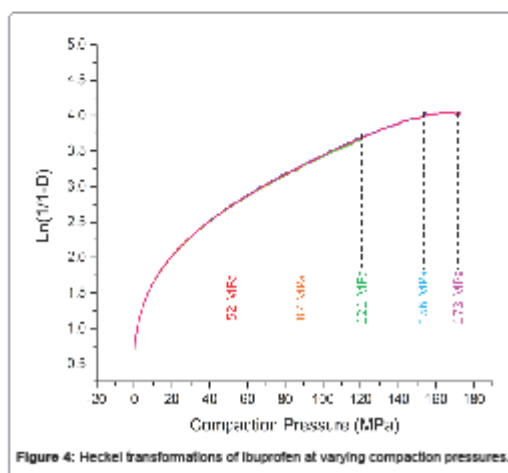
Effect of compaction pressure on derived yield pressure: Heckel transformations for ibuprofen at the different compaction pressures analysed are shown in Figure 4. The plots produced at each compaction pressure overlay suggesting that in principal the same linear region for each pressure could be selected and therefore deriving the same yield pressure results. However, the plot also reveals that the full linear range of the Heckel plot may only become apparent when higher final pressures are used.

Linear regression was performed on six Heckel plots at each compaction pressure for ibuprofen and ibuprofen sodium. During analysis it became apparent that differences in yield pressures arise due to the range of the linear region available for selection at different compaction pressures. Figure 5 shows an example where ibuprofen compacted to 52 MPa returns a yield pressure value of 48 MPa compared to 76 MPa for ibuprofen compacted to 121 MPa. The visually subtle difference in gradient due to the compaction pressure used causes a significantly large difference in yield pressure, 28Mpa. Compacting ibuprofen to higher compaction pressures extends the rate of powder densification which in turn lowers the gradient of the slope and explains the increase in yield pressure values.

Figure 3: An example of the extension of the linear range of the Heckel model in order to achieve the highest regression coefficient.

Figure 4: Heckel transformations of ibuprofen at varying compaction pressures.
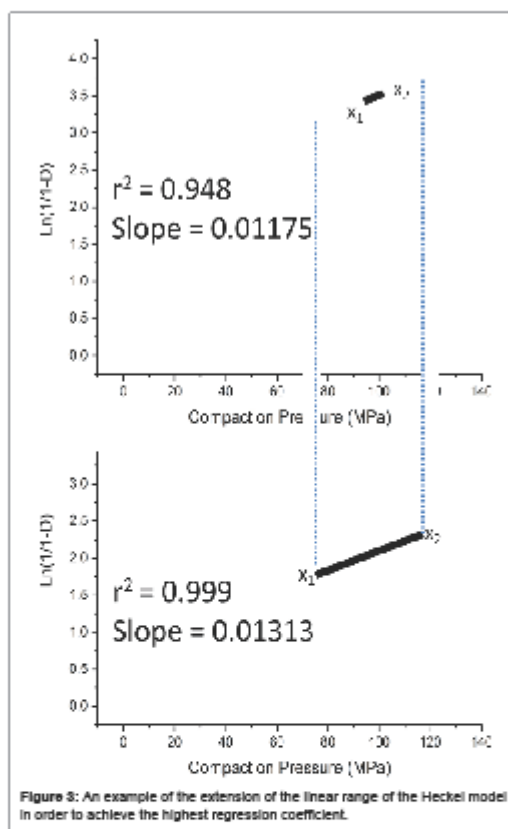
Investigating the effect of error in true density: As discussed previously, it is known that error in measured true density can affect derived yield pressure values. To investigate this further a worst case scenario of ibuprofen sodium compacted to 52 MPa was chosen for investigation, due to ibuprofen sodium containing 0.5% higher error in density compared to ibuprofen. This measurement gave a yield pressure of 50 MPa and when the error in density was included returned values of 46 and 53 MPa which is a difference of around 14%. This large error associated with density is unavoidable due to the logarithmic transformation of the Heckel equation; therefore alternative methods to reduce error are of upmost importance.

Comparison of Ibuprofen and Ibuprofen Sodium: The effect of compaction pressure on yield pressure for ibuprofen and ibuprofen sodium is displayed in Figure 6. The derived value for ibuprofen ranges from 52-78 MPa and ranges from 48-75 MPa for ibuprofen sodium. At the very high compaction pressures (>156 MPa) it is observed that the yield pressure values for both materials reaches a plateau where the standard deviations overlap. This would suggest that at these compaction pressures the highest possible rate of powder densification has been reached however examination of Figure 3 reveals that in order to utilise the greatest range of linearity, final compaction pressures of 121 MPa should be used to report yield pressure values.

The comparison of ibuprofen yield stress to its sodium salt dihydrate reveals that at all compaction pressures ibuprofen sodium exhibits lower yield stress values. It would be expected from the results of previous studies that ibuprofen sodium would exhibit a smaller particle size distribution which would account for the difference [18]. However, examination of the particle size data (Figure 2) reveals that the salt contains a larger particle size. Therefore regardless of particle size, ibuprofen sodium dihydrate possesses an increased powder densification rate suggesting higher plasticity compared to the free acid. The water contained within the crystal structure of the sodium salt could be acting as a plasticiser allowing the easier slip to take place. This could explain the lower yield stress and therefore plasticity of ibuprofen sodium dihydrate compared to ibuprofen free base.

Conclusion

A new approach utilising linear regression has been developed to analyse Heckel plots. Examination of regression coefficients of the linear region of the plot has allowed the selection of the most representative area in which yield stress can be derived. The variation due to the linear region selection has been reviewed and revealed that variations of 10% are possible dependant on which part of the plot is selected.

This linear regression method has been effectively applied to ibuprofen and ibuprofen sodium dihydrate and highlights that increasing compaction pressure results in the calculation of higher yield pressure values. This phenomena reaches its peak at very high compaction pressures (>156 MPa) however the greatest range of linearity is observed when pressures of 121 MPa were used in this study. Therefore it is proposed to enable valuable comparison of yield pressure, high compaction pressures (around 121 MPa) should be used for analysis. We hope to extend this strategy to other pharmaceutical materials.

It is also proposed from this research that when reporting yield pressure values from the Heckel equation that all experimental conditions and linear regression methods should be clear and transparent in order to reliably classify materials.
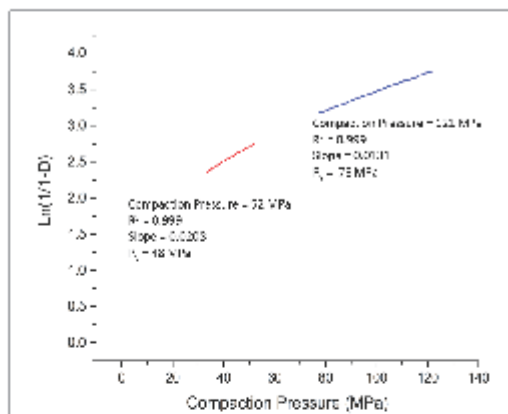
185

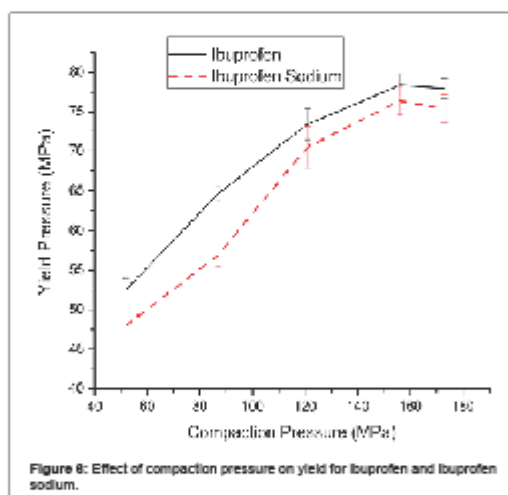**Figure 6:** Derived yield pressure from Heckel plot at 52 MPa and 121 MPa.

Figure 8: Effect of compaction pressure on yield for ibuprofen and ibuprofen sodium.

Acknowledgments

References

1. Taylor LJ, Papadopoulos DG, Dunn PJ, Bentham AC, Mitchell PJ, et al. (2004) Mechanical characterisation of powders using nanoindentation. Powder Technology 179-185.

2. Meier, John E, Wieckhusen D, Wirth W, Peukert W (2009) Influence of mechanical properties on impact fracture: Prediction of the milling behaviour of pharmaceutical powders by nanoindentation. Powder Technology 188: 301-313.

3. Egart M, Ilic I, Jankovic B, Lah N, Srcic S (2014) Compaction properties of crystalline pharmaceutical ingredients according to the Walker model and nanomechanical attributes. International Journal of Pharmaceutics 472: 347-355.

4. Egart M, Ilic I, Jankovic B, Lah N, Srcic S (2015) Nanomechanical Properties of Selected Single Pharmaceutical Crystals as a Predictor of Their Bulk Behaviour. Pharmaceutical Research 32: 469-481.

5. Heckel RW (1961) Density-Pressure Relationship in Powder Compaction. Trans Met Soc AIME 22: 671-675.

6. Alderborn G (2007) Tablets and compaction Churchill Livingstone.

7. Jivraj M, Martini LG, Thomson CM (2000) An overview of the different excipients useful for the direct compression of tablets. Pharmaceutical Science & Technology Today 3: 58-63.

8. Rowe RC, Roberts RJ (1996) Mechanical Properties: Pharmaceutical Powder Compaction Technology, Marcel Dekker, Inc.

9. Sun C, Grant DJ (2001) Influence of elastic deformation of particles on Heckel analysis. Pharm Dev Technol 6: 193-200.

10. Ilic I, Govedarica B, Šibanc R, Dreu R, Srčič S (2013) Deformation properties of pharmaceutical excipients determined using an in-die and out-die method. Int J Pharm 446: 6-15.

11. Roberts RJ, Rowe RC (1985) The effect of punch velocity on the compaction of a variety of materials. J Pharm Pharmacol 37: 377-384.

12. Gabaude CMD, Guilot M, Gautier JC, Saudemon P, Chulia D (1999) Effects of true density, compacted mass, compression speed, and punch deformation on the mean yield pressure. Journal of Pharmaceutical Sciences 88: 725-730.

13. Denny PJ (2002) Compaction equations: a comparison of the Heckel and Kawakita equations. Powder Technology 127: 162-172.

14. Roberts RJ, Rowe RC (1987) The Compaction of Pharmaceutical and other Model Materials - A Pragmatic Approach. Chemical Engineering Science 903: 903-911.

15. Katz JM, Buckner IS (2013) Characterization of strain rate sensitivity in pharmaceutical materials using indentation creep analysis. Int J Pharm 442: 13-19.

16. Fell JT, Newton JM (1971) Effect of particle size and speed of compaction on density changes in tablets of crystalline and spray-dried lactose. J Pharm Sci 60: 1866-1869.

17. McKenna A, McCafferty DF (1982) Effect on particle size on the compaction mechanism and tensile strength of tablets. J Pharm Pharmacol 34: 347-351.

18. Patel S, Kaushal AM, Bansal AK (2007) Effect of particle size and compression force on compaction behavior and derived mathematical parameters of compressibility. Pharm Res 24: 111-124.

19. Sonnergaard JM (1999) A critical evaluation of the Heckel equation. Int J Pharm 193: 63-71.

20. Marshall PV, York P (1993) An investigation of the effect of punch velocity on the compaction properties of ibuprofen Powder Tech. 74: 171-177.

21. Martino D, Beccerica PM, Joiris E, Palmieri GF, Gayot A, et al. (2002) Influence of crystal habit on the compression and densification mechanism of ibuprofen. Journal of Crystal Growth 243: 345-355.

22. Patel S, Kaushal AM, Bansal AK (2010) Mechanistic investigation on pressure dependency of Heckel parameter. Int J Pharm 389: 66-73.

23. Liu LX, Marziano I, Bentham AC, Litster JD, White ET, et al. (2013) Influence of particle size on the direct compression of ibuprofen and its binary mixtures. Powder Tech 240: 66-73.

Effects of crystal habit on the sticking propensity of ibuprofen—A case study

D. Hooper[a,b], F.C. Clarke[b], R. Docherty[b], J.C Mitchell[a,*], M.J. Snowden[a]

[a] Faculty of Engineering and Science, University of Greenwich, Medway, ME4 4TB, UK
[b] Pfizer Ltd., Ramsgate Road, Sandwich, CT13 9NJ, UK

ARTICLE INFO

ABSTRACT

This study demonstrates the effect of active pharmaceutical ingredient (API) particle habit on the sticking propensity of ibuprofen. Four diverse crystal habits with similar physico chemical properties are reported and the sticking propensity was found to increase with shape regularity. The surface energy of the extreme habits were shown to be different where particles that were more regular in shape exhibited surface energies of 9 mJ/m^2 higher than those that were needle-like in habit. Computational and experimental data reveals that the increase in surface energy of the regular shaped particles can be attributed to the increase in the specific (polar) component, which is due to greater presence of faces which contain the carboxylic acid functionality at the surface. The increase in the specific energy component is shown to correlate with the sticking propensity of ibuprofen. It is proposed that investigation of the chemical causality of sticking, for this API and others, using the techniques demonstrated in this paper will be of increasing importance.

1. Introduction

During API development, critical quality attributes (CQAs) are set out in the final specifications for the drug product (Challener, 2014). Solid form and particle size distributions are CQAs with particle shape and surface energy often neglected due to the lack of understanding of their impact.

The engineering of particles with desired properties has become increasingly important and this has led to pharmaceutical Materials Science emerging as a foundation of Quality by Design (QbD) with solid form, crystallization and particle engineering being core elements linking the drug product functional form to the final steps of the API manufacturing process (Shekunov et al., 2007; Chow et al., 2008). More recently the importance of the Materials Science tetrahedron, depicting the relationships between internal structure, particle properties, material processing and performance of a drug product, has been described (Sun, 2009).

For a given API the crystal habit is typically specified through the crystallisation protocol. Different crystal faces of the API produced exhibit different surface chemistry and hence interact differently with solvents, process impurities and excipients. These different crystal faces can be present in different proportions for a given API. The changes in crystal habit, which are generally not controlled in specifications, in combination with particle size can lead to different chemical and physical stabilities, biopharmaceutical properties and processing behaviour (API and drug product) (Storey et al., 2003; Ticehurst and

Docherty, 2006).

This work seeks to outline some of the recent progress on the application of emerging computer modelling technologies for the design strategy of advanced functional particulate products (Waknis et al., 2014). The paper highlights the opportunity for bridging across the chemical, analytical and manufacturing disciplines with a particular focus on understanding punch sticking.

One of the major issues affecting the production of pharmaceutical tablets is the formulation adhering to the tooling surfaces, known as punch sticking. Punch sticking compromises the manufacturing process. Many attempts in the literature have been made to determine the elusive root cause of this phenomenon however no single root cause has been identified (Waknis et al., 2014; Paul et al., 2017a). It is known that sticking may be due to API adherence even when it is present in a formulation at low concentrations (Paul et al., 2017b) and many complex processing and environmental mechanisms such as speed/force/dwell time (Roberts et al., 2004a), temperature/humidity (Danjo et al., 1997), punch geometry/quality where quality is defined as surface roughness and if the punch contains any defects(Roberts et al., 2004a) and lubrication (Roberts et al., 2004b) have been shown to contribute.

There is still a lack of understanding between the particle habit and surface energy of an API and their role in punch sticking despite some recent efforts (Waknis et al., 2014; Pudasaini et al., 2017). One of the challenges often faced when trying to link these properties is punch sticking is not detected until full scale manufacture and there is a

technology gap relating to a small scale test to predict sticking especially when APIs are limited in quantity. This work presents a simple science of scale tool to quantify the sticking of an API with different particle habits and similar physico-chemical properties in combination with emerging computational tools to explore the crystal chemistry in relation to surface energies.

2. Materials and methods

2.1. Computational tools

This study focuses on racemic ibuprofen (RS)-ibuprofen. The Cambridge Structural Database (CSD) was interrogated for (RS)-ibuprofen structures using ConQuest (CCDC 1.18, 2016). The criteria for this search were R-factor of less than 0.0075 and no metals allowed. The crystal structure selected for ibuprofen was IBPRAC and the carboxylic acid hydrogen bonding distance for this hit was measured and compared to all other hits with this functionality using the search criteria above.

The .cif for IBPRAC, was imported into Materials Studio (v7.0, 2013) and the intermolecular interactions were calculated using the following force fields: geometry optimised/fractional charges assigned using COMPASS II/Tripos 5.2 force field, respectively (Sun, 1998; Clark et al., 1989). All further calculations were performed using these parameters. HABIT98 (Clydesdale et al., 1991, 1996) was used to calculate the strength of the non-bonded intermolecular interactions (intrinsic synthons) and lattice energy (E_{cr}). In order to determine if the force field assigned accurately estimated the intermolecular strength of interactions the lattice energy was compared to the sublimation enthalpy (δH_{sub}) as the relationship shown below exists:

$$E_{cr} = \delta H_{sub} - 2RT \tag{1}$$

Where R is the gas constant and T is temperature.

To further validate the force field, the strength of the most dominant intermolecular interaction was compared to validation work published by Dunitz and Gavezzotti (Dunitz and Gavezzotti, 2012).

The Bravais, Friedel, Donnay and Harker (BFDH) (Bravais, 1866; Friedel, 1907; Donnay and Harker, 1937) method was used to predict the most likely growth surfaces based on the rule which states the faces with the largest interplanar spacing (d_{hkl}) are likely to be the most morphologically important at the surface (Docherty et al., 1991; Rosbottom et al., 2015). The lattice energy (E_{cr}) per surface was split into slice energy (E_{sl}) and attachment energy (E_{att}) based on the equation shown below (Docherty et al., 1991):

$$E_{cr} = E_{sl} + E_{att} \tag{2}$$

The morphology of ibuprofen was predicted using the attachment energy model which states that the faces with the lowest attachment energies will be the slowest growing and therefore be the most morphologically important (Hartman and Bennema, 1980).

Previously published studies have revealed that during crystallisation of ibuprofen only three of the surfaces predicted by the BFDH and attachment energy models are present (Cano et al., 2001; Bunyan et al., 1991; Winn and Doherty, 2000). These faces are {1 0 0}, {0 1 1} and {0 0 2} and Materials Studio was used to visualise the chemistry present at each surface (extrinsic synthons).

The relative attachment energy of each face was expressed as centre to face distances then Mercury (CCDC 3.9, 2016) was used to visualise the external morphology. The surface energy of these faces was calculated using the attachment energy calculation shown below (Hartman and Bennema, 1980):

$$\gamma_{hkl} = \frac{Z E_{att} d_{hkl}}{2 V_{cell} N_A} \tag{3}$$

Where Z is the numbers of molecules in the unit cell, V_{cell} is the unit cell

volume, E_{att} is the attachment energy, d_{hkl} is the d spacing and N_A is Avogadro's number.

The area of these faces was compared to scanning electron micrographs of two extreme ibuprofen habits and altered in Mercury (CCDC 3.9, 2016) to represent an average particle habit. The fractional area of each face was expressed using Mercury then the particle surface energy was calculated by summing the face contribution to total surface energy based on area.

2.2. Recrystallisation of ibuprofen

(RS)-ibuprofen (40 µm grade, ≥99.8%) was supplied by Pfizer Ltd and was recrystallised from hexane (95%), toluene (>99.5%), acetonitrile (99.8%) and ethanol (>99.5%) purchased from Fisher Scientific (Loughborough, UK). Supersaturated solutions were prepared at the following concentrations: hexane 1.1 g/mL, toluene 1.5 g/mL, acetonitrile 1.3 g/mL and ethanol 1.5 g/mL. The solubility of ibuprofen in various solvents is documented in the following paper and was used a guide for these experiments (Nguyen et al., 2014). These solutions were heated to 60 °C in a jacketed Optimax reactor (Mettler Toledo, Leicester, UK). The stirred solutions were cooled linearly at a rate of 1 °C/min. The solutions were seeded with 1% of starting material prior to nucleation and then further cooled linearly to 0 °C at a rate of 1 °C/min. Product was obtained through filtering through general-purpose laboratory filter paper (Whatman, UK) and dried in an oven at 50 °C for 24 h. The resultant batches were named according to their crystallisation solvent (i.e. IbuEth is ibuprofen crystallised from ethanol).

2.3. Size and shape characterisation

The recrystallised batches were sieved through a stainless steel sieve (Endecotts Ltd, London, UK) with a mesh size of 150 µm prior to characterisation.

Scanning electron microscopy (SEM) was used to qualitatively assess particle morphology. Electron micrographs were captured using a Zeiss SUPRA 40VP (Carl Zeiss Microscopy GmbH, Cambridge, UK). The samples were mounted onto an aluminium pin stub containing sticky carbon tabs and sputter coated with platinum. A voltage of 3.0 kV and working distance of 10 mm were used.

The particle size and shape of the samples were measured with a dynamic image analysis system QICPIC (Sympatec Ltd., Clausthal-Zellerfeld, Germany). A vibratory feeder system (VIBRI, Sympatec) was combined with a dry air disperser (RODOS, Sympatec) and was operated at 0.5 bar pressure. The system operates using a pulsed light source with sub-nanosecond illumination, and the particles were imaged by a high speed camera with a frame rate of 400 frames per second. Single measurements were made using the M6 lens (measuring range of 5–1705 µm) and a minimum of 200,000 particles were imaged for each run. Images were analysed using WINDOX (Sympatec) software with the size and shape distributions reported using the maximum Feret diameter in order to not lose valuable shape information.

2.4. Physico-chemical characterisation

Powder X-ray diffraction (PXRD) was performed by preparing the samples using a flat plate diffraction patterns collected on a D4 Endeavor (Bruker Corporation, Billerica, Massachusetts, USA). The scan was carried out between 2° and 55° 2θ using CuKα radiation with a secondary graphite monochromator.

Differential scanning calorimetry (DSC) was performed in dry nitrogen gas using a Discovery DSC (TA Instruments – A division of Waters Ltd, Herts, UK). The DSC was calibrated using indium at heating rate of 10 °C/min. The samples (2.5–3 mg) were analysed in a T-zero standard pan at heating rate of 10 °C/min over the range from 30 °C to 100 °C. Due to sample limitations only one measurement was made.

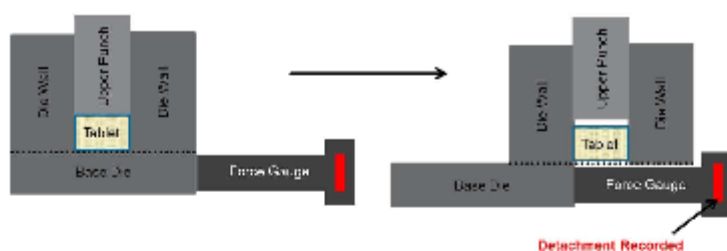Headspace gas chromatography (HS-GC) was performed using a

188

Fig. 1. Gamlen Tablet Press detachment force tool used for the quantification of sticking propensity.

6892N Network GC system coupled to a 7694 HS sampler (Agilent Technologies, CA, US). Around 20 mg of each sample was dissolved in *N,N*-dimethylacetamide (≥99%) purchased from Sigma Aldrich (Dorset, UK). A liquid-vapour equilibrium was established by heating the solution in a sealed vial and an aliquot of the headspace vapour was analysed by capillary GC. Quantification of each volatile impurity was achieved by comparison of the chromatographic peak areas of external reference standards with the peak areas of the test sample solutions.

2.5. Sticking propensity

The sticking propensity was measured using a Gamlen Tablet Press (GTP-1, Gamlen Tableting Limited, Nottingham, UK). 100 mg of sample was compacted in a 6 mm die at the following pressures: 40 MPa, 120 MPa and 180 MPa at a speed of 60 mm/min. A novel approach to quantify the amount of powder adhered to the base die was developed and is illustrated in Fig. 1. Prior to tablet ejection, the detachment stress of the base die was measured manually using a 50 kg hand held force gauge (Mecmesin, Slinfold, UK) placed at the side of the base die. Detachment measurements were made in triplicate (Fig. 2).

2.6. Surface analysis

The specific surface area, pore size distributions and pore volume of the samples was measured using a TriStar II 3020 (Micromeritics U.K. Ltd., Hexton, UK). Between 450–850 mg of sample was filled into 3/8″ flat bottom cell with filler rods and conditioned under a helium purge at 40 °C for 16 h. Nitrogen isotherms were measured at −196 °C. The BET model (Brunauer et al., 1938) based on the linear region of the nitrogen adsorption isotherm (from p/p^* = 0.05–0.9) was used for data calculation. Each batch was measured in duplicate.

Surface energy heterogeneity was measured using inverse gas chromatography – surface energy analyser 2.0 (iGC-SEA, Surface Measurement Systems (SMS) Ltd., Alperton, UK). The samples were packed into 4 mm pre-silanised glass columns and mechanically tapped for 10 min using SMS sample packing device. All samples were packed to yield a total surface area of approximately 0.13 m². The columns were pre-conditioned at 30 °C and 0% RH using helium (carrier gas) at a flow rate of 7 standard cubic centimetres per minute for 120 min and these conditions were maintained throughout the experiment duration. A range of dispersive (non-polar) probes (decane, nonane, octane, heptane and hexane) and specific (polar) probes (ethyl acetate and chloroform) were injected at a range of surface coverages (n/n_m) ranging from 1 to 20%; the column dead volume was determined using methane. Data analysis was performed using the Cirrus Plus SEA Data Analysis software (v1.2, SMS Ltd., Alperton, UK). The Dorris/Gray approach (Dorris and Gray, 1980) was used to determine the dispersive energy contribution, whereas the specific energy contribution was determined by measuring the free energy desorption of a pair of monofunctional acidic and basic probes (chloroform and ethyl acetate), based on the polarisation approach (Dong et al., 1989) and Della Volpe scale (Volpe and Siboni, 1997). Detailed reviews of these approaches can be found elsewhere (Shi et al., 2011; Ho and Heng, 2013). The repeatability and reproducibility of the iGC-SEA system is quoted by the manufacturer as RSD = 1% (SMS, 2016) which is lower than traditional iGC techniques due to the system using the same pipe line and injection manifold for every injection (Gamble et al., 2012). To assess the instrument repeatability batch IbuEth was run in triplicate, but all other batches were run once due to limitations in availability of the iGC-SEA system.

3. Results and discussion

3.1. Crystal chemistry

The molecular structure of ibuprofen consists of a phenyl ring with a propanoic acid group and isobutyl in the para position. The structure can be further divided into four molecular components: A) isobutyl, B) phenyl, C) methyl attached to carbon backbone and D) carboxylic acid. The unit cell, for the crystal structure of ibuprofen (IBPRAC), compromises of four molecules arranged in centro-symmetric hydrogen bonded dimers with dimensions a = 14.667 Å, b = 7.886 Å, c = 10.730 Å and ß = 99.362° (Figure). The hydrogen bonding distance is 1.624 Å. This distance is slightly shorter than the mean value of the hits (1601) returned for carboxylic acid hydrogen bonding search in the Cambridge Structural Database (CSD), 1.743 Å, which suggests that this interaction will be strong.

3.1.1. Lattice energy and intrinsic synthons

The calculated lattice energy was −125.2 kJ/mol which is in excellent agreement with experimental sublimation enthalpies of 125.9 kJ/mol (Bunyan et al., 1991) and 115.9 kJ/mol (Perlovich et al., 2004).

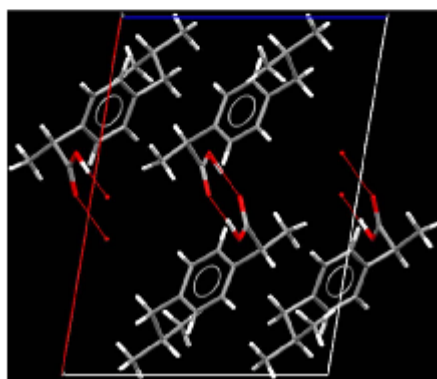The different intrinsic synthon types were investigated and the six

Fig. 2. Ibuprofen unit cell displaying hydrogen bonded carboxylic acid dimers.
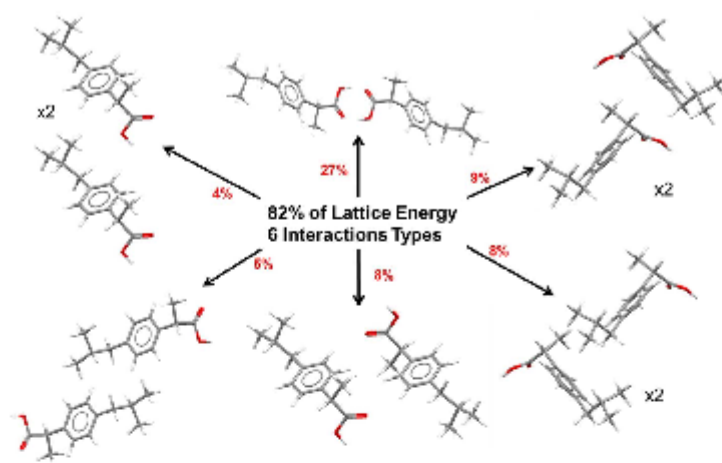
189

key interactions (> 4 kJ/mol) are shown in Fig. 3A total of nine interactions compromising of six types make up 82% of the lattice energy, with the largest contribution coming from the carboxylic acid dimer with a value of -33.7 kJ/mol. This was compared to Dunitz and Gavezzotti's (Dunitz and Gavezzotti, 2012) value of −35 kJ/mol for these types of interactions which validates that the forcefield used has accurately predicted the strength of the interaction energy for this short hydrogen bonded dimer.

The strength of this interaction is highlighted by comparing its contribution to lattice energy with the next strongest π-π stacking interaction which contributes 9% compared with 27%, a three-fold difference. The five other interaction types are Van der Waals interactions and despite being crucial for the formation of the crystal are all relatively weak in comparison to the carboxylic acid dimers.

The lattice energy was collapsed onto the individual atoms and summed across each molecular component and reveals that the strongest intermolecular synthon in the crystal structure is the H bonded carboxylic acid (molecular component D), with its contribution to the lattice energy of 37.5%. The molecular components can also be ranked in terms of their increasing contribution to the lattice energy: D > A > B > C (Fig. 4).

3.1.2. Ibuprofen morphology prediction

The Bravais, Friedel, Donnay and Harker (BFDH) morphology of ibuprofen is shown in Fig. 5a and reveals six predicted morphologically important faces. The attachment energy morphology is shown in Fig. 5b and reveals a flatter habit with the disappearance of faces {1 0 −2}, {0 1 1} and the appearance of {1 1 1}. Although this morphology is similar to what is observed experimentally, literature reveals that the three dominant faces during crystallisation are {1 0 0}, {0 0 2} and {0 1 1} (Cano et al., 2001; Bunyan et al., 1991; Winn and Doherty, 2000). The first two faces are present in both the BDFH and attachment energy models however face {0 1 1} is only present in the BDFH prediction. The attachment energy model was altered to include the three faces present during crystallisation and this is shown in Fig. 5c.

3.1.3. Surface chemistry of ibuprofen

Analysis of the three main faces reveals different crystal chemistry present at the surface of each, as shown in Fig. 6. The dominant (1 0 0) face contains the aliphatic chains; group A at the surface with the molecules linked by the carboxylic acid dimers in the centre of the bulk. This high energy interaction accounts for the directional growth of ibuprofen crystals in the [1 0 0] direction and is confirmed by the lath shaped particles usually produced during crystallisation from non-polar
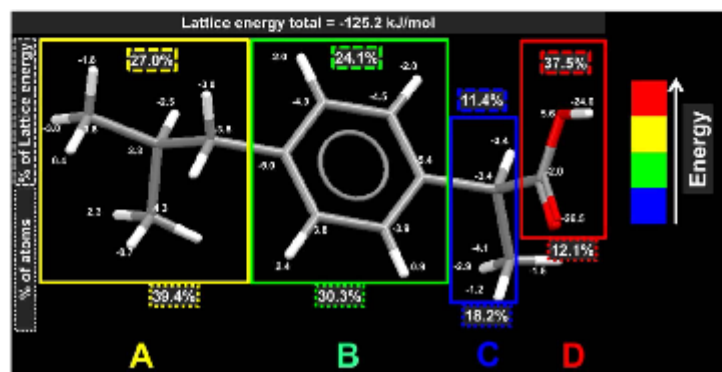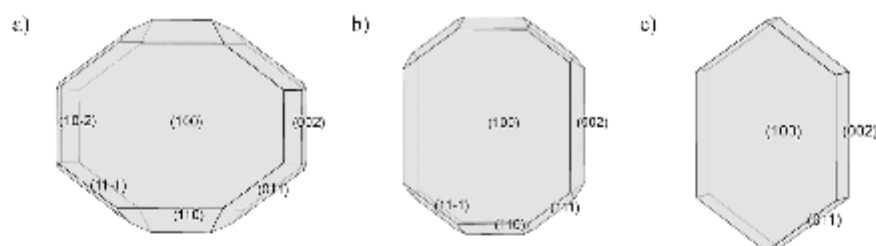
190

Fig. 5. Predicted morphology of ibuprofen where a) BFDH highlighting six morphologically important crystal faces b) attachment energy morphology highlighting five morphologically important crystal faces c) attachment energy morphology edited to only include the three faces observed during crystallisation.

solvents, such as hexane (Bunyan et al., 1991). The (0 1 1) and (0 0 2) face have the carboxylic acid group exposed at the surface allowing for potential hydrogen bonding to occur with Lewis bases. This is confirmed by the habit change when polar crystallisation solvents, such as ethanol, are used and result in a plate like habit due to the slower growth of the (0 1 1) and (0 0 2) face (Cano et al., 2001; Bunyan et al., 1991).

It is evident from the different chemical functionalities present at each surface that the faces will exhibit different surface energies. In order to view this qualitatively, colour coded images relating to the intrinsic synthon contribution to lattice energy for each surface are shown in Fig. 7.

Analysis of the dominant (1 0 0) face reveals that the extrinsic synthon exposed at this face is A. This group is the aliphatic chain and both top and side views of this face show that the surface is flat with no exposure of the other synthons suggesting a relatively low surface energy. Moving to face (0 0 2) the side view reveals that the molecules run at an angle in relation to the surface exposing extrinsic synthons C and D. Synthon C is the lowest energy group however synthon D is the carboxylic acid group involved in the dimer meaning this has to be broken for exposure of this extrinsic synthon. The top view of this face reveals that synthon D is slightly covered by synthon C but is still exposed at the surface. On inspection of the side view of the (0 1 1) face it can be seen that the molecules run parallel to the surface exposing synthon A, C and D. The top view of this face shows that the highest energy synthon (D) is fully exposed and forms channels which imply that this face has high energy due to the dimer not being fully saturated. Qualitative analysis of the three faces ranks them in the following order of increasing surface energy (0 1 1) > (0 0 2) > (1 0 0).

The surface energies of these faces were calculated and these predict the same trends from the qualitative analysis. Face (1 0 0) exhibits the

lowest surface energy of $30.7 \, mJ/m^2$. Face (0 0 2) exhibits a higher surface energy of $47.1 \, mJ/m^2$ due to the slight exposure of Group D and the full exposure of this group increases the surface energy of face (0 1 1) to $73.8 \, mJ/m^2$.

The particle surface energies of the two extreme habits of ibuprofen can be compared, where it can be seen that particles crystallised from polar solvents (e.g. ethanol) which contain a more regular habit exhibit a higher particle surface energy $\sim 48.4 \, mJ/m^2$ than the surface energy of needle-like habit crystallised from non-polar solvents (e.g. hexane) $\sim 38.8 \, mJ/m^2$. These predictions are in agreement with the expected results that an increase in solvent polarity increases the fractional surface coverage of the higher energy faces and in turn results in a larger particle surface energy (Fig. 8).

3.2. Size and shape characterisation of recrystallised batches

Scanning electron micrographs for recrystallised batches are shown in Figure where differences in particle habit are observed. As expected, increasing the solvent polarity (hexane < toluene < acetonitrile < ethanol) increases the shape regularity such that the particles change from needle/lath shaped particles to plate/prismatic shaped.

Particle size and shape analysis (QICPIC) was performed on all batches and the number weighted distributions (most sensitive to smaller particles in the sample) are shown in Fig. 9a and the volume weighted distributions (most sensitive to the large particles in the sample) are shown in Fig. 9b. It should be noted that although the batches were passed through a 150 μm sieve they all contain a proportion of particles greater than this. This is due to elongated particles passing through the mesh along their shortest axis and also reporting the data using Feret Max. IbuAce contains the highest proportion of fine (~5 μm) particles and the lowest proportion of coarse material
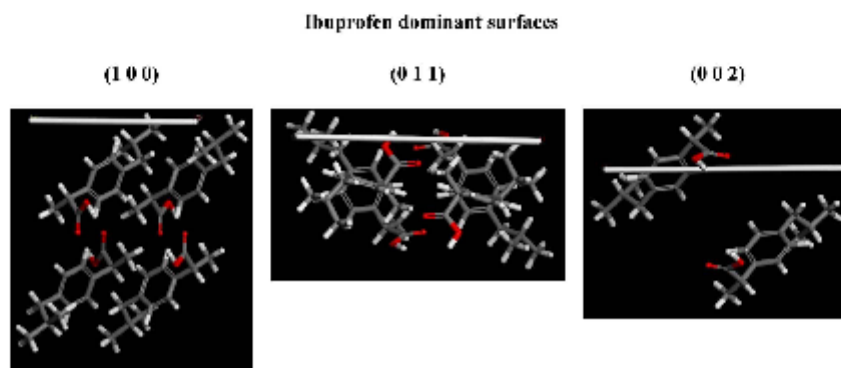
Ibuprofen dominant surfaces

(1 0 0)   (0 1 1)   (0 0 2)

Fig. 6. Crystal chemistry of ibuprofen dominant surfaces.

a) side view
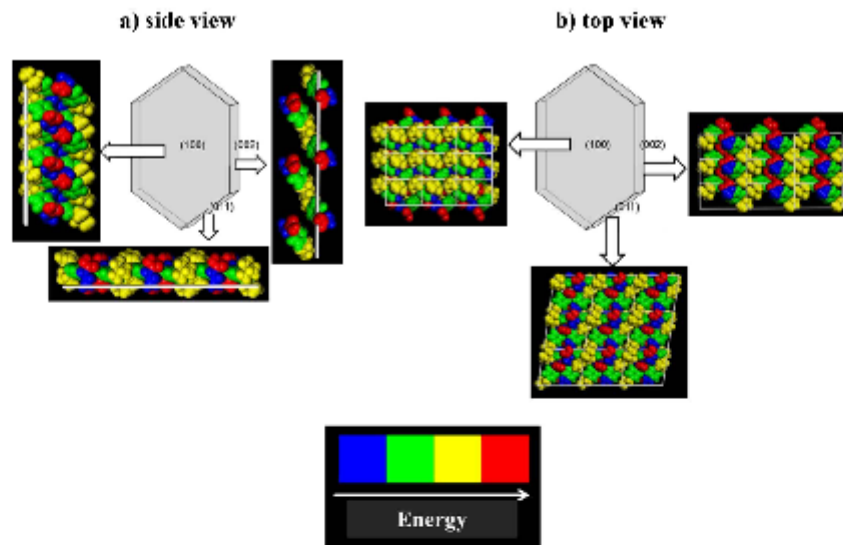
b) top view

Energy

Fig. 7. Crystal chemistry of ibuprofen surfaces colour coded related to the atomic contribution to lattice energy a) side view of the three faces b) top view of the three faces.

(50–400 μm). The volume distribution for this batch is observed to be centered ~250 μm which is higher than all other batches (centered at ~125 μm), inferring that this batch has the widest size distribution. All other batches contain a similar proportion of particles by number and have primary modes centering around 125 μm by volume.

The aspect ratio (width/length) versus particle size (40–400 μm) of

the batches is shown and ranks the batches as follows in terms of decreasing aspect ratio ethanol > acetonitrile > toluene > hexane. This data confirms the visual observation that increasing solvent polarity in turn increases shape regularity.

Fig. 8. Scanning electron micrographs of recrystallised ibuprofen showing changes in particle habit from; a) hexane b) toluene c) acetonitrile d) ethanol. All images captured using × 100 magnification and scale bar is 100 μm.

Fig. 9. QICPIC a) number and b) volume weighted distributions for recrystallised ibuprofen batches; c) QICPIC aspect ratio versus particle size for recrystallised batches.

3.3. Physico-chemical characterisation
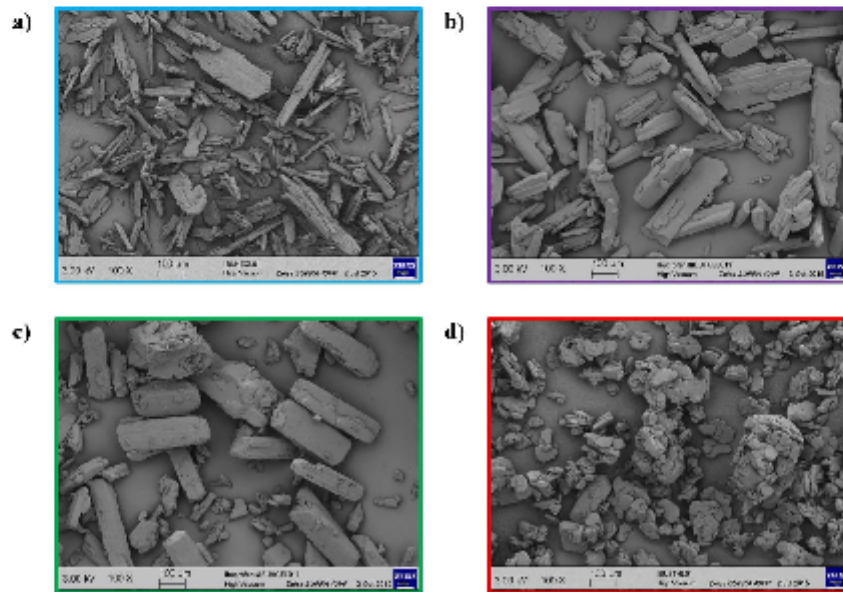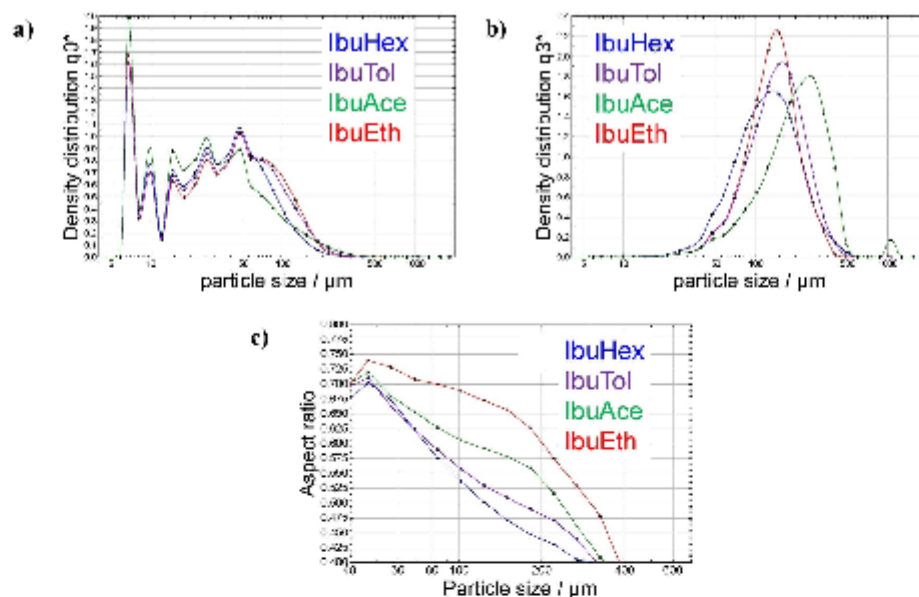
It was expected that no form change, from *(RS)*-ibuprofen form I, would occur during the recrystallisation of ibuprofen as the only other form reported, form II (Dudognon et al., 2008), was prepared by annealing. PXRD was performed to confirm this result. The diffraction patterns for the recrystallised batches are shown in Fig. 10 and reveal that all peaks are aligned. Perhaps not unexpectedly, there is some impact on the PXRD intensities due to the texture of the samples. Some preferred orientation is seen in Fig. 10 especially from needles crystallised from hexane (a). From the single crystal data it is known where every major peak for form I should be and all the PXRD patterns in Fig. 10 are consistent with that. The DSC data (Fig. 11) also shows all four samples are form I. This data confirms that no form change has occurred during the recrystallisation and that the form present is *(RS)*-ibuprofen form I due to the mild crystallisation conditions.

The DSC thermograms for all samples are shown in Figure and reveal no major differences between the melt of the samples. The onset of

the melt was extrapolated using Trios software (TA Instruments – A division of Waters Ltd, Herts, UK) and was shown to be similar for all samples, with the range 73.7–74.5 °C. The peak melting temperatures were found to be within the range 75.8–76.1 °C, again confirming that no form changes had occurred during recrystallisation and all samples are of similar crystallinity. The enthalpy of fusion values for recrystallised ibuprofen batches were shown to be; 123.2 J/g for hexane, 126.8 J/g for toluene, 127.4 J/g for acetonitrile and 118.6 J/g for ethanol. It can be seen that there is some variation between the samples, however they are all form I as the reported enthalpy of fusion for form II is 33.9 J/g and unstable at room temperature (Dudognon et al., 2008).

The respective volatile organic solvent for each recrystallised batch were quantified using HS-GC and the resultant residual solvent levels are shown to be low ($\leq$180 PPM) and are below the maximum acceptable daily exposure guidelines, as set be ICH Q3C (R6) 2016.
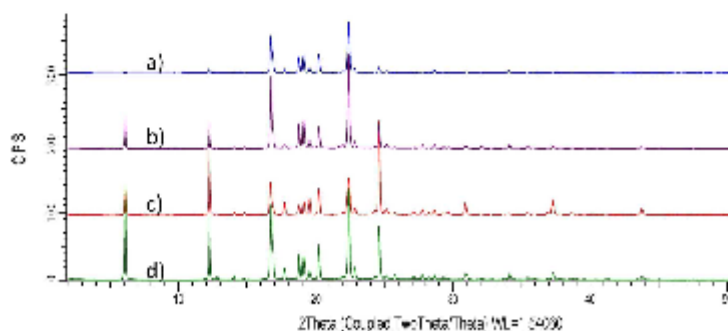

Fig. 10. Powder X-ray diffraction patterns for recrystallised ibuprofen a) hexane b) toluene c) ethanol d) acetonitrile.
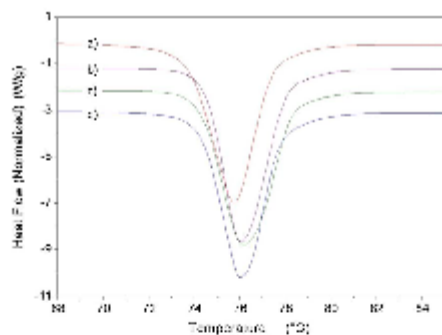
Fig. 11. DSC thermograms of recrystallised ibuprofen a) ethanol b) toluene c) acetonitrile d) hexane.

3.4. Sticking propensity

The sticking propensity of the batches was measured by recording the detachment stress from the base die post compaction. It is proposed that higher stresses relate to more powder adhering to the die in turn inferring a greater sticking propensity. The detachment stress measurements at 3 compaction pressures are shown in Table 1. At the lowest compaction pressures all samples exhibit no sticking and low detachment stress readings (≤ 0.1 MPa). As the pressure increases the detachment stress values diverge and the largest difference is observed at the highest compaction pressure (~ 180 MPa) where batches can be ranked as follows in terms of sticking propensity: IbuHex < IbuTol < IbuAce < IbuEth. When sticking is observed the standard deviations of the measurements generally increase and large variation is observed at 108 MPa for IbuEth however the sticking trend is still clear. From this it can be concluded that the sticking propensity of the batches can be ranked in terms of particle habit with an increase in aspect ratio resulting in an increase in sticking propensity

3.5. Surface analysis

The BET surface area values are presented in Table 2 and show that despite the change in crystal habit the surface area of the particles remains similar, with values between 0.082–0.109 m²/g. The cumulative pore area and volume are also shown in Table 2, where no correlation with sticking propensity can be observed.

Typical isotherms for all batches, as shown in Fig. 12, classify all batches as Type II: non-porous or macroporous according to the IUPAC guidelines (Sing et al., 1985). These results suggest that surface area and pore size are not contributing factors to the observed differences in the sticking propensity of the different habits.

Surface energy heterogenity was calculated for all batches and split into total and dispersive/specific contributions. Studies have suggested surface energy values close to 'infinite dilution' should be reported due to the high energy sites being analysed and hence these values being

Table 1

Detachment stress of recrystallised ibuprofen at three compaction pressures. Standard deviation of three measurements are shown in brackets.

Batch	Detachment Stress		
	40 MPa	108 MPa	180 MPa
IbuHex	0.05 (0.01)	0.08 (0.01)	0.50 (0.01)
IbuTol	0.09 (0.02)	0.27 (0.03)	0.72 (0.22)
IbuAce	0.07 (0.01)	0.63 (0.10)	1.97 (0.39)
IbuEth	0.10 (0.01)	3.38 (0.96)	3.37 (0.24)

Table 2

BET surface area, cumulative pore volume and cumulative pore area for recrystallised ibuprofen samples. Reported values are mean of two measurements.

Batch	BET surface area (m²/g)	Cumulative pore volume (mm³/g)	Cumulative pore area (m²/g)
IbuHex	0.109	0.183	0.114
IbuTol	0.082	0.111	0.070
IbuAce	0.101	0.095	0.054
IbuEth	0.082	0.153	0.074

representative of the entire material surface properties (Gamble et al., 2012). In order to achieve this, energy values are typically reported at surface coverages of < 5%.

The total surface energy (γt) is shown in Table 3 and reveals that the batches IbuAce, IbuTol and IbuHex would rank differently depending on what surface coverage value below 5% was reported. Despite this it is clear that batch IbuEth exhibits the highest total surface energy at all analysed surface coverages (at 1% surface coverage IbuEth has a total surface energy of 67.3 mJ/m² whereas all other batches exhibit lower values between 61.1–62.0 mJ/m²).

The same trends are seen from the specific surface energy (γab) values, Table 3, where IbuEth exhibits a higher specific component at all surface coverages compared to all other batches (at 1% surface coverage batch IbuEth has a specific surface energy of 26.4 mJ/m² whereas all other batches exhibit lower values between 20.7–20.8 mJ/m²). These results agree with the computational work described where crystallisation in a polar solvent (e.g. ethanol) results in particles with a higher aspect ratio due to the greater exposure of the (0 0 2) and (0 1 1) faces. These faces contain a higher surface energy due to the presence of the carboxylic acid groups at the surface and in turn increase the specific surface energy.

At surface coverages below 5% the dispersive surface energy for all batches was similar, with values between 40.3–41.8 mJ/m². The dispersive surface energy was unable to be ranked and reveals that the changes in the total surface energy are due to the variations in specific surface energy only. This implys that the proportion of the main (1 0 0) face stays constant during particle growth and only the proportion of the (0 0 2) and (0 1 1) face are altered when the polarity of the crystallisation solvent is increased.

It would be expected that the total surface energy (influenced by the specific surface energy) would decrease as the aspect ratio of particles decreases. These trends are not observed for IbuAce, IbuHex and IbuTol and these batches would be ranked the same if error is accounted for. This could be due to instrument sensitiviy however an increase in specific surface energy as aspect ratio increases can be inferred from the computational work. Batch IbuEth contains the highest specific surface energy and exhibits the highest sticking propensity. If the findings from the computational work are taken into account then sticking propensity increases as specific surface energy increases. Previous work has shown that a higher surface energy leads to greater cohesion therefore a higher tensile strength of tablets (El Gindy and Samaha, 1982). The findings from this study suggest that the specific contribution to the total surface energy may alter the adhesive properties and a higher specific component leads to greater adhesion and therefore sticking propensity.

It should be noted here that the computational data is derived from a bottom-up approach where the energy is calculated from the unsaturated interactions at the surface of the face. The iGC data is based on a top-down approach where the energy is derived from interactions at the surface from the highest energy sites. In order to compare the two techniques caution must be taken when reporting iGC data due to different surface coverages. It is proposed that as computational modelling accounts for the whole surface and not just high energy sites then reporting iGC at infinite dilution would not be suitable for this comparison. The total surface energy (at 20% surface coverage) for needles is 56.0 mJ/m² compared to 65.1 mJ/m² for prisms. This is a 9.1 mJ/m²
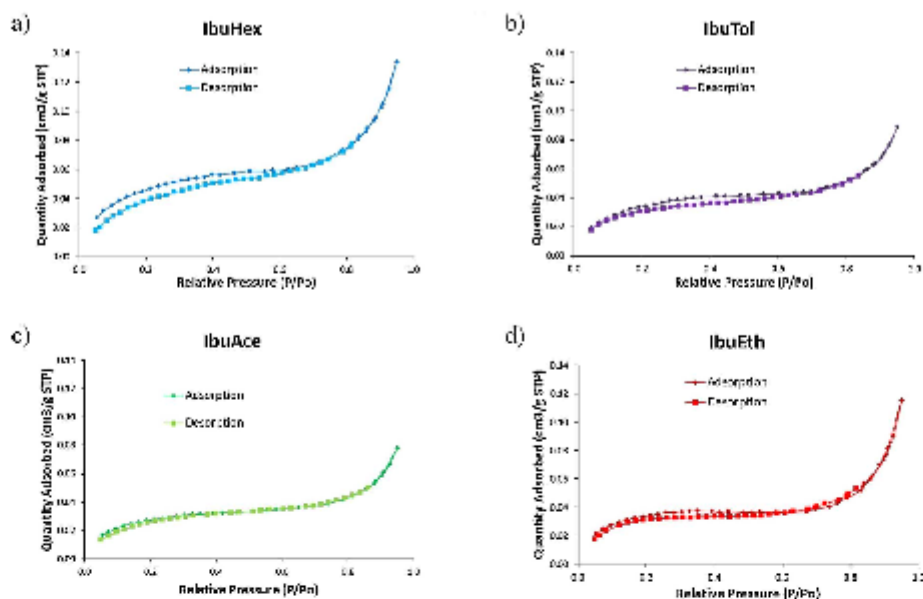
Fig. 12. Typical isotherms for recrystallised ibuprofen batches a) IbuHex b) IbuTol c) IbuAce d) IbuEth.

Table 3
Surface energy (total γt and specific γab) for recrystallised ibuprofen at different surface coverages. Reported standard deviation shown in brackets is of three measurements made on sample with highest variation in surface energy (IbuEth).

Surface coverage	Surface energy (mJ/m^2)							
	IbuHex		IbuTol		IbuAce		IbuEth	
	γt	γab	γt	γab	γt	γab	γt	γab
1	62.0	20.7	61.9	20.8	61.1	20.7	67.3(2.4)	26.4(1.7)
2	60.7	20.1	62.9	21.2	62.1	20.8	67.0(2.1)	26.2(1.6)
4	60.9	20.2	59.3	19.0	62.0	20.2	66.6(1.9)	25.9(1.5)
6	60.0	19.8	59.1	18.6	57.4	17.7	66.3(2.0)	25.8(1.5)
10	57.5	18.8	55.0	16.1	53.5	15.5	65.8(1.8)	25.5(1.5)
15	56.4	18.3	56.2	16.7	52.1	14.6	65.4(1.8)	25.3(1.5)
20	56.0	18.1	54.9	15.4	50.6	13.8	65.1(1.5)	25.1(1.3)

increase for the prisms compared to the needles and the calculated surface energy reveals a similar increase of 9.6 mJ/m^2 (needles: 38.8 mJ/m^2 and prisms: 48.4 mJ/m^2). These values are not alingned due to the differences in the approaches descirved above however do show excellent agreement in the differences.

4. Conclusion

The crystal chemistry of ibuprofen was explored and the importance of the hydrogen bonded carboxylic acid dimers contribution to lattice energy was revealed. The surface chemistry of the three dominant faces was visualised in relation to lattice energy and the calculated surface energy values of the faces increased as the exposure of the carboxylic acid group increased.

The different surface chemistries enabled the proportion of each face to be altered by crystallisation in solvents with differing polarity and ibuprofen was successfully crystallised into four diverse particle habits. The sticking propensity of these batches was shown to be driven by the changes in particle habit, where a more regular particle habit resulted in the material demonstrating a higher degree of sticking. To further investigate if the sticking propensity was driven by a chemical change altered by the difference in physical shape the surface energy of particles was explored.

The particle surface energies of the extreme habits were compared experimentally by iGC and computationally. Although the absolute values did not align both approaches showed that prism shaped particles exhibited a higher energy of around 9 mJ/m^2 compared to needles. The iGC and qualitative modelling data further revealed this difference to be attributed to the increase in the specific (polar) component, which is due to greater presence of faces which contain the carboxylic acid functionality at the surface.

The combination of experimental and computational surface energy techniques reveal that the sticking propensity of ibuprofen is increased by a change in specific surface energy caused by a change in crystal habit. Computational and experimental data reveals that the increase in surface energy of the regular shaped particles can be attributed to the increase in the specific (polar) component, which is due to greater presence of faces which contain the carboxylic acid functionality at the surface. The increase in the specific energy component is shown to correlate with the sticking propensity of ibuprofen. It is proposed that investigation of the chemical causality of sticking, for this API and others, using the techniques demonstrated in this paper will be of increasing importance.

References

Bravais, A., 1866. Etudes Crystallographiques. Gauthiers Villars, Paris.

Brunauer, S., Emmett, P.H., Teller, E., 1938. Adsorption of gases in multimolecular layers. J. Am. Chem. Soc. 60 (2), 309–319.

Bunyan, J., Shankland, N., Sheen, D., 1991. Solvent effects on the morphology of ibuprofen. AIChE Symp. Ser. 45–57.

Cano, H., Gabas, N., Canselier, J.P., 2001. Experimental study on the ibuprofen crystal growth morphology in solution. J. Cryst. Growth 224, 335–341.

Challener, C.A., 2014. QbD in API Manufacture: with a quality-by-design approach, robust processes consistently can help deliver quality product. Pharm. Technol. 38 (9).

Chow, K., Tong, H.H.Y., Lum, S., Chow, A.H.L., 2008. Engineering of pharmaceutical materials: an industrial perspective. J. Pharm. Sci. 97 (8), 2855–2877.

Clark, M., Crammer Jr., R.D., Opdenbosch, N.V., 1989. Validation of the general purpose tripos 5. 2 force field. J. Comput. Chem. 10, 982–1012.

Clydesdale, G., Docherty, R., Roberts, K.J., 1991. HABIT – a program for predicting the morphology of molecular crystals. Comput. Phys. Commun. 64 (2), 311–328.

Clydesdale, G., Roberts, K.J., Docherty, R., 1996. HABIT95—a program for predicting the morphology of molecular crystals as a function of the growth environment. J. Cryst. Growth 166 (1–4), 78–82.

Danjo, K., Kojima, S., Chen, C.Y., Sunada, H., Otsuka, A., 1997. Effect of water content on sticking during. Chem. Pharm. Bull. 45 (4), 706–709.

Docherty, R., Clydesdale, G., Roberts, K.J., Bennema, P., 1991. Application of Bravais-Friedel-Donnay-Harker, attachment energy and Ising models to predicting and understanding the morphology of molecular crystals. J. Phys. D: Appl. Phys. 24 (2), 89.

Dong, S., Brendlé, M., Donnet, J.B., 1989. Study of solid surface polarity by inverse gas chromatography at infinite dilution. Chromatographia 28 (9), 469–472.

Donnay, J.D.H., Harker, D., 1937. A new law of crystal morphology extending the law of bravais. Am. Min. 22, 446–467.

Dorris, G.M., Gray, D.G., 1980. Adsorption of n-alkanes at zero surface coverage on cellulose paper and wood fibers. J. Colloid Interface Sci. 77 (2), 353–362.

Dudognon, E., Danède, F., Descamps, M., Correia, N.T., 2008. Evidence for a new crystalline phase of racemic ibuprofen. Pharm. Res. 25 (12), 2853–2858.

Dunitz, J.D., Gavezzotti, A., 2012. Supramolecular synthons: validation and ranking of intermolecular interaction energies. Cryst. Growth Des. 12 (12), 5873–5877.

El Gindy, N.A., Samaha, M.W., 1982. Tensile strength of some pharmaceutical compacts and their relation to surface free energy. Int. J. Pharm. 13 (1), 35–46.

Friedel, G., Bulletin De La Societe Francaise De Mineralogie Et De Crystallographie. 1907. 30: p. 326.

Gamble, J.F., Leane, M., Olusanmi, D., Tobyn, M., Šupuk, E., Khoo, J., Naderi, M., 2012. Surface energy analysis as a tool to probe the surface energy characteristics of micronised materials—a comparison with inverse gas chromatography. Int. J. Pharm. 422 (1–2), 238–244.

Hartman, P., Bennema, P., 1980. The attachment energy as a habit controlling factor. J. Cryst. Growth 49 (1), 145–156.

Ho, R., Heng, J.Y.Y., 2013. A review of inverse gas chromatography and its development as a tool to characterize anisotropic surface properties of pharmaceutical solids. KONA Powder Part. J. 30, 164–180.

Nguyen, T.T.H., Hammond, R.B., Roberts, K.J., Marziano, I., Nichols, G., 2014. Precision measurement of the growth rate and mechanism of ibuprofen {001} and {011} as a function of crystallization environment. CrystEngComm 16, 4568–4586.

Paul, S., Wang, K., Taylor, L.J., Murphy, B., Krzyzaniak, J., Dawson, N., Mullarney, M.P.,

Moonan, P., Sun, C.C., 2017a. Dependence of punch sticking on compaction pressure—roles of particle deformability and tablet tensile strength. J. Pharm. Sci. 106 (8), 2060–2067.

Paul, S., Taylor, L.J., Murphy, B., Krzyzaniak, J., Dawson, N., Mullarney, M.P., Moonan, P., Sun, C.C., 2017b. Mechanism and kinetics of punch sticking of pharmaceuticals. J. Pharm. Sci. 106, 151–158.

Perlovich, G.L., Kurkov, S.V., Hansen, L.K., Bauer-Brandl, A., 2004. Thermodynamics of sublimation, crystal lattice energies, and crystal structures of racemates and enantiomers (+)- and (±)-ibuprofen. J. Pharm. Sci. 93 (3), 654–666.

Pudasaini, N., Upadhyay, P.P., Parker, C.R., Hagen, S.U., Bond, A.D., Rantanen, J., 2017. Downstream processability of crystal habit-modified active pharmaceutical ingredient. Organic Process Research Development.

Roberts, M., Ford, J.L., Macleod, G.S., Fell, J.T., Smith, G.W., Rowe, P.H., Dyas, A.M., 2004a. Effect of punch tip geometry and embossment on the punch tip adherence of a model ibuprofen formulation. J. Pharm. Pharmacol. 56 (7), 947–950.

Roberts, M., Ford, J.L., Rowe, P.H., Dyas, A.M., Macleod, G.S., Fell, J.T., Smith, G.W., 2004b. Effect of lubricant type and concentration on the punch tip adherence of model ibuprofen formulations. J. Pharm. Pharmacol. 56 (3), 299–305.

Rosbottom, I., Roberts, K.J., Docherty, R., 2015. The solid state: surface and morphological properties of p-aminobenzoic acid in terms of the strength and directionality of its intermolecular synthons. CrystEngComm 17 (30), 5768–5788.

SMS, 2016. iGC-SEA compared to Contact Angle (CA) and Atomic Force Microscopy (AFM). www.surfacemeasurementsystems.com/solutions/inverse-gas-chromatography-sea/.

Shekunov, B.Y., Chattopadhyay, P., Tong, H.H.Y., Chow, A.H.L., 2007. Particle size analysis in pharmaceutics: principles, methods and applications. Pharm. Res. 24 (2), 203–227.

Shi, B., Wang, Y., Jia, L., 2011. Comparison of Dorris-Gray and Schultz methods for the calculation of surface dispersive free energy by inverse gas chromatography. J. Chromatogr. A 1218, 860–862.

Sing, K.S.W., Everett, D.H., Haul, R.A.W., Moscou, L., Pierotti, R.A., Rouquerol, J., Siemieniewska, T., 1985. Reporting physisorption data for gas/solid systems with special reference to the determination of surface area and porosity. Pure Appl. Chem. 57 (4), 603–619.

Storey, R.A., Docherty, R., Higginson, P.D., 2003. Integration of high throughput screening methodologies and manual processes for solid form selection. Am. Pharm. Rev. 6, 104–105.

Sun, H., 1998. COMPASS: an ab initio force-field optimized for condensed-phase applications overview with details on alkane and benzene compounds. J. Phys. Chem. B 102 (38), 7338–7364.

Sun, C.C., 2009. Materials science tetrahedron—a useful tool for pharmaceutical research and development. J. Pharm. Sci. 98 (5), 1671–1687.

Ticehurst, M., Docherty, R., 2006. From molecules to pharmaceutical products – the drug substance/drug product interface. Am. Pharm. Rev. 34–36.

Volpe, C.D., Siboni, S., 1997. Some reflections on acid-base solid surface free energy theories. J. Colloid Interface Sci. 195 (1), 121–136.

Waknis, V., Chu, E., Schlam, R., Sidorenko, A., Badawy, S., Yin, S., Narang, A., 2014. Molecular basis of crystal morphology-dependent adhesion behavior of mefenamic acid during tableting. Pharm. Res. 31 (1), 160–172.

Winn, D., Doherty, M.F., 2000. Modeling crystal shapes of organic materials grown from solution. AIChE J. 46 (7), 1348–1367.

196